LATE PLEISTOCENE EVOLUTION OF GLACIAL LAKE PURCELL: A POTENTIAL FLOODWATER SOURCE TO THE CHANNELED SCABLAND

by

Jared L. Peters
B.S., Bloomsburg University of Pennsylvania, 2009
A.A.S., Garrett College, 2005

THESIS SUBMITTED IN PARTIAL FULFILLMENT OF
THE REQUIREMENTS FOR THE DEGREE OF

MASTER OF SCIENCE

In the
Department of Geography
Faculty of Environment

SIMON FRASER UNIVERSITY

Fall 2012

APPROVAL

Name: **Jared Peters**

Degree: **Master of Science**

Title of Thesis: **Late Pleistocene evolution of glacial Lake Purcell: a potential floodwater source to the Channeled Scabland**

Examining Committee:

Chair: **Dr. Eugene McCann**
Professor, Department of Geography

Dr. Tracy A. Brennand
Senior Supervisor
Associate Professor, Department of Geography

Dr. Olav Lian
Supervisor
Faculty, Department of Geography, University of the Fraser Valley
Adjunct Professor, Department of Geography

Dr. Richard Waitt
Internal Examiner
Research Geologist, Cascade Volcano Observatory

Dr. Dan Smith
External Examiner
Professor
Department of Geography, University of Victoria

Date Defended/Approved: September 18, 2012

ABSTRACT

The Quaternary history of the Channeled Scabland (CS) and its primary floodwater sources during marine isotope stage (MIS) 2 are well documented and understood. However, putative floodwaters from glacial lakes in British Columbia are poorly understood; these lakes may have supplied floodwaters to the CS in late MIS 2 during northward retreat of the Cordilleran Ice Sheet.

This study combines geomorphology, sedimentology, stratigraphy, aerial photograph interpretation, ground penetrating radar, and geographic information science to reconstruct the paleogeography and evolution of glacial Lake Purcell in the Purcell Trench. Glacial Lake Purcell was a proglacial, ice-contact lake that was ~90 km long, up to 12 km wide, and ~360 m deep against its dam (Purcell Lobe). It contained >70 km^3 of water just prior to drainage. It likely drained catastrophically (~47 km^3 of water) down the Kootenay River valley into the Columbia River, though geomorphic evidence is equivocal.

Keywords: Glacial Lake Purcell; ice-contact proglacial lake; jökulhlaup; Channeled Scabland; Cordilleran Ice Sheet; Purcell Trench

For my Hazel Mae (a.k.a. the “Hazelhoff”, the
“Hazinator”, “Hazalea”, “Donkey”, “Donkey
Chowder”, “Chongles”, “Potatoes”,
and “Sweet Petite”).

ACKNOWLEDGEMENTS

The people who live in the Kootenays are among the happiest and friendliest that I have met. They were extremely helpful, curious and tolerant of my explorations on their property. Among those who deserve thanks are Roland Proctor and his neighbours in Johnsons Landing, Bill and Leila McCaw in Balfour, Lenard and his family in Tarrys, and Dan in Castlegar. I am especially thankful to Rob and Sarah, who went above and beyond to make my assistant and I feel down right at home for a week—you guys are great and I will always consider you my friends. I thank you all and wish you the best.

My field assistants, Andrew Perkins and Aaron Dixon were hard working, smart and positive throughout the two demanding field seasons. I couldn't have done this without you guys—and I certainly wouldn't have had as much fun. We spent two months in tents while we ate green hotdogs, cooked in tin cans, weathered storms, got interrogated by the US border patrol, threw axes, slaughtered chickens, drove thousands of kilometres, dug in hundreds of exposures, and counted thousands of clasts. My lab assistant, Lili Perreault saved me hours of tedious data entry that may have cost me my last marbles. Matthew Burke was an integral part of the GPR work in this thesis and served as an impromptu advisor. During his time at SFU he became a good friend and an "uncle Map". Thanks to all my paleo-pals.

My committee members, Olav Lian and Richard Waitt, and my external supervisor, Dan Smith all provided knowledgeable and valuable advice. They all managed to read through my thesis on a very tight timeline and still provide poignant edits. Richard's role was particularly important, for his original questions on Columbia River valley megaflood forms inspired this study—and he proved extremely helpful during the editing process.

Tracy Brennand was an excellent advisor throughout this study. She is knowledgeable, hardworking and selflessly devoted to her students. In both the field and lab she was a leader, and during the occasional downtime she was a lot of fun. Tracy, I consider you a friend and myself lucky. I couldn't have done this without you, thanks.

This study was conducted while my wife, Britta and I started a family by bringing our daughter Hazel into the world. This was crazy. I couldn't have gotten through this project without help from our friends on the "mountain" and in Vancouver, who provided us with much-needed social breaks and babysitting. Thanks to all of our friends. We will miss you.

Most of all, I need to thank Britta and Hazel. Thanks for taking care of each other while I was away in the field or in the lab, and for putting up with me while I was at home.

TABLE OF CONTENTS

LIST OF FIGURES

LIST OF TABLES

1: INTRODUCTION AND RESEARCH RATIONALE

"The history of this old lake country, as it is recorded in the alternations of strata which accumulated at the bottoms of its water basins, will be found to be full of interest."

J. S. Newberry (1871, p.648)

1.1 Introduction

At its last glacial maximum, the last Cordilleran Ice Sheet dammed large amounts of meltwater flowing from the Cordilleran Ice Sheet (CIS) forming (among others) glacial Lakes Columbia and Missoula (Pardee 1910; Bretz 1969; Figure 1-1). Evidence of enormous jökulhlaups from these lakes is abundant and well documented (e.g., Bretz 1923, 1925, 1928, 1969; Baker 1978a, 1978c; Patton & Baker 1978; Baker & Bunker 1985; Atwater 1987; Benito & O'Connor 2003). These megafloods, and similar floods from previous glaciations, were the dominant geomorphic agent in the formation of the Channeled Scablands (CS) of Washington State (Bretz 1923, 1925, 1928, 1969; Baker 1978b, 2009a, 2009b; Smith 2006). Flood events from the drainage of glacial lakes in British Columbia (BC) are also proposed agents of CS evolution (Shaw et al. 1999; Lesemann & Brennand 2009; Waitt et al. 2009).

During the advance and retreat of the CIS, large amounts of meltwater were stored in glacial lakes in southern BC (e.g., Fulton 1969; Fulton and Smith 1978; Fulton et al. 1989; Ryder et al. 1991; Sawicki & Smith 1991; Johnsen and Brennand 2004) and the size and evolution of some of these lakes, as well as their drainage regimes and ages must be deciphered in order to establish the importance of floods from BC as agents of geomorphic change in the CS.

1.2 Rationale

A proposal that glacial Lake Kootenay is the source of floodwater from BC into the CS of Washington State (Waitt et al. 2009) provides the rational for this project. Waitt et al. (2009) and Robert Fulton (pers. comm. 04/21/2010) have differing hypotheses on the character and locations of glacial lakes occupying the Purcell Trench in BC. This thesis will focus on inventorying glaciolacustrine and glaciofluvial sediments and landforms in the Purcell Trench and Kootenay River valley (KRv) in order to assess whether or not a glacial lake existed in the Purcell Trench and drained west along the KRv to the Columbia River valley and thence to the CS.

This research furthers understanding of temporary meltwater storage and catastrophic drainage in BC during the late Wisconsinan (Fraser) Glaciation (MIS 2). This research increases understanding of deglacial hydrology and glacial geomorphology in high-relief terrain.

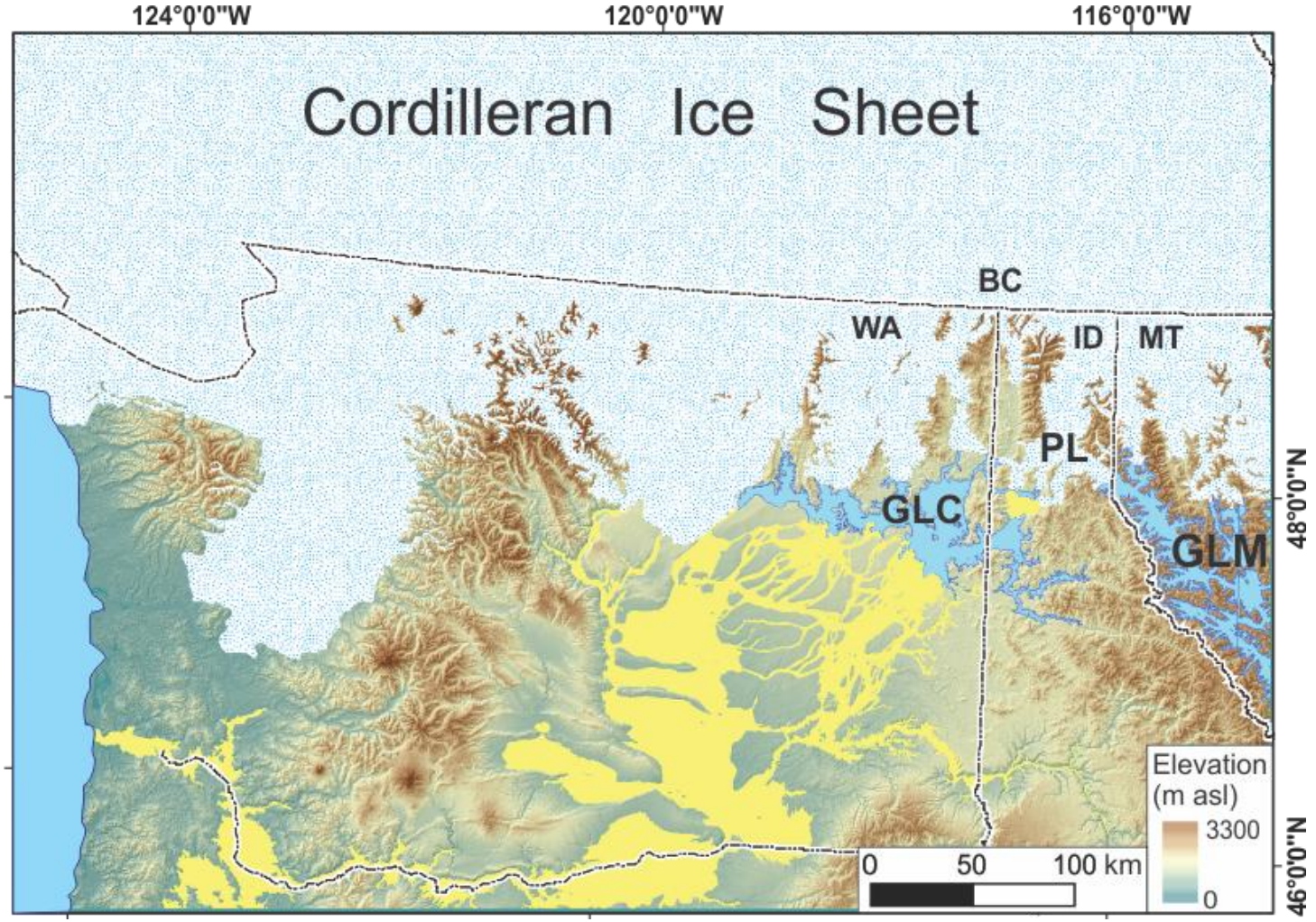

Figure 1-1: Hillshaded DEM (NED; data available from U.S. Geological Survey.) showing the CS (yellow), the Cordilleran Ice Sheet at its late glacial maximum extent (white with blue dots), and glacial Lake Columbia (GLC) and glacial Lake Missoula (GLM) at their non-synchronous maximum extents, and the Purcell Lobe (PL) (Ehlers & Gibbard 2004).

1.2.1 A proposed flood from glacial Lake Kootenay

Geomorphology and tephrachronology suggest that some megaflood landforms in the CS postdate the deposits attributed to the last floods of glacial lakes Columbia and Missoula (Waitt et al. 2009). Along the Columbia River valley near the town of Chelan (Figure 1-2), two low-elevation bars with megaripples are situated below the megaflood surface known as the "Great Terrace". The stratigraphy of these bars is distinct from that of the surrounding Great Terrace because they are devoid of Glacier Peak tephra (Waitt 2009; Waitt et al. 2009), which was deposited by an eruption 11.6 ^{14}C ka BP (13.7-13.4 cal. ka BP) (Kuehn et al. 2009). Waitt (2009) proposed that a large glacial lake in the Kootenay valley, glacial Lake Kootenay, might have been a significant water source late in the Pleistocene and that its drainage could be responsible for the creation of the megaflood deposits along the Columbia River near Chelan (~500 km downflow from glacial Lake Kootenay). The putative flood route of the jökulhlaup proposed by Waitt (2009) is shown in Figure 1-2.

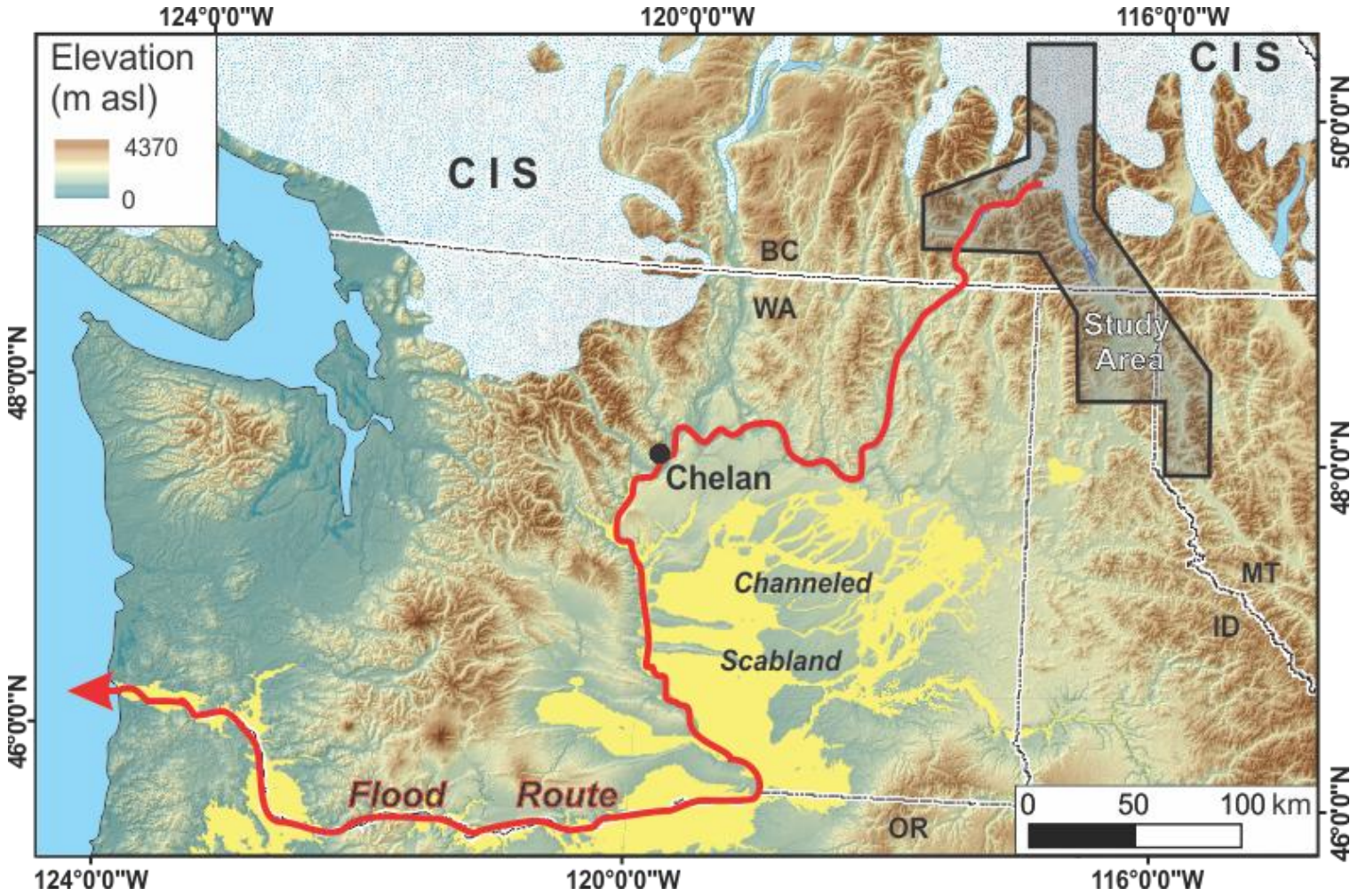

Figure 1-2: Hillshaded DEM mosaic (Geobase® in CA, NED in USA; data available from U.S. Geological Survey.) showing the putative ~500 km long flood route along the CRv associated with the drainage of glacial Lake Kootenay (in this thesis called glacial Lake Purcell, refer to § 3.1.1) as a bold red line (Waitt 2009; Waitt et al. 2009). The CIS marigin is shown at ~12.5 ^{14}C ka BP (Dyke et al. 2003).

1.2.2 Gradual drainage of glacial lakes in the Purcell Trench

Fulton and others have proposed that stagnant ice occupied much of the Purcell Trench during deglaciation of the CIS in MIS 2 (Fulton 1991; Ryder et al., 1991; Fulton pers. comm. 04/21/2010; Figure 1-3). If the Kootenay valley was indeed occupied by a stagnant ice mass, the volume of water stored in the Purcell Trench may have been too small to have resulted in significant flooding ~500 km downflow in the Columbia River valley (even if the lake drained catastrophically). Fulton (pers. comm. 04/21/2010) has suggested that lacustrine sediments in the Purcell Trench are likely the result of low-volume ice-marginal lakes and that drainage of these lakes was likely gradual rather than catastrophic. Likewise, Alden (1953) in his initial assessment of a lake he called glacial Lake Kootenai (gLK, a lake that extended into the Purcell Trench from Montana), and Johns (1970) in his reassessment of this lake, suggest that gradual drainage over its southern spillway near Elmira, ID was responsible for most of the drainage of gLK. In this thesis I show that gLK existed mainly in MT whereas glacial Lake Purcell (gLP) (named as such to distinguish it from gLK) formed in the Purcell Trench (refer to § 3.1.1) and thus is the focus of this thesis.

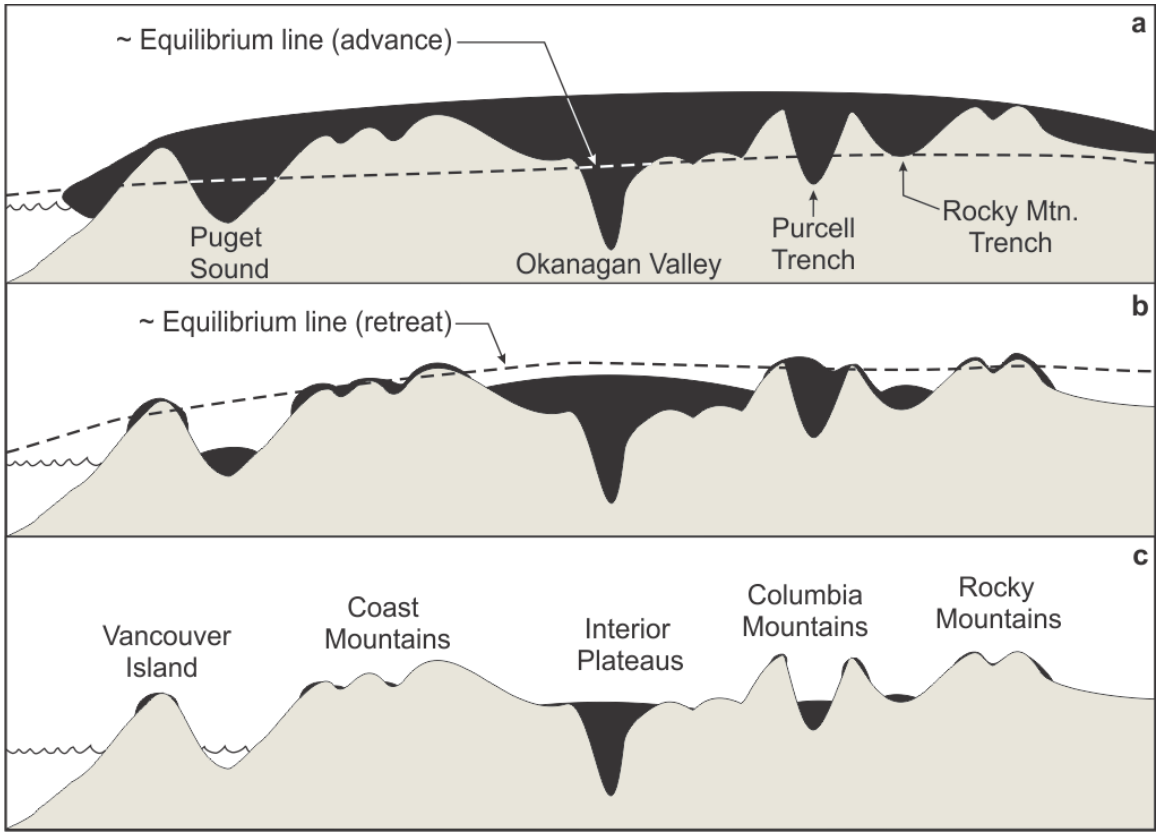

Figure 1-3: Conceptual ice decay model for the CIS (after Fulton 1991). a) CIS (black) at its maximum extent with an approximate advance-phase equilibrium line shown (black dashed line). b) An approximate position of the elevated retreat-phase equilibrium line (black dashed line) causes downwasting across most of the ice sheet leading to the relatively prolonged persistence of the thickest ice. c) Alpine glaciers remain (similar to today) and the CIS is reduced to discrete ice masses in valleys.

1.3 Research questions

1.3.1 Primary research question

Could the Purcell Trench have held a large amount of water and delivered it suddenly to the Columbia River system?

1.3.2 Detailed research questions

Is there evidence of an ice dam in the Purcell Trench? Answering this question will address the likelihood of proglacial lake formation and thus justify the modeling of a glacial lake in the Purcell Trench. Evidence of an ice dam may be provided by kame terrace formation against the valley walls of the Purcell Trench.

What is the paleogeography of glacial Lake Purcell and how did it evolve? Answering this question will help to determine the amount of potentially drainable water contained in the Purcell Trench. To answer this question, the paleolake will be modeled in a geographic information system (GIS).

Is there evidence of catastrophic drainage from glacial Lake Purcell through the Kootenay River valley? Answering this question will address the likelihood of high-energy flood flows through the Kootenay River valley and into the Columbia River system. Evidence of a large flood flow may be provided by large-scale bedforms, soft-sediment rip-up clasts, hyperconcentrated-flow deposits, smoothed bedrock, or deep incision through valley fill sediment.

2: LITERATURE REVIEW

"The scablands are wounds only partially healed – great wounds in the epidermis of soil with which Nature protects the underlying rock. … The region is unique: let the observer take the wings of the morning to the uttermost parts of the earth: he will nowhere find its likeness"

J Harlen Bretz (1928)

2.1 Ice-dammed lakes

Ice-dammed lakes occur where drainage systems are interrupted by glaciers (Tweed & Russell 1999). Glacial lakes are classified according to their damming mechanism and their position on the terrain (Tweed & Russell 1999; Clague & Evans 2000; Roberts et al. 2005) (Figure 2-1,

Table 2-1). To ensure relevance and brevity, this review will focus on subaerial ice-marginal and proglacial lakes.

2.1.1 Lake types

Ice-dammed lakes are "substantial bodies of standing water" whose existence depends, to some extent, on damming by glacier ice (Blachut & Ballantyne 1976). Ice-dammed lakes form when a basin is created and meltwater is supplied. These requirements can be met when: (1) increased rates

of melt caused by topographically-reflected solar radiation fill topographic lows (Maag 1969; Blachut & Ballantyne 1976), (2) advancing ice cuts off a valley, (3) a tributary glacier retreats from a trunk glacier, or (4) a trunk glacier retreats/backwastes from its terminal or recessional moraine (Tweed & Russell 1999). Ice-dammed lakes are primarily classified by their position on the local terrain and their position relative to the damming glacier (Hutchinson 1957; Maag 1969). Other considerations of ice-dammed lake categorization include the type of damming glacier and the potential drainage style (Blachut & Ballantyne 1976; Costa & Schuster 1988; Tweed & Russell 1999). Costa and Schuster (1988) have documented nine types of ice-dammed lakes (Figure 2-1;

Table 2-1). A combination of geomorphic, sedimentologic and stratigraphic observations are used to differentiate ice-dammed paleolake types (e.g., Eyles & Clague 1991; Knight et al. 2000; Johnsen & Brennand 2006).

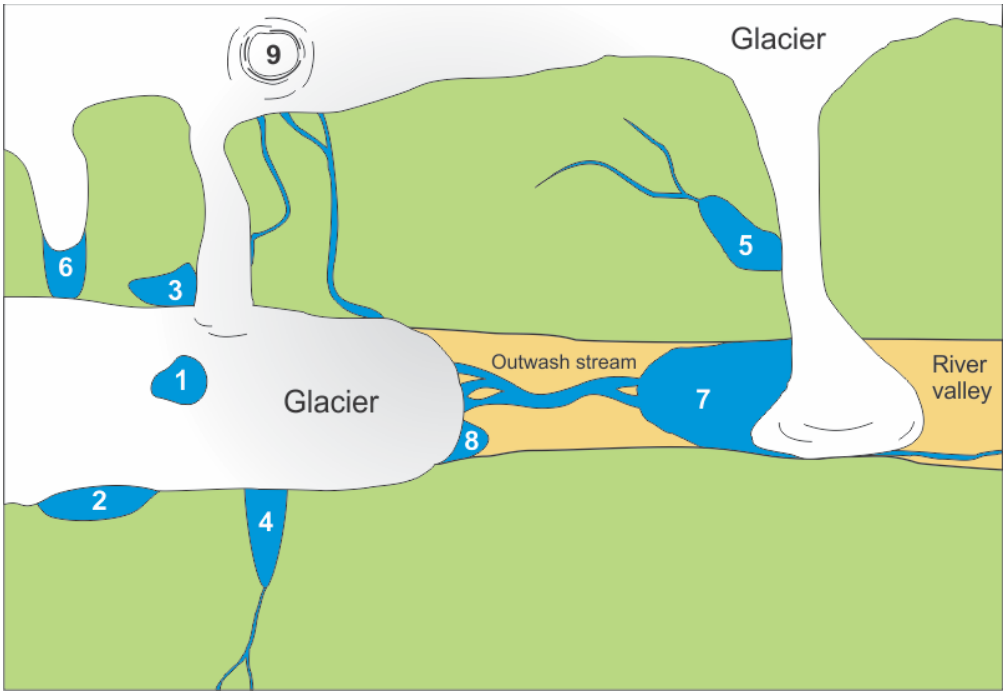

Figure 2-1: Ice-dammed lake (blue) types numbers refer to lake types listed in

Table 2-1: Ice-dammed lake types (adapted from Costa and Schuster 1988).

Number[1]	**Lake type**	**Description (example and references)**
1	Supraglacial[2]	Occupy depressions on a glaciers surface (Bjornsson 1976; Luthje et al. 2006)
2	Ice-marginal[2]	Occupy depressions between ice margin and valley wall (Sugden 1985; Knight et al. 2000)
3	Converging ice ponded	Formed where local drainage is disrupted by the confluence of two glaciers (Maag 1969; Costa & Schuster 1988)
4	Trunk glacier-valley ponded[2]	Formed where a tributary stream is impounded by a trunk glacier (Clark & Waldron 1984)
5	Tributary glacier-valley ponded[2]	Formed where a tributary stream is impounded behind a tributary glacier (Nichols & Miller 1952; Costa & Schuster 1988).
6	Interglacier[2]	Occupy the basin between a tributary and trunk glacier; relatively common in BC and Alaska; requires two ice dams (Marcus 1960).
7	Tributary glacier-dammed[2]	Formed in trunk valleys behind tributary glaciers (Gunn 1930; Costa & Schuster 1988)
8	Proglacial	Formed in contact with the front of advancing or retreating glaciers or ice sheets; can be extremely large; (not all ice-contact proglacial lakes are necessarily ice-dammed) (Pardee 1910; Atwater 1987; Teller et al. 2002)
9	Subglacial or englacial[2]	Formed in subglacial or englacial settings with adequate water supply and ice-substrate interactions conducive to storage; effects ice dynamics (Bjornsson 2002; Pattyn et al. 2004; Siegert et al. 2005; Lesemann & Brennand 2009)

[1] Numbers refer to those in Figure 2-1.

[2] High jökulhlaup potential.

2.1.2 Dam failures

Ice dams impounding subaerial lakes can fail by five general mechanisms: (1) hydrostatic ice-dam flotation (e.g., Thorarinsson 1939; Nye 1976; Clarke 1982), (2) viscoplastic deformation (Glen mechanism) (Glen 1954), (3) hydrofracture (e.g., Fowler 1999; Anderson et al. 2003), (4) Darcian basal flow (Walder & Fowler 1994; Fowler 1999), and (5) thermomechanical erosion through supraglacial overspill (Roberts 2005). Ice creep can reclose ice dams after a breach (Glen 1955; Nye 1976). Thus, ice-dammed lakes are prone to a recurrent cycle of filling and draining (e.g., Clarke et al. 1984; Waitt 1985).

Thorarinsson (1939) proposed a simple theory for ice-dam flotation employing the $9/10^{ths}$ density ratio of clean, freshwater ice to water. Advancements have since refined the theory of ice-dam flotation (e.g., Fowler 1999). Ice dam flotation occurs when the downward pressure of the cryostatic stress is overcome by the pressure of the hydrostatic stress (i.e. the water pressure head) causing a loss of the basal seal (Nye 1976; Clarke 1982; Fowler 1999). When subglacial water flow is initiated, frictional heat enlargement allows lake drainage to continue despite the requisite loss of hydrostatic pressure (Nye 1976; Clarke 1982). Lake drainage ends when hydrostatic pressure decreases sufficiently to allow ice creep to reform the basal seal (Nye 1976). Walder and Fowler (1994) describe a theory of subglacial meltwater drainage that evolves from darcian flow through the till to sheet flows at the ice/till interface as discharge increases (and thus pore-water pressure increases). Because sheet flow is unstable, flow bifurcation and channelization at the ice/till interface ensues

(Walder & Fowler 1994). These channels can remain stable with sufficient discharge to remove inwardly creeping till and can effectively drain subglacial lakes (Walder & Fowler 1994).

Lake drainage via the Glen mechanism occurs when hydrostatic stress exceeds the confining strength of the ice dam (Glen 1954; Roberts 2005). Glen (1954) proposed that an uneven distribution of hydrostatic stress applied to the ice dam can lead to focused strain and higher local rates of flow. This allows the horizontal stress from hydrostatic pressure to surpass the vertical compressive stress generated by the weight of the overlying ice (Glen 1954). Although deformation of an ice dam may occur from the viscoplastic deformation described by Glen (1954), complete failure of the dam is unrealistic (Fowler 1999). It is more likely that, as the lake reaches levels of hydrostatic pressure sufficient to induce viscoplastic deformation, the lake will fail via hydraulic fracturing (hydrofracture) causing lateral channel enlargement at the ice bed (Fowler 1999; Anderson et al. 2003).

Glacial lake drainage via overspill is common when glacial lakes form at the margins of cold-based glaciers (Costa & Schuster 1988; Tweed & Russell 1999). Supraglacial lakes drain through thermodynamic spillway erosion when spillway melt is faster than lake level lowering (Raymond & Nolan 2000). Warm lake water and large lake volume contribute to the likelihood of rapid supraglacial drainage (Raymond & Nolan 2000).

2.2 Megafloods and deglaciation

The term ‘megaflood’ is employed to describe high-energy, high-discharge, subaerial or subglacial flood events that have long recurrence intervals and irreversibly modify the landscape (Carling et al. 2009a). Typically, a flood is deemed deserving of the “mega” prefix when its discharge approaches or exceeds a sverdrup (10^6 m^3/s) (Baker 2002, 2009a; Carling et al. 2009a). Megafloods result from a multitude of causes and play an important role in surface morphology and climate change on Earth and Mars (Baker 2009a).

The signatures of megafloods are left behind as erosional (remnant) and depositional (constructional) landforms (e.g., Bretz 1923, 1925, 1928, 1969; Baker 1978a, 1978c, 2009b; Waitt 1980, 1985; Carrivick et al. 2004; Carling et al. 2009c). The massive deposits and erosional forms generated by megafloods are best described by the non-genetic term ‘landform’ rather than the standard moniker for fluvial deposits ‘bedform’ because the spatial implications of bedform are inadequate for megaflood morphology (Carling et al. 2009a). Some typical erosional megaflood landforms include: crescentic scours (obstacle marks), streamlined (residual) hills, plunge pools, overfit stream channels and cataracts (e.g., Bretz 1923, 1925; Baker 1978a; Carling et al. 2009c; Waitt et al. 2009). In many cases, megaflood depositional landforms are preserved by rapid waning of flow and a general resistance to mundane erosion owing to their unusual scale (Bretz 1925; Carling et al 2009a). Common depositional landforms consist of large-scale bars, dunes, antidunes, and slackwater deposits (e.g., Bretz 1923, 1925; Baker 1978a, 2009b; Waitt 1980, 1984, 1985; Carling et al. 2009a).

Paleohydraulics of some megafloods have been reconstructed by numerical modelling and geologic evidence (e.g., Baker 1978b; Baker & Bunker 1985; Waitt 1985; Benito & O'Connor 2003; Alho et al. 2010; Denlinger & O'Connell 2010). Most terrestrial megafloods are caused by glacier and ice sheet interruptions to stream flow patterns (e.g., Bretz 1923, 1925, 1928; Bretz et al. 1956; Waitt 1980, 1984, 1985; Clarke et al. 1984; Shaw et al. 1999; Kovanen & Slaymaker 2004; Baker 2008, 2009a; Hanson et al. 2011). Terrestrial megaflood reconstructions usually reveal maximum discharges of <10 sverdrups (Baker 1978; Clarke et al. 1984; O'Connor & Baker 1992; Benito & O'Connor 2003; Denlinger & O'Connell 2010). However, some reconstructed megafloods in the Altai Mountains, Siberia have discharges of ~10 sverdrups (Baker et al. 1993; Carling et al. 2009b) and the largest terrestrial megafloods (that carved the Channeled Scablands, WA) had maximum discharges of ~17-25 sverdrups (O'Connor & Baker 1992; Alho et al. 2010; Denlinger & O'Connell 2010).

2.2.1 The Channeled Scabland

The CS is a palimpsest landscape comprised of erosional and depositional megaflood landforms that extends from central Idaho to the Pacific Ocean, covering much of eastern Washington State (Figure 1-1). The terrain of the CS results from numerous megafloods across the Columbia Plateau from glacial lakes, which were impounded by the CIS (Waitt 1980; Benito & O'Connor 2003). These megafloods occurred over multiple glaciations (Waitt, 1980, 1985; Clark et al., 1984; Baker and Bunker, 1985; Atwater, 1987; Benito and O'Connor, 2003; Clague et al., 2003; Smith 2006b; Baker, 2009). Plucked basalt stripped of

its loess and soil overburden, and coulees (huge, dry, steep-walled channels) are characteristic of the CS (e.g., Bretz, 1969; Baker, 2008b; Waitt et al., 2009). The structural characteristics of the underlying Yakima Basalt governs the formation of some of the erosional CS landforms. Other common features of the CS include rounded loess hills, cataracts, boulder bars and erratics (Bretz 1928; Baker, 1978a, 2009b).

The primary source of floodwater for the CS was glacial Lake Missoula (gLM) (Bretz et al. 1956; Bretz 1969; Clark 1984; Baker & Bunker 1985; Figure 1-1). This lake was impounded in the drainage system of the Clark Fork River in the Bitterroot Mountains of ID and MT by the Purcell Lobe of the CIS (Pardee 1910, 1942; Bretz 1969; Figure 1-1). At maximum stage it is estimated to have contained 2,600 km^3 of water (Smith 2006; Alho et al. 2010), and to have been >600 m deep against its dam (the Purcell Lobe) (Pardee 1942; Bretz et al. 1956; Bretz 1969). Glacial Lake Columbia (Figure 1-1) and Lake Bonneville (to the south) also sent floodwaters down the Snake and Columbia river valleys (Oviatt et al. 1992; Atwater 1987; Baker 2008a; Waitt et al. 2009).

Estimates of flood magnitudes through the CS vary depending on the source waters and the method of paleoflood calculation. GLM floods have been reconstructed using one-dimensional (1-D) (step-backwater) and two-dimensional (2-D) numerical modeling techniques (Clark 1984; O'Connor & Baker 1992; O'Connor et al. 1995; Benito & O'Connor 2003; Miyamoto et al. 2007; Alho et al. 2010; Denlinger & O'Connell 2010). Peak floodwater discharge estimates at the point of dam failure are ~20 x 10^6 m^3/s from 1-D calculations

(Baker 1973; O'Connor & Baker 1992), and ~17 x 10^6 m^3/s from 2-D models (Alho et al. 2010). Peak floodwater discharge estimates by 2-D methods from within the Columbia Gorge are ~6 x 10^6 m^3/s (Denlinger & O'Connell 2010).

Although the aforementioned discharge estimates through the CS are many orders of magnitude higher than the likely floods through the KRv, they provide an example of the maximum erosive force of megafloods. In the CS, discharges of ~2.6 x 10^6 m^3/s (Alho et al. 2010) have carved channels into basalt (Baker 1978b). Many of the channels terminate at cataracts, indicating headward knickpoint propagation (Bretz 1928; Baker 1978b). The turbulent floodwaters from gLM jökulhlaups produced vertical hydraulic vortices termed "kolks" (Matthes 1947; Baker 1978b; Figure 2-2). These kolks were capable of producing hydraulic lift sufficient to pluck large basalt boulders out of the stream bed and into the flow of the floodwater (Figure 2-2). The well-jointed Yakima basalt of the Columbia Plateau is particularly suited to hydraulic erosion via plucking, the majority of which occurred on tension-jointed anticlinal crests (Baker 1978b). The structural characteristics of the basalt are controlled by differential rates of cooling (Swanson 1967; Baker 1978b) and form a plucking-resistant entablature that overlies readily plucked columnar basalt (Baker 1978b; Figure 2-3). Areas of basalt that experienced rapid cooling developed hackly columns (fractures) in the entablature, which causes the entablature to be receptive to plucking (Mackin 1961; Swanson 1967; Baker 1978b; Figure 2-3). The interaction between the deep, fast and turbulent Missoula floodwaters and

the easily plucked basalt is the reason for the large amounts of incision in the CS.

Estimates on the number of CS floods during the late Wisconsin vary greatly. Evidence of subaerial exposure (optical dating, eolian sediment, Mount St Helens set-S tephra, bioturbation assemblages and animal bones on top of slackwater rhythmites) between flood events and a correlation of regional slackwater rhythmites show as many as 89 catastrophic gLM floods swept through the CS in the late Wisconsin, with an average recurrence interval of ~20-35 years (Waitt 1980, 1984, 1985; Atwater 1987; Hanson et al. 2012). Further evidence for multiple draining's (at least 29) of gLM comes from optically dating gLM varves (Hanson et al. 2012). In counterpoint, other researchers have suggested that most rhythmic deposits are likely the result of pulses within the flow of a single flood (Baker & Bunker 1985; Shaw et al. 1999).

Optical and radiocarbon dating have recently established that MIS 2 gLM floods occurred from 19.6-12.6 cal. ka BP and that at least one pre-gLM flood deposit dates to >22 cal. ka BP (Zuffa et al. 2000; Hanson et al. 2012). Baker (1978c) lists sedimentologic evidence for pre-Wisconsin floods through the CS that includes loess beds capped with paleosols and saprolitic cobbles. Although not necessarily proof of a pre-gLM flood, Benito and O'Connor (2003) hypothesised from stratigraphic relationships that one large flood event pre-dated the blockage of the Columbia River valley by the Okanagan Lobe of the Cordilleran Ice Sheet. These pre-gLM flood events may record jökulhlaups during earlier glaciations.

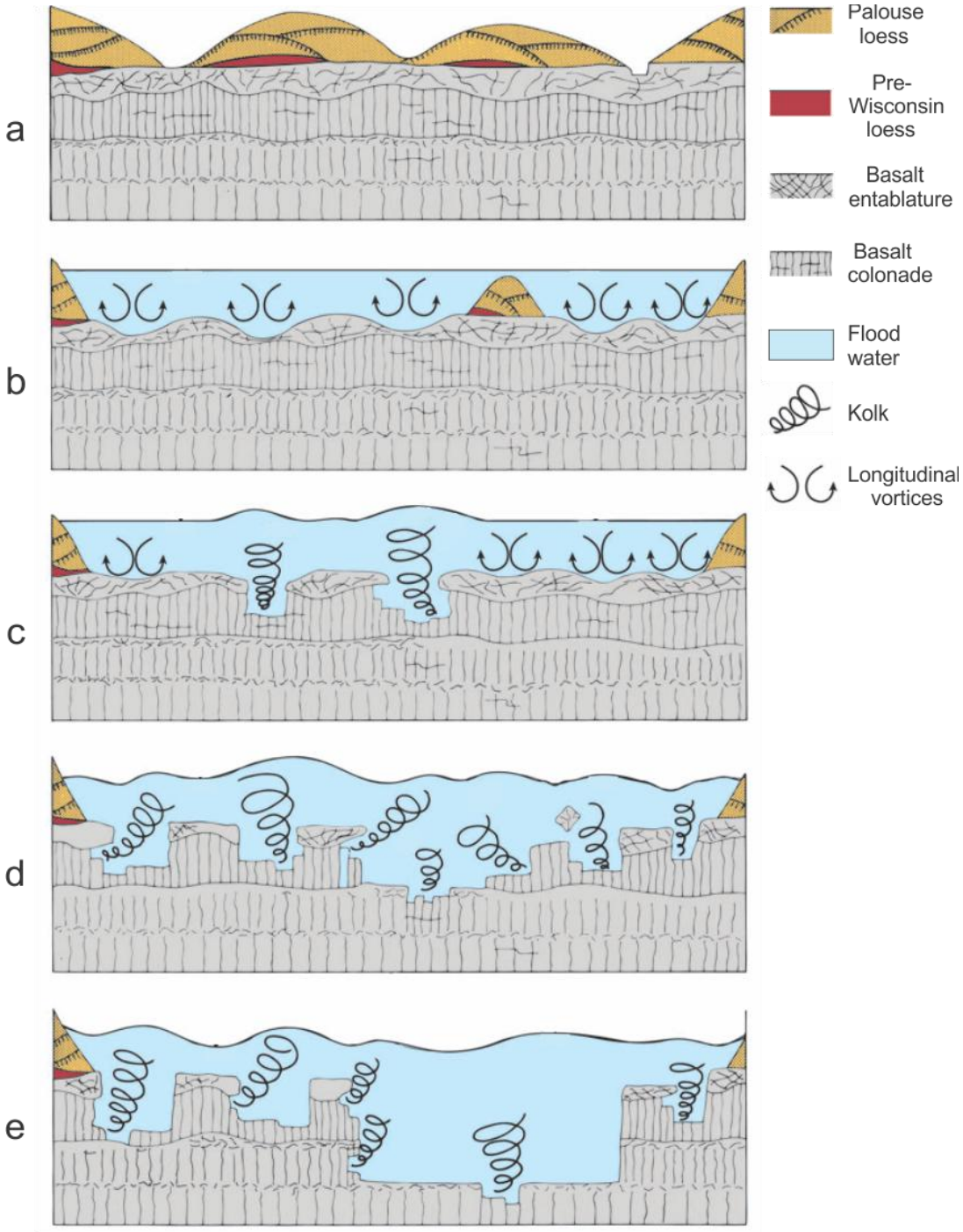

Figure 2-2: Hypothetical sequence of turbulent floodwater erosion in the Channeled Scablands, WA (modified from Baker (2008). Republished with permission of Annual Review of Earth and Planetary Sciences, from The Channeled Scabland: a retrospective, Victor R. Baker, Issue 37, 2008; permission conveyed through Copyright Clearance Center, Inc.). a) Pre-flood, loess-covered landscape shaped by dendritic stream drainage. b) Flood water is introduced; loess cap is reduced to discrete streamlined hills and basalt entablature erosion is initiated by longitudinal vortices. c) Longitudinal vortices develop grooves that expose the basalt colonnade; kolks (vertical vortices) remove colonnade. d) Erosion from kolks enlarges and merges potholes. e) Prominent channels are developed – possibly by headward knickpoint erosion.

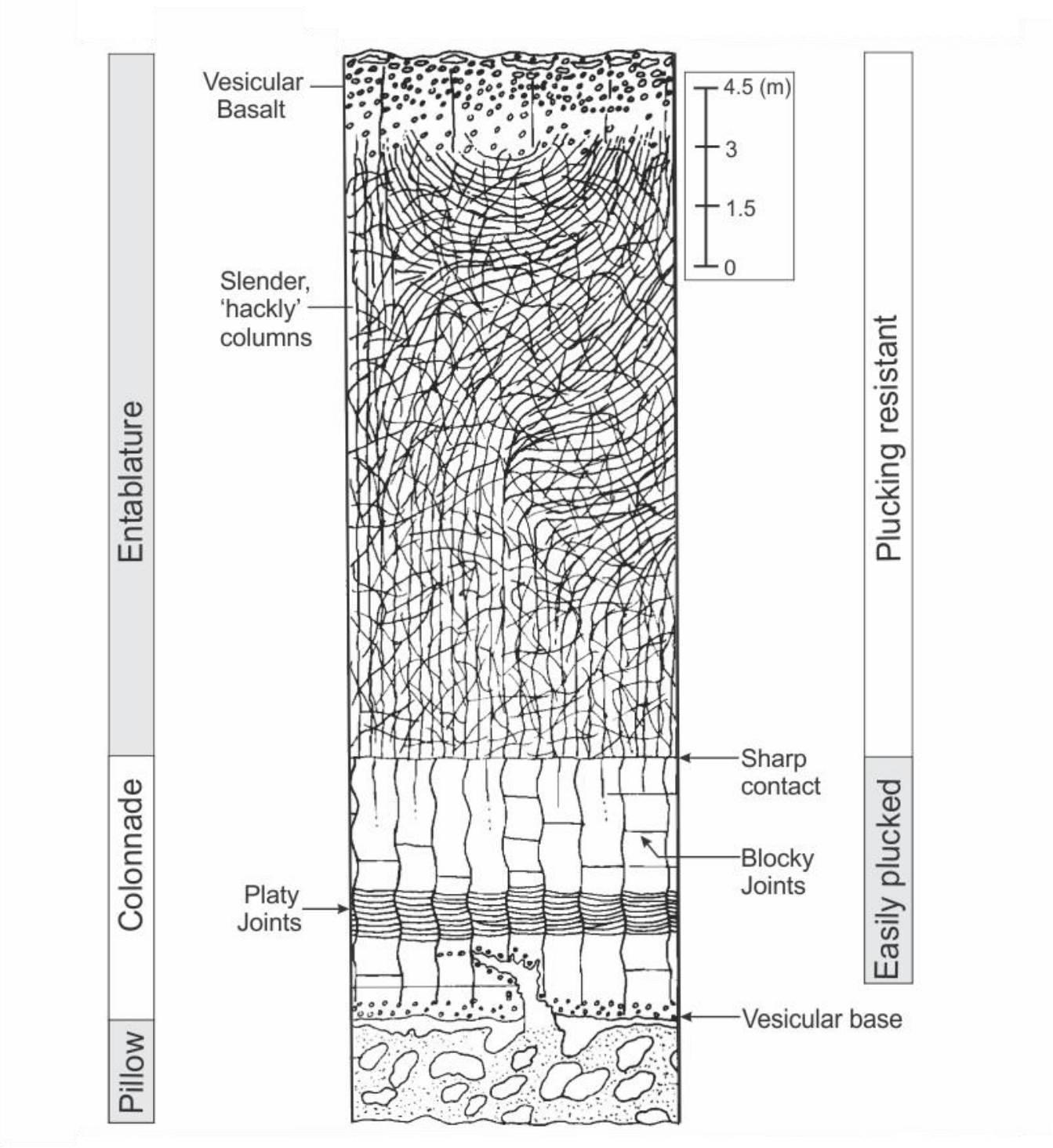

Figure 2-3: Typical characteristics of Yakima Basalt, Channeled Scablands, WA. Hackly columns form in areas of rapidly cooled basalt and detract from the resistance to plucking of the entablature (modified from Swanson (1967), republished with 'fair use' permission from the Geological Society of America).

2.3 Deglacial history of southern BC valleys

The Interior Plateau, Columbia and Rocky mountain regions of southern BC possess deep, elongate basins with features similar to coastal fjords (Eyles et al. 1990). These basins are oriented roughly parallel to regional orogenic landforms and are the result of intense glacial and fluvial erosion (e.g., Eyles et al. 1990; Vanderburgh and Roberts 1996). These deep basins contain a rich record of CIS decay at the end of the Fraser Glaciation (MIS 2).

Considerable valley fill thicknesses are common in southern BC valleys: the Okanogan Valley contains up to ~800 m of Quaternary deposits (Fulton 1965; Eyles et al 1990; Lesemann & Brennand 2009); the Thompson Valley exposes silt bluffs >150 m thick (e.g., Fulton 1965; Ryder 1971; Johnsen & Brennand 2004, 2006); and incision by the Fraser River has exposed >400 m of Late Wisconsinan sediment (Eyles & Clague 1991; Lian & Hicock 2001). Much of the thickness of the valley-fill records glacial lakes because regional ice stagnation (downwasting and backwasting) resulted in stagnant ice blocks within the valleys which impounded drainage (e.g., Fulton 1969; Eyles et al. 1990; Johnsen & Brennand 2004, 2006).

Three broad deglacial lake types have previously been recognized in southern BC: type 1 – supraglacial lakes that may have evolved into proglacial lakes through thermokarstic enlargement (e.g., Eyles et al. 1987; Ward & Rutter 2000; Burke et al 2012); type 2 – proglacial and ice-marginal lakes with significant ice contact (e.g., Fulton 1967; Shaw & Archer 1979); and type 3 –

proglacial lakes with negligible ice contact (except at the ice dam) (e.g., Johnsen & Brennand 2006).

Deglacial lacustrine deposits are pervasive throughout BC valleys and typically overlie debris flow diamictons, till or glaciofluvial sediment (Fulton 1965; Ryder 1971; Eyles & Clague 1991; Sawicki & Smith 1991; Lian & Hicock 2001; Johnsen & Brennand 2004, 2006; Lesemann & Brennand 2009). Some deglacial lakes (type 3, above) were relatively high-energy water bodies with multiple, sediment input points (tributary valleys) that resulted in the rapid deposition of lake bed sediments from hyperpycnal flows (Johnsen & Brennand 2004, 2006). Other deglacial lakes (types 1 and 2 above) were lower energy depositional environments as evidenced by rhythmic (perhaps varved) silt-clay couplets resulting from suspension settling (e.g., Shaw & Archer 1979; Eyles & Clague 1991).

Following lake drainage, or following ice decay in valleys not containing glacial lakes, valleys began to experience the combined effects of paraglacial conditions and base level change: sediment was redistributed on unstable hillslopes forming alluvial and colluvial fans in the valley bottom, floodplains aggraded and rivers incised (e.g., Ryder 1971a, 1971b; Church & Ryder 1972; Lian & Hickin 1996; Ballantyne 2002). There have been no similar studies of the deglacial record of the Purcell Trench in BC, however, the observations and interpretations from adjacent valleys suggest what might be expected in the Purcell Trench.

2.3.1 Deglacial history of the Arrow Lakes basin

The Arrow Lakes basin, ~70 km west of the Purcell Trench, is part of the Columbia River valley (Figure 2-4). Elevated “valley-wall terraces” and “kettled terraces” (above lacustrine deposits) are abundant on the valley walls of the Arrow Lakes basin (Fulton et al. 1970). These terraces are interpreted as elevated kame terraces built from glaciofluvial deposition along the margin of the downwasting CIS (Fulton et al. 1970; Fulton et al. 1984; Fulton pers. comm. 04/21/2010). They suggest stagnant ice occupied much of the Arrow Lakes basin (Fulton pers. comm. 04/21/2010).

When the CIS retreated northward across southeastern BC a glacial lake (“glacial Lake Arrow”) formed in the high-relief valleys now occupied by the Arrow Lakes (Figure 2-4) (Fulton 1970; Fulton et al. 1989; Fulton & Warner 1990). Plant remains (likely detrital) from lacustrine sediments within the Arrow Lakes basin provide ages of 9-10 ^{14}C ka BP (10.1-11.5 cal. ka BP) (Fulton et al. 1989). Whether these glacial lakes drained gradually or catastrophically is unknown. With continued glacial retreat, nonglacial lakes developed in the Arrow Lakes basin; these lakes were ~25 m higher than modern lake levels (Fulton et al. 1970; Fulton et al. 1988).

2.3.2 Deglacial history of the southern Rocky Mountain Trench

The southern Rocky Mountain Trench (RMT) is ~100 km east of the Purcell Trench, separated from it by the Columbia Mountains (the Purcell Range), and contains the headwaters of the Columbia River (Figure 2-4). During deglaciation of the RMT the northward flow of the Columbia River was blocked

by the CIS. In the southern RMT valley fill restricted drainage, which resulted in the formation of glacial Lake Invermere (gLI) (Sawicki & Smith 1991). Radiocarbon dating constrains the drainage of gLI to before ~10 ^{14}C ka BP (11.5 cal. ka BP) (Sawicki & Smith 1991). At its maximum extent gLI occupied 210 km of the RMT with an average width and depth of 2.5 km and 100 m, respectively (Sawicki & Smith 1991). The initial drainage of gLI was southward over a breach in the valley fill sediment; when the RMT ice melted the lake drained to the north. This transfer to a northern drainage route established the modern drainage route of the Columbia River (Sawicki & Smith 1991).

2.3.3 Glacial Lakes in the Purcell Trench and northwestern Montana

Previous studies have reconstructed glacial Lake Kootenai (gLK), from thick deposits of lake bed sediments (sand and silt), in valley systems in northern Idaho and northwestern Montana (Alden 1953; Johns 1970; Smith 2006a). This lake formed when the Kootenai, Yaak, and Moyie River systems (Figure 2-4) were impounded between a terminal moraine (Figure 2-4) and valley fill sediment to the south and the stagnant ice of the Purcell Lobe to the north (Alden 1953; Johns 1970; Smith 2006a).

Sediments recording glacial Lake Kootenai are over 90 m thick and record rapid deposition proximal to inflows (Alden 1953; Smith 2006a). Valley-side benches composed of lake bed sediments attributed to gLK range in elevation from 700-740 m asl in ID and from 730-762 m in MT (Alden 1953). The different lake-bench elevations result from different spillway heights.

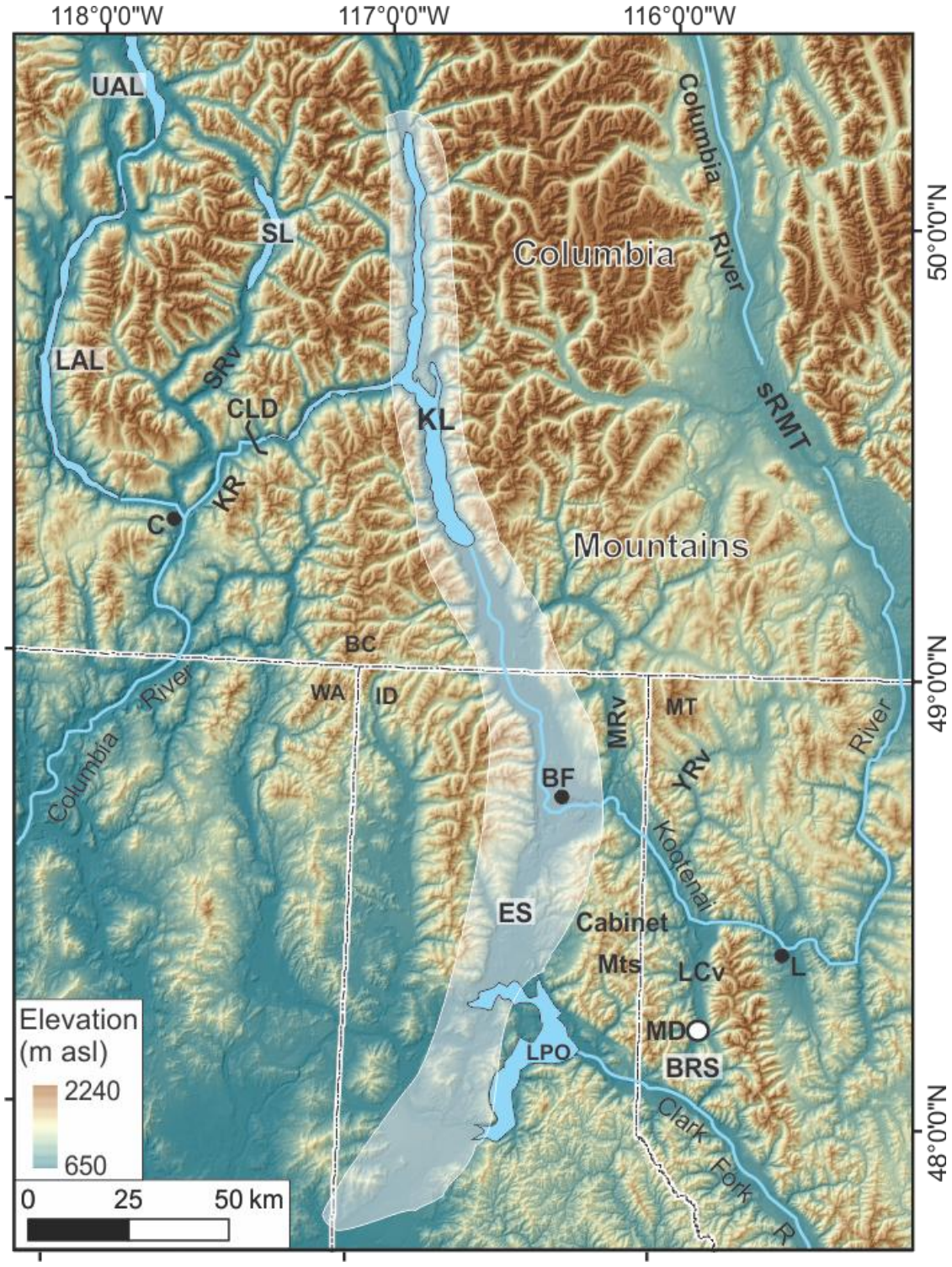

Figure 2-4: Places mentioned in the text. The Purcell Trench is highlighted white. Abbreviations: UAL = Upper Arrow Lake; SL = Slocan Lake; LAL = Lower Arrow Lake; SRv = Slocan River valley; CLD = Corra Linn Dam; KR = Kootenay River; C = Castlegar; KL = Kootenay Lake; sRMT = southern Rocky Mountain Trench; MRv = Moyie River valley; YRv = Yaak River valley; BF = Bonners Ferry; ES = Elmira spillway; LCv = Lake Creek valley; L = Libby; MD = moraine dam (that formed the Bull River spillway); BRS = Bull River spillway; LPO = Lake Pend Oreille.

The Bull River spillway in MT (Figure 2-4) was the first to be activated (Alden 1953). Activation of the Bull River spillway would have commenced following a lowering of the final stage of gLM in the Clark Fork River valley to the south of gLK (Alden 1953). The current elevation of the incised Bull River spillway is 714 m asl; the estimated pre-incision elevation of the terminal moraine at the Bull River spillway is ~732 m asl (Alden 1953). After sufficient northward retreat of the Purcell Lobe gLK occupied the southern Purcell Trench and lake level was dictated by the Elmira spillway (Figure 2-4) (Alden 1953). The geomorphology of the Elmira spillway suggests that its original height was ~710 m asl and that incision from gLK drainage is responsible for its current elevation of 655 m asl (Alden 1953).

The evolution of gLK is complex and controlled by glacial sediments (acting as earthen dams), backwasting and downwasting ice (ice dam), and high relief terrain (Alden 1953; Johns 1970; Smith 2006a). The evolution of gLK as described by Alden (1953) is summarized in Table 2-2 and Figure 2-5. While gLK occupied the Kootenai and Yaak valleys in MT, the Purcell Lobe of the CIS still occupied much of the Purcell Trench to the west and dammed the westward flow of the Kootenai River (Alden 1953) (stage 1, Table 2-2, Figure 2-5). The lake level of gLK was controlled by a moraine that forms the Lake Creek/Bull River drainage divide (Johns 1970) (Figure 2-4). Simultaneously, as the Purcell Lobe backwasted to the north an unnamed proglacial lake was formed in the southern Purcell Trench, ID; its lake level was controlled by a deposit of glacial drift that formed the Elmira spillway (Alden 1953) (stage 1, Table 2-2, Figure 2-5).

Table 2-2: Summary of gLK evolution after Alden (1953).

Stage[1]	Description	Spillway in use	~Elevation (m asl)
1	Small, discreet proglacial lakes in MT (gLK) and ID (unnamed)	Bull River and Elmira	~732 (MT) ~710 (ID)
2	GLK lowers as Bull River spillway is incised; unnamed proglacial lake in ID grows as CIS backwastes	Bull River and Elmira	≤732 (MT) ≤710 (ID)
3	CIS retreat enables gLK to jökulhlaup west into the Purcell Trench and merge with unnamed lake in ID	Elmira	≤710
4	GLK expands north as the CIS backwastes northward up the Purcell Trench	Elmira	<710
5	CIS retreat enables gLK to drain through the Kootenay River valley	Kootenay River valley	unknown

[1] A cartoon depiction of evolutionary stages (same stage numbers) is presented in Figure 2-5.

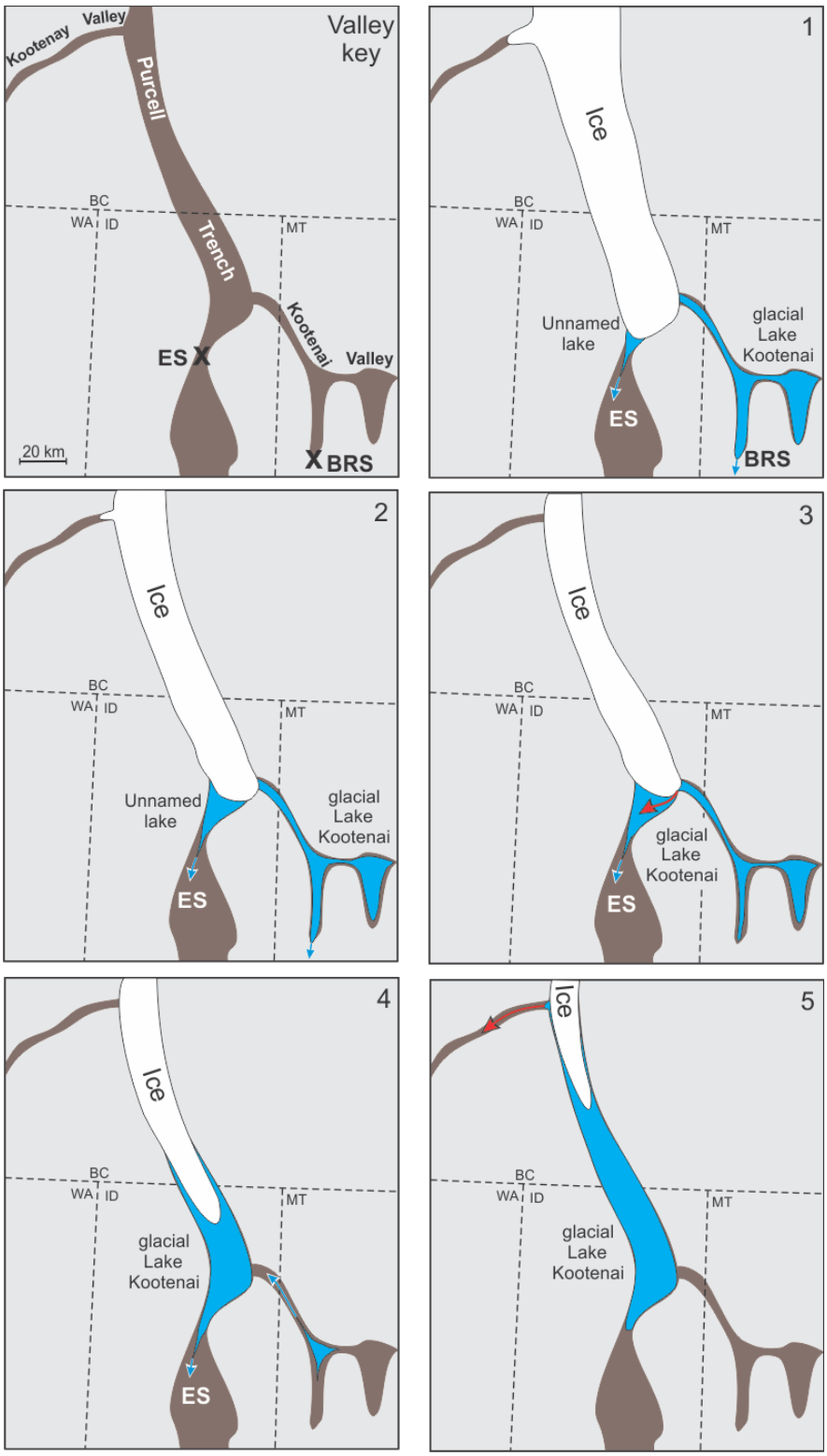

Figure 2-5: Cartoon of glacial Lake Kootenai evolution (after Alden 1953). First panel (upper left) shows valleys and spillway locations (X) (BRS = Bull River spillway, ES = Elmira spillway), remaining five panels show lake stages (stage numbers in upper right as numbered in Table 2-2). Blue arrows indicate active lake spillways. Red arrows indicate jökulhlaup routes.

The unnamed lake expanded as the Purcell Lobe backwasted, and gLK lowered as the Bull River spillway was incised (stage 2, Table 2-2, Figure 2-5). Upon sufficient northward retreat of the Purcell Lobe, much of gLK emptied into the unnamed proglacial lake in the Purcell Trench via the Kootenai River valley (Alden 1953); this resulted in what Alden (1953) described as a merger of the two lakes (stage 3, Table 2-2, Figure 2-5). The initial transferring of the MT-occupying gLK into the Purcell Trench resulted in a large fan-shaped deposit that stretches from Bonners Ferry to Lake Pend Oreille, ID (Alden 1953) (Figure 2-4). The newly established Purcell Trench-occupying gLK lowered its lake level as its spillway (Elmira spillway) was incised, and expanded north as the Purcell Lobe backwasted northward up the Purcell Trench (Alden 1953, Smith 2006a) (stage 4, Table 2-2, Figure 2-5). Southward drainage would have continued as long as the stagnant ice mass in the Purcell Trench (the Purcell Lobe) blocked northward drainage via the Kootenay River valley, BC (Alden, 1953). Alden (1953) speculated that a northern drainage route through the West Arm of Kootenay Lake was initiated gradually as the stagnant ice mass occupying Kootenay valley melted (Alden, 1953) (stage 5, Table 2-2, Figure 2-5).

Alden's lake naming conventions adopted by later authors (Johns 1970; Smith 2008), are not followed in this study. A new scheme strives for descriptive clarity and accuracy. Refer to § 3.1.1 for a detailed explanation.

Waitt et al. (2009) suggest that a glacial lake in the Purcell Trench, that he called "glacial Lake Kootenay", was a potential water source for a flood down the Columbia River valley after glacial Lakes Missoula and Columbia and Lake

Bonneville ceased to exist. Geomorphic evidence that supports the occurrence of post-Missoula late Wisconsin flood(s) in the Columbia River valley exists in the form of two relatively low level megaflood bars marked by giant current ripples near Chelan Falls, Washington (Waitt 1994). Figure 2-6 illustrates the proposed floodwater route from glacial Lake Kootenay and its timing relative to the earlier CS floods (Waitt et al., 2009). They infer the timing of the gLK drainage to be ~11.2 ^{14}C ka BP (13.1 cal. ka BP).

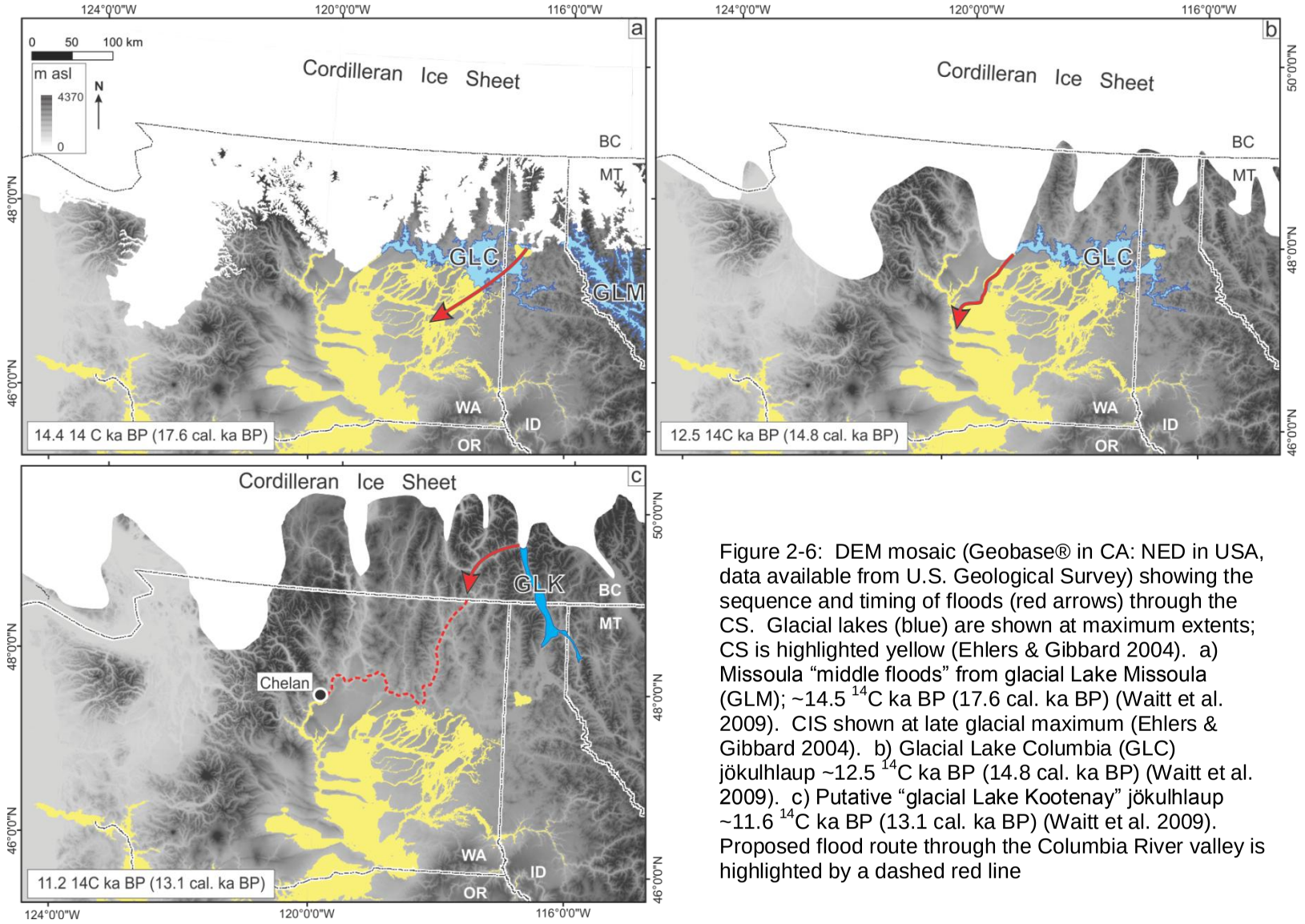

Figure 2-6: DEM mosaic (Geobase® in CA: NED in USA, data available from U.S. Geological Survey) showing the sequence and timing of floods (red arrows) through the CS. Glacial lakes (blue) are shown at maximum extents; CS is highlighted yellow (Ehlers & Gibbard 2004). a) Missoula "middle floods" from glacial Lake Missoula (GLM); ~14.5 ^{14}C ka BP (17.6 cal. ka BP) (Waitt et al. 2009). CIS shown at late glacial maximum (Ehlers & Gibbard 2004). b) Glacial Lake Columbia (GLC) jökulhlaup ~12.5 ^{14}C ka BP (14.8 cal. ka BP) (Waitt et al. 2009). c) Putative "glacial Lake Kootenay" jökulhlaup ~11.6 ^{14}C ka BP (13.1 cal. ka BP) (Waitt et al. 2009). Proposed flood route through the Columbia River valley is highlighted by a dashed red line

3: STUDY AREA

3.1 Geography

The study area explored for this research is in the west Kootenay region of the Columbia Mountains in south-eastern BC (Figure 3-1). The region is dominated by three distinct valley systems with a roughly north-south orientation. The Columbia and Slocan valleys and the Purcell Trench (listed from west to east) contain the upper and lower Arrow Lakes, Slocan Lake and Kootenay Lake, respectively (Figure 2-4). Data were gathered for this study within the roughly north-south trending Purcell Trench (PT) and its high-relief tributary valleys, and along the Kootenay River valley (Figure 3-1). The study area covers ~4500 km^2.

The Purcell Trench extends from ~40 km south of Lake Pend Oreille, Idaho into the Kootenay Lake basin, BC (Figure 2-4) and separates the Selkirk and Purcell mountain ranges (Figure 3-1). Much of the floor of the Purcell Trench in Canada is occupied by Kootenay Lake, which is a ribbon-shaped lake >100 km long with an average width of ~6.5 km. Its water surface elevation of ~532 m asl (Kyle 1938; International Kootenay Lake Board of Control 2003) is controlled by the Corra Linn Dam in the KRv, just west of the town of Nelson, BC (Kyle 1938) (Figure 3-4). The Corra Linn Dam is mandated to add no more than 6 feet (1.83 m) to the original surface of Kootenay Lake at the time of its

construction (which was ~530 m asl) (Davis 1920; Kyle 1938). Numerous rivers, streams and creeks flow into Kootenay Lake. The largest of these are the Kootenai, Kaslo and Duncan Rivers (Figure 3-2, Figure 3-3). Duncan River is controlled by the Duncan Dam (the first dam constructed to satisfy the Columbia River Treaty of 1961, Kyle 1938) and drains Duncan Lake, which is situated north of Kootenay Lake in the Purcell Trench (Figure 3-3).

Kootenay Lake marks the change in spelling from the Kootenai River to the Kootenay River; the lake is essentially a stagnation point in the flow of the Kootenai/y River along its circuitous route from the Rocky Mountain Trench, BC around the southern margin of the Purcell Mountains (Figure 2-4). A terminal moraine from the CIS near Libby, Montana (Figure 2-4) diverts the river to the west toward Idaho (ID) where it follows the Hope Fault (§ 3.2), taking advantage of the weakness through the Cabinet Mountains (Figure 2-4). In ID, the Kootenai flows north through the Purcell Trench to Kootenay Lake, just north of Creston, BC (Figure 3-2). Kootenay Lake drains out of its West Arm via the Kootenay River (Figure 3-2, Figure 3-4), which is the first major tributary of the Columbia River; in this study, the West Arm and the Kootenay River are jointly referred to as the “Kootenay River valley” (KRv).

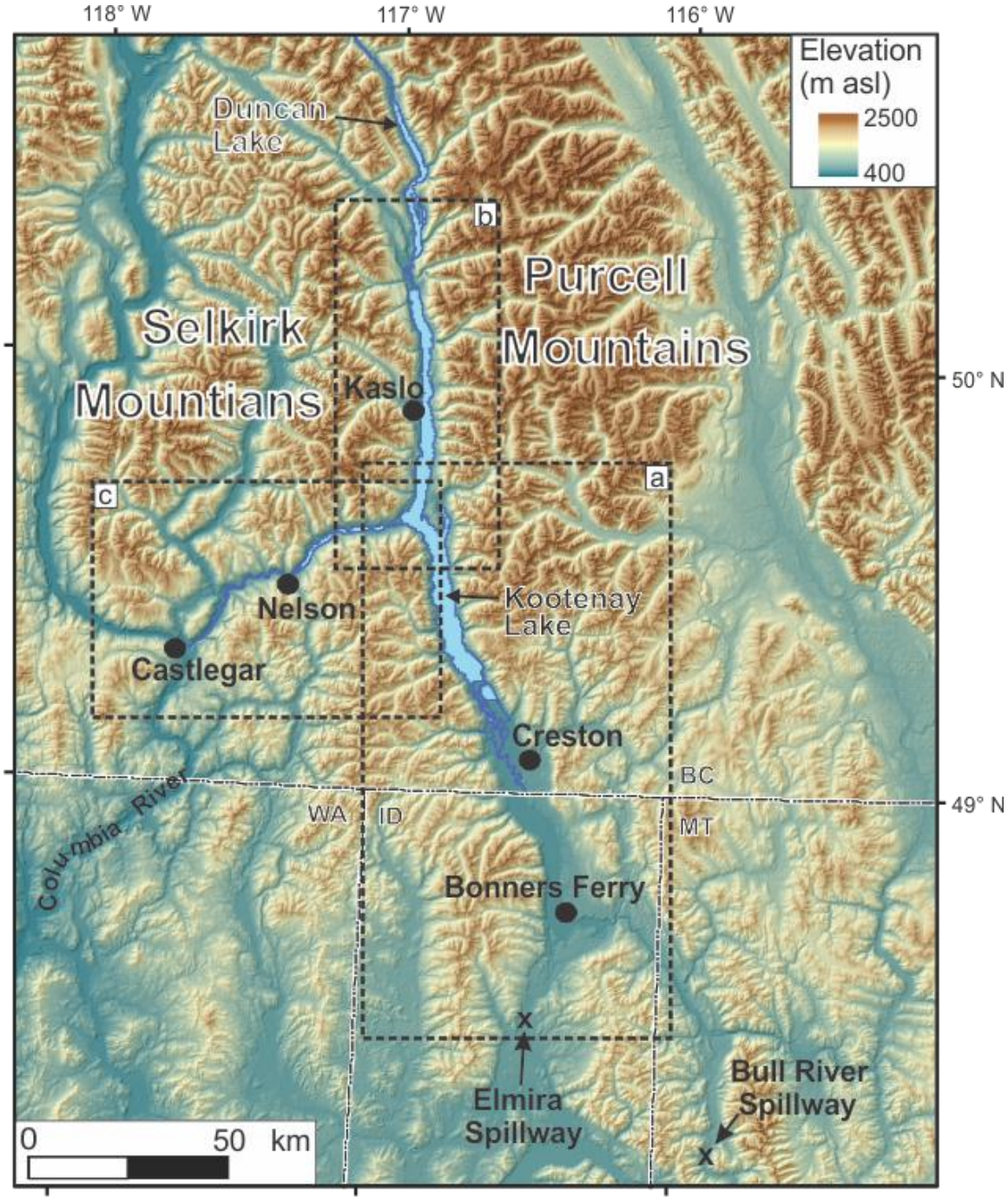

Figure 3-1: Hillshaded DEM (Geobase®) of the study area. The Purcell Trench extends roughly the entire length of the DEM and contains Kootenay and Duncan Lakes. The spillways (Elmira and Bull River) of glacial Lakes Kootenai and Purcell (see § 3.1.1) are labeled. Box a outlines the southern study area shown in Figure 3-2; box b outlines the northern study area shown in Figure 3-3; box c outlines the western study area (along the Kootenay River valley) shown in Figure 3-4.

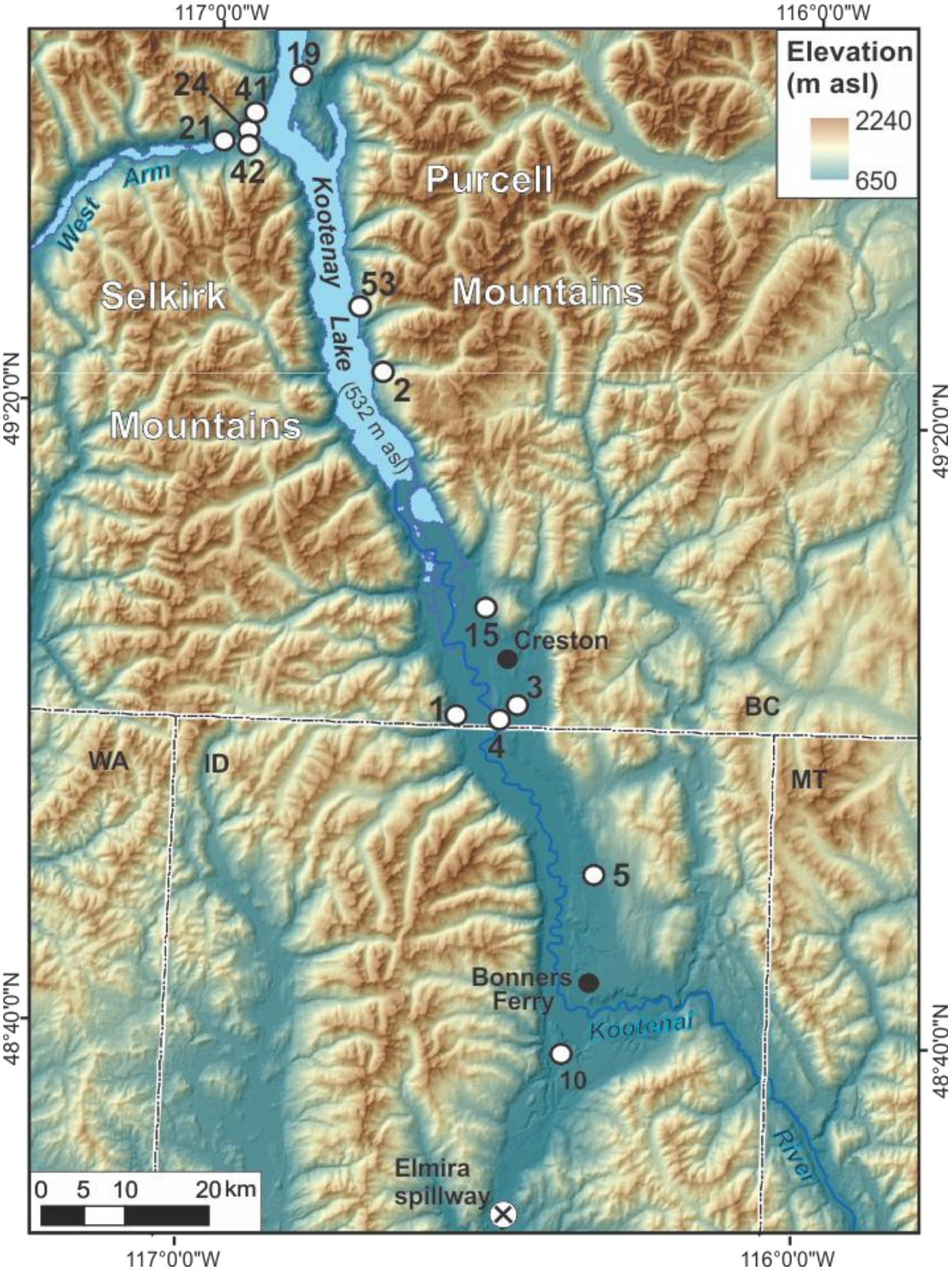

Figure 3-2: Hillshaded DEM (Geobase®) of the southern study area showing field site locations described in this thesis as numbered white dots. The Kootenai River flows northward into Kootenay Lake.

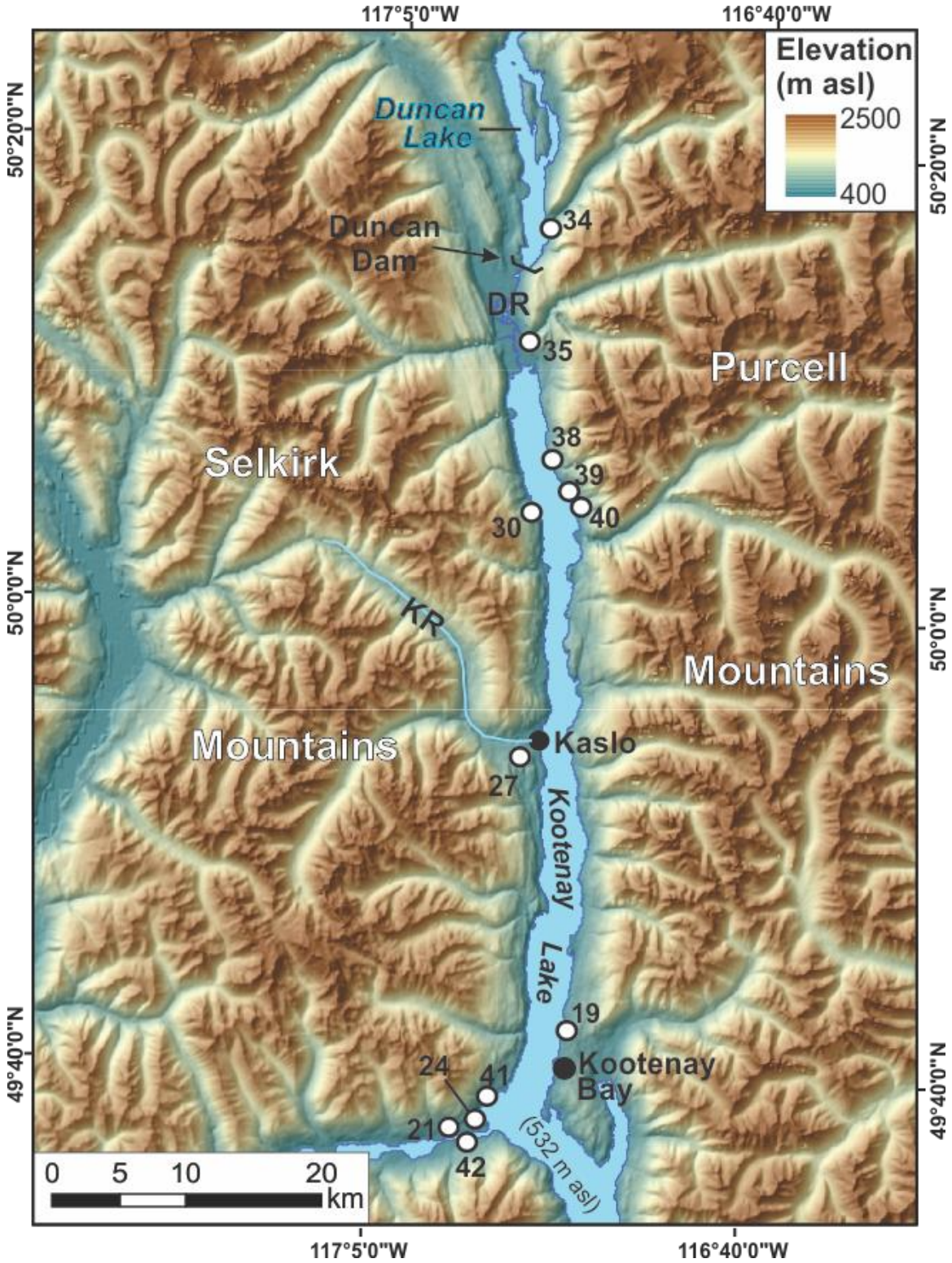

Figure 3-3: Hillshaded DEM (Geobase®) of the northern study area showing field site locations described in this thesis as numbered white dots. KR = Kaslo River; DR = Duncan River.

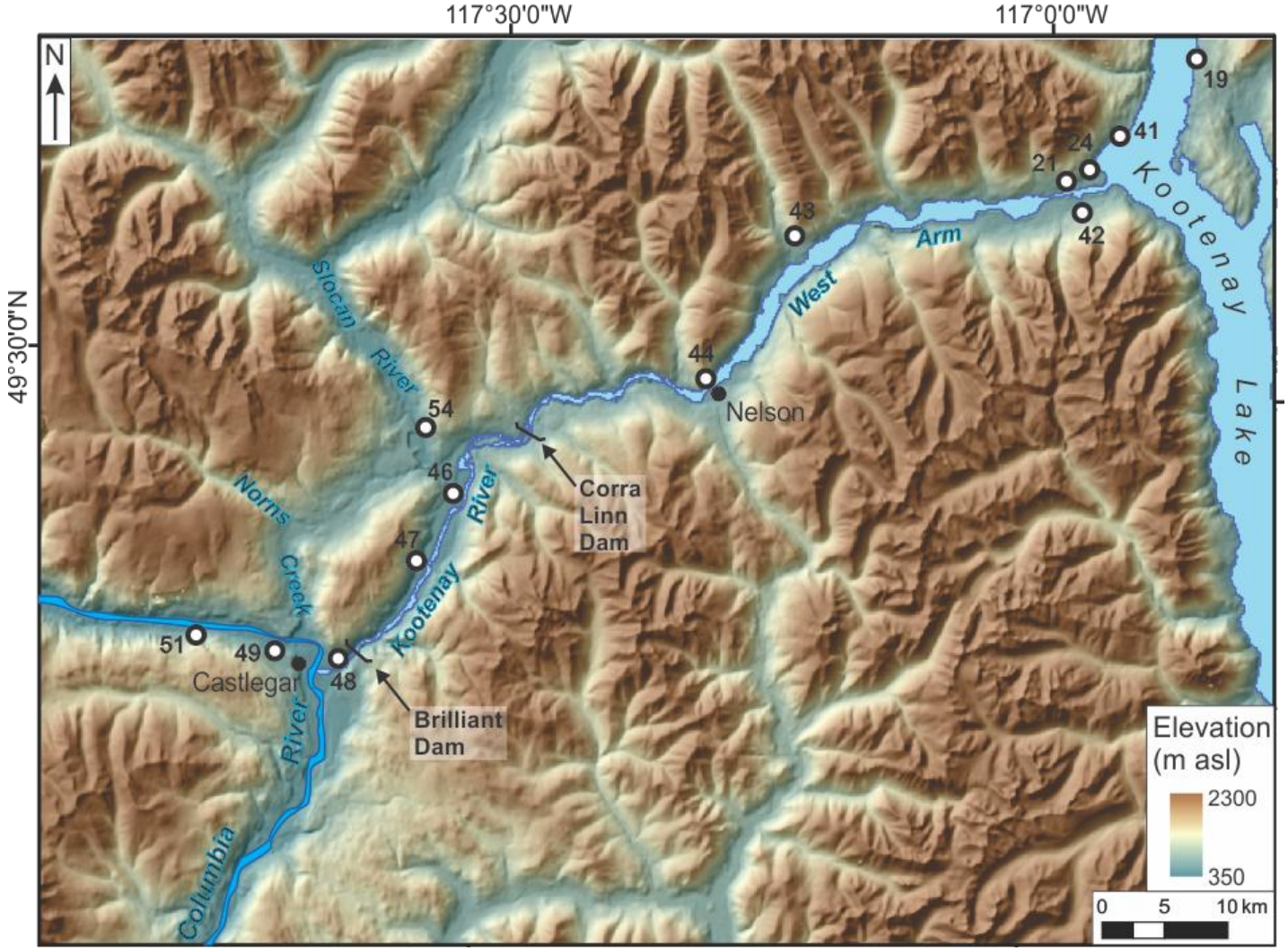

Figure 3-4: Hillshaded DEM (Geobase®) of the western study area showing field site locations described in this thesis as numbered white dots. Corra Linn Dam separates the west Arm of Kootenay Lake from the Kootenay River.

3.1.1 Lake naming conventions used in this thesis

The naming conventions used by Alden (1953; Figure 2-5) and adopted by Johns (1970) and Smith (2008) are not embraced in this study. Instead, a more descriptive and geographically accurate naming system is employed that distinguishes discrete, possibly contemporaneous, lakes that occupied separate basins (Table 3-1, Figure 3-5). This new naming scheme retains Alden's glacial Lake Kootenai in ID and MT, but names the unnamed lake and its northern expansion in the Purcell Trench, glacial Lake Purcell.

Henceforth in this thesis glacial Lake Kootenai (gLK) describes the glacial lake, identified by Alden (1953), that occupied the Lake Creek, Libby Creek and Kootenai River valleys of MT (Figure 2-4, Figure 3-5). This lake existed while the westward flow of the Kootenai River into the Purcell Trench was blocked by the Purcell Lobe of the CIS (stages 1-4, Table 3-1, Figure 3-5). Lake levels (Table 3-1) in gLK were governed by the Bull River spillway (into the Clark Fork River) (Figure 2-4) and, briefly by drainage into the Purcell Trench around the margin of the retreating CIS (stages 1-4, Table 3-1, Figure 3-5).

Glacial Lake Purcell (gLP) refers to the glacial lake in the Purcell Trench. It existed when the northward drainage of the Kootenai River was blocked by the Purcell Lobe of the CIS (stages 1-5, Table 3-1, Figure 3-5). Lake levels in gLP were controlled by the Elmira Spillway (into the Clark Fork River, Figure 2-4) and, briefly by drainage into the Kootenay River past a northern ice dam (stage 5, Table 3-1, Figure 3-5).

Table 3-1: Summary of gLK and gLP evolution used in this study (modified from Alden 1953).

Stage[1]	**Description**	**Spillway in use**	**~Elevation gLK**[2] (m asl)	**~Elevation gLP**[2] (m asl)	**Timing (~^{14}C ka BP)**[3]
1	Small, discreet proglacial lakes in MT (gLK) and ID (gLP)	Bull River and Elmira	~732	~710	13.5-12.5
2	gLK lowers as Bull River spillway is incised; gLP grows as CIS backwastes	Bull River and Elmira	≤732	≤710	13-12
3	CIS retreat enables gLK to jökulhlaup west into gLP	Elmira	≤710	≤710	13-12
4	gLK dwindles as it drains via the Kootenai River; gLP expands north as the CIS backwastes northward up the Purcell Trench	Elmira	<710	<710	12.5-11.5
5	CIS retreat enables gLP to drain through the Kootenay River valley	Kootenay River valley	na	unknown	12-11

[1] A cartoon depicting evolutionary stages (using same stage numbers) is presented in Figure 3-5.

[2] Spillway elevations from Alden (1953).

[3] Chronology estimated from Easterbrook (1992), Carrara et al. (1996), Clague & James (2002), Dyke et al. (2003) and Waitt et al. (2009).

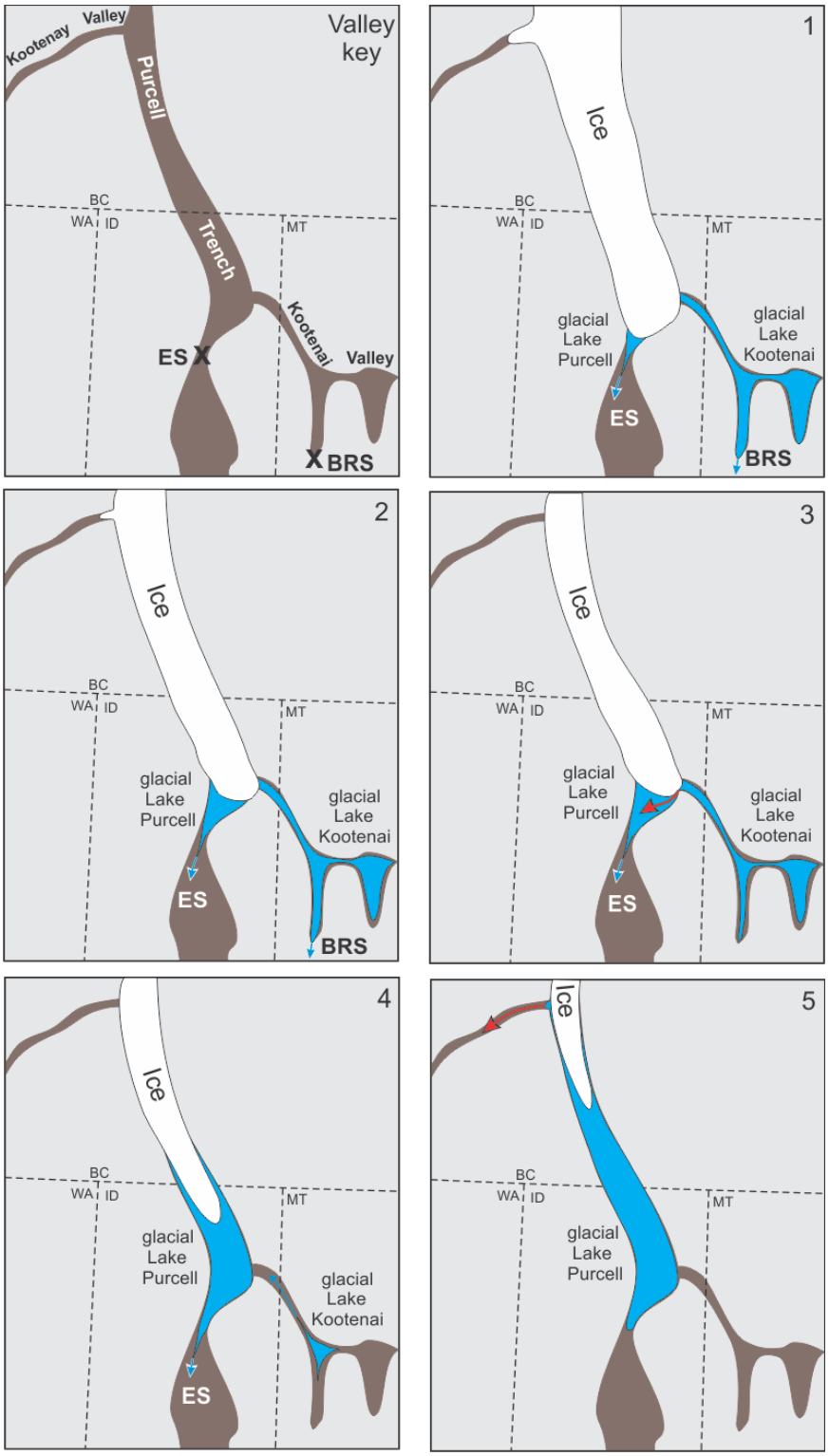

Figure 3-5: Cartoon of glacial Lakes Kootenai and Purcell showing evolutionary stages used in this thesis (modified from Alden 1953). First panel (upper left) shows valleys and spillway locations (X) (BRS = Bull River spillway, ES = Elmira spillway), remaining five panels show evolutionary stages (stage numbers are in upper right of each panel and refer to stages numbered in Table 3-1). Blue arrows indicate active lake spillways. Red arrows indicate jökulhlaup routes.

3.2 Geology

The terrane of the study area consists of intrusive igneous plutons (with varying degrees of metamorphism): the Lardeau Group (of the Kootenay terrane), and the Windermere and Purcell Supergroups (of the North American Miogeocline) (Figure 3-6). These groups and supergroups are situated within the Kootenay Arc of the Canadian Cordillera near the suture of the North American and Intermontane superterranes (Fyles 1964; Colpron & Price 1995; Paradis 2007) (Figure 3-6). In places, the metamorphic and granitic bedrock is capped by sedimentary rocks (Doughty & Price 2007).

The Kootenay Arc is deformed bedrock that extends from ~100 km south of Sandpoint, Idaho to ~400 km north of Revelstoke, BC (Fyles 1964; Paradis 2007; Figure 3-6). The arc delineates the structural divergence between the Purcell Anticlinorium (characterized by upright folds) and accreted Permian and Jurassic rocks of the Eagle Bay Assemblage (Colpron & Price 1995; Paradis 2007; Figure 3-6).

The bedrock is heavily faulted. Two of the largest faults in the region, the Northern and Southern Purcell Trench faults, have undergone preferential erosion by rivers and glaciers to form the basin of the Purcell Trench (Doughty & Price 2007). Approximately 15 km of terrane with no obvious faulting separates the two faults (Figure 3 6). These two normal faults dip steeply to the east (Figure 3-6) with several lower-angle detachment faults (Doughty & Price 2000). Mineral assemblage mapping indicates that no significant post-metamorphic faulting occurred between the two Purcell Trench faults (Doughty & Price 2000).

The Southern Purcell Trench Fault has a large amount of offset resulting in the juxtaposition of metamorphosed plutonic rock against the argillaceous rocks of the Purcell Supergroup (Doughty & Price 2000; Figure 3-6).

Considerable cross-valley variation in terrane (at a scale not identifiable in Figure 3-6) exists in the Purcell Trench. The western side of the Purcell Trench is generally characterised by mafic plutons of Mesoproterozoic age, and near the tops of gabbro sills quartz diorite and biotite granophyre are common (Burmester et al. 2010). Central and eastern parts of the Purcell Trench consist of argillaceous rocks of the Purcell Supergroup (Doughty & Price 2000; Burmester et al. 2010). Metamorphic rocks (quartzite, gneiss, amphibolite, schist and mylonite) are abundant throughout the study area (Doughty & Price 2000; Burmester et al. 2010). KRv bedrock generally consists of Mesoproterozoic plutons that have undergone varying amounts of metamorphosis.

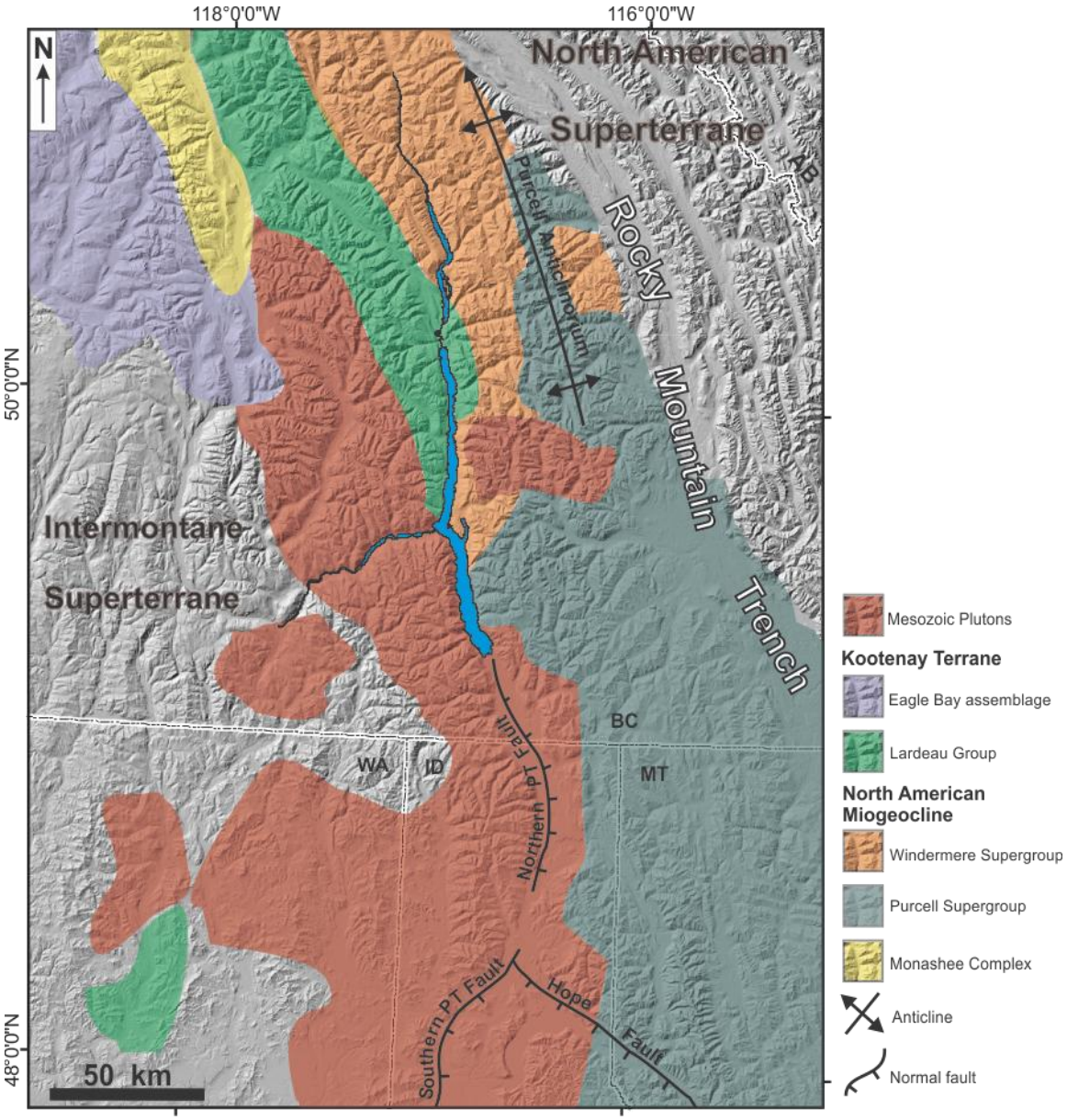

Figure 3-6: Generalized geologic map of the Kootenay Arc (coloured terrane) and surrounding terranes (modified from Archibald et al. 1983; Colpron & Price 1995; Doughty & Price). Kootenay and Duncan Lakes (blue, Figure 3-3) occupy the northern Purcell Trench.

4: METHODOLOGY

"The method of science, as stodgy and grumpy as it may seem, is far more important than the findings of science."

Carl Sagan (1995, Chapter 1).

4.1 Field preparation

Field preparation for this study consisted of four steps: (1) data mining, (2) data compilation, (3) initial data interpretation, and (4) logistics. Data integral to this study includes topographic maps, aerial photographs, geologic maps, surficial geology (Quaternary) maps, water well logs (Appendix F), published Quaternary studies conducted in or near the Purcell Trench, and associated digital data (digital elevation models (DEMs), geotiff orthophotographs, water well data, bathymetric maps). Digital data were gathered from publicly available sources through governmental agencies in Canada and the United States (e.g., Geobase®, the National Elevation Dataset (NED), The National Aerial Photograph Library, Environment Canada, Idaho Geologic Survey, Montana Geologic Survey, United States Geologic Survey).

All available data was digitized and geo-referenced into a GIS to be employed in the field during data collection and in the lab during analysis. Digital elevation models (DEM) from Canada and the United States were resampled to compatible cell sizes and merged into one continuous DEM mosaic. A DEM resolution of 90 m was used to facilitate the resampling and eliminate artifacts of the raster merger. Resampling was completed using the mosaic to new raster function in ESRI ArcGIS® version 10. This is not the highest resolution DEM available for the study area (10 m resolution DEMs are available for ID and MT; 100 m subsampled to 25 m is available in BC); consequently, this continuous 90 m DEM mosaic was used in conjunction with local, higher resolution DEMs when the continuous DEM was not required.

Landforms that may help identify the presence of an ice dam, the extent and evolution of gLP, and a flood route along KRv (e.g., valley bottom benches and plains, elevated valley-side benches and fans) were identified from the compiled digital data and stereographic aerial-photograph analysis.

4.2 Field data collection and analysis

Detailed geomorphic observations, sedimentologic and stratigraphic observations and measurements, and Ground Penetrating Radar (GPR) data were collected in the field as sites allowed during July 2010 and May 2011. Observations were made at >250 field sites (Appendix G), but only 28 sites are described in detail and included in this thesis (Figure 3-2, Figure 3-3, Figure 3-4, Appendix A). Local geomorphic observations included qualitative descriptions of landforms and landform associations, slope measurements (using a Brunton®

Pocket Transit), and elevation and position measurements (using a real-time kinematic Leica® GPS System 500 differential global positioning system (dGPS)).

Sedimentary investigations entailed photographing and centimetre-scale, qualitative logging of exposures and identification of lithofacies. Lithofacies are defined as distinct, relatively homogeneous sediment packages delineated by non-genetic physical characteristics (Reading 1986; Walker 1992). Lithofacies descriptions included observations of texture, structure, the nature of the lower contact, thickness, lateral extent, geometry, and, occasionally, colour. Secondary geologic structures (shear and fault planes, intrusive dikes, dewatering structures, folds, and boudinage structures) were also described; fault and shear plane orientation (strike and dip) and offset were recorded. Field descriptions of recurring sedimentary characteristics were compiled into fifteen lithofacies types (summarized in Table 4-1). Quantitative sedimentologic data on textural and structural attributes (grain size (axial measurements on gravel clasts), grain roundness (Wentworth 1922; Wadell 1933; Olsen 1983), grain sphericity (Wadell 1933), clast concentration (visual estimate of % area), bed thickness and lateral extent (lengths), bedding orientations, and fabric) were gathered where possible.

Table 4-1: Lithofacies descriptions, associations and interpretations.

	Code[1]	Lithofacies Name	Log Symbol	Description	Lithofacies associations	Interpretation[2]	References[3]
Silt and Clay	Fl	Laminated silt and clay	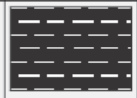	Parallel laminated silt and/or clay up to 1 cm thick; occasionally rhythmic.	Fm, Fd Occasionally with Sp, Sr	Suspension settling likely from overflow or interflow into deep a lake; possibly a seasonal signature (i.e. varves)	2, 4, 8, 25
	Fm	Massive silt or clay		Massive silt or clay.	Fl, Fd, Sp, Sr	Suspension settling from ice distal overflows or interflows, or ice proximal interflows and underflows in a lake.	25
	Fd	Deformed silt or clay		Laminated silt and/or clay with soft-sediment deformation structures including convolutions, shears, flames, and ball-and-pillows.	Fl, Fm, St, Sp, Sd, Dmm	Deformation of lake sediment from removal of ice support, incision, slumping, loading, or glacitectonism.	9, 20
Sand	Sp	Planar-stratified sand	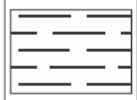	Fine to coarse planar-stratified sand, may contain some granules. Sediments are typically normally graded.	St, Sc, GRd, Fl	Upper or lower flow regime deposition from traction in rivers, on alluvial fans or fan-deltas, or in underflows on the lake bottom.	1, 4, 5, 7, 12, 13, 14, 16, 17, 22, 23
	St	Trough cross-stratified sand		Trough cross-stratified sand, may contain some granules; coset lateral extent varies from ~0.5 - ~3 m.	Sp, Gt	Scour and fill structures, or 3-D dunes from fluvial deposition.	1, 7, 15, 24
	Sc	Planar cross-stratified sand		Planar cross-stratified sand; usually with sharp lower contacts. May contain some granules. Beds may be horizontal or dipping.	St, Sp, Sr, Gc, Gt, Gp, GRd, Gm	Traction deposition during 2D bedform or barform migration in a river or on an alluvial fan.	1, 13, 15, 23
	Sr	Cross-laminated sand		Type A, B or S cross-laminated sand with varying amounts of ripple form lee-side preservation. Angles of climb range from 7° - 46°.	Sr, Sc, Sd, Gp, Fl, Fm	Deposition from suspension and/or traction by rivers or underflows into lakes.	1, 3, 13, 18, 22
	Sd	Deformed sand	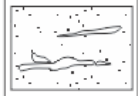	Bedding is dominated by secondary structures (i.e. shear planes, load-structures, fault planes) and little to no primary structure is preserved.	Fd, Fm, St, Sc, Gm, Gt, Dmm, Dcm	Compressional stress from glaciotectonism or loading. Extensional stress from removal of buttressing sediment or ice.	10, 21
	Sm	Massive sand	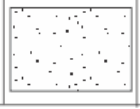	Massive fine to coarse sand. Occasional weak stratification.	Fm, Fd, Fl, Sd	Deposition from underflows into a lake; or grain-flows on fan-deltas or alluvial fans.	4, 5, 16

	Code[1]	Lithofacies Name	Log Symbol	Description	lithofacies associations	Interpretation[2]	References[3]
Gravel	Gp	Planar-stratified gravel		Planar-stratified granule to cobble gravel with some boulders; normally graded beds; sharp lower contacts.	Gt, Gc, Gm, Gd, Dmm, Dcm, St, Sp,	Traction deposition during high-velocity flows in rivers or on alluvial fans.	13, 14, 15, 18
	Gt	Trough cross-stratified gravel	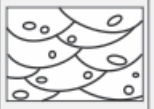	Trough cross-stratified pebble to boulder gravel (usually clast supported, occasionally openwork). Lateral extent ranges from 2.5 m - >7 m.	Gp, Gc, Gm, Gd, Dmm, Dcm, St, Sp	Scour and fill structures, or 3D dune migration in a river.	1, 13, 14, 15, 24
	Gc	Planar cross-stratified gravel	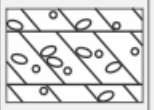	Planar cross-stratified pebble to boulder gravel beds. Beds are clast supported with some imbricated clasts; occasionally openwork.	Gp, Gt, Gm, Gd, Dmm, Dcm, St, Sp	2D dune or barform migration in a river.	1, 15, 18
	Gm	Massive gravel	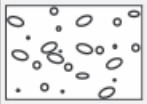	Massive gravel with varying amounts of matrix; occasionally imbricated or openwork. Matrix of poorly-sorted sand and granules. Bed thicknesses range from 0.2 - 0.8 m.	Gd, Gc, Dcm, Sd, Sr, St, Sc	Rapidly deposited water lain sediment in a river or on an alluvial fan; or water lain deposits reworked by gravity.	13, 18, 21, 23
Diamicton	Dmm	Massive matrix-supported diamicton		Massive clayey-silt to silty-clay diamicton; typically <25% clasts (pebbles to boulders, occasionally exhibit glacigenic wear features); occasionally foliated; typically overconsolidated.	Gp, Gt, Gc, Gd, Dcm, Sr, Sc, St, Sp, Fl, Fd	Subglacial till or colluvial debris flows.	10, 11
	Dcm	Massive clast-supported diamicton	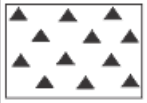	Massive, clast rich (>50% pebbles to boulders), silty-sand to coarse sand diamicton; no glacigenic wear features on clasts.	Gc, Gt, Gp, Gm, Sc, Fd	Debris flows in alluvial fans or on recently deglaciated terrain.	6, 7, 19

[1] This table lists only the most commonly occurring lithofacies in the Purcell Trench and the Kootenay River valley. Some infrequently occurring lithofacies are not listed here, but are described in the text.

[2] Only interpretations applicable to the observations of this study are included.

[3] References: (1) Allen 1984, (2) Ashley 1975, (3) Ashley et al 1982, (4) Burbridge & Rust 1988, (5) Cheel 1990, (6) Eyles & Clauge 1987, (7) Eyles et al. 1987, (8) Gustavson et al. 1975, (9) Hart et al. 1990, (10) Hicock et al 1996, (11) Lian & Hicock 2000, (12) Lowe 1982, (13) Maizels 1993, (14) Marren et al 2009, (15) Miall 1977, (16) Nemec 1990, (17) Nemec et al. 1999, (18) Postma 1990, (19) Pugin 1989, (20) Reinick & Singh 1980, (21) Rovey & Borucki 1995, (22) Russell 2009, (23) Salamon 2008, (24) Smith 1974 (25) Smith & Ashley 1985

In each fabric sample no less than 30 clast a-b plane fabric measurements (maximum dip and down-dip direction of the a-b plane) were taken from gravel deposits and clast a-axis fabric measurements (plunge and down-plunge direction of the a-axis) were taken from diamictons (Appendix C). Samples were extracted from <0.07 m^2 zone of the exposure. Data was plotted on lower hemisphere, equal area (Schmidt) diagrams as scattergrams and/or contoured stereonets (Figure 4-1). Fabrics were contoured using the cosine sums method (Stereo32 software) with a cosine exponent of 20 for gravels and 125 for diamictons (Roeller 2008) (Figure 4-1). Eigenvalues and eigenvectors were calculated using the orientation tensor method (Mark 1973) (Figure 4-1). For diamicton fabrics, modes were identified visually from the fabric scatterplots (cf. Hicock et al. 1996) and tested against randomness using the critical values and statistical protocol of Woodcock and Naylor (1983). The mode with the highest number of clasts is considered to be the primary or main mode (M1), and the mode with fewer clasts is considered to be the secondary mode (M2). Only modes that are significant to the 95% confidence level (Woodcock and Naylor 1983) are labelled as such on the scatterplots (Figure 4-1).

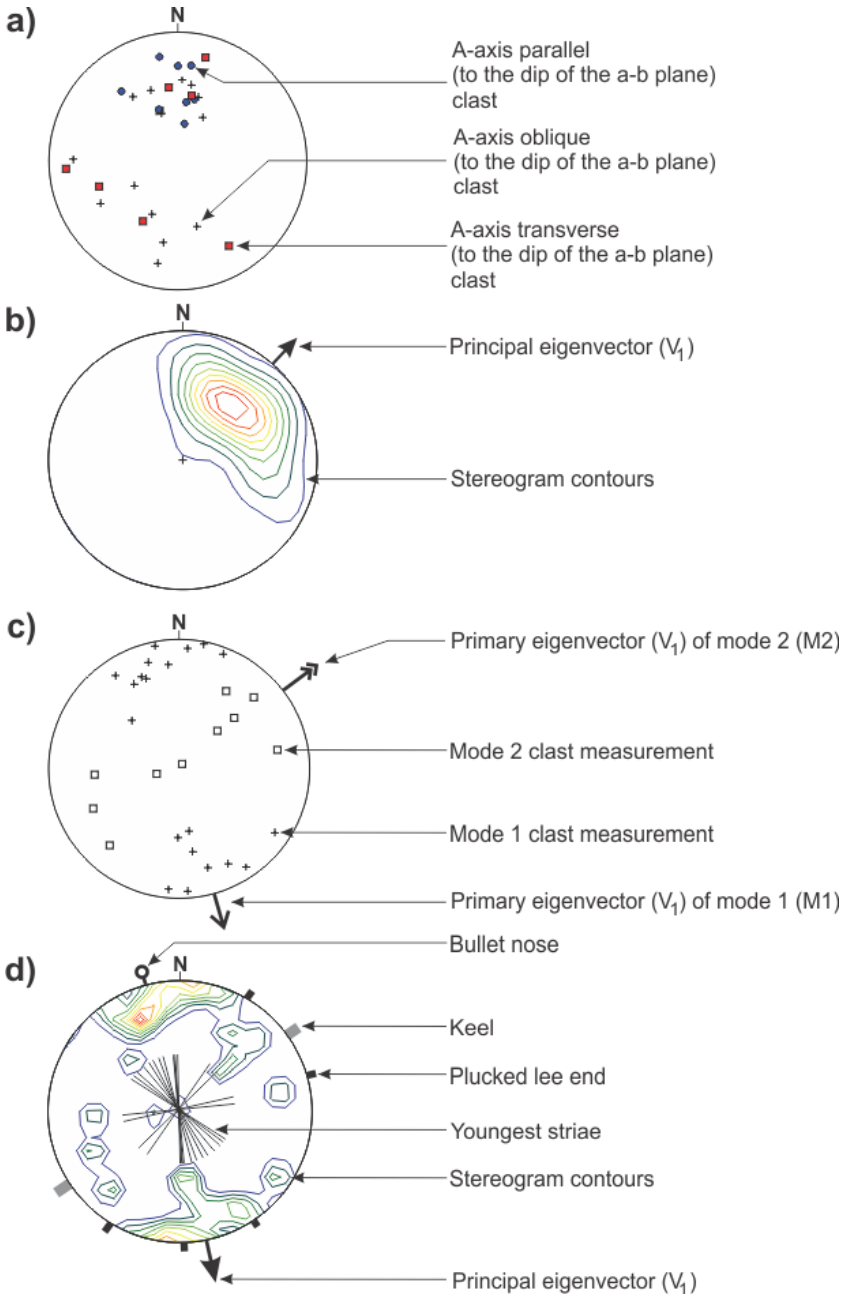

Figure 4-1: Legends for fabric diagrams. All data is presented on lower-hemisphere, equal-area Schmidt nets. a) Scatterplot for trough cross-stratified gravel. The dips and dip directions of clast a-b planes are plotted and classified according to the orientation of the a-axis (a(t), a(p), or (a(o)) with respect to the dip and direction of the a-b plane. b) Gravel fabric stereogram. The dips and dip directions of the a-b plane of gravel clasts in a sample are presented as a contoured stereogram. Contour density is calculated using the cosine sums method with a cosine exponent of 20 in Stereo32 software. The principal eigenvector (V1) depicts the azimuth of maximum cluster for all clasts. Diamicton fabric scatterplot (c) and contoured stereogram (d) record the a-axis plunge and azimuth of measured pebbles. Orientation and direction of glacigenic wear features and the V1 for all the clasts are displayed. Contour density is calculated using the cosine sums method with a cosine exponent of 125 in Stereo32 software. The principal eigenvectors of the sample is shown in (d), and the primary and secondary eigenvector of modes in bimodal distributions are shown in (c).

Additional clast size, shape, lithology, orientation and wear data were also collected from clasts sampled for fabric analysis (Appendix C). Clast a-, b- and c-axis measurements were used for grain size and sphericity (Sneed & Folk 1958) estimation (Appendix D). Clast roundness was estimated using Krumbein's (1941) scale. From gravel fabric samples the orientation of the a-axis to the maximum dip of the a-b plane was also collected (Appendix C). This affords an estimation of the likely mode of grain transport just prior to deposition. A dominance of clast a-axes transverse to dip direction (a(t)) suggests clasts rolled along the bed, whereas a dominance of clasts parallel to dip direction (a(p)) favour clast sliding across the bed (or clast deposition from suspension in a hyperconcentrated flow) (cf. Brennand 1994). This logic allows a(p) clasts in gravel fabrics from trough cross-beds to be used as a proxy for the true direction of dip of slip- or avalanche-faces and hence an estimation of paleoflow direction in cases where this is not obvious from exposures (i.e. where Gt (Table 4-1) presents as troughs rather than cross-sets). From diamicton fabric samples the presence and orientations of obvious surface wear features (SWFs; i.e., keels, striae, bullet noses, plucked ends; Krüger 1984) on clasts were also recorded following the protocol of Lian (1997) (Appendix C; Figure 4-1).

Lithostratigraphic units in this thesis are defined as distinct bodies of sediment that have been deposited in a depositional environment different from that of surrounding or nearby lithostratigraphic units. They are defined at a finer scale than geoclimatic (i.e. glacial-interglacial) because the research questions in this thesis require elucidation of environmental changes (in time) and differences

(in space) during deglaciation. Lithostratigraphic units are defined by their lithofacies associations, physical characteristics, relative stratigraphic position and geomorphic context. Measurements of lithostratigraphic unit thickness were made with a tape measure on simple exposures, and by Impulse® laser range finder on more complex, inaccessible or high exposures. Measurements of lithostratigraphic unit lateral extent were made using a tape measure. Elevations of lithostratigraphic unit lower contacts and the tops of exposures were measured using a hand-held Pretel® barometric altimeter (calibrated to the known elevation of Kootenay Lake) or, a real-time kinematic Leica® GPS System 500 dGPS (vertical accuracy reported by Leica®: within ± 0.1 m). All elevations reported in this thesis are supplemented with DEM elevations to normalize the data to a single datum. This also establishes a single accuracy for all elevation measurements to within 10 m at a 90% confidence interval (Beaulieu et al. 2007). Lithostratigraphic data is presented in photographic panoramas and vertical logs (refer to Figure 4-2 for lithostratigraphic log legend).

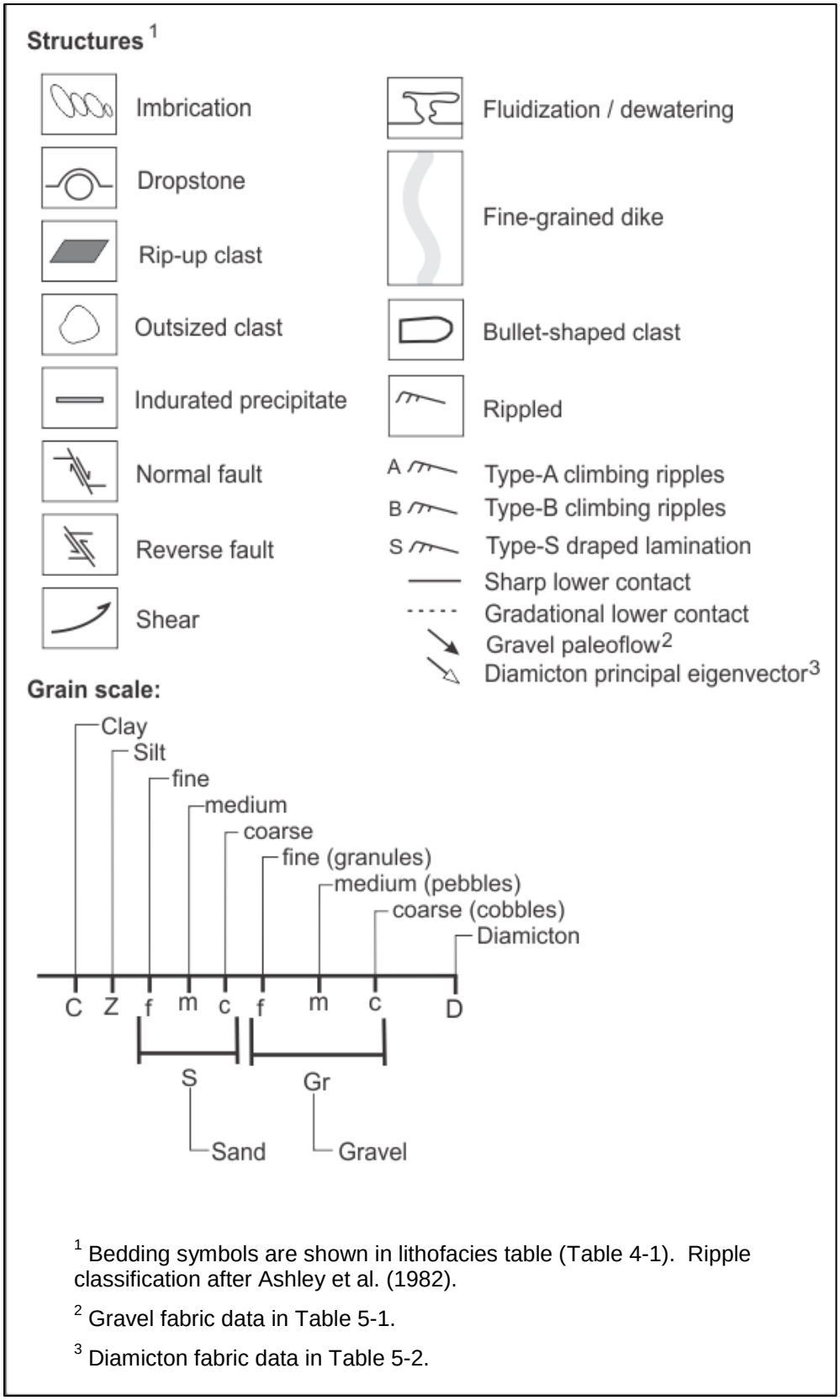

[1] Bedding symbols are shown in lithofacies table (Table 4-1). Ripple classification after Ashley et al. (1982).

[2] Gravel fabric data in Table 5-1.

[3] Diamicton fabric data in Table 5-2.

Figure 4-2: Legend for lithostratigraphic logs.

When no exposures were available, sedimentary architectural information was obtained using a pulseEKKO® IV ground penetrating radar (GPR) system (site 48 in KRv, Figure 3-4). GPR lines parallel to the KRv are termed “X-lines”; GPR lines perpendicular to the KRv are named “Y-lines”. A total of 530 m of 100 MHz common offset (CO) GPR lines were collected (Appendix E). During CO data collection, the GPR antennas were co-polarised and perpendicular-broadside to the survey line, to reduce reflections from offline sources (Arcone et al. 1995). Antennas were kept at a constant separation of 1 m and data were collected in step mode (0.25 m) along the lines to improve ground coupling and trace stacking (32 traces). Two common mid-point (CMP) profiles, collected at site 48 (Figure 3-4), provide an estimated subsurface average velocity of 0.097 m/ns, which was used to convert two-way travel time (TWT) into depth and for data processing. Detailed topographic data was gathered on the survey lines using a real-time kinematic Leica® GPS System 500 dGPS to allow for topographic correction of the processed lines. The GPR data processing was carried out in REFLEXW® v6.0 (Sandmeier 2011) and included time-zero correction, ‘dewow’ filtering, bandpass filtering, migration, background removal filtering, application of a gain function, and topographic correction (§ 4.2.2).

The digital data and field observations encompassing the geomorphology, sedimentology and stratigraphy of the study area are integrated and analysed in order to verify landform classifications, elucidate different paleoenvironments and paleoenvironmental change, and thus address the research questions. This

landform and paleoenvironmental information was used with DEMs and bathymetric data to reconstruct gLP and better explain its evolution.

4.2.1 Landform definitions

Kame terraces, river terraces, lake-bed benches, fan-deltas, and alluvial fans are identified in the study area. *Kame* (originally spelled *kaim* or *cam*) is a Scottish word that describes a sediment mound with steep sides or a crooked path (Jamieson 1874; Gregory 1912; Holmes 1947), which has come to vaguely describe any alluvial or lacustrine sediment that was once in contact with ice (e.g., Holmes 1947; Price 1973). Because of its ambiguity, there is little scientific use for the word *kame* as a stand-alone descriptor of glacial sediment, however, when used with an adjective, such as terrace, the term is specific enough to warrant its use. In this study the term *kame terrace* describes glaciofluvial sedimentation in a temporary topographic low formed between the ice margin and the valley wall (Embleton & King 1975). *Bench* is the non-genetic term used to describe a relatively flat-topped sediment deposit, whereas the term *terrace* is reserved for deposits of fluvial or glaciofluvial origin, a fluvial terrace denoting an elevated river floodplain. *Lake bed benches* are flat-topped, frequently gullied and incised, fine-grained sediment deposits on valley floors and walls that were deposited on a lake bed.

Alluvial fans are defined as fan-shaped fluvial and debris flow deposits that radiate downslope from a mountainous sediment source into a lowland area or larger valley (Bull 1963; Ryder 1971; Church & Ryder 1972). Alluvial fans prograde from their sediment point source through some combination of braided

stream, sheet flow, or debris flow deposition (Church & Ryder 1972; Blair 1987; Postma 1990; Blair & McPherson 1994). They have steeply-dipping (2° - 25°), convex-up profiles (Blair & McPherson 1994; Ryder 1971) and may build into bodies of water creating a *fan-delta* (Nemec 1990; Postma 1990). Most fans in the study area have undergone extensive post-depositional modification through incision, which occurs either through a lowering of the local base level (Hooke 1967; Ryder 1971), or by "fan-head trenching" due to changes in sediment supply and/or stream gradient (Hooke 1967).

4.2.2 GPR processing and analysis

The GPR data were processed using REFLEXW® software version 6.0 (Sandmeier 2011) to improve the signal to noise ratio (Woodward et al. 2003; Burke 2008), thereby providing a clear and less distorted cross-sectional view of the underlying sedimentary architecture. The following paragraphs will document the processing steps applied to the data (in sequential order) and, when necessary, discuss the shortcomings and benefits of the parameters.

4.2.2.1 Time-zero correction

This processing step aligns the airwave arrival to zero on the y-axis of the graphical display. This is necessary to account for a delayed airwave arrival time (Woodward et al. 2003). The delay is caused by some combination of equipment warm-up (acquisition of ambient temperature), damaged optic cables or electronic malfunctions (Woodward et al. 2003). An uncorrected airwave delay can be propagated into the lower reflections of the graphic profile (Neal, 2004).

4.2.2.2 Dewow filter

The dewow filter removes low frequency noise ('wow') from the data, onto which the real data is overlain. Due to its low frequency, the 'wow' has sufficiently large amplitude to obscure the real data (Woodward et al. 2003). The 'wow' in the signal is the result of electronic saturation caused by the short interval between airwave and ground wave arrivals (Neal 2004).

The manipulated parameter in the dewow filter is the time window over which a mean value is calculated for each trace. The goal during the dewow processing step is to select a time window value that effectively mitigates the 'wow' while keeping the real data unaffected. The smaller the time window value, the greater the 'wow' is diminished; however, if the time window value is too small, or too large, the real data will be adversely affected. A time window of 21 ns was deemed optimal for this study (Figure 4-3).

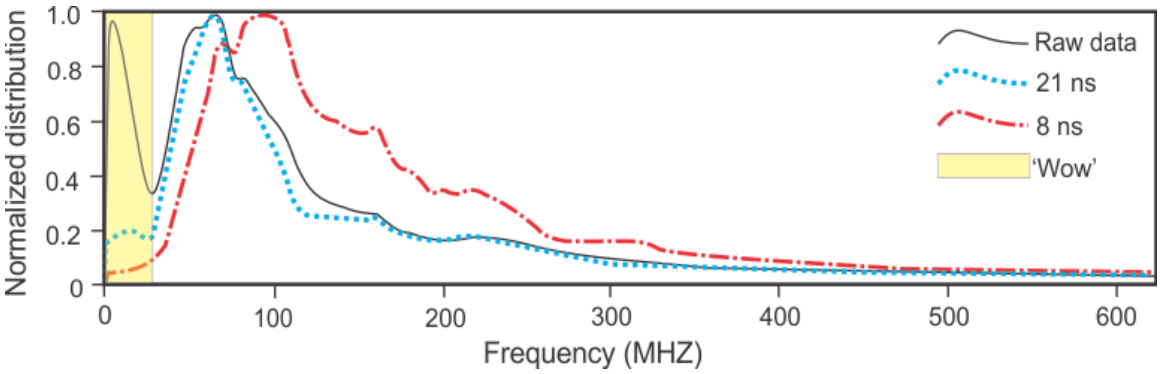

Figure 4-3: Effects of the dewow filter. Plot is from the application of the REFLEXW® dewow filter to site 48B, GPR line X1. The 21 ns window was chosen over the 8 ns window because the actual data was minimally distorted and the 'wow' was greatly diminished.

4.2.2.3 Bandpass filter

The bandpass filter removes high and low frequency noise from the GPR amplitude spectrum (Woodward et al. 2003). Two types of bandpass filters are available through the REFLEXW® software: *Bandpass Frequency* and *Bandpass Butterworth*. *Bandpass Frequency* was selected for this study because it removed more background noise. Four parameters can be adjusted in the application of the *Bandpass Frequency* filter: lower-cutoff frequency (LCF), lower plateau (LP), upper plateau (UP), and upper-cutoff frequency (UCF). These four frequency parameters define a trapezoidal filter. Lower and upper value pairs are held to octaves – the LCF and UP frequencies are each half of the LP and UCF, respectively. The doubling relationship ensures that the taper of the trapezoid is not too steep, which can result in high frequency ringing in the data (Woodward et al. 2003). For all lines in this study, the following parameters, in LCF-LP-UP-UCF format, were selected as optimal: 15-30-115-230 MHz.

4.2.2.4 Velocity analysis

A velocity analysis is used to determine the velocity of electromagnetic (EM) propagation through the subsurface. The EM velocity then allows the recorded raw data in two-way travel time (TWTT) to be converted into depth measurements.

Two common midpoint (CMP) surveys taken from lines X1 and X2 at site 48B (Figure 3-4) were used to assess EM velocity. The velocity is calculated using the semblance analysis function in the REFLEXW® software by regressing antenna distance from the common midpoint against the TWTT of the EM pulse

(Woodward et al. 2003). The analysis results in a graph of TWTT vs. velocity that displays the normalized output-to-input energy ratio as 'bullseyes', which are superimposed onto nonlinear reflections (Burke 2008). The bullseyes are visually fit to diffraction hyperbolas generating interval velocities; the deepest bullseye used in the analysis provides an average profile velocity. Individual layer velocities (V_{Lay}) are calculated manually (Equation 4.1; pers. comm. Matthew J. Burke 22/07/2011) to ensure that no spurious values have been used in averaging the profile velocity. The average layer velocity at site 48B was found to be 0.097 m/ns.

$$V_{Lay} = (V_{int} \times L_{\#}) - (\sum V_{ov}) \qquad \text{(Equation 4.1)}$$

Where V_{int} is the interval velocity, $L_{\#}$ is the stratum number (increasing sequentially from the top of the profile), and V_{ov} is the velocity of the overlying strata(um).

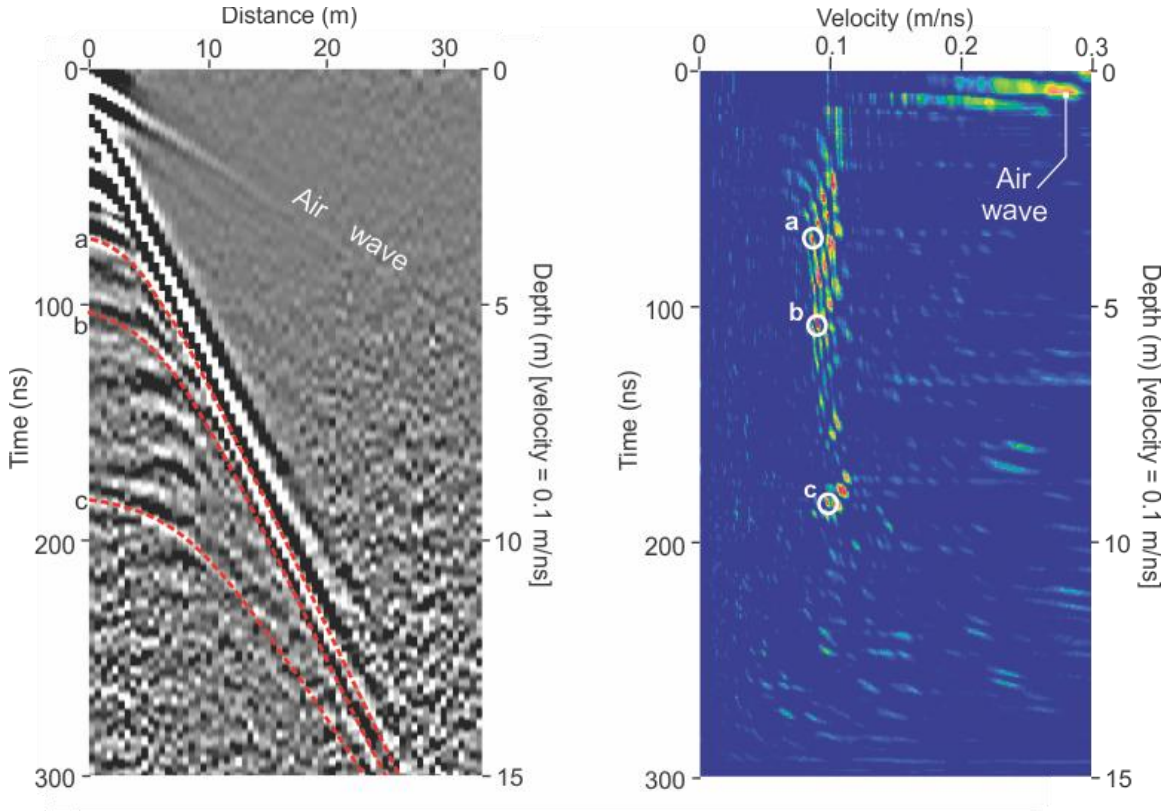

Figure 4-4: CMP velocity analysis. Images are from the semblance analysis at site 48B, GPR line X1. Normalized output/input energy ratio bullseyes are marked with white circles and labeled (on right). Bullseyes correspond to the labeled diffraction hyperbolas, which are highlighted with dashed red lines (on left). The REFLEXW® software utilizes a computer assisted visual coupling of bullseyes (velocities) to hyperbolas (distances) to generate an actual measurement of the EM wave velocity.

4.2.2.5 Migration

This processing step attempts to minimize distortion caused by generating a 2D survey from a 3D EM cone. Because the EM pulse radiates from the transmitter as a complex 3D cone, out-of-line reflections are imaged, which result in diffractions, displacements and distortions (Neal 2004).

The REFLEXW® software provides several methods of reducing image distortion from out-of-line reflections; of these, the Kirchoff migration method was

used because it removed the most diffraction hyperbolae without adversely affecting the real data. Three parameters are needed to run the algorithm: 1) summation width, which directs the algorithm to sum each data point to a width dictated by the largest diffraction hyperbolae (Burke 2008), 2) velocity, which is the average EM velocity calculated in the velocity analysis, and 3) start time, which allows specific depths of the profile to be targeted. The optimum values for these parameters were found to be 10, 0.09 m/ns, and 25 ns (just below the ground wave), respectively. When the summation width was too high the data appeared over-migrated and developed inverted hyperbolae termed 'migration smiles' (Burke 2008). When the summation width was too low some real data was removed from the profile and noise was introduced.

4.2.2.6 Background removal

Background removal attempts to remove coherent, airwave-parallel banding in the data introduced by ringing in the antennas, which is caused by signal repetition (Woodward et al. 2003). Peak results for this processing step were obtained through the subtracting average algorithm in the REFLEXW® program. The algorithm calculates a reference trace over a distance chosen by the user; the reference trace is then subtracted from every trace in the profile. The optimum number of traces used for the average was found to be 20. Banding persisted when <20 traces were averaged, and some planar reflections in the data were lost when >20 traces were averaged.

4.2.2.7 Gain

Gains serve to counteract progressive signal weakening with depth caused by signal attenuation, geometrical spreading, reflection and scattering (Woodward et al. 2003; Neal 2004). An automatic gain control (AGC) algorithm was run on the data through the REFLEXW® software. An AGC calculates average amplitude for each trace over a specified time window (Woodward et al. 2003). Then, values for all points along individual traces are held constant to the calculated average. A time window of 5 ns was deemed optimal for this study because it resulted in an amplification of the data without amplifying noise.

4.2.2.8 Topographic correction

Topography along the survey line must be accounted for to display the landform geometry and the actual dips of the internal reflections. To accomplish this field data on position and elevation, gathered from a dGPS, was converted into elevation change relative to the highest point on the line. Then the elevation change was converted into TWTT through the use of the EM pulse velocity obtained through the velocity analysis. These changes in TWTT are then applied to the profile.

4.2.2.9 GPR analysis

Analysis (interpretation) of the processed GPR data was conducted to describe sedimentary architecture and infer a probable mechanism of deposition. Interpretations were guided by established methods outlined in peer-reviewed literature, especially Neal (2004) and Woodward et al. (2003).

All of the GPR profiles were printed at the same scale and with a one-to-one ratio (no vertical exaggeration); this enabled the profiles to be viewed at different angles, which elucidates reflection geometry characteristics that may otherwise remain ambiguous. Radar bounding surfaces, which are high amplitude reflections that can be traced across multiple lines and mark changes in reflection geometry (Burke 2008), were identified and traced onto the hard copies. The bounding surfaces define discrete radar elements (RE), which are labelled in stratigraphic order (RE-a – RE-ee in text and a – ee in figures) and described in terms of their geometry, boundaries and character of their constituent reflections (Neal 2004). The properties of the radar elements are used to infer the mode of deposition (Woodward et al. 2003; Neal 2004).

Radar elements consist of radar surfaces, radar packages and radar facies (Neal et al. 2002; Neal 2004). These terms have similar definitions to the equivalent seismic stratigraphy terms (Neal 2004). Radar surfaces delineate radar packages, which are depositional units interpreted to consist of genetically related strata (Mitchum et al. 1977; Neal 2004). Radar facies are the reflection sets that occupy space between the stronger reflections of the radar surfaces (Mitchum et al. 1977; Neal 2004).

4.2.3 GLP extent and volume calculations

Typically, glacial lake extent is reconstructed from the distribution of lake bed sediments and by correlating water plane indicators (e.g., deltas, shorelines; Johnsen and Brennand 2004). However, a dearth of gLP water-plane indicators were identified on the steep bedrock valley walls of the Purcell Trench in the

study area, so gLP extent is estimated by modeling (in a GIS) a tilted water plane (Appendix G) fixed to the Elmira spillway, lake extent limited by the topographic DEM and the lake bed DEM (Figure 4-5). Given that a lack of water-plane indicators in the Purcell Trench precludes calculation of glacioisostatic tilt of the water plane, a reasonable range of tilts (Appendix G) are applied based on an assessment of known glacioisostatic tilt values reported for the CIS (§ 6.2). The orientation of glacioisostatic tilt is assumed to be parallel to the Purcell Trench (352°).

GLP paleo-volume can be estimated from the topographic DEM, tilted water plane, lake extent map, a simplified gLP lake bed DEM and Kootenay lake bathymetry using raster mathematics in a GIS (Figure 4-5). The gLP lake bed DEM was extrapolated from the elevation of the lake bed bench and surrounding topography (§ 5.3). The elevation of a series of measured points on the gLP lake bed bench were interpolated using the inverse distance weighting function in ESRI ArcGIS® (Figure 4-5). By integrating this surface with the topographic DEM, a simplified reconstruction of the gLP lake bed prior to lake drainage and Holocene incision is produced. The extent of gLP for each tilt scenario is provided by the intersection of the tilted water plane with the interpolated lake bed DEM and the topographic DEM. The volume and depth of gLP is ascertained by adding the volume of the proglacial portion of the Kootenay Lake bathymetric raster to the volume of the topographic DEM below a tilted water plane (all volume calculations were performed using the surface volume function in ESRI ArcGIS®) (Figure 4-5).

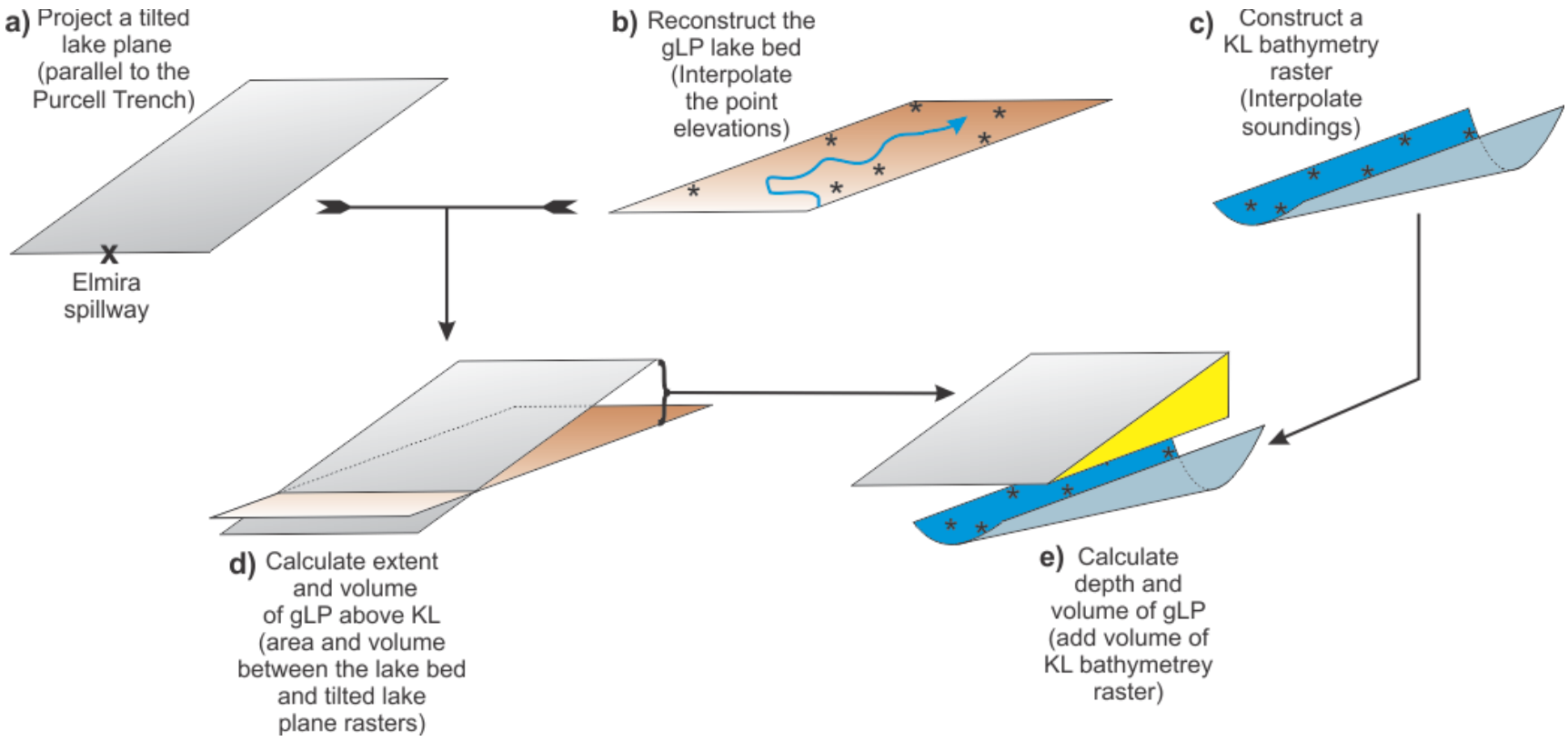

Figure 4-5: Flow chart describing the methodology developed to calculate gLP extent, depth and volume. a) A water plane tilt is assumed following a review of previously reported tilts (see text) and projected northwards from the Elmira spillway parallel to the Purcell Trench. b) The elevation of the gLP lake bed bench is measured at a series of points using a Leica® dGPS system and a DEM (Geobase®), then the elevation data is interpolated and limited by the topographic DEM to produce a simplified lake bed DEM. Stars on the brown lake plane represent point elevations and blue line represents the Kootenai River. c) Individual bathymetric soundings are interpolated in a GIS to produce a simplified Kootenay Lake (KL) bathymetry raster. d) For each water plane (see text), the extent of gLP and volume above the surface of Kootenay Lake (~530 m asl) is calculated from the intersection of the tilted lake plane and simplified lake bed DEM. e) The depth and volume of gLP is calculated as the volume from d) plus the volume of Kootenay Lake within the gLP extent.

5: RESULTS

This chapter provides descriptions and interpretations for all major study sites. Section 5.1 describes sites recording ice advance. The elevations of these sites define full glacial valley fill elevations in the Purcell Trench. Section 5.2 describes sites recording ice position during decay of the Purcell Lobe in the Purcell Trench. Section 5.3 describes sites containing a sedimentary record of glacial Lake Purcell. Section 5.4 explores the terraced geomorphology of the valley fill and describes sites in the Kootenay River valley that may contain some record of gLP drainage. Section 5.5 describes sites that contain a record of postglacial (Purcell Trench) or post-gLP drainage (KRv) sedimentation. In this chapter most sites are interpreted individually. Sites that occur within the same landform are interpreted as a group. A summary of the findings of each section is also provided. Regional interpretations are addressed in chapter 6.

5.1 Sites recording ice advance

The sites in this § are interpreted to record the advance of the marine isotope stage 2 (MIS 2) Cordilleran Ice Sheet (CIS) south through the Purcell Trench, because each site is capped by, or composed of glacigenic diamicton (till). These sites record remnants of the full glacial valley fill because they occupy positions south (downstream of ice advance) of distinct bedrock protrusions in the Purcell Trench.

5.1.1 Site 19

5.1.1.1 Observations

Site 19 is an active gravel pit that abuts the eastern wall of the Purcell Trench ~78 m above the surface of modern Kootenay Lake (top of exposure is ~610 m asl), and ~2.6 km north of Kootenay Bay (Figure 3-3). The pit is on the northwest side of a saddle that bisects the Bluebell Mountain/Pilot Point ridgeline and connects Kootenay Bay and Crawford Bay (Figure 5-1). The deposit occupies a slight alcove in the Purcell Trench (Figure 5-1).

The pit exposes a 27 m thick sediment package containing two lithostratigraphic units plastered onto the bedrock valley wall (Figure 5-2). Talus slopes between vertical exposures precluded a continuous vertical log of this sediment package; thus, to document the stratigraphy, two logs were constructed at the site one of which is a composite log (Figure 5-3; see Figure 5-2 for locations of log measurements).

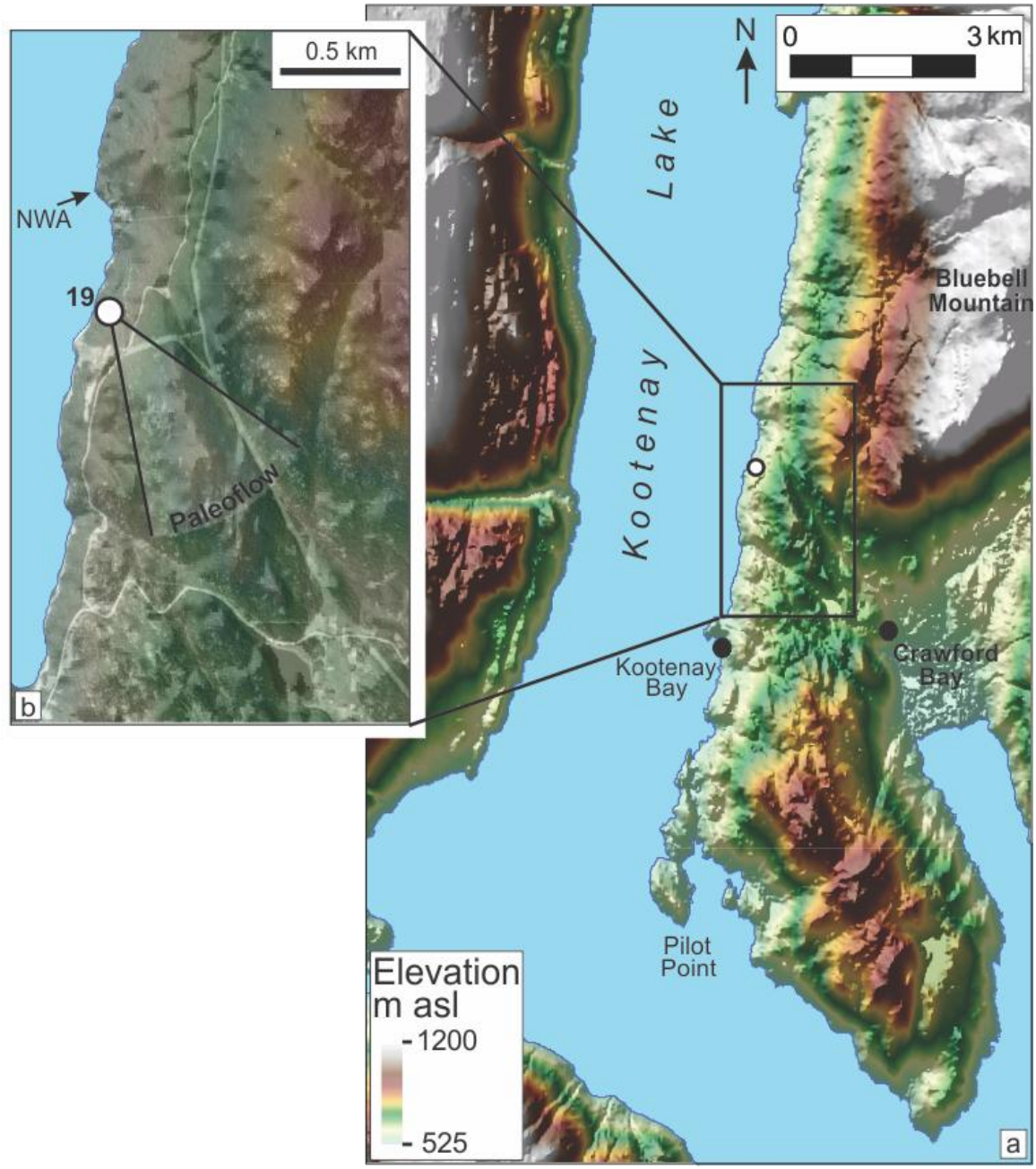

Figure 5-1: a) Hillshaded DEM (Geobase®) showing the geomorphology around site 19 (white dot). Site 19 is located in the saddle between Bluebell Mountain and Pilot Point. b) Hillshaded DEM superimposed on an aerial photograph (clip from BC5347_248. © Province of British Columbia. All rights reserved. Reprinted with permission of the Province of British Columbia.) showing local terrain. The northernmost wall of this gravel-harboring alcove is marked NWA. The range of paleoflow directions gathered at site 19 is displayed as a cone extending from the site. (The deposit does not cover the geographic area of the cone.) Refer to Figure 3-1 and Figure 3-3 for site location within the Purcell Trench.

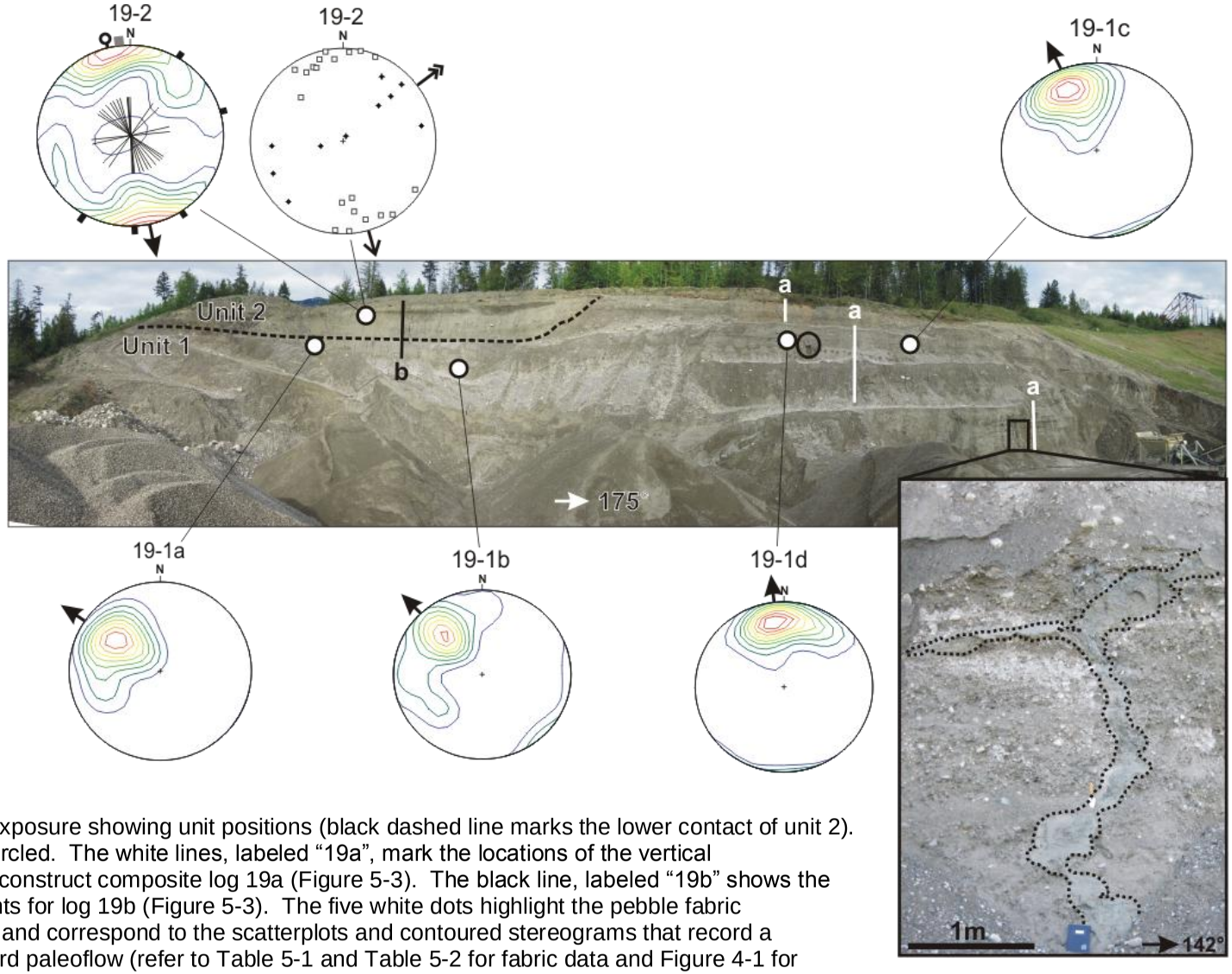

Figure 5-2: a) Site 19 exposure showing unit positions (black dashed line marks the lower contact of unit 2). For scale, a person is circled. The white lines, labeled "19a", mark the locations of the vertical measurements used to construct composite log 19a (Figure 5-3). The black line, labeled "19b" shows the location of measurements for log 19b (Figure 5-3). The five white dots highlight the pebble fabric measurement locations and correspond to the scatterplots and contoured stereograms that record a southward/southeastward paleoflow (refer to Table 5-1 and Table 5-2 for fabric data and Figure 4-1 for stereogram legend). Table 5-1 for gravel fabric data and Table 5-2 for diamicton fabric data) Refer to Figure

Table 5-1: Pebble fabric data listed in order of appearance in Chapters 5.

Fabric name	**Litho-facies code**[1]	**Elevation** (m asl)	**n**	**Roundness**[2] (%)			**a-axis orientation**[3] (%)			V_1[4] (trend / dip)	S_1[5]	S_3[6]
				R	**S**	**A**	**a(p)**	**a(t)**	**a(o)**			
19-1a	Gp	598	30	60	40	0	40	27	33	298° / 42°	0.81	0.07
19-1b	Gp	597	30	47	53	0	27	50	23	308° / 27°	0.70	0.06
19-1c	Gp	598	30	53	40	7	30	43	27	336° / 30°	0.85	0.05
19-1d	Gp	602	30	43	50	7	63	13	24	359° / 27°	0.81	0.05
41-4	Gm	557	30	17	70	13	3	67	30	171° / 14°	0.52	0.21
27-1	Gp	700	31	74	23	3	3	65	32	346° / 31°	0.70	0.09
30-1	Gp	569	30	37	56	7	33	33	33	31° / 16°	0.53	0.21
38-1a	Gp	587	30	40	43	17	20	47	33	169° / 48°	0.85	0.06
38-1b	Gp	589	30	37	57	6	20	30	50	195° / 33°	0.75	0.10
38-1c	Gp	590	31	37	47	16	20	47	33	203° / 31°	0.65	0.13
39-6	Gp	573	30	16	47	37	47	23	30	252° / 51°	0.65	0.13
39-7	Gm	571	30	20	50	30	23	43	31	244° / 36°	0.66	0.09
40-1	Gt	622	50	37	48	15	40	16	44	248° / 34°	0.59	0.14

Fabric name	Litho-facies code[1]	Elevation (m asl)	n	Roundness[2] (%)			a-axis orientation[3] (%)			V_1[4] (trend / dip)	S_1[5]	S_3[6]
				R	S	A	a(p)	a(t)	a(o)			
24-1a	Gp	578	30	47	50	3	7	50	43	51° / 37°	0.70	0.07
24-1b	Gp	577	30	67	33	0	10	43	47	65° / 38°	0.66	0.08
24-1c	Gp	584	30	70	30	0	23	27	50	69° / 34°	0.77	0.06
24-1d	Gp	586	30	~100	0	0	na[7]	na[7]	na[7]	48° / 42°	0.80	0.05
35-1	Gp	611	30	40	47	13	53	10	37	333° / 31°	0.76	0.10
1-2[8]	Gp	598	30	63	20	17	17	67	16	8° / 32°	0.65	0.12

[1] – Refer to Table 4-1.

[2] – R: rounded and well-rounded; S: subrounded and subangular; A: angular and very angular. (after Wadell 1933 and Barrett 1980).

[3] – A-axis orientation relative to the maximum plunge of the a-b plane: parallel (a(p)), transverse (a(t)), oblique (a(o)). (Refer to § 4.2.)

[4] – Principal eigenvector (vector aligned with maximum clustering).

[5] – Principal eigenvalue (highest clustering value, corresponding to the Principal eigenvector).

[6] – Weakest eigenvalue. (Lowest clustering value, corresponding to the third eigenvector, which is normal to the principal eigenvector and aligned with the direction of minimal clustering).

[7] – Data not collected.

[8] – Site presented in Appendix B.

Table 5-2: Diamicton pebble fabric data listed in order of appearance in chapter 5.

Fabric name[1]	Elevation (m asl)	n	Roundness[2]			V_1[3] (trend / plunge)	S_1[4]	S_3[5]	SWFs[6]				Interpretation[7]
			R	S	A				K	B	P	S	
19-2	605	30	20	70	10	355° / 2°	0.61	0.16	1	1	5	15	Subglacial till
41-6a	568	30	5	75	20	185° / 3°	0.61	0.10	1	0	2	11	Subglacial till
41-6b	571	30	0	75	25	166° / 13°	0.64	0.06	1	0	1	7	Subglacial till
53-1	602	30	7	63	30	19° / 17°	0.76	0.07	0	2	7	8	Subglacial till
39-2	570	30	0	30	70	320° / 5°	0.64	0.15	0	0	0	2	Debris flow
40-2	627	31	19	61	20	344° / 10°	0.56	0.11	0	0	0	0	Flow till / debris flow
47-X	539	30	3	53	44	168° / 21°	0.58	0.15	0	0	0	0	Debris flow
1-3[8]	597	40	55	40	5	116° / 25°	0.46	0.12	0	0	0	0	Debris flow
49-2[8]	510	30	33	63	4	219° / 43°	0.63	0.17	0	0	0	0	Debris flow

[1] - All fabrics are bimodal except 53-1, which is unimodal. All fabrics are from Dmm except 39-2, which is Dcm (Table 4-1).

[2] – R: rounded and well-rounded; S: subrounded and subangular; A: angular and very angular (after Wadell 1933 and Barrett 1980).

[3] – Principal eigenvector (vector aligned with maximum clustering.) All fabrics have a >99% confidence level and are bimodal except 53-1, which is unimodal.

[4] – Principal eigenvalue (highest clustering value, corresponding to the Principal eigenvector).

[5] – Weakest eigenvalue (lowest clustering value, corresponding to the third eigenvector, which is normal to the principal eigenvector and aligned with the direction of minimal clustering).

[6] – Surface wear features: K – keel; B – bullet nose; P – plucked lee; S – clasts with striae (not an individual count of striae) (after Kruger 1979 and Sharp 1982).

[7] – Refer to text for explanation.

[8] – Sites presented in Appendix B.

Unit 1 is at least 25 m thick (lower contact not exposed) and mainly composed of tabular to lenticular beds of planar-stratified, rounded to well-rounded (19-1a-d, Table 5-1) cobbles and pebbles (Gp, Table 4-1) below ~610 m asl (Figure 5-3). Clasts are dominantly intrusive igneous and metamorphic and are highly spherical. Gravel beds are predominantly clast supported and in places openwork. Beds are differentiated by geometry (tabular or lenticular), texture and grading. Most beds are 0.25-0.5 m thick, tabular, have sharp lower contacts and contain imbricate gravel clasts that fine upward from cobbles to large pebbles supported by a matrix of coarse sand (Gp, Table 4-1). Similar beds with lenticular geometry are less frequent, representing only 9% of the beds intersecting the vertical logs. These lenses extend laterally 6–12 m. The amount of matrix is highly variable between beds; typically, the beds with large amounts of matrix also have gradational lower contacts. Some beds are composed entirely of planar-bedded, well-imbricated pebbles and granules and have little to no matrix. Rarely, gravel beds are separated by lithofacies of massive sand (Sm, Table 4-1). These lithofacies are thin (0.10-0.20 m), lenticular (lateral extent: 2.5-6 m), and composed mainly of coarse sand with granules. The planar-stratified sand beds fine upwards and have gradational lower contacts. The uppermost gravel beds (top 2.5 m of log 19A, Figure 5-3) in unit 1 are composed of crudely cross-bedded to massive boulder and large cobble gravel in a matrix of sandy granules and pebbles (Gm and Gc, Table 4-1). These coarse upper beds have sharp lower contacts. Gravel fabrics on imbricate a(t) and a(o) clasts within unit

1 (19-1a, 19-1b, 19-1c and 19-1d, Figure 5 4, Figure 5 5, Table 5-2) record southward to southeastward paleoflows.

A dike composed of deformed, vertically-laminated (Fd, Table 4-1) dark grey clay and light grey silt (~65% and ~35%, respectively) with rare small granules cuts vertically into the unit 1 gravel beds (Figure 5-2). The dike averages ~0.30 m wide and extends for ~5 m with a sill (~0.2 m thick and ~1.5 m long) extending from the main dike (Figure 5-2). In places the dike texturally varies across its width with the coarsest sediment (silt) located near the centre of the dike.

Unit 2 is ~6 m thick with a sharp lower contact. It is composed of massive, well-consolidated, matrix-supported diamicton (Dmm, Table 4-1) that consists of ~15% clasts (pebbles and cobbles) in a clayey silt matrix. In places a faintly discernible fissile structure can be distinguished in the matrix. The majority of the clasts in the diamicton are subrounded and the majority of the clasts have striae on their tops, bottoms and sides (19-2, Table 5-2). Typically striations align with the a-axes of clasts. Some clasts also displayed polished and striated facets (on clast tops), bullet noses, keels (on clast bottoms), and freshly plucked lee ends (19-2, Table 5-2). A diamicton fabric measured within unit 2 is bimodal with its principal eigenvector and primary mode eigenvector toward 355° (19-2, Figure 5-2, Table 5-2).

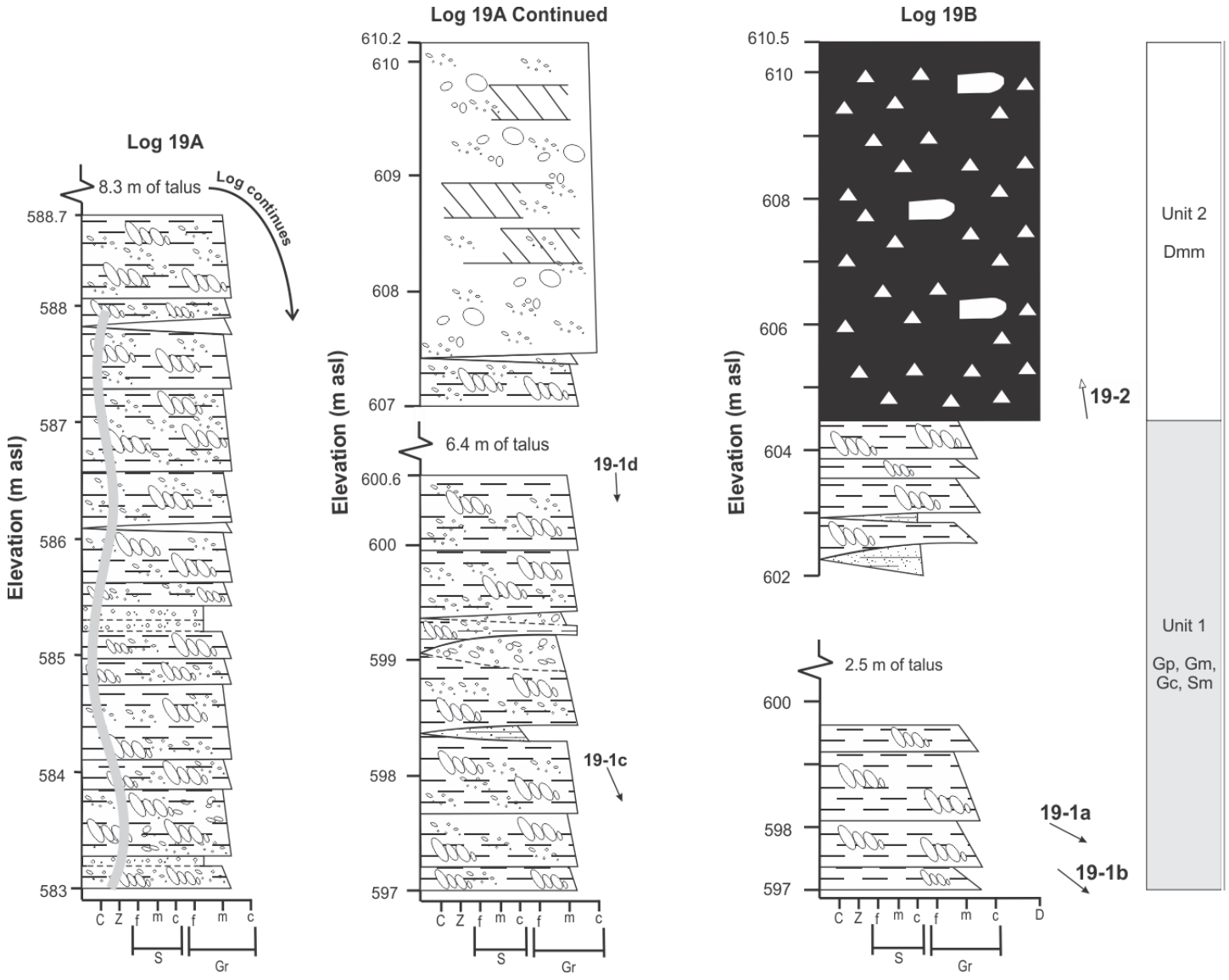

Figure 5-3: Log 19A and 19B from site 19 (Figure 5-2). Log 19A records the sedimentology of unit 1; covered intervals (talus) are not drawn to scale. Log 19B records the sedimentology of the top of unit 1 and unit 2. Refer to Figure 4-2 for legend and Table 4-1 for lithofacies codes. Paleoflow arrows correspond to data in Tables 5-2 and 5-3, and Figure 5-4a.

5.1.1.2 Interpretation

Unit 1 is interpreted as a braided-stream deposit, because it contains rounded, imbricated clasts and lithofacies consistent with this interpretation (Allen 1982). Imbrication is deduced from the dominance of a(t) clasts in fabrics 19-1b and 19-1c (Table 5-1); the dominance of a(p) clasts in fabrics 41-1a and 41-1b may be caused by rotation around larger obstacle clasts in cluster bedforms. The elevated position of the deposit on the valley wall and its valley-parallel paleoflow direction suggest a glacial outwash or ice-marginal depositional environment. The lithofacies at this site (Gp, Gt, Gm and Sp, Table 4-1) are consistent with previous reports of ice-proximal glacial outwash deposits (Boothroyd and Ashley 1975; Aitken 1998; Salamon 2008).

Surface wear features (bullet noses, plucked lee ends, facets, keels, striae) on clasts in unit 2 are interpreted to be glacigenic wear features. The presence of these glacigenic wear features is consistent with lodgement or clast shaping within shear zones in a subglacial environment (Krüger 1979; Sharp 1982; Benn 1994). The high level of consolidation, fissile structure and bimodal distribution of a-axis orientations suggests that unit 2 records a subglacial till (cf. Hicock et al. 1996) emplaced during advance of the Purcell Lobe in MIS 2 (Fraser glaciation).

The stratigraphic sequence of subglacial till (unit 2 at the land surface) directly overlying outwash gravel (unit 1) suggests that the outwash gravel was emplaced in front of the advancing Purcell Lobe. The clay dike is interpreted as a large dewatering structure from loading, which resulted from glacial overriding

(Jolly & Lonergan 2002; Heron & Etienne 2005). A possible source of sediment for the clay dike may be an underlying, unexposed lacustrine deposit. This unconfirmed lacustrine deposit may record a pre-Fraser glaciation Kootenay Lake, possibly associated with Purcell Lobe advance. The elevation of the top of the outwash deposit (unit 1 ~610 m asl) specifies the minimum height of the valley fill at site 19 before ice occupied the site. Assuming no significant deglacial or Holocene infill of Kootenay Lake, the difference in elevation between the top of the outwash and the current floor of Kootenay Lake represents the minimum incision performed by the Purcell Lobe in the Purcell Trench. Kootenay Lake is ~124 m deep (Fisheries and Oceans Canada 2011) near site 19, and so the Purcell Lobe was responsible for >200 m of incision.

5.1.2 Site 41

5.1.2.1 Observations

Site 41 exposes a valley-fill sequence within a ~1.9 km long hummocky bench located just north of the West Arm (Figure 3-1, Figure 3-3) and near the shore of Kootenay Lake within a large alcove in the Purcell Trench named Queens Bay (Figure 5-4). This valley fill sequence extends to an elevation of at least 575 m asl, and has been sheltered from glacial erosion by two bedrock ridges that form the northernmost wall of the alcove (Figure 5-4).

Two exposures, 41A and 41B, were explored (Figure 5-4). Exposure 41A contains *in situ* sediments but most of exposure 41B is located in a slump block. Both exposures reveal a similar six-unit lithostratigraphy (Figure 5-5), but only *in*

situ units in exposure 41A was logged in detail. Unit 6, exposed in the *in situ* foot-wall scarp at exposure 41B is also described.

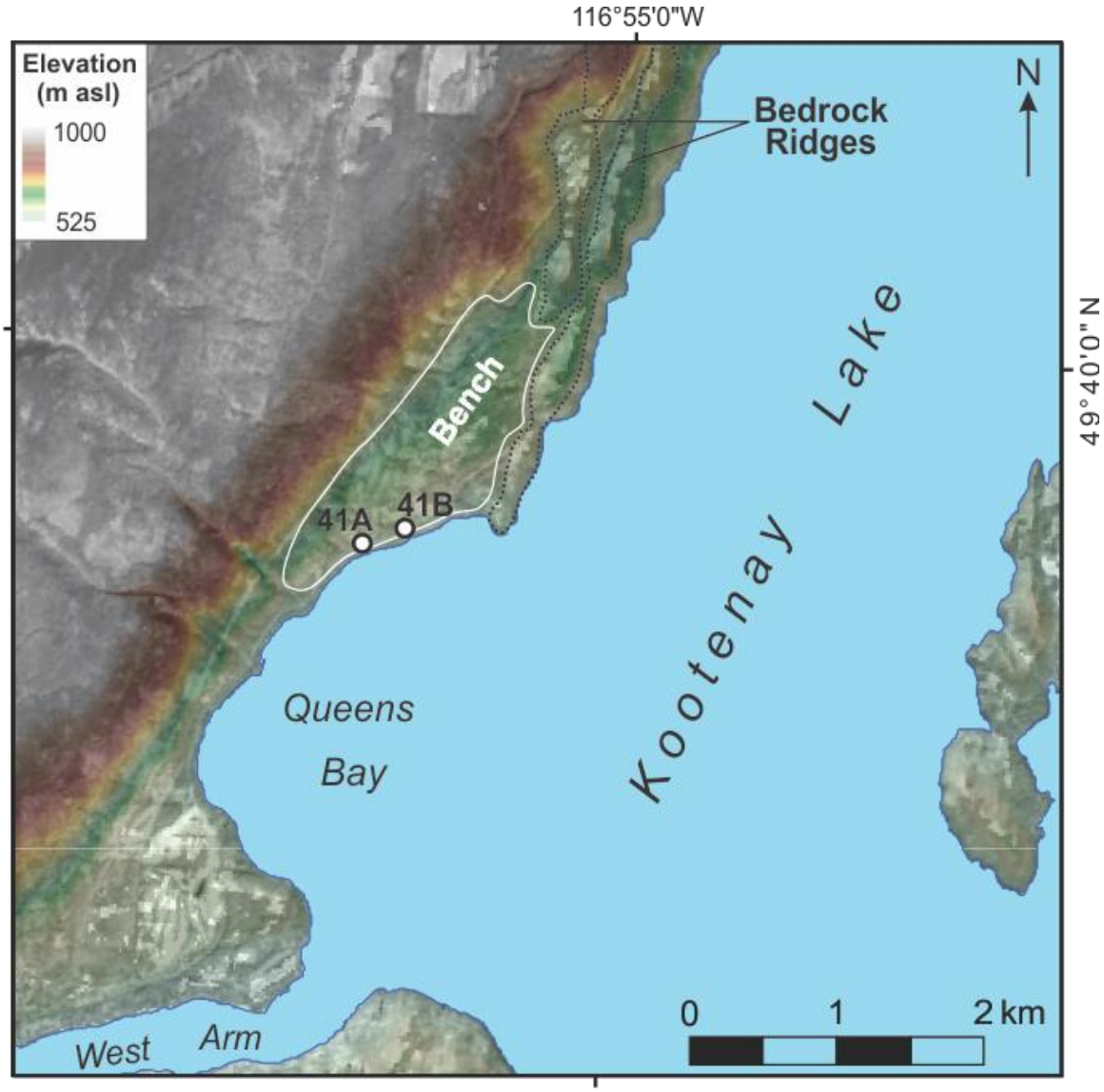

Figure 5-4: Hillshaded DEM (Geobase®) superimposed onto an orthophotograph (clip from 1:250 000 orthophotograph mosaic, 82F. © Province of British Columbia. All rights reserved. Reprinted with permission of the Province of British Columbia.) showing site 41 (exposure 41A and 41B denoted as white dots) located on a bench (white outline) positioned between the western wall of the Purcell Trench and two bedrock ridges (within black dotted lines) to the east. Refer to Figure 3-3 for the site location within the Purcell Trench.

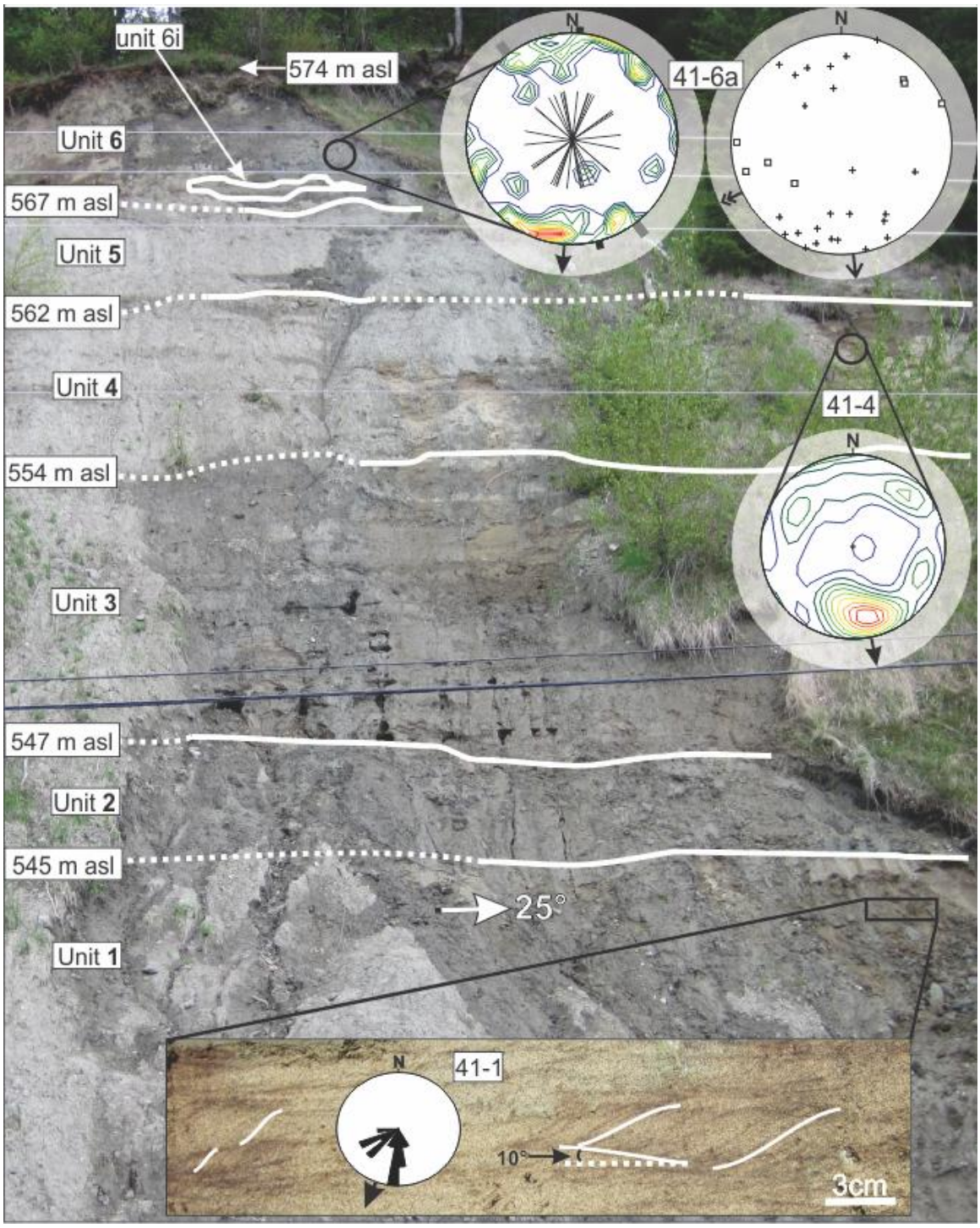

Figure 5-5: Site 41 exposure 41A showing unit boundaries and their elevations as well as locations and stereograms for gravel fabric 41-4 (Table 5-1) and diamicton fabric 41-6a (Table 5-2). Refer to Figure 4-1 for stereogram legend. Unit 6 contains an intra-unit sand lens (unit 6i) highlighted in unit 6 (Figure 5-7). Inset photograph (bottom) shows type-A ripples in unit 1 (white lines highlight some laminae) and a rose diagram of paleoflow measurements from them (41-1, Table 5-3).

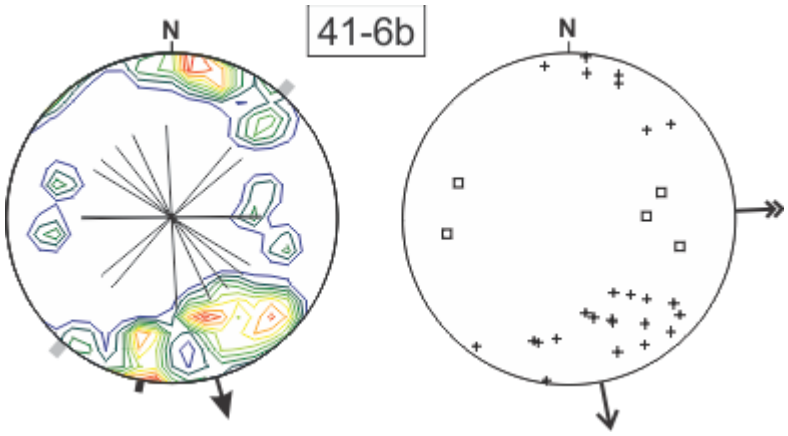

Figure 5-6: Bimodal diamicton fabric 41-6b from exposure 41B, site 41. Refer to Figure 4-1 for stereogram legend.

Table 5-3: Ripple drift cross lamination paleoflow data listed in order of appearance in chapter 5.

Name	**Elevation** (m asl)	**Sand texture**	**Ripple type** (A, B)[1]	**Angle of climb** (°)	**n**[2]	**Azimuth of mean vector** (°)	**Max petal length**[3]
41-1	555	Medium / coarse	A	7-15 (avg = 10)	15	203	3
41-6i	568	Medium	A	2–15 (avg = 7)	15	197	6
21-1b	573	Fine	B	27–30 (avg = 28)	22	250	6
47-1a	529	Medium / fine	B	15-61 (avg = 36)	15	61	5
47-1e	544	Fine	A	15-54 (avg = 32)	15	94	4
46-1	481	Fine	A	15–21 (avg = 18)	19	123	4

[1] After Ashley 1982.
[2] Number of measurements.
[3] Number of measurements within dominant class of the corresponding rose diagram. All corresponding rose diagrams are constructed with 10° classes.

Unit 1 is at least 1.5 m thick (lower contact is not exposed) and forms a groundwater aquifer. It is composed of type A cross-laminated coarse and medium sand with some fine sand and frequent granules (Sr; Table 4-1) recording a southwestward paleoflow (41-1, Figure 5-5, Table 5-3). Cross-laminated cosets with modest angles of climb (7°-15°) range from 1-6 cm thick; generally, the coarsest sand forms the thickest cosets.

Unit 2 is ~2 m thick (Figure 5-5) with a sharp lower contact and tabular architecture. It is composed of saturated, blue, massive clay (Fm, Table 4-1). The lower contact is defined by a 5 cm thick, highly consolidated bed of orange clay.

Unit 3 is 5-7 m thick, has tabular architecture and a sharp lower contact intruded into by burst-out structures (Nichols et al. 1994) the blue clay of unit 2. It is composed of laminated (<0.01 m thick laminae) to bedded (up to ~0.3 m thick beds) sand, silt and clay lithofacies (Sr, Sd, Sm, Fd, Fm and Fl, Table 4-1). The unit is dominated by cross-laminated sand capped by laminated silt and clay; massive and deformed lithofacies are common near the bottom (lowest 0.6 m) of the unit; cross-laminated sand beds are often capped by laminated fine-grained sediment through most of the unit. Whereas the vast majority of lithofacies are laterally continuous through the exposure and appear planar, but a few are lenticular. Most Sd and Fl beds fine upwards, and are capped by clay; however, some beds display inverse grading and coarsen up from fine and medium sand to granules or coarse sand. Soft sediment deformation structures (convolutions, flame structures, ball and pillow structures, burst-out (Nichols et al. 1994)

structures) are common. A prominent (0.09 m thick) silty, calcareous precipitate bed crops out near the middle of unit 3 (~1.5 m below the contact with unit 4). This bed is bounded by deformed clay and sand lithofacies. In places, the clay has ruptured through the precipitate as small (<0.05 m long) vertical dikes.

Unit 4 is ~8 m thick with a sharp lower contact and tabular architecture. It is composed of alternating unconsolidated planar-stratified and massive gravel lithofacies (Gp and Gm, Table 4-1) that have an average thickness of ~13 cm. The gravel beds display inverse grading, coarsening up from coarse sand and granules to clast-supported pebbles and cobbles (maximum b-axis of 0.06 m) in a silty, sandy granule matrix; in places the gravel is openwork. Pebbles and cobbles are composed of foliated metamorphic rock with a metallic luster, dominantly subrounded (41-4, Table 5-1) and imbricated (clasts a-axes are dominantly a(t), 41-4, Table 5-1). A fabric from a massive, imbricated gravel bed records a southward eigenvector (41-4, Figure 5-5, Table 5-1).

Unit 5 is 5 m thick with a sharp lower contact and tabular architecture. It is composed of planar and lenticular coarse to fine sand, silt and clay lithofacies (Sr, Sd and Fd; Table 4-1). Typically the coarse and fine-grained lithofacies alternate and deformation is strongest low (bottom ~1 m) in the unit. Some sand beds coarsen upwards. Though similar in structure to units 1 and 3, unit 5 possesses very few coarse sand lithofacies, resulting in finer overall texture.

Unit 6 is 7 m thick at exposure 41A with a sharp lower contact and tabular architecture; the top ~3 m of the unit is visible at exposure 41B. Unit 6 is composed of massive, matrix-suported silty clay diamicton (Dmm, Table 4-1)

containing many subrounded pebbles and cobbles (41-6a, Table 5-2) with surface wear features (striae, bullet noses, plucked lee ends, 41-6a and 41-6b, Table 5-2), and a ~2.5 m long, deformed sand lens (Figure 5-5). Diamicton fabrics are bimodal with southward principal eigenvectors (41-6a, 41-6b, Table 5-2, Figure 5-5, Figure 5-6). Pebble striae exhibit no preferred orientation (Figure 5-5, Figure 5-6); however, the highly foliated clast lithology made identification of all but the most obvious striations difficult.

Unit 6 also contains an irregularly shaped intra-unit sand lens (unit 6i, Figure 5-5, Figure 5-7) containing mainly deformed (sheared) type A cross-lamination in medium and coarse sand interbedded with fine sand and a single 1 cm thick clay bed located near the stratigraphic center of the unit (Sd and Sr, Table 4-1) (Figure 5-7). The shearing in unit 6i is oriented roughly north-south (Figure 5-7b). Relatively undeformed ripples record a southward paleoflow (41-6i, Table 5-3, Figure 5-7).

5.1.2.2 Interpretation

With the available observations, there is no way to rule out the possibility that the sharp lower contacts separating the six units at site 41 record erosional unconformities. However, until independent dating controls are established the available geomorphic and stratigraphic associations, as well as Occam's razor—suggest that the deposit is best interpreted as part of the record of a single glaciation (in this case, the Fraser Glaciation).

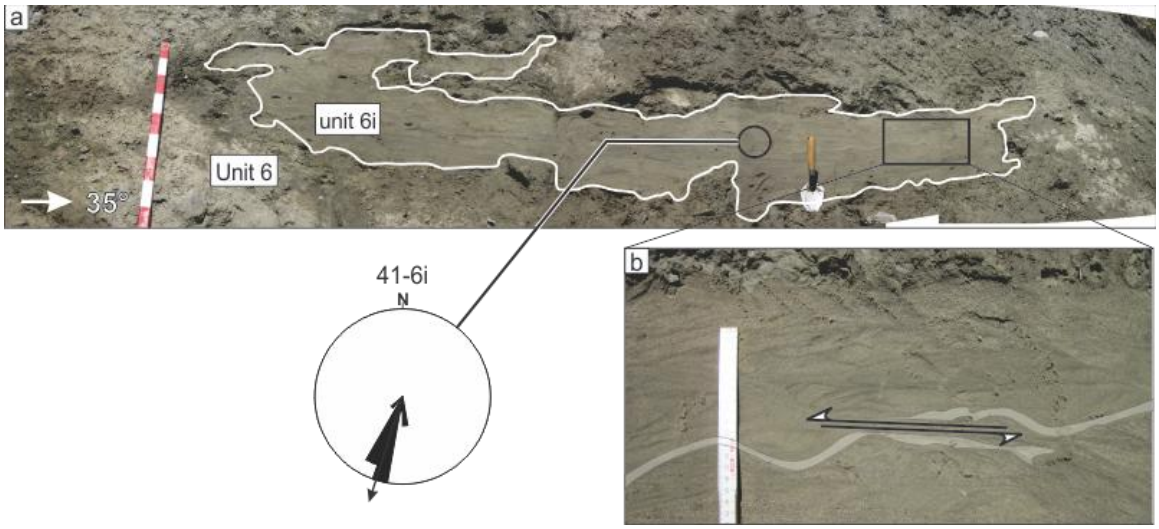

Figure 5-7: a) Site 41, unit 6 contains an irregular, intra-unit sand lens (unit 6i, bounded by white line). The location of the ripple paleoflow measurements (41-6i, Table 5-3) and corresponding rose diagram are displayed. Metre stick has decimetre markings. b) Unit 6i exhibits shears. Sense of shear (arrows) through a clay bed (outlined in grey) in unit 6i is highlighted; displacement along this shear is 10 cm. Ruler is ~1.5 cm wide.

The coarse sand ripples of unit 1 record deposition in a fluvial or inflow-proximal) (possibly ice-proximal) lacustrine depositional environment (Smith 1974; Maill 1977; Postma 1990; Aitken 1995) by a southward flowing river or turbidity current. The thick massive clay of unit 2 records a period of suspension settling in a lake (Smith & Ashley 1985). Unit 3 consists of normally- and inversely-graded cross-laminated sand capped with clay, suggesting deposition by low-energy grain flows and turbidity flows into a lake environment (Nemec 1990; Postma 1990). Clay intrusions from unit 2 and load structures low in unit 3 record deformation from increased interstitial pore pressures possibly caused by rapid deposition onto saturated sediment (Nichols et al. 1994). The inversely-graded planar and massive beds of unit 4 indicate dispersive pressure and rapid deposition during grain flows (Sallenger 1979; Lowe 1982; Postma 1990; Eyles

et al. 1987). Grain flow deposits with openwork areas and some imbrication suggest deposition on a steep alluvial-fan delta prograding off the valley wall (Lowe 1982; Nemec & Steel 1988; Nemic 1990; Nemec et al. 1999). The weakness of the 41-4 gravel fabric (principal eigenvalue of 0.52, Table 5-1) may be attributed to space-filling in the open-framework gravel. The steep, near angle of repose, depositional environment of a confined fan delta and the southward orientation of the primary eigenvector suggest that the inclination of the bedding (about normal to the exposure face) is steeper than the principal plunge of imbricated clasts. Thus, paleoflow is interpreted as southward and unit 4 is interpreted as a rapidly-deposited, steep alluvial-fan delta prograding from the valley wall toward the Purcell Trench. The well-sorted fine-grained laminae and sand beds of unit 5 also indicate water lain sediment. The inversely graded and massive planar sand beds interbedded with lenticular sand beds indicate deposition from grain flows or low-energy turbidity currents (Lowe 1982; Nemec 1990; Postma 1990). Thus, unit 5 is interpreted as a return to low-energy lake-bed sedimentation, possibly resulting from a reduction in sediment supply to this site.

The surface wear features (bullet noses, plucked lees, striations) on clasts in unit 6 are interpreted to be glacigenic wear features (Krüger 1984). The presence of these glacigenic wear features is indicative of lodgement or clast shaping within shear zones in a subglacial environment (Krüger 1979; Sharp 1982; Benn 1994). The high level of consolidation, fissile structure, and southward principal eigenvector of the bimodal diamicton fabrics further suggest

unit 1 is a subglacial till (e.g., Lian & Hicock 2000) emplaced by the southward flowing Purcell Lobe. In this context, the intra-till deformed and rippled sand lens (unit 6i) likely records deposition in a small meltwater conduit at the ice bed (e.g., Berthelsen 1979; Hart & Roberts 1994; Evans et al. 1995; Benn and Evans 1996). Ice-bed recoupling resulted in the shearing of this sand; the north-south shear plane displacement is consistent with glaciotectonism during southward advance of the Purcell Lobe.

In summary, the stratigraphy exposed at site 41 is interpreted to show a record of the southward Purcell Lobe advance in MIS 2. This ice advance resulted in a period of ponded water in the topographic low formed between the Purcell Lobe, the bedrock ridges, and the valley wall. The till cap was deposited after the Purcell Lobe overtopped the bedrock ridges. It is important to note that no lacustrine sediment is found above till in this stratigraphic sequence—no evidence of a proglacial or postglacial lake exists above the subglacial sediment at this location in the Purcell Trench.

The elevation of the top of unit 5 (~567 m asl) specifies the minimum local height of the preglacial valley fill that occupied the Purcell Trench at site 41. Assuming no significant glacial, deglacial or Holocene infill of Kootenay Lake, the difference in elevation between the top of the glacial advance lake sediments and the current floor of Kootenay Lake represents the minimum incision performed by the Cordilleran Ice Sheet in the Purcell Trench. Near site 41 Kootenay Lake is ~132 m deep (Fisheries and Oceans Canada 2011), which results in a minimum of ~167 m of incision by the Purcell Lobe.

5.1.3 Site 53

5.1.3.1 Observations

Site 53 is a small roadside exposure located on the east side of the Purcell Trench at 605 m asl (top of exposure; DEM, Geobase®) (Figure 3-2, Figure 5-8a). The roadcut exposes two lithostratigraphic units emplaced next to, and on top of, a 4 m high, striated (striae orientation: ~200°) bedrock knob (Figure 5-8b). The bedrock apparently sheltered the sediment from glacial erosion because no other valley-wall geomorphology offers a preservation mechanism for the deposit (Figure 5-8b).

Unit 1 is at least 4 m thick and composed of well-consolidated, fissile, grey-coloured, matrix-supported clayey-silt diamicton (lithofacies Dmm, Table 4-1) containing 10-15% clasts that range from 1-10 cm along their b-axes and are dominantly subrounded and subangular (53-1, Table 5-2). Many clasts exhibit surface wear features (plucked lee ends, bullet noses, keels, facets and/or striae; Table 5-2). The diamicton fabric (53-1, Figure 5-8c, Table 5-2) within unit 1 is unimodal with striae, plucked ends and bullet noses aligned with the principal eigenvector and parallel to the local valley wall. Plucked lee ends and bullet noses show no preferred direction.

Unit 2 is up to 3 m thick and has a conformable lower contact (Figure 5-8b). It is composed of orange-coloured, massive, unconsolidated, clast-rich (>50% clasts) sandy diamicton (Dcm, Table 4-1). Most clasts are angular cobbles.

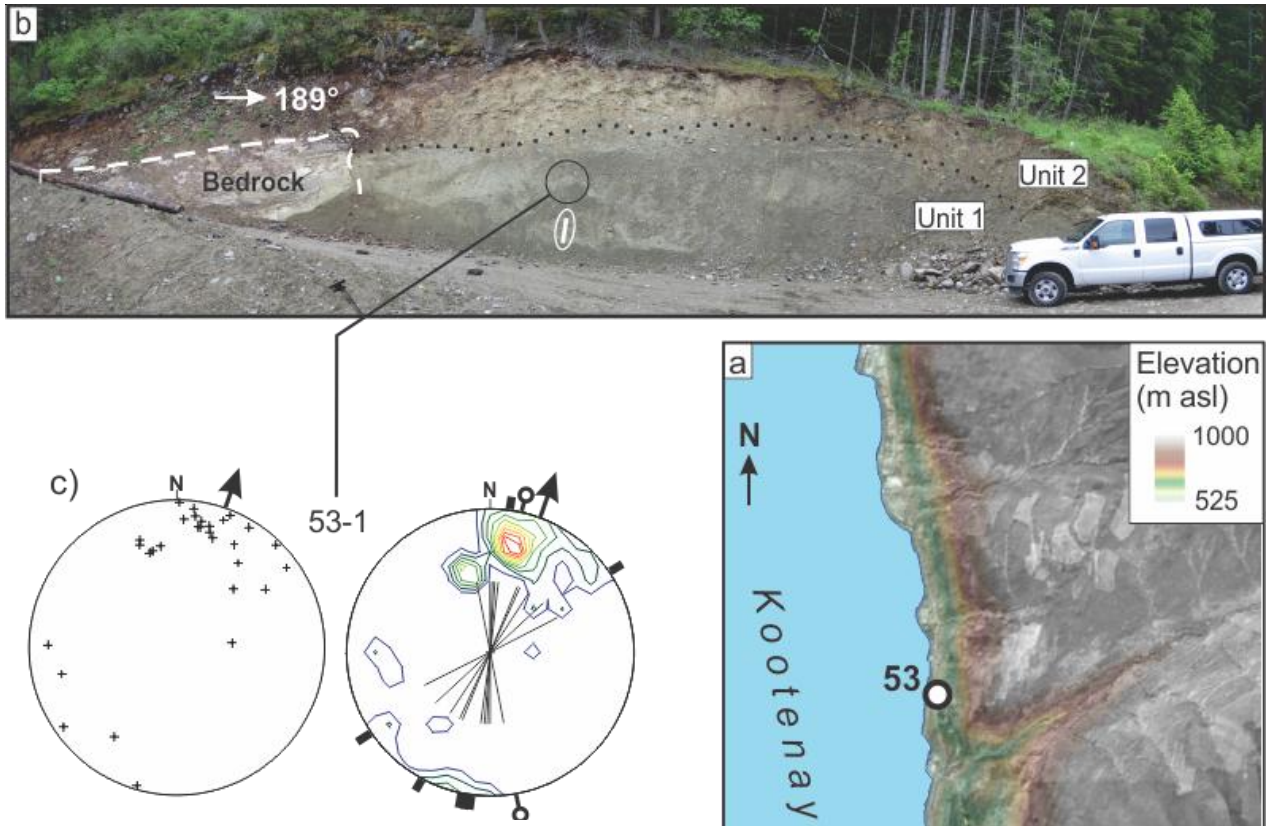

Figure 5-8: a) Hillshaded DEM (Geobase®) superimposed onto an orthophotograph (clip from 1:250 000 orthophotograph mosaic, 82F, Province of British Columbia) showing the location of site 53. The geomorphology of the Purcell trench offers no protection from glacial erosion at this site; deposit preservation is enabled locally by the bedrock knob outlined in "b". Refer to Figure 3-2 for site location within the Purcell Trench. b) Site 53 exposure showing contact between units 1 and 2 and their relationship to the local bedrock knob. The location of diamicton fabric 53-1 (Table 5-2) is circled and corresponding scatter and contour stereograms are presented. Refer to Figure 4-1 for stereogram legend.

5.1.3.2 Interpretation

Surface wear features (bullet noses, plucked ends, facets, keels, striae) of clasts in unit 1 are interpreted to be glacigenic wear features (Kruger 1979, 1984). The presence of these glacigenic wear features is indicative of subglacial lodgement or clast shaping within shear zones in a deforming bed (Krüger 1979, 1984; Sharp 1982; Benn 1994). The high level of consolidation, fissile structure and a valley-parallel unimodal distribution of a-axis orientations also support a subglacial till interpretation (Hicock et al. 1996). The orientation of the glacigenic wear features suggest lodgement and deformation (rotation) during till formation (e.g., Lian & Hicock 2000). The valley-parallel fabric is consistent with emplacement by the south-flowing Purcell Lobe during its advance.

The unsorted sediments and angular clasts that comprise unit 2 may have resulted from deposition as colluvium (Eyles et al. 1987). Unit 2 is interpreted as postglacial colluvium based on its geomorphic (sloping land surface) and stratigraphic (above subglacial till) context.

5.1.4 Ice advance summary

The sites in this § record MIS 2 till overlying glacial-advance outwash and lake sediments. The minimum elevation of the top of the Purcell Trench valley fill prior to ice occupation was 610 m asl at site 19 and 567 m asl at site 41 (average elevation 590 m asl). This datum provides important context for differentiating potential retreat-phase ice-marginal deposits (including kame terraces) from advance-phase outwash and lake deposits in the Purcell Trench.

5.2 Sites recording ice position during decay

The following sites exposed elevated (above the modern valley floor and Kootenay Lake) interfluve-occupying deposits interpreted as recording ice-contact deposition. They record the height of the decaying Purcell Lobe during the termination of MIS 2. Deposits in this § reach elevations of ~600-725 m asl (up to 115 m above the advance-phase outwash/till contact).

5.2.1 Site 27

5.2.1.1 Observations

Site 27 is an inactive gravel pit near Kaslo on a ~700 m asl (at site 27) gravel bench that occupies an alcove at the junction of the Kaslo River valley and the Purcell Trench (Figure 3-3, Figure 5-9a). Just south of the site, the gravel bench abuts a series of subparallel bedrock ridges oriented roughly north-south (Figure 5-9a). East of the site, Kaslo occupies the modern Kaslo River delta (at ~550 m asl) (Figure 5-9a).

A 2.5 m tall exposure at site 27 contains a single lithostratigraphic unit (unit 1) composed of ~1 m thick, normally-graded planar-stratified gravel (Gp, Table 4-1) (Figure 5-9b). This exposure is positioned above and adjacent to the main pit wall, which is ~10 m tall and has been covered by talus; this suggests a likely unit thickness of at least 10 m. The gravel clasts range in size from small pebbles to small boulders and are typically well-rounded to rounded (27-1, Table 5-1). The unit is clast supported in a matrix of poorly-sorted sand. A paleoflow estimate from imbricate, dominantly a(t) pebbles is southward, which is

consistent with the gentle southward slope of the gravel beds (Figure 5-9b, Figure 5-9c; 27-1, Table 5-1).

5.2.1.2 Interpretation

The single lithostratigraphic unit exposed at site 27 is inferred to record deposition by a south-flowing gravel-bed river because of its clast size and roundness, planar-stratified character, normally-graded bedding and fabric. The planar-stratified, normally-graded gravel lithofacies containing dominantly a(t) clasts is consistent with deposition from traction transport (dominated by rolling) in shallow stream flows (Eynon & Walker 1974; Miall 1977; Maizels 1993; Kjaer et al. 2004). A paleoflow direction towards the south is interpreted from the clast imbrication.

The elevated (700 m asl) valley-wall position of the gravel bench and its valley-parallel paleoflow direction suggest that the gravel-bed river was supported by ice or valley fill sediment in the Purcell Trench. Because the bench is at least 100 m higher than the identified till-advance phase outwash contact (567 m asl, site 41, Figure 5-5; 610 m asl, site 19, Figure 5-3) and there is no evidence of overriding by the Purcell Lobe (capping till or gravel deformation), it is unlikely that this deposit is advance-phase outwash. Thus, this gravel is interpreted as an ice-marginal gravel-bed stream deposit—a kame terrace.

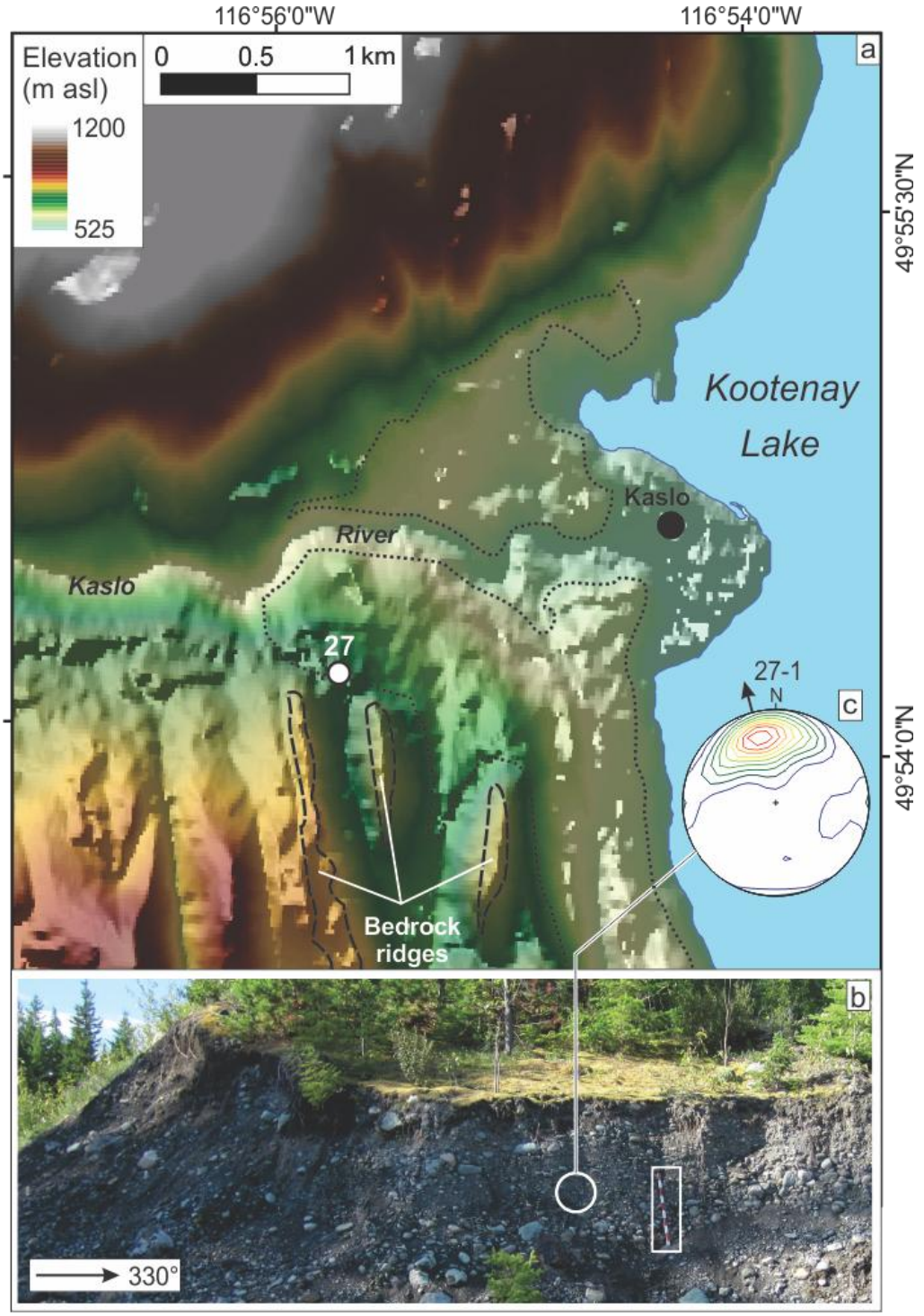

Figure 5-9: a) Hillshaded DEM (Geobase®) showing the location of site 27 (white dot) on top of an elevated gravel bench (outlined by black dotted lines) west of Kaslo, BC (Figure 3-3) that occupies the alcove formed at the junction of the Kaslo River valley and the Purcell Trench (Kootenay Lake) just north of a series of valley-parallel bedrock ridges (black dashed outlines). b) Inclined, planar-stratified imbricate gravel (Gp, Table 4-1) at site 27. Metre stick (in white box) has decimetre markings. White circle marks location of gravel fabric 27-1. c) Contoured stereogram of gravel fabric 27-1 (southward paleoflow) (Table 5-1). Refer to Figure 4-1 for stereogram legend.

5.2.2 Site 30

5.2.2.1 Observations

Site 30 is on the west side of the Purcell Trench 19 km north of Kaslo (Figure 3-3). It comprises two exposures and three lithostratigraphic units. Exposure 30A is ~25 m tall and positioned 90 m northwest of exposure 30B (Figure 5-10b). Most of exposure 30A was inaccessible or unsafe (Figure 5-11a), but exposure 30B (~3 m tall) afforded safe access to unit 1 (Figure 5-11b). Both exposures and a large, abandoned gravel pit (GP, Figure 5-10b) south of exposure 30B occur within a poorly defined and gullied valley-side bench that is ~320 m long (Figure 5-10b) at an elevation of ~600 m asl. A rockslide (~1.8 km^2) borders the north end of the bench. The bench does not exist north of the landslide and pinches out ~150 m south of the steep-sided gully that dissects the bench (Figure 5-10b).

Three lithostratigraphic units show at exposure 30A; unit 1 is also revealed at exposure 30B (Figure 5-11). Unit 1 is at least 6 m thick (lower contact not exposed) and lies below 596 m asl. It is composed of packed (but not consolidated), planar-stratified gravel (Gp, Table 4-1). Fining-upward gravel beds with sharp lower contacts that truncate lower beds range in thickness from 0.2-0.6 m and in texture from clast-supported cobbles in a coarse-sand matrix to coarse sand with few pebbles; there is a positive relation between bed thickness and coarseness. Clasts are subangular to rounded (30-1, Table 5-1). Clast a-axis orientations are variable, and the gravel fabric records a northeastward principal eigenvector (30-1, Table 5-1). Some isolated massive sand lenses

(0.1–0.15 m thick; 2–3 m lateral extent; Sm, Table 4-1) exist between the gravel beds (Figure 5-11b).

Unit 2 is ~1.75 m thick with a sharp, irregular lower contact that truncates beds in unit 1 (Figure 5-11a). The unit has an apparent dip of 5° towards an azimuth of 100°. It is composed of clast-poor (pebbles to large cobbles), matrix-supported, silty-fine sand diamicton (Dmm, Table 4-1).

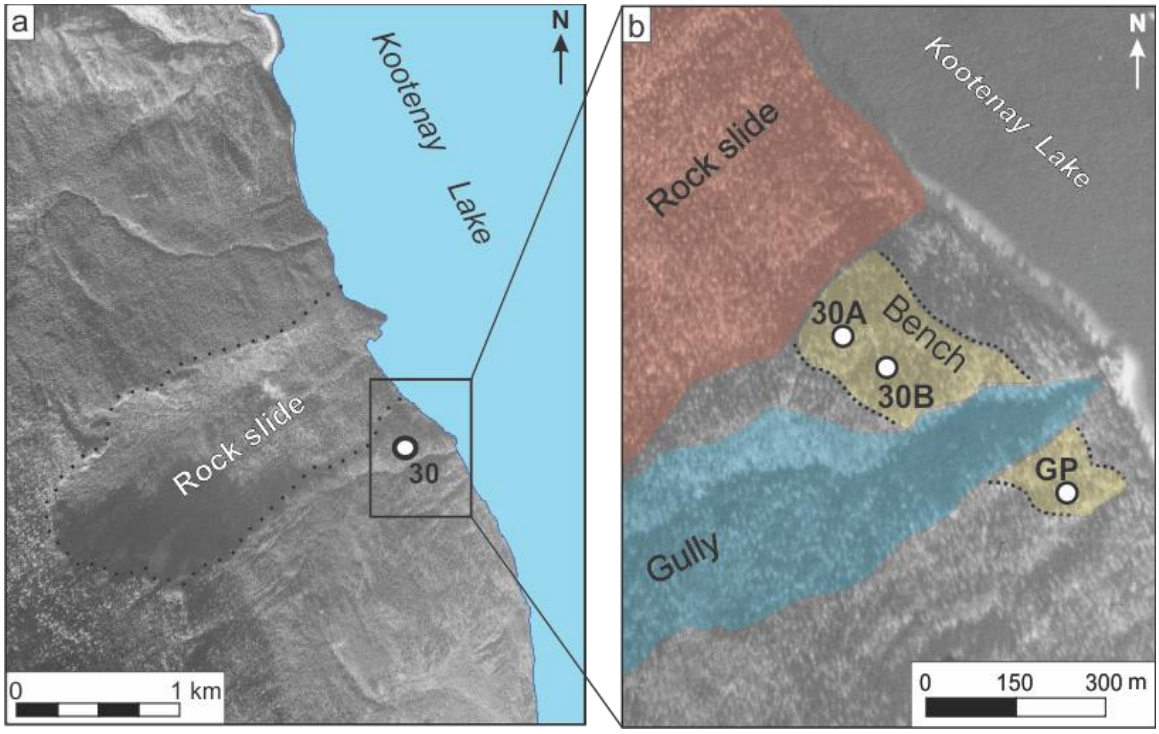

Figure 5-10: a) Aerial photograph (A13796-69; © Department of Natural Resources Canada. All rights reserved.) displays the location of site 30 (labeled circle) on the west side of the Purcell Trench (Figure 3-3), south of a large rock slide (delimited by the dotted line). Box shows location of b). b) Close-up of aerial photograph (op. cit.) showing locations of sections 30A and 30B and an abandoned gravel pit (GP) (labeled circles). These sections occur within a gullied (blue) valley-side bench (yellow) south of the large rock slide (red).

Unit 3 is up to 4 m thick with a deformed and sheared lower contact that incorporates diamictic intrusions from unit 2 (Figure 5-11a). It is composed of coarse gravel beds (Gm, Table 4-1) that exhibit an apparent dip of 10°-20° east (100°). This dip is approximately conformable to the modern land surface slope. Beds are composed of clast-supported large cobbles and small boulders in a sand matrix, or openwork cobbles and/or boulders. Binocular inspection of the gravel beds revealed clast imbrication recording an apparent eastward paleoflow into the Purcell Trench.

5.2.2.2 Interpretation

Unit 1 is inferred to record deposition in a southward-flowing gravel-bed river because of its clast size and roundness, well-sorted and planar-stratified character, normally-graded bedding and fabric. Subrounded, clast-supported gravel beds in a matrix of coarse sand interbedded with some lenses of sand have previously been associated with gravel outwash (Eynon & Walker 1974; Smith 1974; Hein & Walker 1976; Salamon 2008). The variability in clast a-axis orientations may be attributed to cluster bedform geometry (smaller clast rotating around larger obstacle clasts before coming to rest).

Unit 2 is interpreted as a debris flow deposit because of its diamictic texture, massive structure, dip, position at the base of a steep slope (on the bench tread), and a lack of glacially-worn clasts (Lowe 1982). The sharp and irregular lower contact of unit 2 is interpreted as an erosional unconformity.

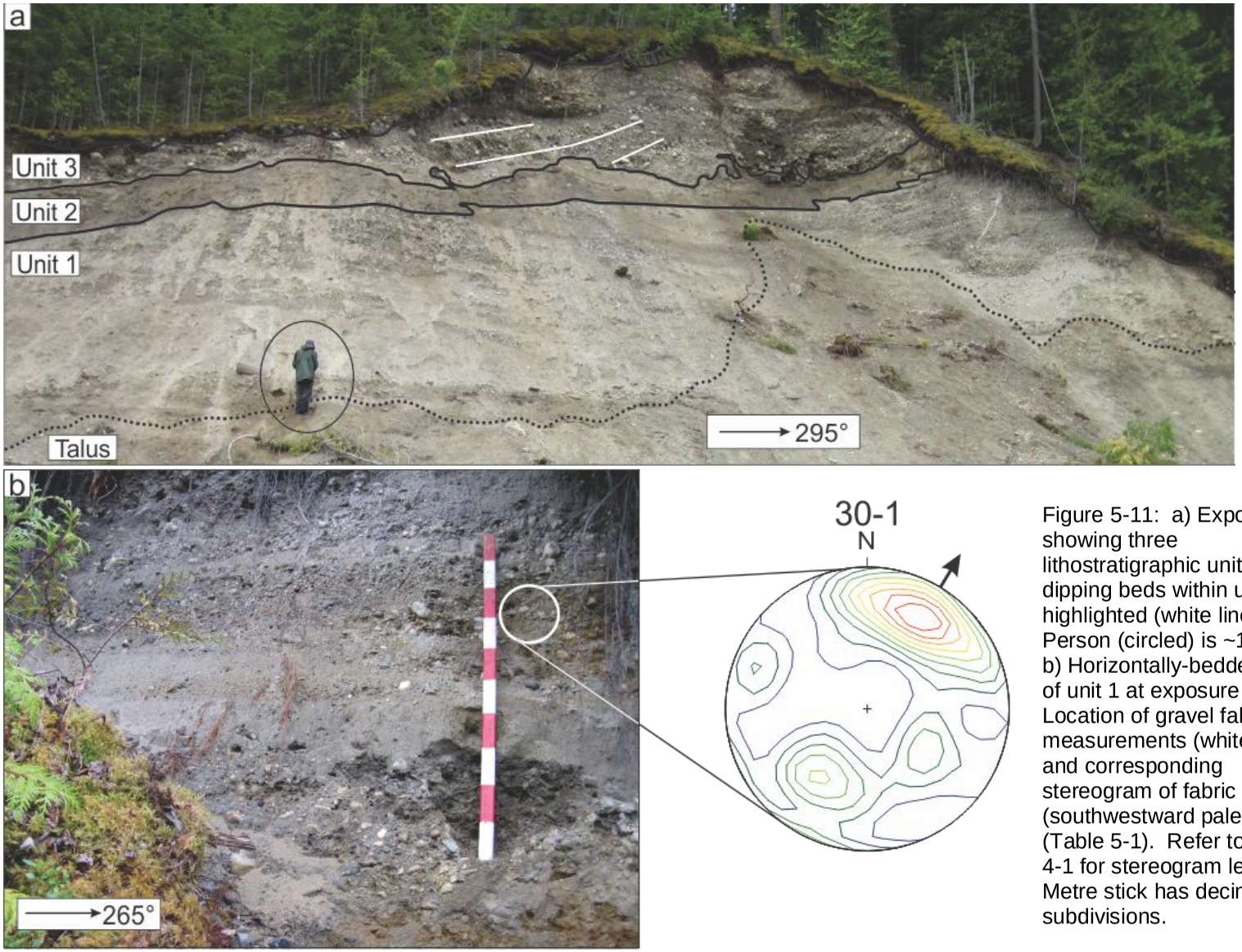

Figure 5-11: a) Exposure 30A showing three lithostratigraphic units. Some dipping beds within unit 3 are highlighted (white lines). Person (circled) is ~1.9 m tall. b) Horizontally-bedded gravel of unit 1 at exposure 30B. Location of gravel fabric measurements (white circle) and corresponding stereogram of fabric 30-1 (southwestward paleoflow) (Table 5-1). Refer to Figure 4-1 for stereogram legend. Metre stick has decimetre subdivisions.

Unit 3 exposes sediment within a subtle, gently-sloped, apron-shaped landform on the northwestern side of the gravel bench (Figure 5-10b). The inclined and massive tabular gravel beds of unit 3 indicate deposition during non-cohesive debris flows and fluvial sheet flows (Blair 1987; Eyles et al. 1987; Blair & McPherson 1994). The diamictic intrusions into the base of unit 3 record shearing and possible fluidization of the underlying diamicton (unit 2) during emplacement of unit 3 (Nichols et al. 1994). Apparent bed dip indicates an eastward (~100°) paleoflow consistent with flow out of the small incised gully (blue, Figure 5-10b). Therefore, unit 3 is interpreted as the progradation of alluvial or colluvial sediments supplied either by the gully-forming creek or a stream in the slide area through a combination of fluvial sheet flows and debris flows (Lecce 1990).

The southwestward paleoflow of unit 1 suggests deposition from a stream flowing parallel to the valley wall. The elevated position of the gravel suggests deposition as advance-phase outwash that filled the Purcell Trench, or as a kame terrace deposited marginal to the Purcell Lobe. Although the gravel is at an elevation consistent with the advance-phase outwash at sites 19 and 41, the lack of a till cap, surface wear features, and glaciotectonisum consistent with a subglacial environment, and a local valley-wall shelter (e.g., bedrock knobs or ridges) from glacial erosion suggests unit 1 is a kame terrace (Figure 5-10a).

5.2.3 Sites 38–40

5.2.3.1 Sites 38–40 geomorphology

Sites 38–40 lie on the east side of Kootenay Lake (Figure 3-3) in the riser of a long (>4 km), thin (0.2-0.7 km) gully-dissected, valley-side gravel bench with an undulatory tread surface that slopes west ~5° (0.08 m/m). The bench reaches an elevation of ~725 m asl at its contact with the Purcell Trench valley wall near its southern extent and slopes north (parallel to the Purcell Trench) ~1° (0.01 m/m) to ~670 m asl (Figure 5-12).

Site 38 is located in the riser of the bench (top of exposure 595 m asl), and the bench is located on an interfluve ~70 m above the north eastern shore of Kootenay Lake (Figure 3-3). At site 39 the bench has been incised by three ephemeral streams (Figure 5-13). Gully 1 terminates at a west-sloping gravel fan below the bench tread; gullies 2 and 3 extend to Kootenay Lake (Figure 5-13). Site 40, the southernmost exposure in the gravel bench, also lies high on the bench riser reaching an elevation of ~630 m asl (top of the exposure) (Figure 5-12). Near site 40 the bench tread widens to 0.7 km (Figure 5-12).

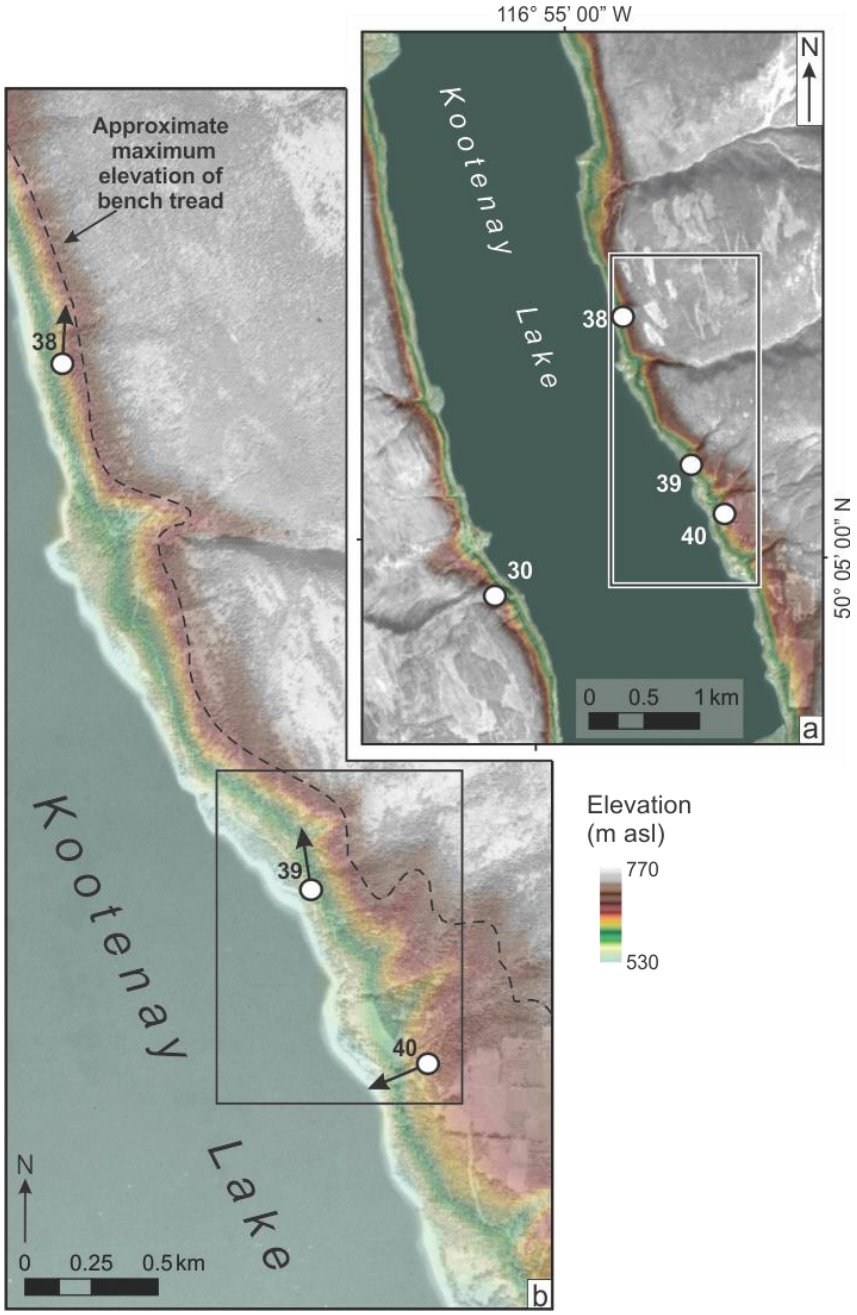

Figure 5-12: a) Hillshaded DEM (Geobase®) superimposed onto an orthophotograph (clip from 1:250 000 orthophotograph mosaic, 82K. © Province of British Columbia. All rights reserved. Reprinted with permission of the Province of British Columbia.) showing the geomorphology around sites 30, 38, 39 and 40. Sites are shown as labeled white dots and the area of b) is outlined (black box). b) Hillshaded DEM (Geobase®) superimposed onto an aerial photograph (A11105-102, NAPL; © Department of Natural Resources Canada. All rights reserved.) showing the extent of the elevated gravel bench exposed by sites 38, 39 and 40. Sites are shown as white dots with arrows indicating local mean paleoflow direction measured in gravel lithofacies. Paleoflows at sites 38 and 40 are derived from gravel fabrics 38-1a, b, c and 40-1, respectively (Figure 5-14, Figure 5-18, Table 5-1). Paleoflow at site 39 is inferred from the orientation of dipping gravel beds (site 39, exposure 39D, unit 3, Figure 5-17). Black box shows the location of Figure 5-13. Refer to Figure 3-3 for locations within the Purcell Trench.

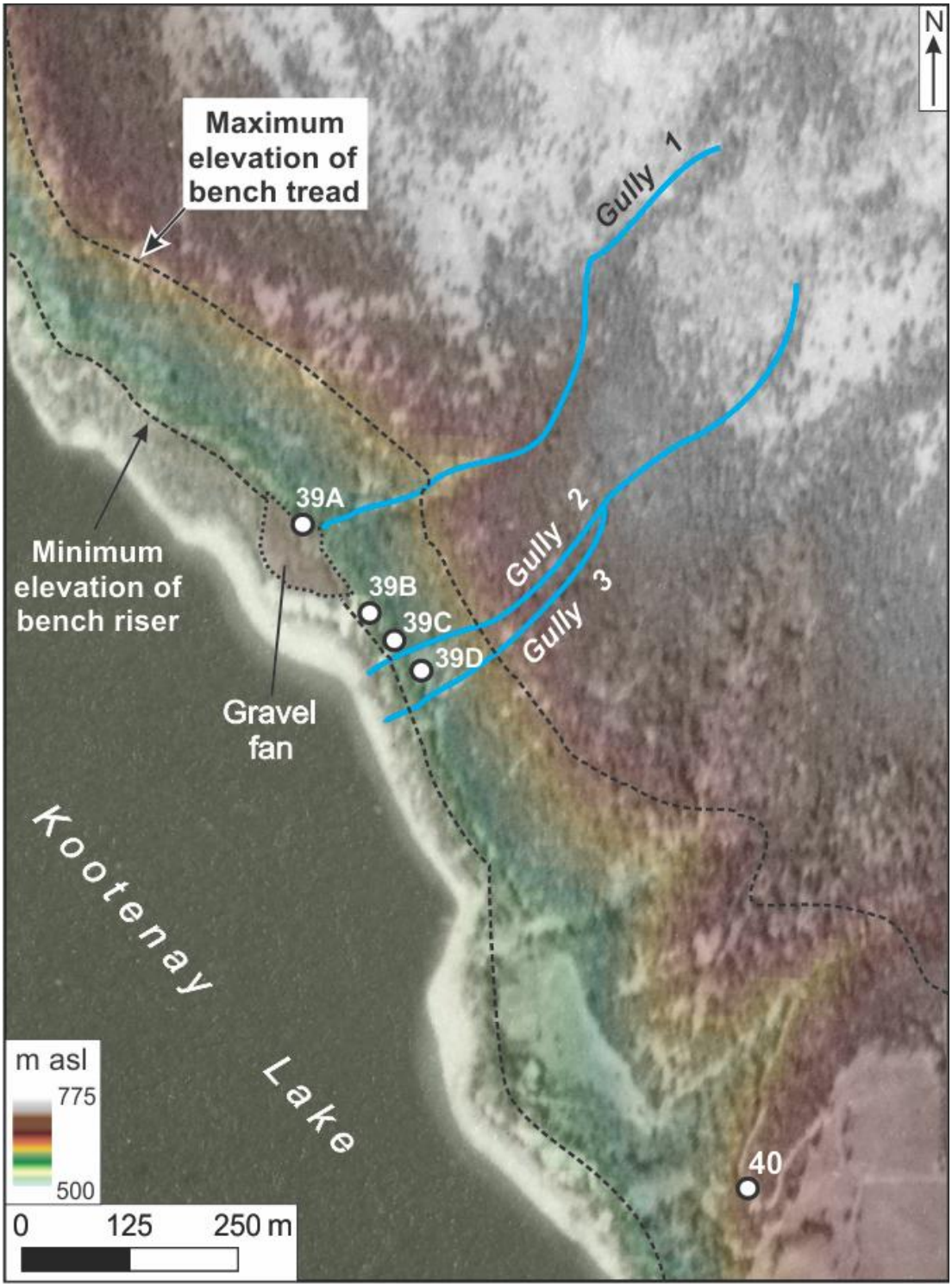

Figure 5-13: Hillshaded DEM (Geobase®) superimposed onto an aerial photograph (A11105-131; © Department of Natural Resources Canada. All rights reserved.) showing the four exposures (39A-39D) at site 39, and site 40 (white dots) within an elevated and gullied valley-side bench. Gully 1 terminates in a gravel fan below the bench riser, whereas gullies 2 and 3 extend to Kootenay Lake and do not terminate in topographically-distinct gravel fans. The area between the dashed lines denotes the thin bench tread (red and yellow tones) and the bench riser (green tones). Refer to Figure 3-3 and Figure 5-12 for site location within the Purcell Trench.

5.2.3.2 Site 38 sedimentology

A single lithostratigraphic unit (unit 1) containing planar-stratified and trough cross-stratified sand and gravel lithofacies (Sp, Gp and Gt, Table 4-1) is revealed at the >190 m long, 7 m high exposure at site 38. Gravel beds 0.1–0.25 m thick are composed of upward-fining, imbricated, clast-supported cobbles and pebbles in a poorly sorted matrix of sand and granules. Planar-stratified medium and coarse sand forms a few lenses >10 m in length. Most gravel clasts display a similar lithology: foliated, metamorphic rock with a metallic lustre. Clast roundness varies from angular to well-rounded, most clasts are subrounded (38-1a, 38-1b, 38-1c, Table 5-1). Imbricated clasts are dominantly a(t) or a(o) and record northward paleoflow directions (38-1a, 38-1b, 38-1c, Figure 5-14, Table 5-1). Two small (0.1 – 0.25 m apparent length), imbricated, unconsolidated, medium sand clasts (Figure 5-13c) within the gravel beds also record a northward paleoflow direction. Four near vertical faults, with offsets ranging from ~0.1 – 0.15 m, occur in the far northern end of the exposure adjacent to a small gully (Figure 5-14).

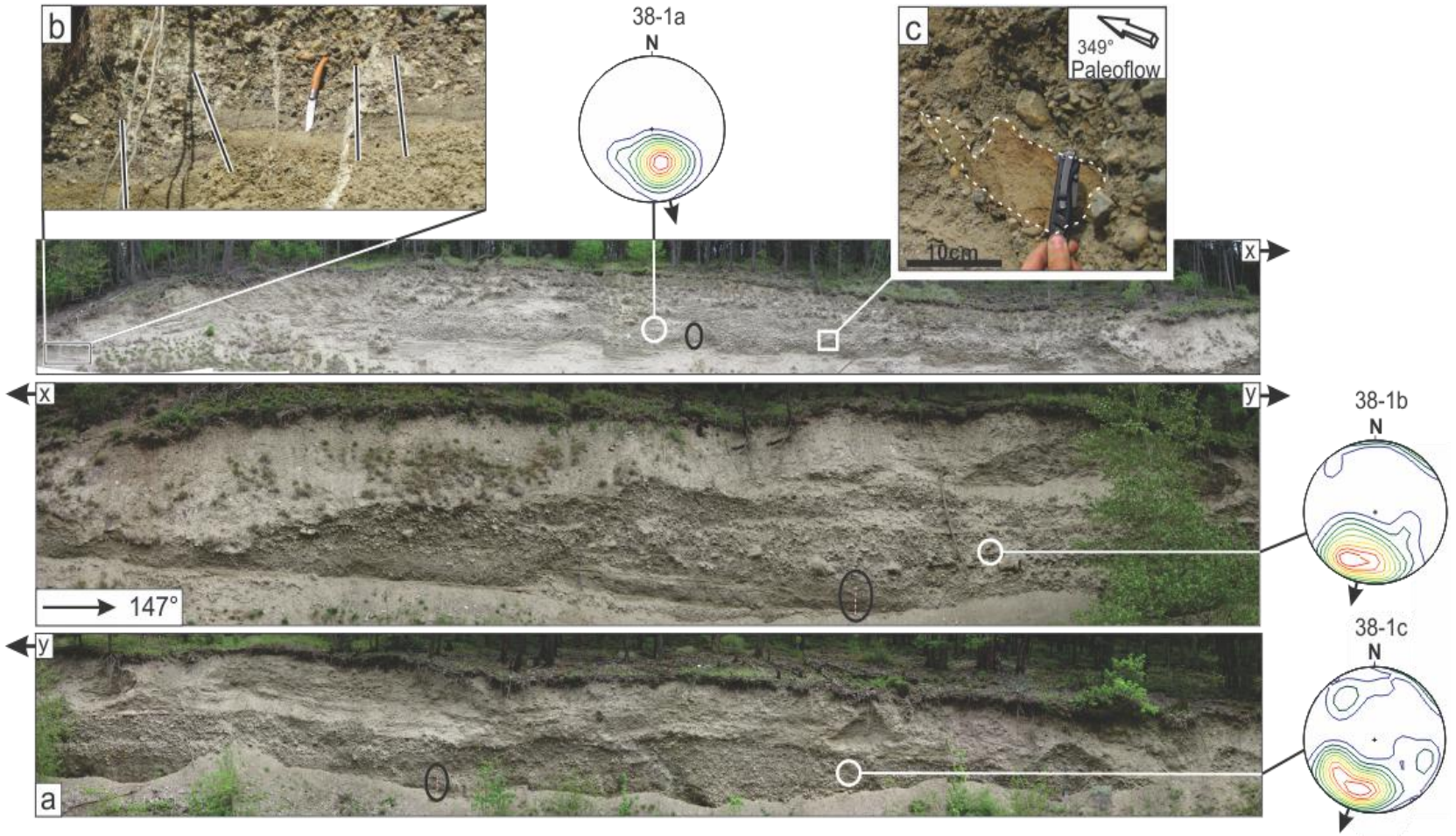

Figure 5-14: a) Panorama of the single lithostratigraphic unit exposed at site 38 (190 m long exposure). Locations of gravel fabrics are shown and corresponding stereograms, which record a northward paleoflow, are provided. Refer to Table 5-1 for fabric data and Figure 4-1 for stereogram legend. Metre sticks are circled (black circles). b) Steep faults in the northern end of the exposure. The knife is 16 cm long. c) Imbricated medium sand rip-up clast records a northward paleoflow.

5.2.3.3 Site 38 interpretation

Planar-stratified sand and gravel lithofacies (Sp and Gp) with some cross-stratified gravel lithofacies (Gt) and northward paleoflows at site 38 indicate deposition in a north-flowing gravel-bed stream (Smith 1974; Miall 1977; Salamon 2008). The subrounded gravel suggests relatively short transport distances (Mills 1979). The preservation of imbricated soft-sediment rip-up clasts suggest that the sand was frozen and/or it was ripped up, transported only a short distance before deposition, and rapidly buried (high sedimentation rates) (Allen 1982; Knight 2009). Fluvial deposition at this height makes the gravel part of a valley fill, or an ice-marginal stream (kame terrace). The northward paleoflow is difficult to explain using a valley-fill interpretation because advance or retreat-phase outwash would likely flow south away from the southern margin of the Purcell Lobe. Thus, the gravel at site 38 is interpreted to record kame terrace formation.

5.2.3.4 Site 39 sedimentology and stratigraphy

Seven lithostratigraphic units are revealed in four exposures at site 39 (Figure 5-13): unit 1 at exposure 39B; units 2-5 at exposure 39D; unit 6 at exposure 39C; and unit 7 at exposure 39A (Figure 5-15). Unit 1 constitutes the lithostratigraphically oldest unit at site 39, being located lowest on the riser of the bench (exposure 39B, Figure 5-13, Figure 5-15) 554 - 571 m asl (Figure 5-16). It consists of laminated and massive fine-grained lithofacies and planar-stratified and massive sand lithofacies (Fl, Fm, Fd, Sp and Sm, Table 4-1) that show an overall upward fining (Figure 5-16). The thinly-bedded and laminated sediments

are tilted 21° towards 208° (i.e. towards the Purcell Trench; Figure 5-13) and typically display a cyclic normal-grading from fine sand and silt to clay (they are rhythmites). The sediment at exposure 39B is highly consolidated and most of the clay laminae are oxidized an orange colour. Indurated white precipitate beds appear throughout the exposure (Figure 5-16). Some silt – clay couplets contain very small silt rip-up clasts (~554.5 m asl, log 39B-1, Figure 5-16). Near the bottom of log 39B-3 laminated very fine silty sand drapes a large highly spherical and rounded granitic pebble (Figure 5-16). Normal faulting in unit 1 is pervasive (Figure 5-16) with no preferred direction and with displacements ranging from <0.01-0.30 m. Some normal faults propagate through the entire exposure, though most are limited to only a few beds; reverse faults are rare (Figure 5-16). Dewatering structures (flame and ball-and-pillow structures) are also common in unit 1 (Figure 5-16).

Exposure 39D reveals four lithostratigraphic units (units 2-5) towards the top of the bench riser (Figure 5-15, Figure 5-17a). Lowest in the exposure is unit 2 (Figure 5-17a), which is at least 1.3 m thick (lower contact not exposed) and composed of massive clast-supported silty diamicton (Dcm, Table 4-1). The clasts range from pebbles to small cobbles, mostly angular (39-2, Table 5-2). Clast surface wear features are rare: two of the clasts sampled for fabric analysis from unit 2 were striated (39-2, Figure 5-17a). A diamicton fabric reveals a bimodal distribution with primary and secondary mode eigenvalues oriented toward the northwest and west, respectively (39-2, Figure 5-17a; Table 5-2).

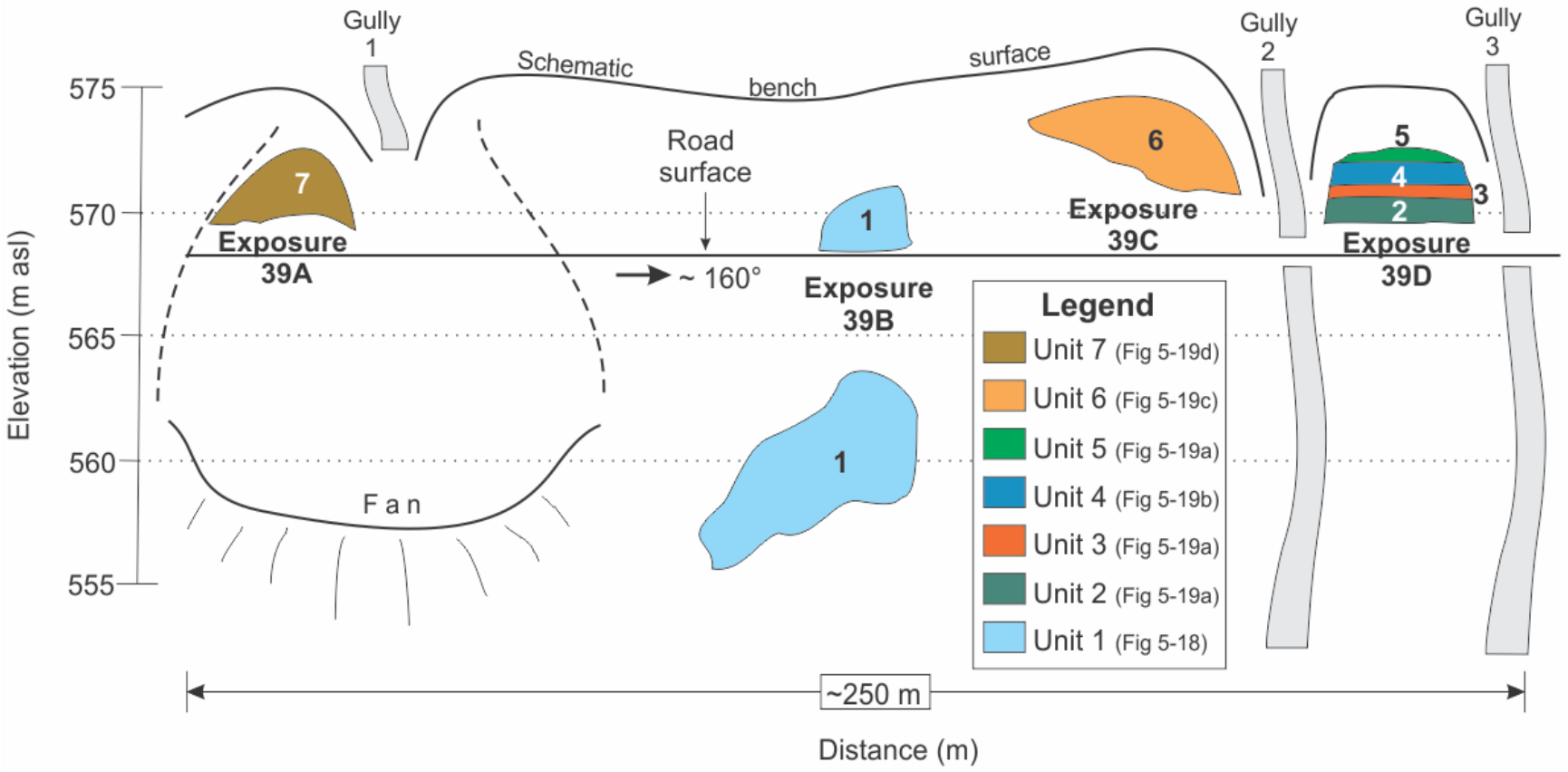

Figure 5-15: Sketch of relative position and stratigraphy at exposur es 39A-39D at site 39 as viewed from Kootenay Lake looking east. Figures detailing individual lithostratigraphic units are referred to in the legend.

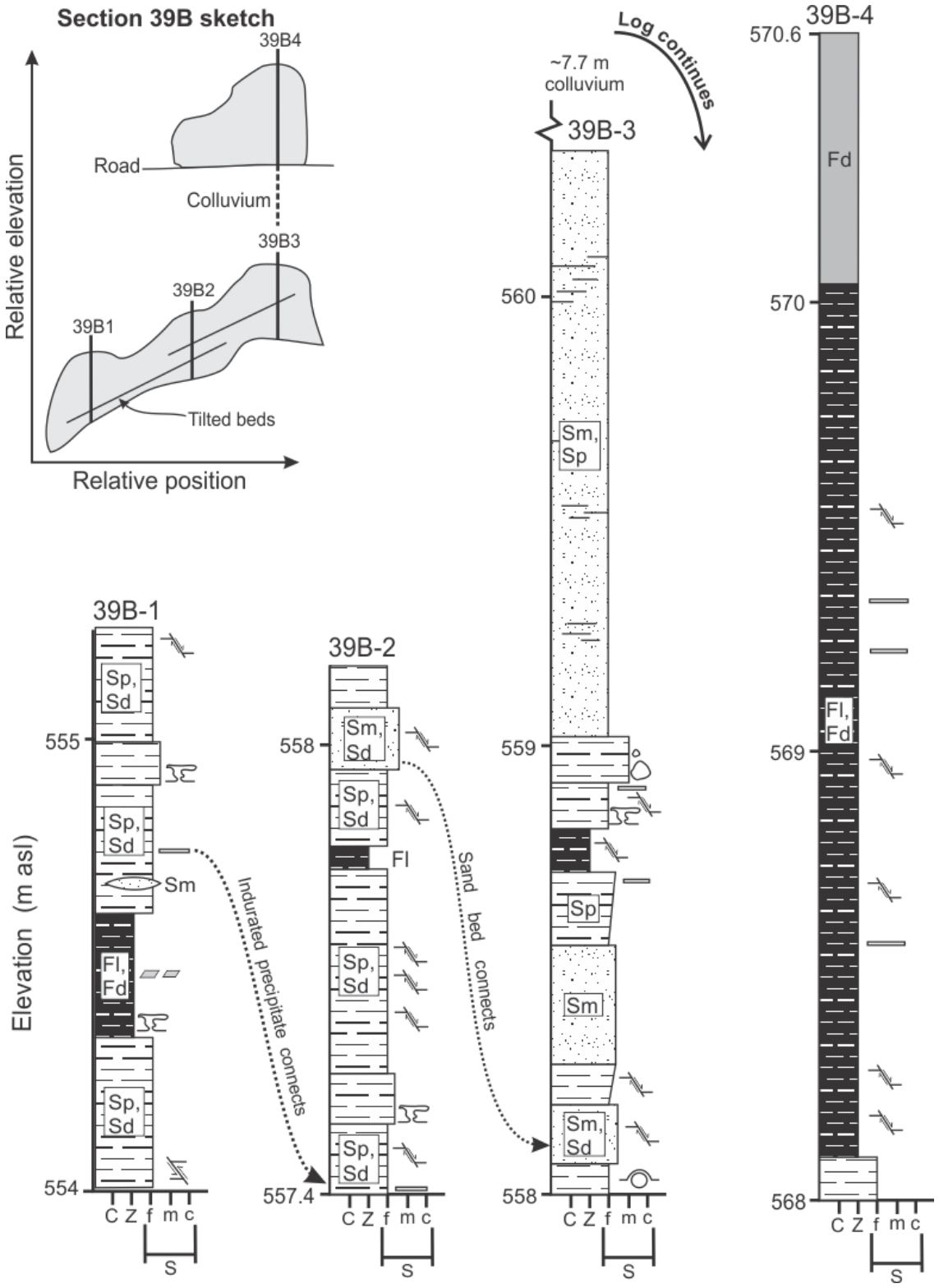

Figure 5-16: Composite vertical log of lacustrine sediments (lithostratigraphic unit 1) at exposure 39B (Figure 5-13). Sketch shows the relative position of the logs (sediment exposures are shaded grey) and the tilt of the beds (21° down towards 208°). The top 0.6 m of log 39B4 (grey bar) consists of fine sand and silt that is desiccated and heavily bioturbated with few areas of lamination preserved. Refer to Figure 4-2 and Table 4-1 for legends.

Unit 3 is ~0.4 m thick, has a sharp lower contact and consists of tabular cross-stratified pebbles (2-5 cm b-axis) (Gc, Table 4-1). The cross-stratified gravel beds have been oxidized orange, are predominantly openwork and have an apparent dip of 23° toward 350° (Figure 5-17a). Pebbles are typically subangular or subrounded.

Unit 4 is ~1 m thick, has a sharp lower contact (Figure 5-17a) and consists of horizontally-laminated silt-clay rhythmites (Fl, Table 4-1; Figure 5-17b). Rhythmites range in thickness from 1-10 mm. They are desiccated and, in places, bioturbated.

Unit 5 is up to 1.4 m thick, has a sharp lower contact and consists of clast-supported (>80% clasts) silty-sand diamicton (Dcm, Table 4-1). The clasts display no surface wear features, range in roundness from angular to subrounded and vary in size from small cobbles to small boulders (b-axes up to 0.30 m).

Unit 6 is revealed at exposure 39C, toward the top of the bench riser on the north shoulder of gully 2 (Figure 5-13, Figure 5-15). The unit is at least 2 m thick and mainly composed of planar-stratified gravel lithofacies (Gp, Table 4-1) (Figure 5-17c). The planar-stratified, normally-graded gravel (small pebbles to cobbles) beds of unit 6 average ~0.40 m thick with sharp lower contacts, and consist of clast-supported, relatively angular (39-6, Table 5-1) pebbles and cobbles in a coarse sand matrix. A fabric on the planar-stratified gravel of unit 6 reveals a southwestward principal eigenvector and a dominance of a(p) clasts (39-6, Figure 5-17c and Table 5-1). Two rip-up clasts (up to ~10 cm long)

composed of grey clay are present in the gravel beds. Unit 6 also contains a thin (~0.1 m) intra-unit lens of laminated clay and silt and planar-stratified fine sand (Fl and Sp, Table 4-1, Figure 5-17c). The fine-grained laminae display both normal and inverse grading. The lower contact of the lens is sharp and conformable with the gravel beds in unit 5.

Unit 7 is revealed at exposure 39A within the gravel fan (near its apex) that extends below the bench riser at the mouth of gully 1 (Figure 5-13, Figure 5-15). This geomorphic context dictates that unit 7 is the youngest lithostratigraphic unit exposed at site 39. Unit 7 is at least 2.5 m thick (lower contact not exposed) and composed of inclined, poorly-sorted, planar-stratified and massive, inversely and normally-graded pebble to large cobble (b-axis >0.2 m) beds (Gp and Gm, Table 4-1) (Figure 5-17d). The beds average ~0.35-0.4 m in thickness and have an apparent dip of 29° towards 274° (Figure 5-17d). At exposure 39A the surface of the gravel fan slopes ~30° towards the southwest (~200°). A gravel fabric (39-7) from imbricated, dominantly subangular and subrounded clasts is strongly unimodal with clast orientation and dips roughly parallel to those of the containing beds; clasts are dominantly a(t) or a(o) (39-7, Figure 5-17d, Table 5-1).

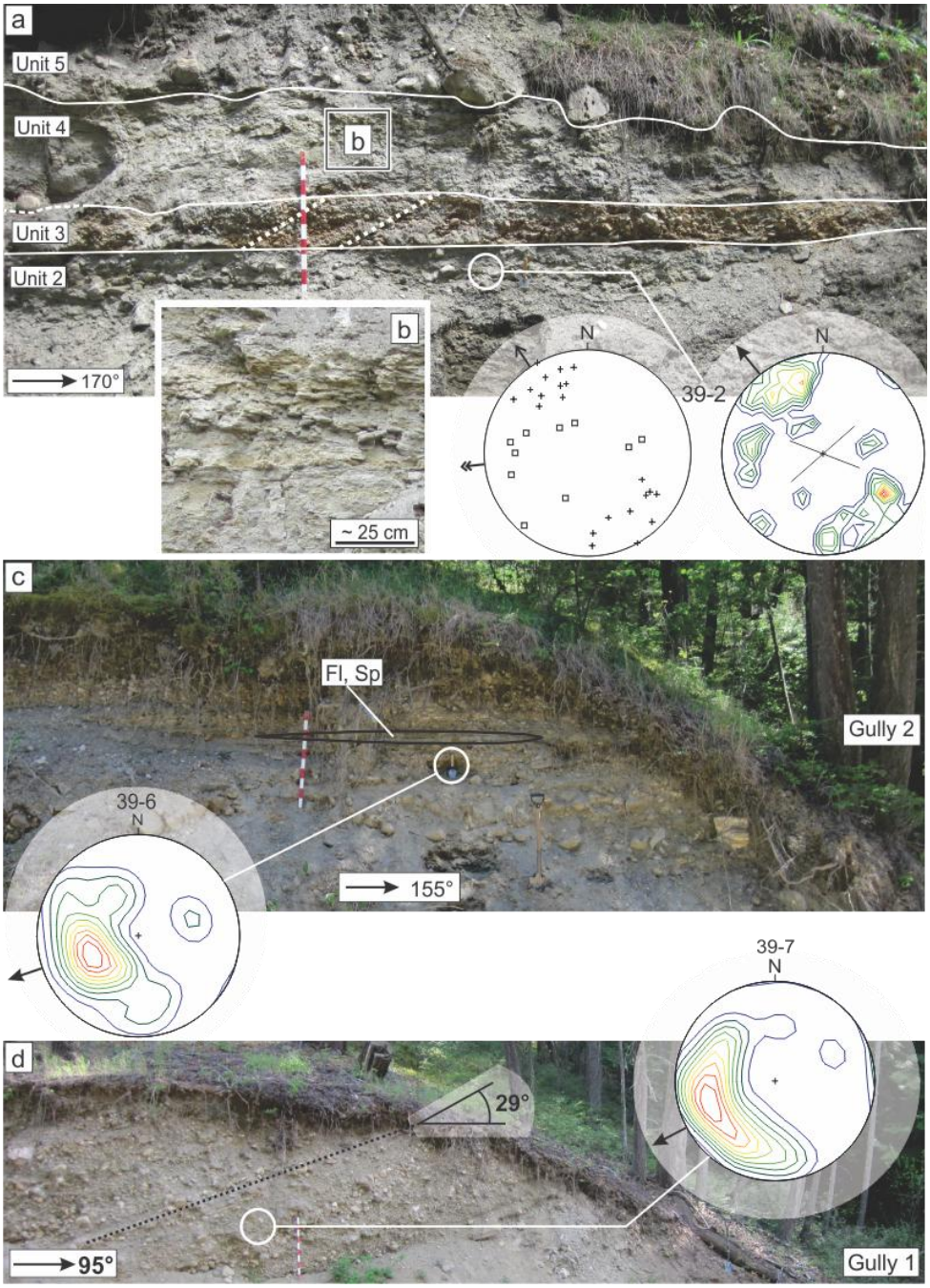

Figure 5-17: a) Exposure 39D reveals four lithostratigraphic units (labeled units 2-5). The location and corresponding stereograms of diamicton fabric 39-2 (Table 5-2) are shown. The cross-stratified gravel beds (Gp) in unit 3 dip northward (white dashed lines). Black box (labeled b) marks location of b). b) Close-up of laminated fine-grained lacustrine sediment (Fl) of unit 4 in exposure 39D. c) Exposure 39C is located north of gully 2 and contains the planar-stratified gravel (Gp) and interbedded fines (Fl, Sp) of lithostratigraphic unit 6. The location of gravel fabric 39-6 (Table 5-1) and its corresponding contoured stereogram (southwestward paleoflow) are shown. d) Exposure 39A reveals west-dipping planar-stratified and massive gravel beds (Gp and Gm) of unit 7 adjacent to gully 1. Location of gravel fabric 39-7 and its corresponding contoured stereogram (southwestward paleoflow) are shown. Metre stick has decimetre markings. Refer to Figure 5-13 for exposure locations, Table 4-1 for lithofacies codes and Figure 4-1 for stereogram legend.

5.2.3.5 Site 39 interpretation

The tabular sand-silt-clay rhythmites of unit 1 (revealed at exposure 39B) indicate deposition from suspension settling in a lake, the textural rhythmicity likely resulting from diurnal or seasonal inflow variations (cf. Church and Gilbert 1975; Smith & Ashley 1985). Dewatering structures reveal rapid deposition onto saturated sediment (Lewis 1984). The presence of icebergs and dropstones is inferred from the draped granitic lonestone (Smith & Ashley 1985). The overall upward-fining in unit 1 indicates a progressive reduction of energy in the lake. This may be the result of a deepening of the lake, the migration of its water and sediment supply to a more distal location, or a combination of the two (Smith & Ashley 1985). Faulting is pervasive throughout unit 1 and records the application of extensional and, more rarely, compressional stress. Most fault planes only propagate through a few beds, thus indicating syn-depositional stress; these stresses may have resulted from saturated sediment mobilization on a sloping lake bed, or incremental melt of the lake-marginal ice. Other fault planes propagate through the entire deposit recording post-depositional stress (which may have been caused by slumping after ice buttress removal; see below). The elevated position (~570 m asl) of the rhythmites indicates deposition into a Purcell Trench-occupying lake that was at least 38 m higher than modern Kootenay Lake or deposition into an elevated ice-marginal lake. Although unit 1 is located below the till/advance-phase outwash contact identified in the Purcell Trench (sites 19, 41), it lacks a till cap and geomorphic protection from erosion by the advancing Purcell Lobe. Consequently, unit 1 is interpreted to record an ice-marginal lake that formed against the backwasting and downwasting Purcell

Lobe, and likely existed after the drainage of gLP (because gLP likely required an ice dam >200 m higher than the bench at site 39; § 6.2).

Unit 2 is inferred to be a debris flow deposit or a till because of its diamictic texture and massive structure, stratigraphic and geomorphic context, and bimodal to multimodal fabric. A paucity of glacigenic surface wear features suggests that the unit is likely a debris flow. Elsewhere in the PT, till is found preserved behind bedrock obstructions (cf § 5.1); there are no such obstructions to glacial erosion at site 39. Unit 2 is lies stratigraphically within the elevation range of unit 1, suggesting that the unit may have been deposited into the ice-marginal lake recorded by unit 1 (Levson & Rutter 1989). Striae can be produced during debris flow transport of clasts (Atkins 2003). But, the two striae may owe to the debris flow being remobilized till. The bimodal fabric records both compressional (primary eigenvector 39-2, Figure 5-19a) and extensional (secondary eigenvector 39-2, Figure 5-19a) stresses during debris flow transport (e.g., Rappol 1985; Major 1998). Whether the debris flow flowed from the valley walls or off the Purcell Lobe is uncertain.

The sorted and tabular cross-stratified gravel of unit 3 (at exposure 39D) with a northward paleoflow records traction deposition during bedform migration in lake underflows (Allen 1982; Postma 1990), or fluvial barform migration (Miall 1977; Allen 1983; Rust 1984; Salamon 2008) possibly during lake drainage towards the north or following lake drainage. Openwork gravel may indicate high-energy flows (Smith 1974; Lunt & Bridge 2007), rapidly waning flows (Steel

& Thompson 1983), or sorting due to avalanching and flow separation in the lee of bedforms or bars (Rust 1984; Carling & Glaister 1987; Carling 1996).

The stratigraphic context of the silt-clay rhythmites of unit 4 (at exposure 39D) indicate an abrupt return to deposition from suspension settling in a lake marginal to the downwasting and backwasting Purcell Lobe and experiencing diurnal or seasonal changes in sediment influx (Church and Gilbert 1975).

The massive, clast-supported diamicton of unit 5 is inferred to be a debris flow deposit because it is poorly consolidated and lacks glacigenic wear features. Furthermore, the unit consists of a single bed that conforms to the exposed topography, which suggests deposition by modern (Holocene-aged) slope processes (Eyles et al. 1987). Therefore, unit 5 is interpreted as a Holocene colluvium.

The unit 6 gravel beds (exposure 39C) are dominated by angular and subangular clasts and display varying amounts of sorting, which suggests short transport distances. The massive and inversely-graded beds indicate rapid deposition in fluvial sheet flows (Allen 1984; Postma 1990) or during non-cohesive debris flows (Blair 1987; Eyles et al. 1987; Blair & McPherson 1994). The high percentage of a(p) clasts (39-6, Table 5-1) suggest sliding in a fluvial sheet flow on a steep fan surface or flow extension in a non-cohesive debris flow. A southwestward paleoflow is inferred from these a(p) sliding clasts. The lens of laminated fine-grained sediment is interpreted as lower flow regime channel fill or pond sediments that were deposited between ephemeral stream flows or debris

flow events (Miall 1977; Blair 1987). Thus, unit 6 is interpreted as an alluvial or colluvial fan deposit building from the valley walls into the Kootenay Lake basin.

Unit 7 (revealed at exposure 39A) is interpreted as an alluvial fan deposit because of its geomorphic context, well-sorted gravel texture, dominance of subangular clasts, angled planar-stratified structure, and imbricate (dominantly a(t)) gravel fabric. Unit 7 is exposed in the apex of a gravel fan at the terminus of gully 1, inset into the riser of the bench containing units 1-6 (Figure 5-13, Figure 5-15). Upward-fining, planar-stratified gravel beds with dominantly subangular clasts indicate short transport distances and deposition in shallow streams or sheetflows consistent with sedimentation styles on alluvial fans (Blair 1987; Blair & McPherson 1994; Goedhart & Smith 1998). Clast imbrication plunge is high as expected on steeply dipping beds, and in this context the fabric is interpreted as recording southwestward flows, consistent with an alluvial fan building from the valley walls into the Kootenay Lake basin.

In summary, landforms and sediments at site 39 record sedimentation in an ice-marginal lake during decay of the Purcell lobe (units 1-4), formation of a kame terrace when ice support was removed through melting, and post-glacial colluvial processes and alluvial fan formation (units 5-7). The ice-marginal lake experienced diurnal and/or seasonal variations in sediment influx, suspension settling, an energetic underflow, sediment rafting by icebergs and a debris flow.

5.2.3.6 Site 40 sedimentology

Two lithostratigraphic units are exposed at site 40 (Figure 5-18). Unit 1 is at least 3 m thick (lower contact not exposed) and is composed of planar-

stratified and trough cross-stratified gravel and sand (St, Sp, Gp and Gt, Table 4-1). The beds fine upwards (typically from gravel to sand), range in thickness from 0.15 – 0.65 m and have sharp lower contacts. Troughs extend laterally for up to 8 m, whereas planar-stratified beds maintain a uniform thickness throughout the entire ~20 m long exposure. The coarsest gravel beds fine up from clast-supported cobbles in a granule matrix to matrix-supported small cobbles, pebbles and granules in a coarse sand matrix. Several beds contain coarse sand rip-up clasts (up to 0.4 m apparent length). Gravel clasts are dominantly rounded to subangular (Fabric 40-1, Table 5-1). A gravel fabric from the centre of a large cross-stratified trough contains dominantly a(p) or a(o) clasts and records a southwestward principal eigenvector (40-1, Table 5-1, Figure 5-18c). The sand beds fine up from coarse sand with granules to coarse sand with medium and fine sand. Some sand beds coarsen then fine upward from coarse sand to granules and back to coarse sand.

Unit 2 is ~6 m thick with a sharp and slightly undulatory lower contact (Figure 5-18). It is composed of massive, matrix-supported and consolidated diamicton (Dmm, Table 4-1) containing <50% small cobble to boulder clasts (some with >1 m b-axis; Figure 5-18). Clasts are composed of metamorphic and intrusive igneous lithologies and are usually rounded (40-2, Table 5-2) and highly spherical (Appendix C). Some (*ex situ*) clasts exhibited striae, and more rarely, bullet-noses and plucked ends. Many clasts are highly foliated or composed of coarse-grained rock making identification of striae difficult. A diamicton fabric is

bimodal to multimodal with a primary mode eigenvector towards 350° and a secondary mode eigenvector towards 265° (40-2, Figure 5-18).

5.2.3.7 Site 40 interpretation

Unit 1 is inferred to record deposition in a southwest-flowing gravel-bed river in an ice-marginal environment because of its clast size and roundness, well-sorted, planar-stratified and trough cross-stratified character, normally-graded bedding, fabric, elevation and geomorphic context. Trough cross-stratified gravel records the migration of three-dimensional dunes or barforms in subcritical flow (Miall 1977, Ashley 1990). A southwestward paleoflow direction is interpreted from the distribution of a(p) clasts in a fabric taken in trough cross-stratified gravel (40-1, Table 5-1, Figure 5-18b, Figure 5-18c). This paleoflow direction is consistent with regional grade (flow from the valley wall into the Purcell Trench) and thus does not require a local topographic reorganisation from ice support, though it is achievable in an ice-marginal environment. The preservation of imbricated soft-sediment rip-up clasts suggest that the sand was frozen and/or it was ripped up, transported only a short distance before deposition, and rapidly buried (high sedimentation rates) (Allen 1982; Knight 2009). An ice-marginal depositional environment is supported by the elevation of unit 1 (unit top ~624 m asl), at least 15 m higher than the recorded valley fill before ice occupation (§ 5.1), and its geomorphic context within the riser of a valley-wall bench with a maximum elevation of 725 m asl.

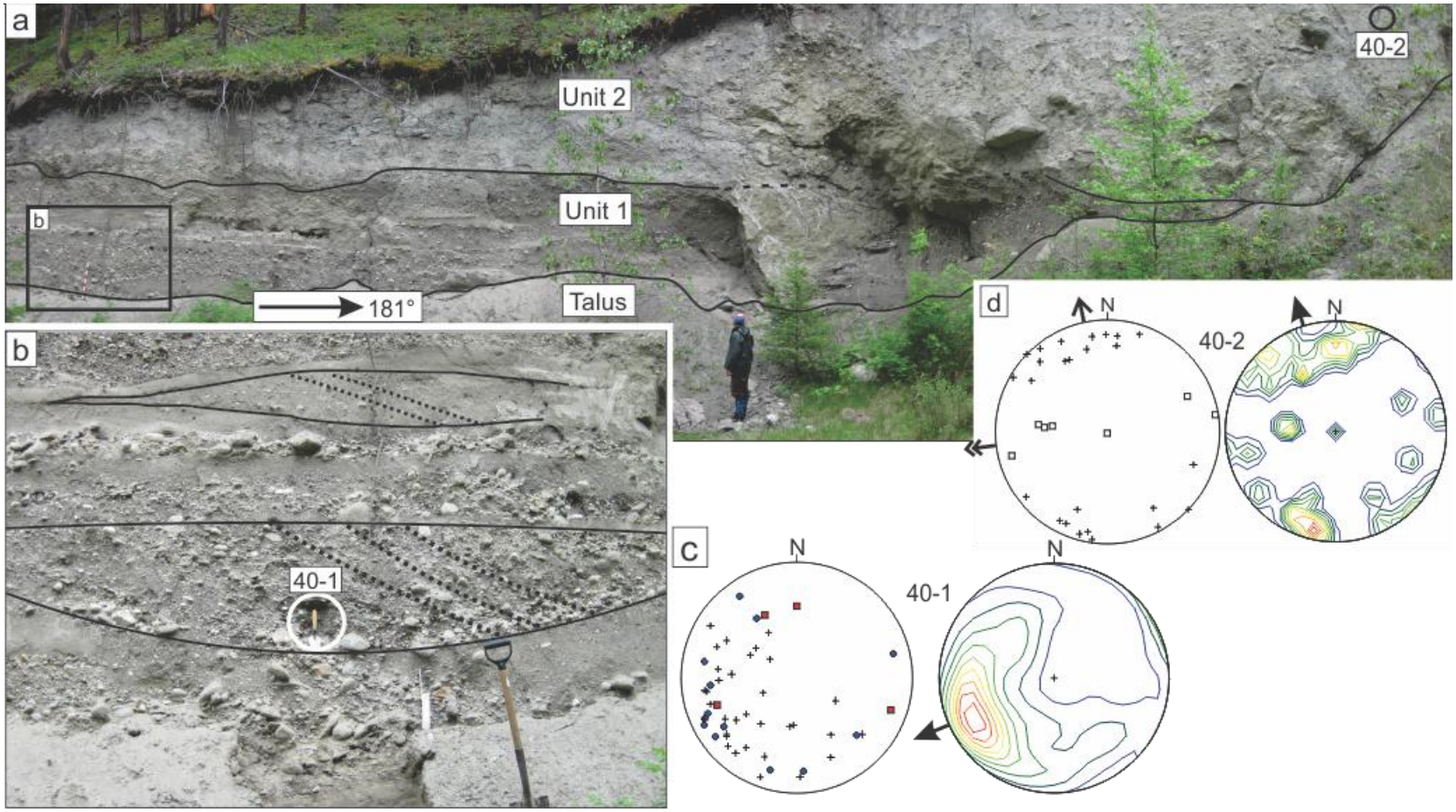

Figure 5-18: a) Site 40 (Figure 5-12) exposes two lithostratigraphic units (units 1 and 2). Unit contacts demarked by a solid black line, dashed black line denotes the approximate location of the unit 2 lower contact (the contact is hidden by a large slumped block of unit 2). Black circle (on right) denotes the location of diamicton fabric 40-2 (shown in d; Table 5-2). Black rectangle (labeled b) marks the location of b. Person is ~1.9 m tall. b) Lenses of Gt (bottom) and St (top) outlined by solid black lines are surrounded by beds of Gp and Sp (Table 4-1). Some cross-stratification is traced with black dotted lines. White circle denotes the location of trough cross-stratified gravel fabric 40-1 (shown in c). The trowel within the circle is 26 cm long. c) Contoured stereogram of gravel fabric 40-1 (southwestward paleoflow). d) Scatter plot and contoured stereogram of diamicton fabric 40-2. Refer to Figure 4-1 for stereogram legend.

Unit 2 is interpreted as a debris flow deposit because of its geomorphic and stratigraphic context (within an elevated valley-side bench above unit 1 as discussed above), texture, structure, rarity of glacigenic wear features on clasts and fabric. Its diamictic texture, massive structure and bimodal to multimodal fabric are consistent with deposition in a debris flow (Lowe 1982; Rappol 1985). In this scenario, the primary mode (M1) of fabric 40-2 (Figure 5-18d) records compressional stress in a west-flowing debris flow off the valley wall onto the alluvium of unit 1, and the *ex situ* glacigenic stones are attributed to debris flow reworking of an antecedent subglacial till. Alternatively, unit 2 may be interpreted as a subglacial till with a southward paleoflow; but this interpretation is not favoured because of its stratigraphic and geomorphic context.

In summary, site 40 records ice-marginal river flow along-side the downwasting and backwasting Purcell Lobe followed by colluvial activity. The westward paleoflow of unit 1 suggests that site 40 may record the delivery of non-ice marginal stream flow to the ice marginal system.

5.2.3.8 Sites 38–40 interpretation

That the top of the valley-side bench at sites 38–40 is up to ~100 m higher than the Purcell Trench valley fill prior to MIS 2 ice occupation (recorded elsewhere in the study area; sites 19 and 41), is preserved despite a lack of sheltering valley structures, and is not capped by till, suggests that sediments within the bench must record ice-marginal deposition in a kame terrace during ice retreat (Holmes 1947; Goodwin 1985).

Faulting in kame terrace deposits may record post or syn-depositional extensional stress from ice buttress removal, or from local slope steepening by gullying or road construction. The paucity of faulting through the deposit at sites 38-40 may be the result of the steepness of the valley wall: sediments in the residual narrow bench having experienced minimal ice support. Hummocky, kettled topography is not preserved or visible on the bench tread because of the narrow and forested nature of the deposit, areas of capping alluvial sediment, and agricultural use (which resulted in terrain smoothing) on the wider areas of the bench.

5.2.4 Ice position summary

The kame terraces in the Purcell Trench (~600 to >700 m asl; sites 27, 30 and 38-40) record the position of the Purcell Lobe during MIS 2 CIS decay. The evidence for ice-marginal rivers and lakes also suggests that the Purcell Lobe had a valley wall seal that was sufficient to dam gLP. The elevation of the kame terraces suggests ice thicknesses of at least 171 m (in the Purcell Trench near site 30) and up to 290 m (in the Purcell Trench at site 27) at the time of their formation.

5.3 Sites recording glacial Lake Purcell

The following sites are located in a silty bench on the eastern floor of the Purcell Trench south of Kootenay Lake and are interpreted as a record of the minimum paleogeographic extent of gLP in Idaho and BC. Most of the sites reported here are located in BC because there is no existing mapping or reports

on gLP sediments in BC. The presence of lake sediments associated with gLP and gLK is well documented in Idaho and Montana (Alden 1953; Johns 1970; Smith 2006; Breckenridge et al. 2009; Burmester et al. 2009; McFaddan et al. 2009; Breckenridge et al. 2010; Burmester et al. 2010; Russell et al. 2010).

5.3.1 Site 2

5.3.1.1 Observations

Site 2 is a small gravel pit located ~1.3 km east of the eastern shore of modern Kootenay Lake in an elevated bench north of Sanca Creek (Figure 3-2; Figure 5-19). This dissected bench is located in an alcove created by the widening of the Sanca Creek valley at its intersection with the Purcell Trench (Figure 5-19). The exposure is 675 m asl, or 143 m above present Kootenay Lake. A separate 0.3 m high exposure, at least 2 m below the gravel pit reveals lacustrine sediment similar to that exposed in the gravel pit.

Site 2 exposes a single lithostratigraphic unit (unit 1) composed of deformed fine sand, silt and clay (Figure 5-20). This unit is described as three subunits (1a, 1b, and 1c), subdivided based on textural and structural differences. Subunit 1a is at least 2.5 m thick and consists of normally-graded rhythmic beds (0.01-0.06 m thick) with sharp lower contacts (Figure 5-20). Each bed fines upward from fine sand to varying amounts of silt and clay (Sm and Fl, Table 4-1; Figure 5-20). The beds are apparently tilted 14° down towards 230°

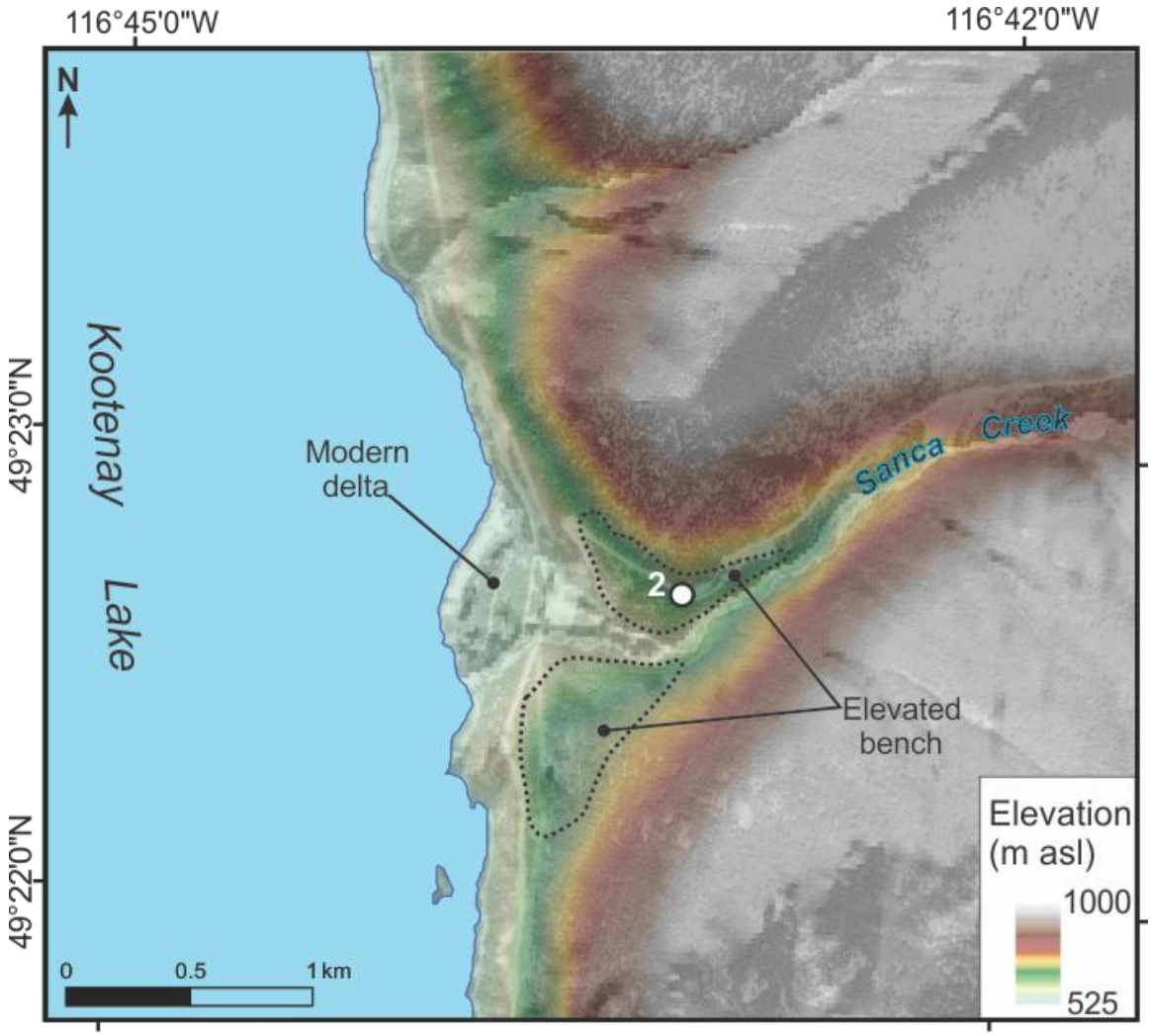

Figure 5-19: Hillshaded DEM (Geobase®) overlain with an aerial photograph (BC80116-210. © Province of British Columbia. All rights reserved. Reprinted with permission of the Province of British Columbia.) showing elevated benches (black dotted lines) around site 2 (white dot). Refer to Figure 3-2 for site location within the Purcell Trench.

(roughly parallel to the Sanca Creek valley). Subunit 1a also exhibits thrust faults (Figure 5-20) scattered throughout most of the subunit and typically propagate through less than five rhythmites (Figure 5-20). The faults are larger and appear more frequently towards the top of the subunit; at the base of the exposure the beds of subunit 1a are tabular, horizontal and unfaulted. Subunit 1b is up to 0.5 m thick with a sharp lower contact that truncates the bedding of subunit 1a. It is

composed tilted (apparently ~23° towards 230°), thrust faulted (apparent direction of thrust ~245°) and convoluted silty fine sand (Sd, Table 4-1). Subunit 1c is ~1 m thick with a sharp lower contact that truncates the beds of subunit 1b, and consists of desiccated and highly consolidated silt. Horizontal lamination (up to ~2 cm thick) is discernible in places (Fl, Table 4-1); however, most of the subunit is massive and has undergone a large amount of bioturbation from roots (Figure 5-20).

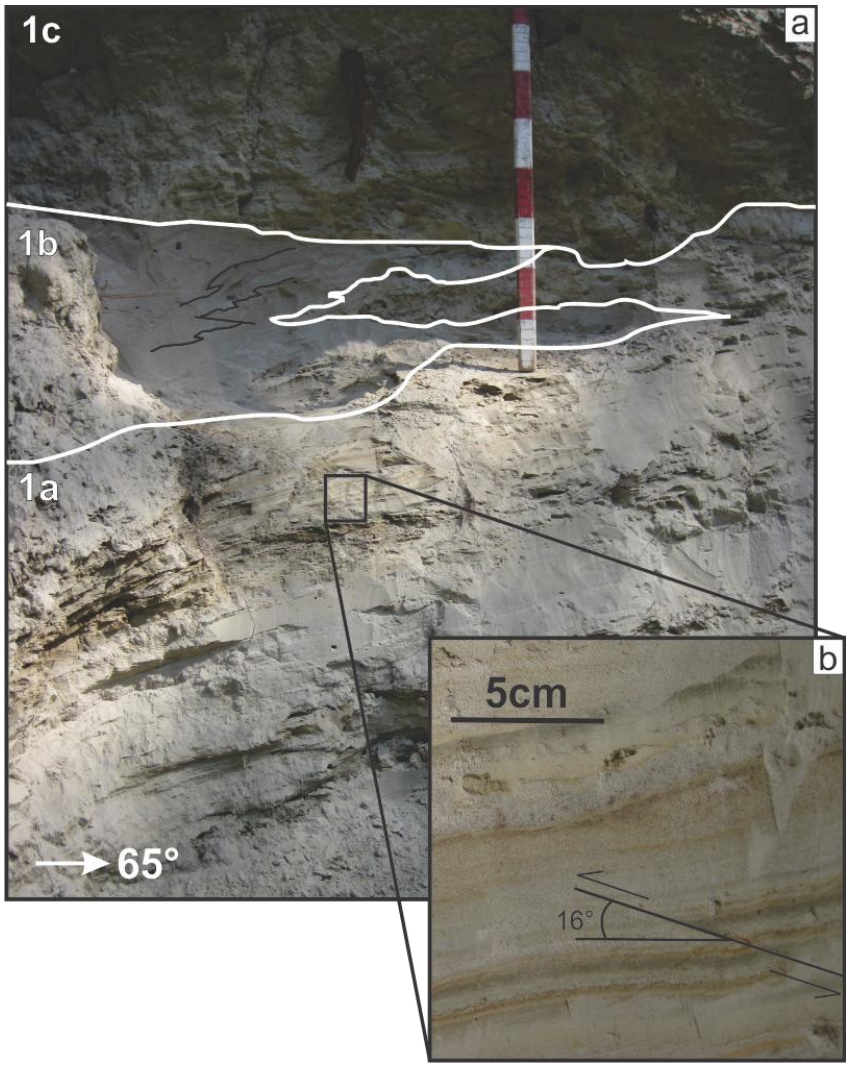

Figure 5-20: a) Site 2 exposure showing subunit boundaries (white lines) and sediment structures (traced in subunit 1b by thin black lines). Metre stick has decimetre subdivisions (only 0.74 m visible). b) Close up of subunit 1a sand beds showing a syndepositional thrust fault with ~2 cm of displacement.

5.3.1.2 Interpretation

The rhythmic sand, silt and clay beds in subunit 1a were deposited on a lake bed. The presence of rhythmites indicates a depositional environment that experienced small, repetitive changes in energy over time; these rhythmites may be the result of diurnal or seasonal variations in sediment influx (Church and Gilbert 1975). The lack of ripples within the rhythmites suggests sediment and meltwater delivery via overflows and/or interflows, or that site 2 is distal to inflows that may include turbidity currents (Gilbert & Shaw 1980; Smith & Ashley 1985). In this context, the well-sorted silty fine sand of subunit 1b is interpreted as evidence of higher energy inflows into the lake, perhaps a turbidity current (Smith & Ashley 1985), and the desiccated and bioturbated (roots) silty laminated subunit 1c records a return to suspension settling on the lake bed. Syndepositional thrust faults in subunits 1a and 1b, recording a compressional stress from the east (~65°), suggest minor downslope (toward the PT) gravity-driven compression of lake bed sediments during accumulation on the lake bottom (cf. Smith & Ashley 1985). The lower contacts between subunits are interpreted as shear planes because they truncate the rhythmites or laminae in the subunit below. The presence of shear planes accounts for the tilting of the rhythmites and suggests that the subunits may have post-depositionally slumped toward Sanca Creek when buttressing sediment was removed by Sanca Creek incision.

5.3.2 Sites 3, 4, 5 and 15

Sites 3, 4, 5 and 15 are all located within a large silt and clay bench that extends from the Elmira spillway (~10 km south of Bonners Ferry, ID) to ~5 km north of Creston, BC (Figure 3-2, Figure 5-21). The sites are all located north of Bonners Ferry, Idaho, although, the gLP bench continues much farther to the south (Figure 3-1, Figure 3-2, Figure 5-21a). The sites possess similar geomorphic, stratigraphic, and sedimentologic characteristics, so they are described and interpreted as a group.

5.3.2.1 Observations

Site 3 exposes ~5 m (thickness) of massive silty-clay (Fm, Table 4-1) that has a maximum elevation of ~630 m asl (~100 m above the modern surface of Kootenay Lake). Site 4 exposes 7 m (thickness) of deformed (convolute bedding with flame structures) and tilted (36° towards 330°, apparent tilt) silt-clay rhythmites (~70% clay) (Fd, Table 4-1) (Figure 5-22c) at a maximum elevation of 604 m asl. The thickness of the rhythmites varies from 1 mm to 20 mm (Figure 5-22c). Rare quartz granules are present throughout the exposure (Figure 5-22c). Site 5 exposes over 14 m (thickness) of massive and laminated silt (Fm and Fl, Table 4-1) containing occasional clasts (pebbles to cobbles, some exhibit striated facets, and plucked ends) at a maximum elevation of ~640 m asl. Rarely, thin beds (~0.02 m thick) of clast-supported, planar-stratified granules in a silt matrix (Gp, Table 4-1) punctuate the silt beds.

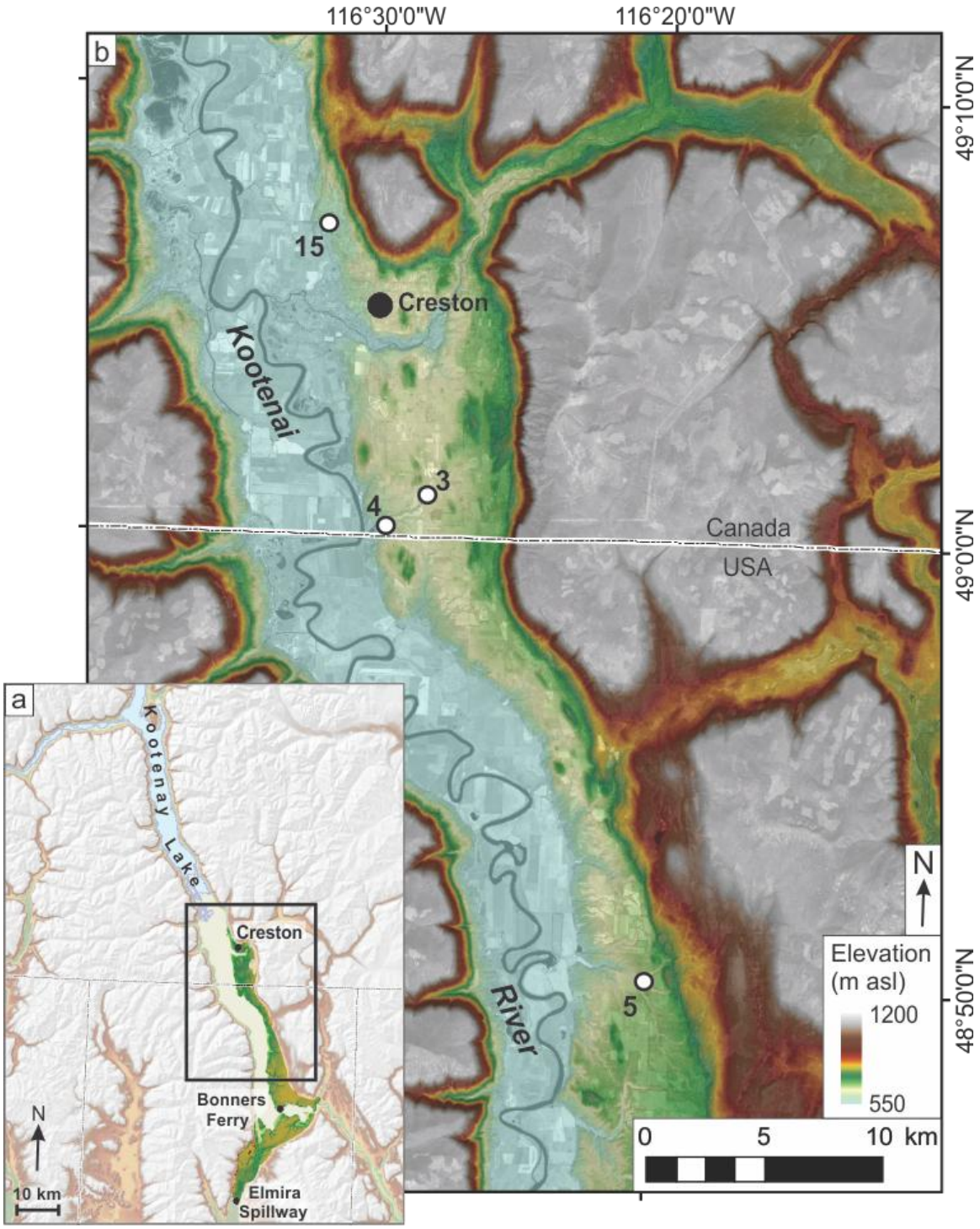

Figure 5-21: a) Hillshaded DEM mosaic (Geobase® in CA, NED in USA; data available from U.S. Geological Survey) showing the gLP lake bed bench (unmuted green and orange) on the southern and eastern floor of the Purcell Trench. Black box shows location of b. b) DEM mosaic (op. cit.) overlain with an orthophotograph (clip from 1:250 000 orthophotograph mosaic, 82F, Province of British Columbia) of the northernmost part of the gLP bench (light yellow and green) showing locations of sites (white dots) between Creston and Bonners Ferry that expose gLP lake-bottom sediment.

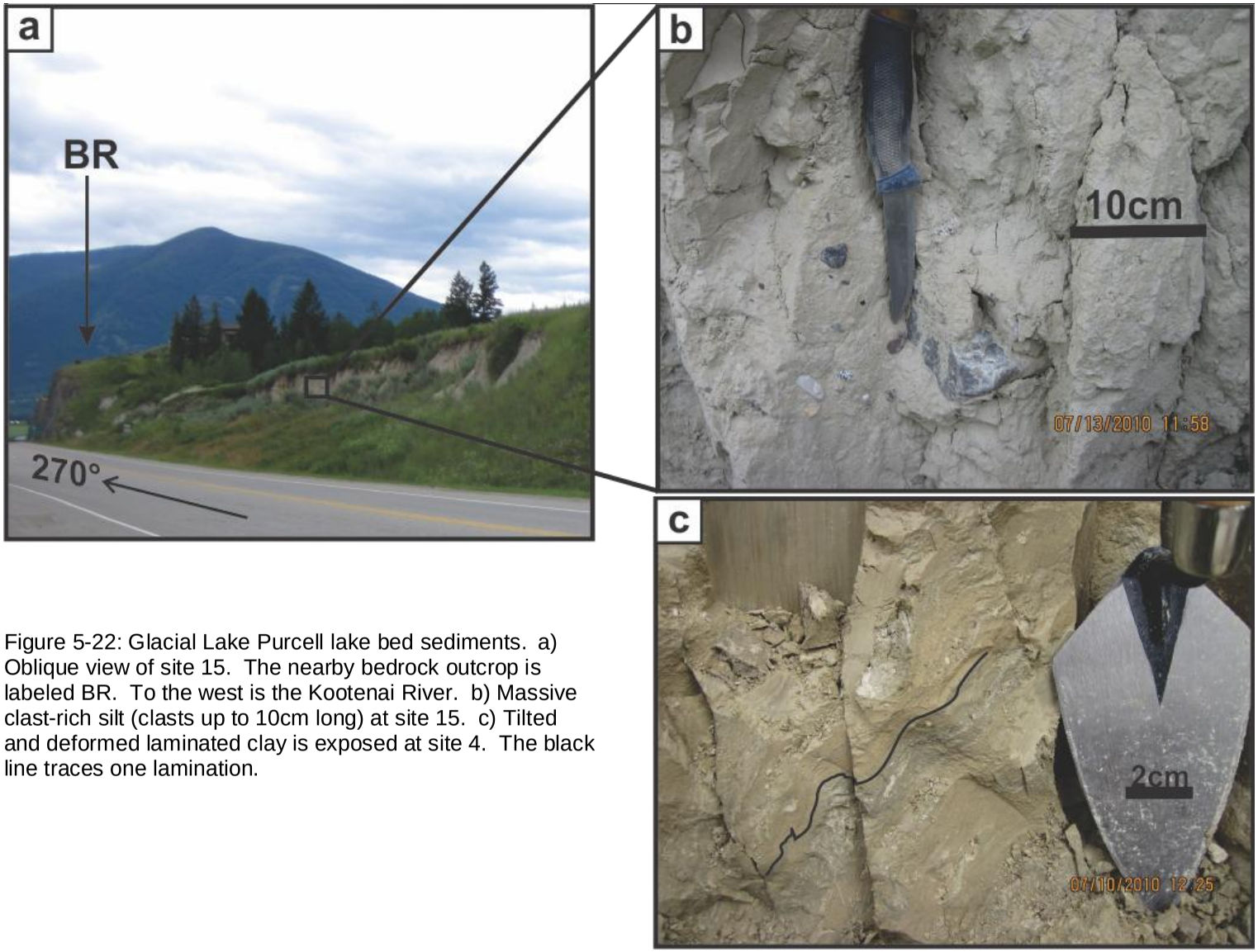

Figure 5-22: Glacial Lake Purcell lake bed sediments. a) Oblique view of site 15. The nearby bedrock outcrop is labeled BR. To the west is the Kootenai River. b) Massive clast-rich silt (clasts up to 10cm long) at site 15. c) Tilted and deformed laminated clay is exposed at site 4. The black line traces one lamination.

Site 15 exposes ~4 m (thickness) of massive and rhythmically laminated silt and clay (Fm, Fl and Fd; Table 4-1) at a maximum elevation of 565 m asl (dGPS) (577 m asl, DEM) that is separated from the Kootenai River floodplain by a series of low relief bedrock knobs (Figure 5-22a). The bottom 3 m of the exposure consists of massive, clast-rich (~20%) silt (Figure 5-24b). Clast roundness ranges from subrounded to rounded and many clasts are heavily striated. The top metre exhibits rhythmically-laminated silt-clay couplets that thin and fine upwards through the exposure. The lower couplets are dominated by silt and average 0.02 m thick. The upper couplets grade upwards from silt to clay and are <0.01 m thick. Silt dikes (average ~0.02 m wide, at least 0.30 m vertical extent) are injected upwards from the top of the massive silt into the rhythmites.

5.3.2.2 Interpretation

Rhythmites at sites 3, 5, and 15 record varying sediment influx and deposition from suspension settling on a lake bed (Smith & Ashley 1985). The dominance of silt and clay at sites 3, 4 and 15 suggests a distal sediment inflow source (Smith & Ashley 1985). The paucity of clay at site 5 suggests more energetic lake conditions, possibly from valley side sediment influx, or the close proximity of the Kootenai River alluvial fan (§ 6.2). Flame structures (site 4) and vertical silt dikes (site 15) record dewatering caused by loading, and thus relatively high sedimentation rates (Nichols et al. 1994). Stones within the rhythmites at site 5 may be dropstones that record the presence of icebergs. Stones within the massive silt at site 15 could be the result of iceberg rollover events, ice-marginal debris flows, or debris rain-out from the ice front (Smith &

Ashley 1985), and suggest that gLP was an ice-contact, proglacial lake. Site 15 likely records the oldest sediments described from the gLP lake bottom sediment bench because this site is the lowest in elevation and close to bedrock.

5.3.3 Site 10

5.3.3.1 Observations

Site 10 is located ~20 km north-northeast of the Elmira spillway in Idaho (Figure 3-2) within an extensive silt bench (Figure 5-23). It exposes ~11 m of sediment and reaches an elevation of ~560 m asl (DEM, NED; data available from U.S. Geological Survey). The site lies south of the Kootenai River and east of Deep Creek in a northeast-southwest trending channel (channel B) that is ~0.80 km wide, ~2.20 km long and ~0.12 km deep (Figure 5-23). Channel B meets a geomorphically similar channel (channel C) that is oriented approximately north-south (Figure 5-23). These channels have dissected the silt bench (Figure 5-23).

Three lithostratigraphic units are exposed at site 10 (Figure 5-24a). Unit 1 is at least 10 m thick and is composed of dipping (30° towards 221°, apparent dip), normally-graded and massive, ~1.5 m thick gravel beds (Gp and Gm, Table 4-1) (Figure 5-24a). The beds typically fine upwards, from clast-supported large cobbles and pebbles with small amounts of a sandy granule matrix, to mainly clast-supported large pebbles and rare small cobbles in a sand and granule matrix (Figure 5-24b). Clasts are typically rounded to well-rounded (Figure 5-24b).

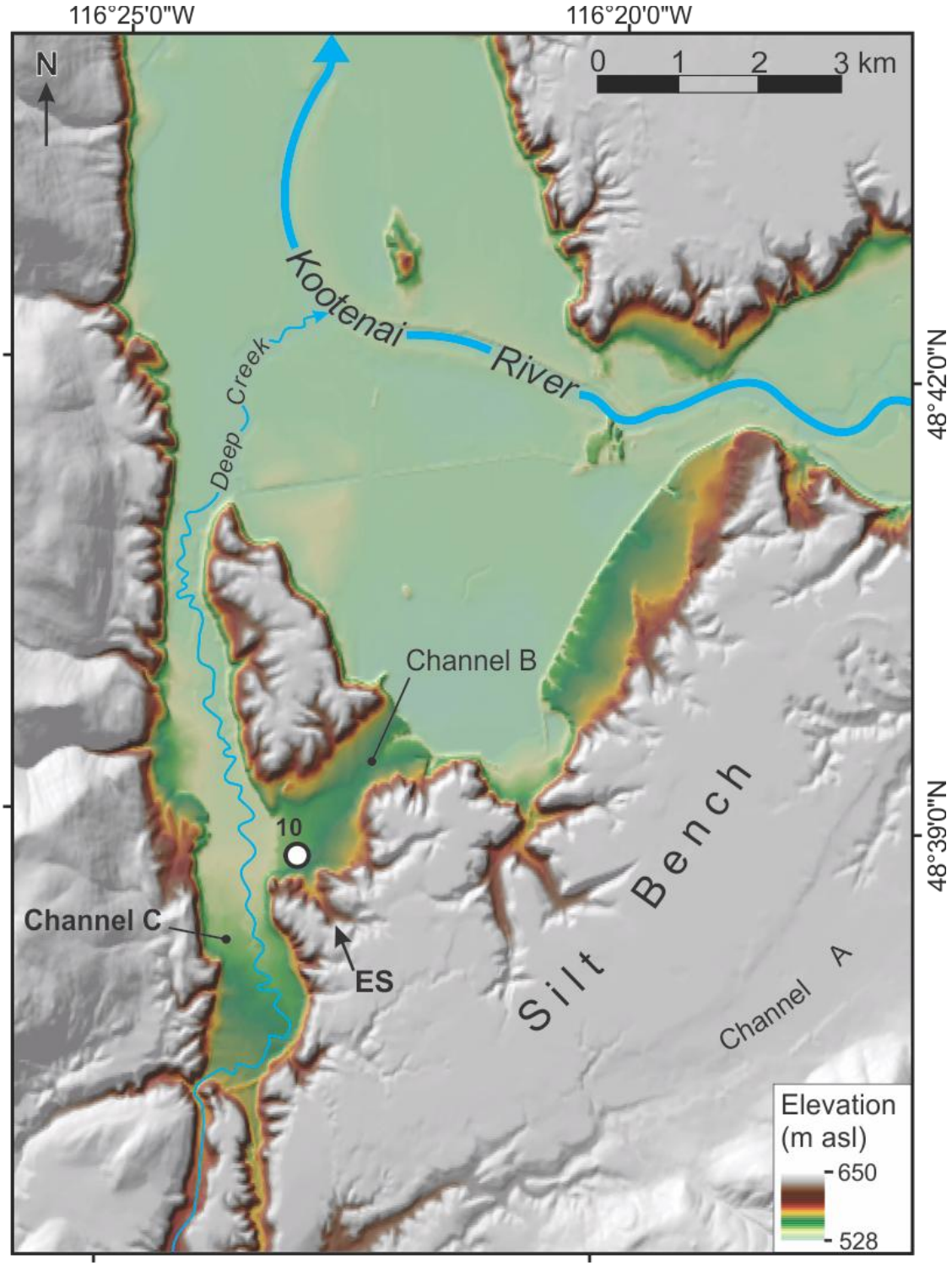

Figure 5-23: Site 10. Hillshaded DEM (NED; data available from U.S. Geological Survey) showing site 10 (white dot) and the surrounding geomorphology of the incised silt bench. Deep Creek flows north within Channel C to its confluence with the northward flowing Kootenai River. The arrow labeled ES points to an ephemeral stream that flows towards site 10. Refer to text for discussion of channels A-C and Figure 3-2 for site location within the Purcell Trench.

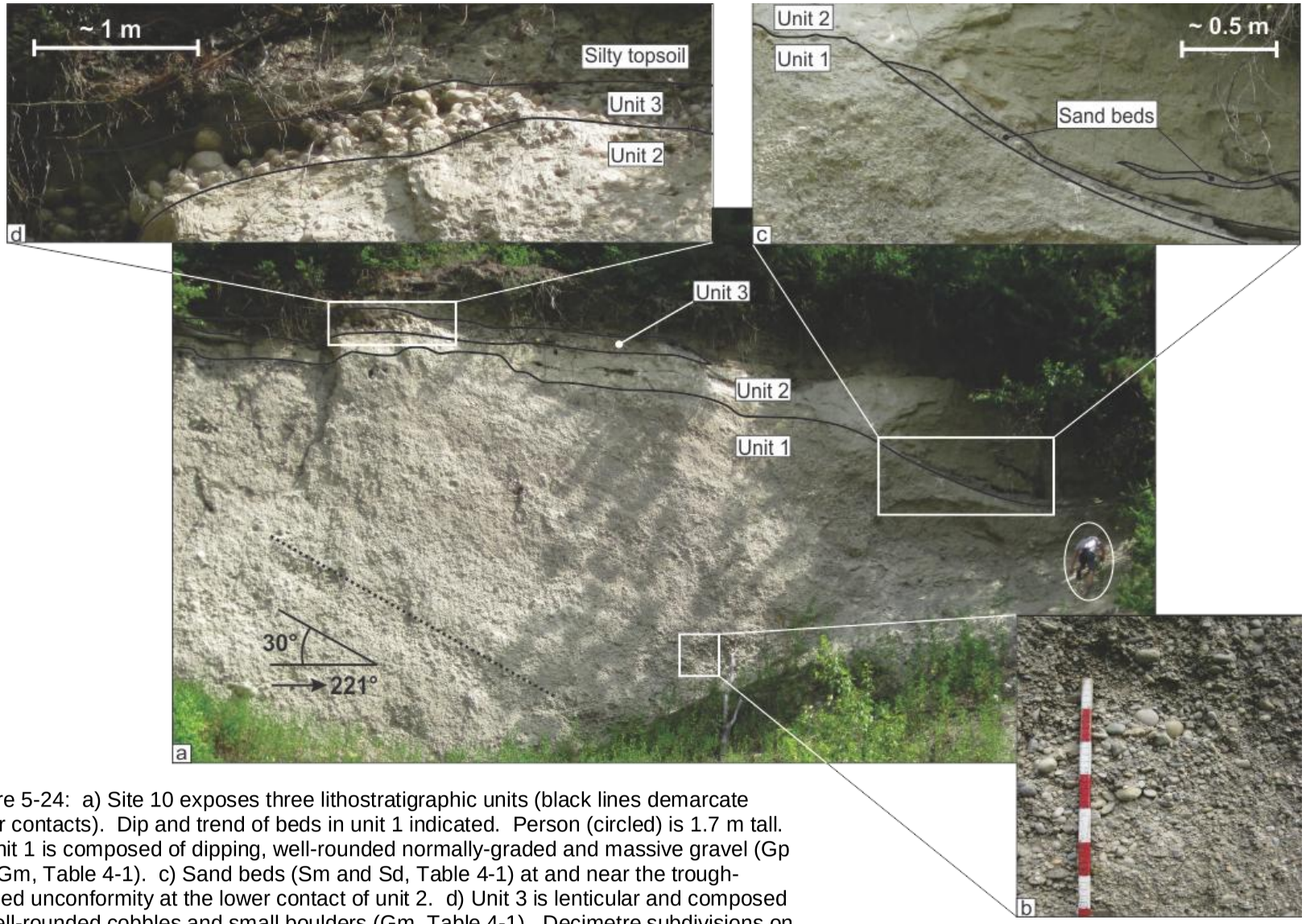

Figure 5-24: a) Site 10 exposes three lithostratigraphic units (black lines demarcate lower contacts). Dip and trend of beds in unit 1 indicated. Person (circled) is 1.7 m tall. b) Unit 1 is composed of dipping, well-rounded normally-graded and massive gravel (Gp and Gm, Table 4-1). c) Sand beds (Sm and Sd, Table 4-1) at and near the trough-shaped unconformity at the lower contact of unit 2. d) Unit 3 is lenticular and composed of well-rounded cobbles and small boulders (Gm, Table 4-1). Decimetre subdivisions on

Unit 2 is 0.3-3 m thick (thickening to the southwest) and is composed of massive silt (Fm, Table 4-1, Figure 5-24a). It has a sharp lower contact that truncates the gravel beds of unit 1. Low in the unit and at the unit's lower contact, ~0.2 m thick sand beds (Sm and Sd, Table 4-1) with convolute structure are interbedded within the silt (Figure 5-24c).

Unit 3 is a ~1 m thick, ~12 m wide massive gravel lens (Gm, Table 4-1) that has a sharp lower contact and is overlain by silty topsoil (Figure 5-24a, Figure 5-24b). The clasts are well-rounded and range in size from cobbles to small boulders (b-axes averaging ~20 cm) (Figure 5-24d). The unit has little to no matrix and most of the lens is openwork while its periphery cobbles (cobbles near the lower contact and the overlying silty topsoil) are surrounded by silt (Figure 5-24b).

5.3.3.2 Interpretation

Unit 1 is inferred to record southwestward progradation of an alluvial fan or delta because of the dip and orientation of its well-sorted gravel beds. A southwestward progradation suggests that deposition resulted from flowing water originating in the Kootenai River valley.

The trough-shaped unconformity between units 1 and 2 on the southwest side of the exposure indicates a period of erosive flow. This channel could be the result of incision by a small ephemeral stream (marked ES in Figure 5-23) that flows north-northwest into channel B, or the channel may have resulted from local Kootenai River incision during the building of the large Kootenai River alluvial fan (§ 6.2). Interstratified and convolute sand beds near the bottom of

unit 2, within the trough-shaped unconformity, likely record grain flows on the steep channel margins. The sorted silt of unit 2 indicates deposition from suspension settling in a lake. The massive structure of the silt may be the result of rapid sedimentation rates, or a shallow water body that experienced mixing from wave- or wind-generated currents (Smith and Ashley 1985).

Unit 3 is inferred to record deposition in a river because it contains well rounded cobles and boulders with an openwork texture. This texture suggests deposition in a fluvial environment characterized by high-energy flows (Smith 1974; Lunt & Bridge 2007), rapidly waning flows (Steel & Thompson 1983), or sorting due to flow separation in the lee of bedforms or bars (Rust 1984; Carling & Glaister 1987; Carling 1996).

The geographic position (within the southern Purcell Trench), geomorphic relationship to the gLP lake bottom bench (§ 5.3.2; Figure 5-23), and silty composition of unit 2 indicate deposition in gLP. The stratigraphic position of the southwest-inclined gravel beds in unit 1 below gLP lake bottom-sediments, suggest that unit 1 records part of the large alluvial fan or fan-delta, first identified by Alden (1953) that was built into the southern Purcell Trench during the draining of the original gLK basin in Montana (cf. § 2.4; Table 2-2; Figure 2-5) into the Purcell Trench and gLP. In context, unit 3 is interpreted as alluvium deposited by flows in Deep Creek (after sufficient drainage of gLP) or the small ephemeral stream (ES, Figure 5-23). The commencement of northward flow and ensuing excavation of channel C by Deep Creek would only have been possible after a northern drainage route through the Kootenay River valley was

established. The orientation of channels A and B suggest that the subaerial flow that carved them originated in the Kootenai River valley. Channel B is interpreted to record incision from an abandoned meander of the Kootenay River.

In summary, the sediments at site 10 record the initial transfer of water from the Bull River gLK lake basin in MT to the Purcell Trench gLP lake basin in ID. The geomorphology at site 10 reveals a change from subaqueous (gLP) to subaerial conditions, followed by stream activation and incision.

5.3.4 gLP summary

GLP was a proglacial, ice-contact lake. The sites described in § 5.3 record only the minimum paleogeographic extent of gLP because much of the silt bench has been fluvially eroded during the Holocene, sediment deposits have been poorly preserved on the steep valley walls of the Purcell Trench, and the sediment fill of Kootenay Lake is unknown (obscuring any potential gLP evidence). Consequently, a more accurate estimate of gLP extent must be derived through modelling in a GIS (§ 4.2.3). The GIS modeling reveals all of the sites in § 5.3 to be within the paleogeographic extent of gLP (§ 6.2). Because these sites fall within the estimated boundaries of gLP and exhibit sedimentologic characteristics consistent with a glacial lake environment, they are interpreted as a record of gLP.

5.4 Sites relevant to gLP drainage

Glacial lake drainage can be gradual or catastrophic (Bretz 1923; Waitt 1980, 1985; Shaw et al. 1999; Benito & O'Connor 2003; Teller 2004; Alho et al. 2010), the latter resulting in jökulhlaup deposits. Evidence for jökulhlaups can be erosional (pot holes, cataracts, smoothed bedrock, bedrock canyons) and/or depositional (bars, antidunes, dunes, ice-rafted erratics, hyperconcentrated flow deposits, obstacle marks, kettle holes) depending on the flow characteristics and sediment supply (Baker 1978a; Maizels 1993; Magilligan et al. 2002; Davies et al. 2003; Herget 2005; Carling et al. 2009a, 2009c; Russell 2009), though no one piece of evidence alone is diagnostic of a jökulhlaup event. The KRv is likely to have experienced glacial and postglacial (pre-jökulhlaup) valley fill and Holocene colluvial and fluvial aggradation and incision (pre- MIS 2 sediments may also have been preserved). Differentiating putative jökulhlaup evidence from pre-jökulhlaup valley fill and the Holocene record must rely on geomorphic and stratigraphic context and elevation in combination with sedimentology. Even then, many interpretations remain equivocal and thus alternative interpretations are provided here. The putative geomorphic signature of the gLP jökulhlaup (valley-fill incision) is further examined in § 6.3.

5.4.1 KRv geomorphology

The KRv contains elevated sediment benches, and elevated, bisected and truncated alluvial fans, remnants of thicker valley fill. Figure 5-25 presents select topographic profiles across KRv. Inflections in the topographic profiles mark sediment benches that are used to reconstruct pre-incision valley-fill above modern Kootenay River and West Arm (Figure 5-25). Inferred valley fill thickness is >100 m (excluding alluvial fans) and varies along KRv (Figure 5-15, Figure 5-26). Valley fill thickness increases abruptly between the middle and lower reaches (Figure 5-25); sediment transport along the Slocan River valley has contributed to valley-fill thickness in the lower reach (Figure 3-4). Incision through the upper part of the valley fill (top ~100 m, including the alluvial fans) is manifested as a steep, continuous (non-terraced) truncation (Figure 5-26); stepped terraces and alluvial fan remnants, which would indicate a gradual incision through KRv valley fill, are absent. Incision through the lower part of the valley fill (lower 20-30 m) is recorded by numerous stepped terraces and Holocene alluvial fans (Figure 5-26), indicative of gradual incision through KRv valley fill. It is plausible that incision through the upper 100 m (possibly more if waning jokulhlaup flows and Holocene alluvial and colluvial action resulted in significant post-gLP drainage aggradation) of the valley fill may have been accomplished by a jökulhlaup from gLP. Alternatively, deep valley-fill incision and a lack of terraces may record a powerful, early-Holocene Kootenay River that was able to remove sediment across the width of the KRv. The ~10 km reach of the KRv between the Corra Linn Dam and its confluence with the Slocan River valley (Figure 3-4) is a steep bedrock canyon that ranges from ~200-400 m

wide and is up to ~70 m deep. The bottom of this canyon is situated at ~525 m asl (~125 m below the top of the pre-gLP drainage valley fill).

Sites included in this § are located within and above the upper ~100 m of KRv valley fill (Figure 5-26b) and are described from northeast to southwest along the KRv (following the direction of putative gLP drainage) (Figure 3-4). Sites 42, 43, 44, and terrace 1 at site 48 are at the top of inferred pre-gLP drainage valley fill. Site 47 is in the steep riser leading to the top of the valley fill. Sites 21 and 24 are near the base of the putative jökulhlaup incision and thus may record waning stage deposits. Sites in the lower 20-30 m of valley fill (Figure 5-26b) are excluded from this § (e.g., site 46 is at an elevation confidently attributed to Holocene Kootenay River activity; § 5.5.3).

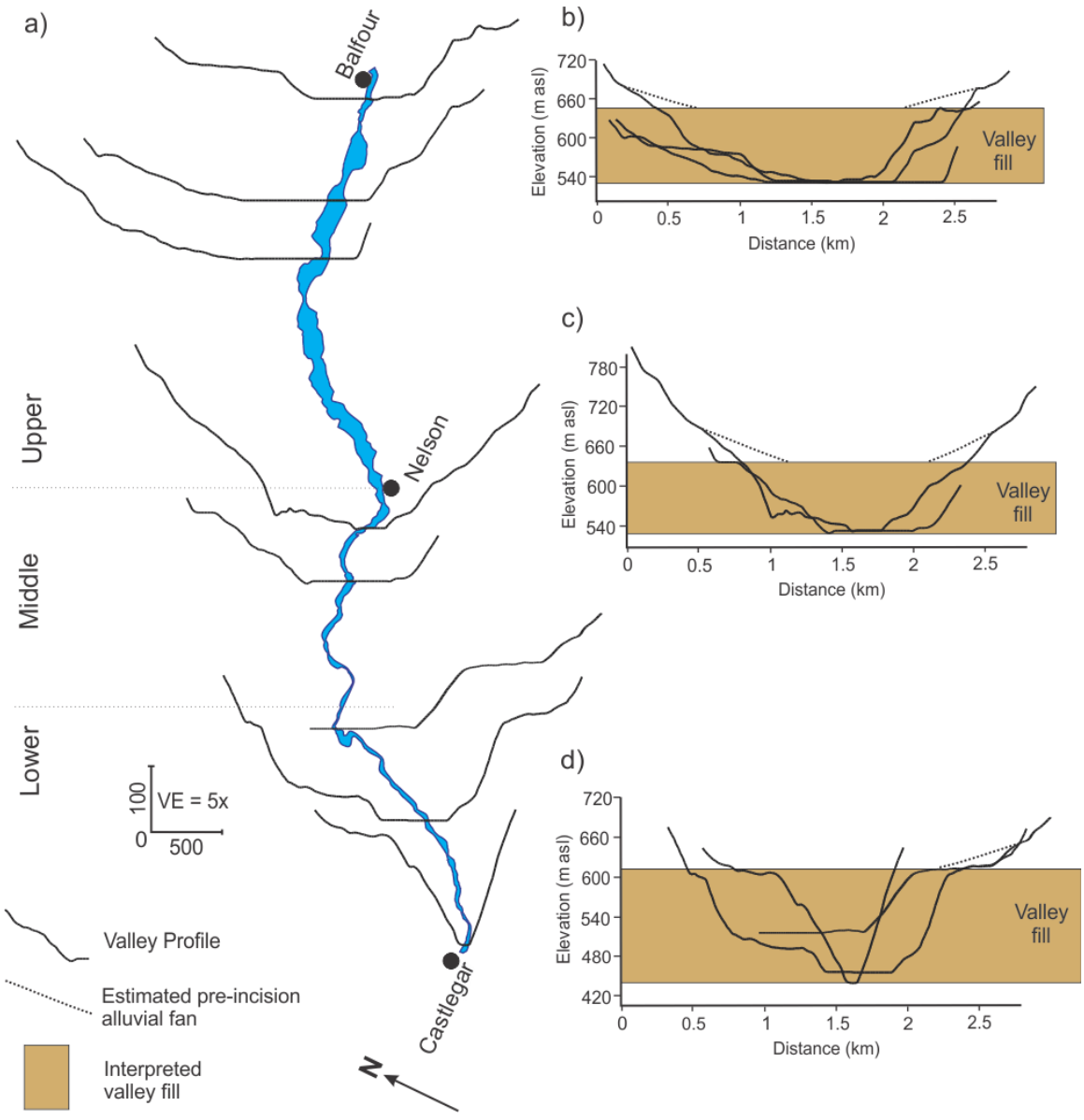

Figure 5-25: a) KRv, oriented with flow from top to bottom, shown with select topographic profiles across the upper, middle and lower reaches of the valley. Stacked topographic profiles across the upper (b), middle (c) and lower (d) reaches of KRv showing the interpreted pre-incision valley fill thickness inferred from elevated sediment benches and truncated alluvial fans.

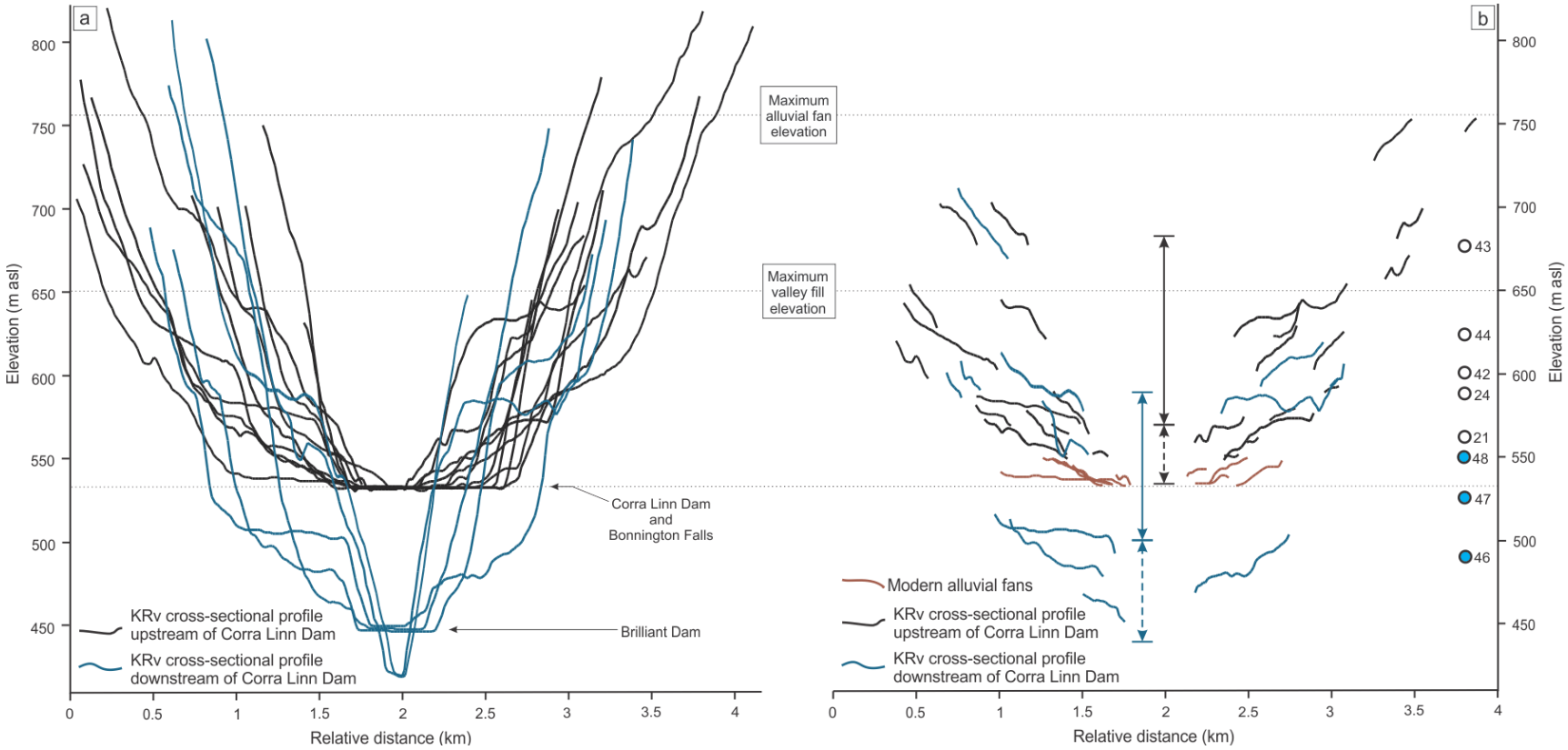

Figure 5-26: a) Sixteen topographic profiles across KRv from along the entire 68 km long valley (vertical exaggeration 10x). Horizontal-trending inflections represent the treads of sedimentary landforms and typically occur only once per cross section; note that tread elevations are usually paired. Upstream from the Corra Linn Dam (black profiles) the valley bottom is fixed at ~532 m asl. Dams located at the two prominent knickpoints are labeled. b) The same topographic profiles with only the most prominent sediment treads displayed and differentiating known modern alluvial fans (brown lines). Upstream of the Corra Linn Dam the elevation range of frequently observed, continuous (non-stepped) valley fill truncation is demarcated by the solid black arrow and elevation ranges containing Kootenay River terraces and Holocene alluvial fans are shown with the dashed black arrow. Downstream of the Corra Linn Dam elevation ranges of frequently observed, continuous (non-stepped) valley fill truncation are demarcated by the solid blue arrow and elevation ranges containing Kootenay River terraces are shown as a dashed blue arrow. Elevations of sites are indicated to the right (black circles demarcate sites above Corra Linn Dam, and blue circles denote sites below the dam).

5.4.2 Sites 21 and 24

5.4.2.1 Geomorphology

Sites 21 and 24 expose sediments of the riser (site 21) and tread (site 24) of a ~2.5 km^2 sediment bench on the northern wall of the KRv (Figure 5-27a) at its confluence with the Purcell Trench (Figure 3-4). The western boundary of the bench terminates at a topographic low near the eastern margin of an alluvial fan-delta and the eastern boundary terminates at a bedrock outcrop that marks the shore of modern Kootenay Lake (Figure 5-27a). The sediment bench and the bedrock outcrop reach elevations of ~590 m asl.

5.4.2.2 Site 21 observations

Site 21 is a ~8 m tall scarp cut during residential construction into the southern riser of the sand and gravel bench on the northern shore of the KRv (Figure 5-27). It exposes one lithostratigraphic unit (unit 1), which is described as two subunits (1a and 1b) with differing texture and structure. Subunit 1a consists of at least 0.2 m of planar cross-stratified, rust-coloured coarse sand with granules and few rounded to well-rounded pebbles (~1 cm across their b-axes) (Sc, Table 4-1; Figure 5-28b). The beds have an apparent dip of 31° towards 170°. Subunit 1b is ~2.5 m thick and composed of very well sorted cross-laminated (lower 1.7 m) and planar-stratified (top 0.8 m) fine sand (Sr and Sp, Table 4-1). Type-A ripples occur low in the subunit and are overlain by type-S ripples, and only rarely by type-B ripples (Figure 5-28c). The ripples record a mean paleoflow direction of 250° (21-1b; Figure 5-28d; Table 5-3), the angles of

climb of the ripple cosets range from 1° to 19° in the type-A ripples and 22° to 30° in the type-B ripples.

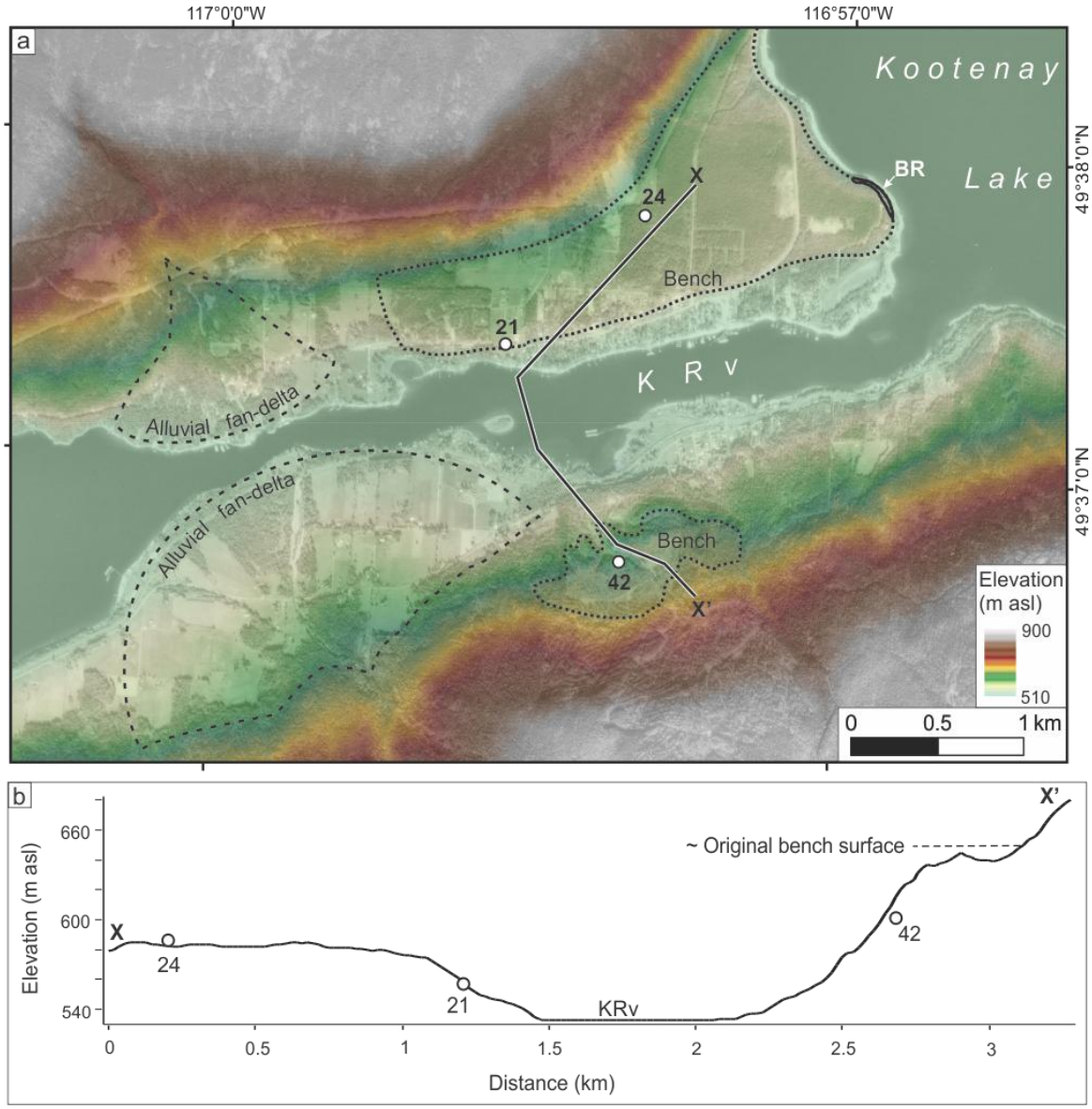

Figure 5-27: a) DEM (Geobase®) overlain by an aerial photograph (BC80137-216. © Province of British Columbia. All rights reserved. Reprinted with permission of the Province of British Columbia.) showing locations of sites 21, 24 and 42 (labeled white dots), the sediment benches they expose (labeled black dotted lines), and the nearby alluvial fan-deltas that grade to the modern Kootenay Lake elevation (labeled dashed lines). The eastern boundary of the northern gravel bench terminates at a bedrock outcrop (BR). Line X-X' marks the position of the topographic profile in b. b) Topographic profile along X-X' showing locations of sites 21, 24 and 42 (labeled white dots) (5x vertical exaggeration). Sites 21 and 24 are located on the riser and tread, respectively, of the lower, northern sediment bench; site 42 is located within a gully on the riser of the higher, southern sediment bench. The approximate original (un-gullied) surface of the high southern sediment bench is shown as a dashed line.

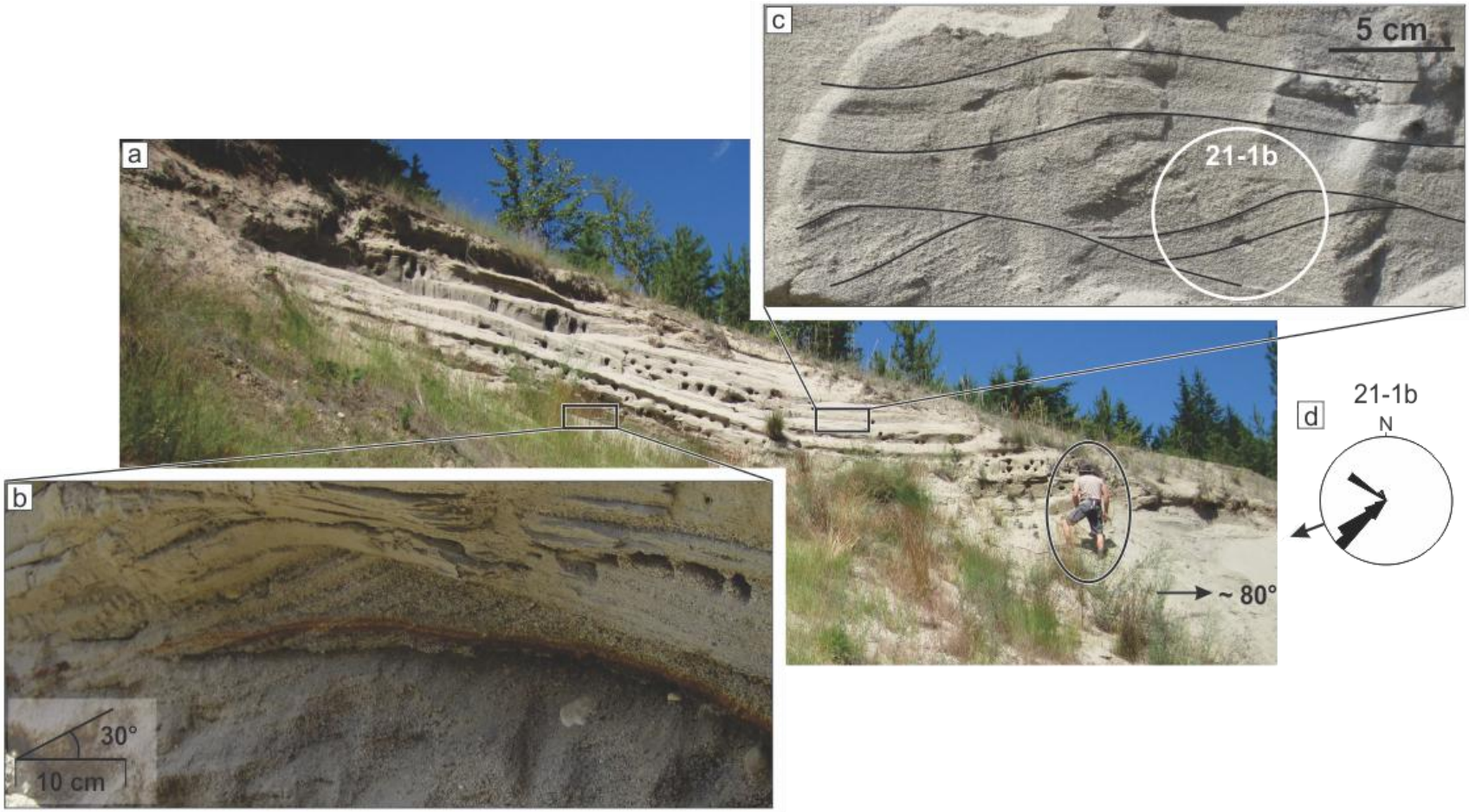

Figure 5-28: a) Site 21 exposes Sc, Sr and Sp (Table 4-1). Person (circled) is 1.7 m tall. Black boxes locate b and c. b) Subunit 1a consists of coarse Sc, (apparent dip angle shown). c) Type-A (bottom of photograph) and overlying type-B and S cross-lamination (highlighted by black lines) in subunit 1b from the area of ripple measurements displayed in d. d) Rose diagram of ripple measurements (21-1b, Table 5-3) taken in subunit 1b reveal a southwestward paleoflow direction. Refer to Table 4-1 for lithofacies codes, Figure 5-27 for site geomorphology and Figure 3-4 for location within the Purcell Trench.

5.4.2.3 Site 21 interpretation

The well-sorted character of the sand in subunit 1b, and the rounding of the pebbles in subunit 1a suggest that unit 1 records a water-lain environment. The cross-stratified sand and granule beds of subunit 1a record a unidirectional flow to the southwest and deposition from traction (Boothroyd & Ashley 1975; Miall 1977). The cross-laminated and planar-stratified sand of subunit 1b record a reduction in flow energy upwards through the deposit.

5.4.2.4 Site 24 observations

Site 24 is an active BC Ministry of Highways gravel pit that exposes a single ~13 m thick lithostratigraphic unit (unit 1) composed of planar-stratified and trough cross-stratified, normally-graded sand and gravel lithofacies (dominated by gravel) (Sp, St, Gp and Gt; Table 4-1) with sharp lower contacts. The gravel beds range in thickness from 0.1-0.6 m and are typically laterally continuous, although some beds are lenticular. Most beds consist of large subrounded to well-rounded (24-1a, 24-1b, 24-1c, 24-1d, Table 5-1) pebbles and cobbles supported by a matrix of medium and coarse sand; some beds exhibit clast-supported cobbles. Gravel fabrics on imbricated clasts (clast are dominantly a(t)) in planar-stratified gravel beds record paleoflows towards the west and southwest (24-1a, 24-1b, 24-1c, 24-1d, Figure 5-29a, Table 5-1). Trough cross-stratified sand exposed in a small gully toward the centre of the exposure (that provides a pseudo-3D view of the sedimentary structure) (Figure 5-29b) appear to have a paleoflow direction to the west (aligned with the West Arm). The sand beds are composed of normally-graded medium and coarse sand.

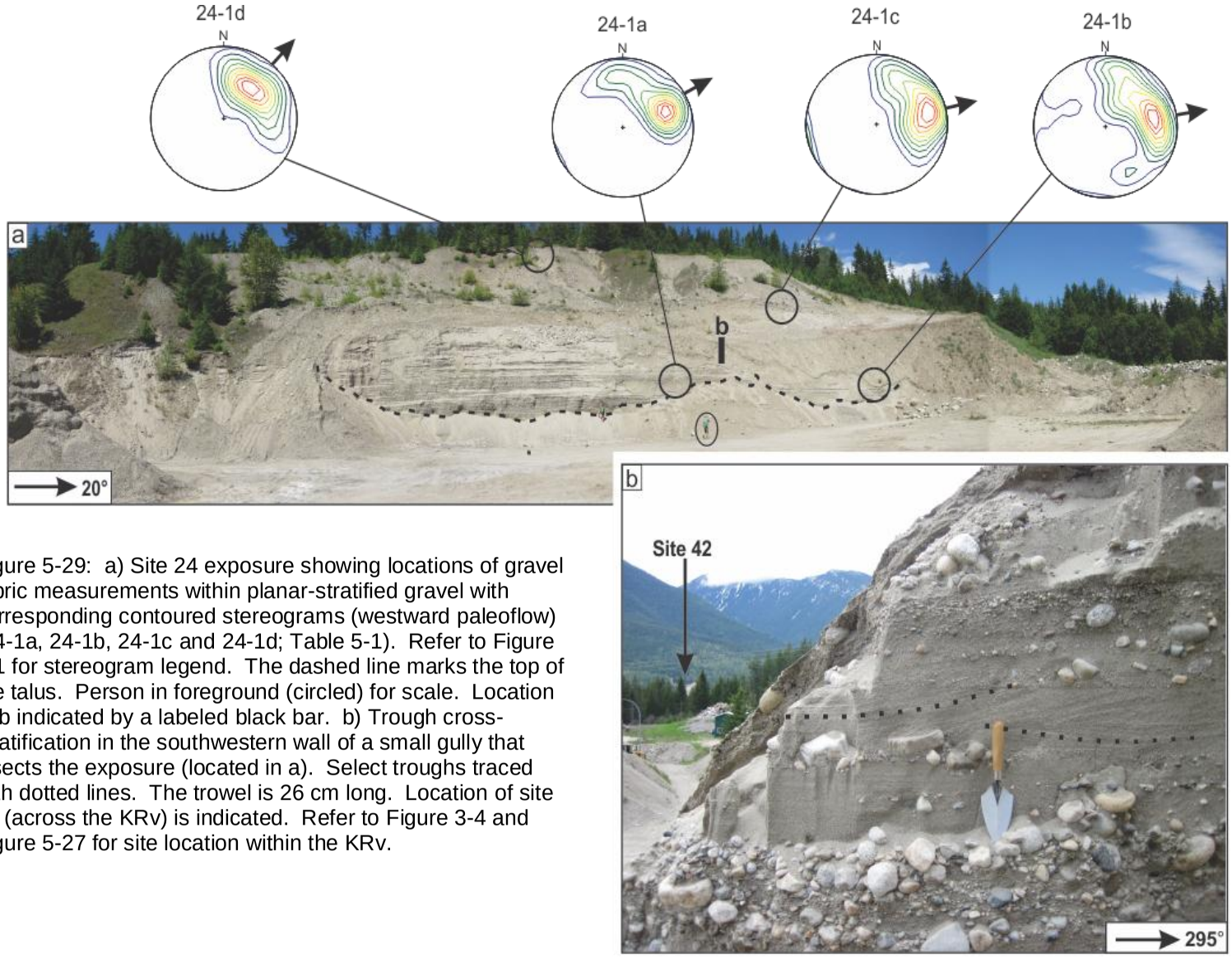

Figure 5-29: a) Site 24 exposure showing locations of gravel fabric measurements within planar-stratified gravel with corresponding contoured stereograms (westward paleoflow) (24-1a, 24-1b, 24-1c and 24-1d; Table 5-1). Refer to Figure 4-1 for stereogram legend. The dashed line marks the top of the talus. Person in foreground (circled) for scale. Location of b indicated by a labeled black bar. b) Trough cross-stratification in the southwestern wall of a small gully that bisects the exposure (located in a). Select troughs traced with dotted lines. The trowel is 26 cm long. Location of site 42 (across the KRv) is indicated. Refer to Figure 3-4 and Figure 5-27 for site location within the KRv.

5.4.2.5 Site 24 Interpretation

Unit 1 is interpreted as a braided river deposit because it contains coarse, imbricated, planar stratified, normally-graded gravel and trough cross-stratified sand and gravel (Miall 1977; Allen 1982). Paleoflow was towards the southwest, consistent with river flow through the KRv that originated in the Purcell Trench.

5.4.3 Site 42

5.4.3.1 Observations

Site 42 is an active BC Ministry of Highways gravel pit that exposes sediments in a gullied, elevated (~601 m asl at top of exposure, ~645 m asl on top of the bench) sediment bench on the west side of the Purcell Trench, ~2.5 km west of Kootenay Lake and ~0.5 km south of the West Arm (the KRv) (Figure 3-4, Figure 5-27). A single lithostratigraphic unit (unit 1) is exposed. It is composed of trough cross-stratified (Gt; Table 4-1) mainly matrix-supported, rounded to well-rounded pebbles and cobbles in a coarse sand matrix with inter-bedded planar-stratified sand (Sp; Table 4-1) (Figure 5-32a, c). Clast-supported beds form <10% of the exposure. Normally-graded gravel beds are up to ~0.6 m thick and form cross sets up to 1.25 m thick. The troughs have sharp lower contacts and some troughs are at least 11 m wide (Figure 5-30). Smaller (<4 m wide) lenses of trough cross-stratified gravel are typically finer in texture, consisting of pebbles with some small cobbles and rare outsized clasts (b-axes up to 15 cm) (Figure 5-30c, small troughs). The sand beds fine upwards and consist of coarse and medium sand with some granules and rare small pebbles.

The sand beds range in thickness from 0.07 – 0.20 m and have sharp lower contacts.

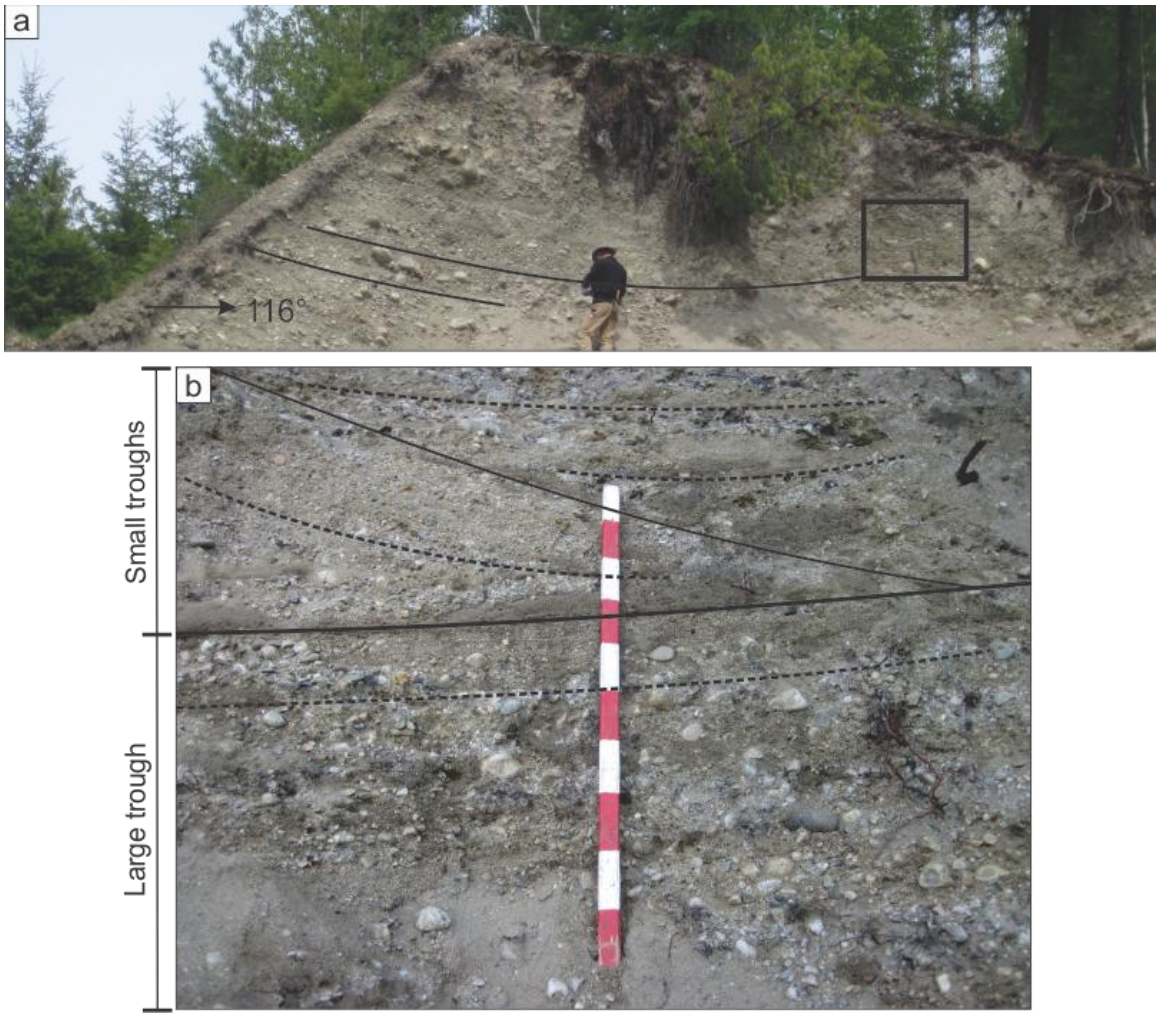

Figure 5-30: a) Site 42 exposes trough cross-stratified gravel (some troughs highlighted as black lines). Black square locates photograph in b. Person is 1.7 m tall. b) Detail of trough cross-stratified gravel (solid lines delimit set boundaries, dashed lines highlight some beds). Decimetre subdivisions on rod.

5.4.3.2 Interpretation

The large trough cross-stratified well-rounded gravel beds, and planar-stratified sand beds may record channel fills in a braided stream environment

(Eynon & Walker 1974; Miall 1977; Allen 1984; Salamon 2008), or large-scale dune migration during flood flow through the KRv (Carling 1996; Maizels 1997; Marren & Matthias 2009). The upward fining in individual beds indicates successive flows, longitudinal sediment sorting, or pulses within the flow with deposition during the waning stages of flow.

5.4.4 Site 43

5.4.4.1 Observations

Site 43 is located in the KRv, ~1.2 km north of the north shore of the West Arm of Kootenay Lake (Figure 3-4; Figure 5-31a). It is an ~8 m high exposure (maximum elevation of ~670 m asl, DEM (Geobase®)) that reveals the sediments within an elevated (maximum ~700 m asl, DEM (Geobase®)), sloping (~4.5°), gullied and truncated, fan-shaped gravel bench (Figure 5-31). Much of the sloping bench is situated in the valley of Duhamel Creek >100 m above the Duhamel Creek delta, which has prograded ~1 km into the West Arm (Figure 5-31). Duhamel Creek is centrally located on the West Arm, ~11 km northeast of Nelson, BC and ~25 km northeast (upstream) of the Corra Linn Dam (Figure 3-4).

One lithostratigraphic unit (unit 1) is exposed. It consists of steeply-dipping planar-stratified sand and gravel lithofacies (Sp and Gp, Table 4-1). The gravel is composed of loosely-consolidated, well-rounded boulders, cobbles and pebbles supported by a matrix of poorly-sorted sand with small amounts of granules. The finest beds consist of poorly-sorted sand and granules and average ~10 cm thick, while coarse beds consist of cobbles and boulders in a

poorly-sorted sand matrix and reach thicknesses >1 m. All of the observed clasts are of a similar, granitic lithology. The beds are tabular and normally graded with sharp lower contacts.

5.4.4.2 Interpretation

The fan-shaped, sloping bench at site 43 suggests that this site is located in a remnant alluvial or colluvial fan that prograded into the KRv from Duhamel Creek (cf. Church and Ryder 1972; Blair & McPherson 1994; Ballantyne 2002). Its elevated position (~670 m asl) in the KRv suggests that the fan prograded onto an elevated KRv floor. The lobate shape of the enduring sediment deposit is interpreted to be the result of incision (gullying) due to a reduction in sediment supply and a lowering of the Duhamel Creek base level (cf. Church and Ryder 1972; Ballantyne 2003), which may have resulted from gLP drainage or Kootenay River incision.

The well-rounded cobbles and boulders at site 43 were water-lain. The normally-graded, poorly-sorted and planar-stratified beds indicate deposition during non-cohesive debris flows (e.g. Blair 1987; Eyles et al. 1987; Blair & McPherson 1994). Thus, the deposit revealed by site 43 is interpreted to be a colluvial fan deposited at the entrance of Duhamel Creek into the KRv. Its elevated position suggests progradation onto an elevated valley floor.

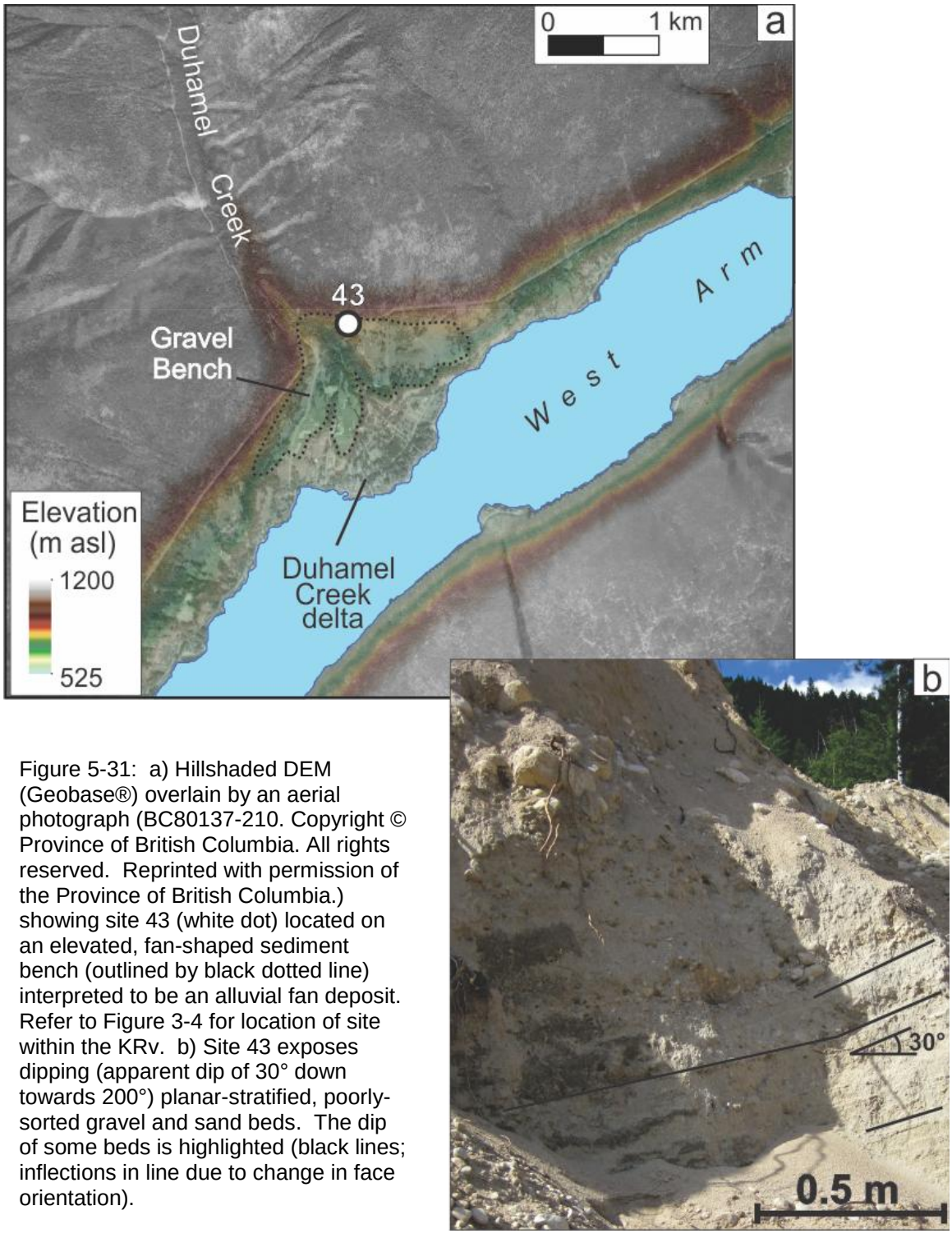

Figure 5-31: a) Hillshaded DEM (Geobase®) overlain by an aerial photograph (BC80137-210. Copyright © Province of British Columbia. All rights reserved. Reprinted with permission of the Province of British Columbia.) showing site 43 (white dot) located on an elevated, fan-shaped sediment bench (outlined by black dotted line) interpreted to be an alluvial fan deposit. Refer to Figure 3-4 for location of site within the KRv. b) Site 43 exposes dipping (apparent dip of 30° down towards 200°) planar-stratified, poorly-sorted gravel and sand beds. The dip of some beds is highlighted (black lines; inflections in line due to change in face orientation).

5.4.5 Site 44

5.4.5.1 Observations

Site 44 is located ~0.2 km north of the West Arm of Kootenay Lake and ~2 km west of the town centre of Nelson (Figure 5-32a). The site is ~624 m asl, which is 92 m above Kootenay Lake. It is bordered to the north by Mt Nelson in the Kokanee Range of the Selkirk Mountains, and to the south by the West Arm of Kootenay Lake and north-flowing Cottonwood Creek (Figure 5-32a).

Exposed at site 44 is an outcrop of smoothed granite bedrock with several smooth circular depressions (Figure 5-32a, b); outcrops of the same bedrock occurring higher (above site 44, investigated to an elevation of ~900 m asl) on the valley wall are not smooth. The depressions range from 0.1-0.3 m in diameter (Figure 5-32b, c) and the largest is filled with ~5 cm of vegetated medium and fine sand (Figure 5-32c).

5.4.5.2 Interpretation

The circular depressions are interpreted as potholes that indicate fluvial erosion (Alexander 1932; Zen & Prestegaard 1994). Potholes typically indicate erosion by a high-velocity stream in which erosion was dominated by corrasion (Zen & Prestegaard 1994). This vigorous stream flow may have been associated with a gLP jökulhlaup, the Kootenay River (likely post-jökulhlaup), which flowed atop the thick valley fill (Figure 5-25), or a combination of the two.

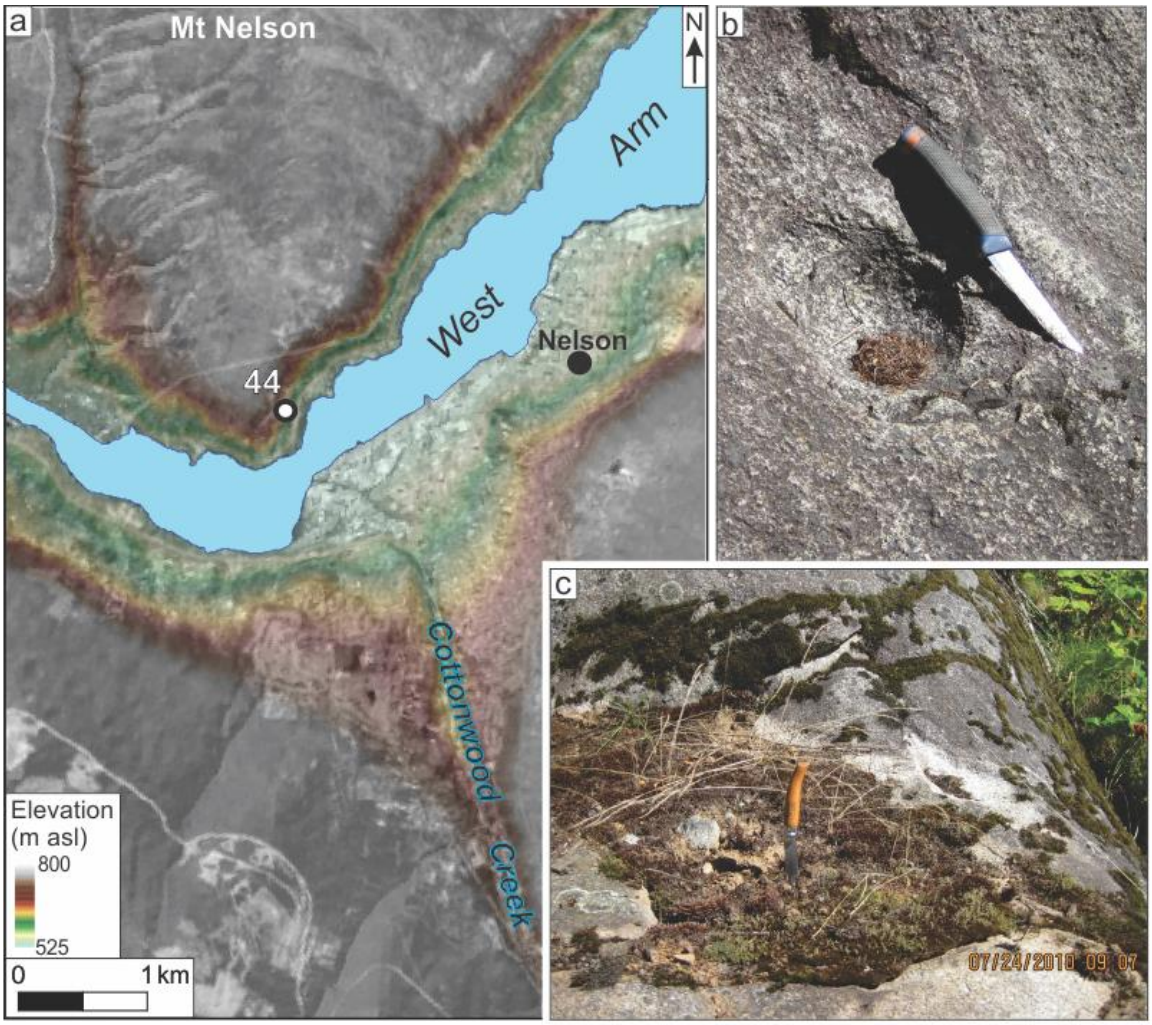

Figure 5-32: a) Hillshaded DEM (Geobase®) superimposed onto an orthophotograph (clip from 1:250 000 orthophotograph mosaic, 82F. © Province of British Columbia. All rights reserved. Reprinted with permission of the Province of British Columbia.) showing the location of site 44 (white dot) and its elevated (~624 m asl) position on the northern KRv wall near Nelson, BC. b) Pothole in granite bedrock; knife is ~18 cm long. c) Sand-filled pothole in granite bedrock; knife is ~17 cm long.

5.4.6 Site 47

5.4.6.1 Observations

Site 47 is located in the KRv, in the riser of an elevated and gullied bench above the western side of the Kootenay River (Figure 5-33a) ~11 km northeast of Castlegar (Figure 3-4). The bench is paired in elevation (maximum elevation ~600 m asl, DEM (Geobase®)) to a similar bench on the eastern side of the

Kootenay River (Figure 5-33b). The risers of both benches are steep and continuous (non-stepped) for >100 m before terminating at a low terrace on the western side of the KRv, which is ~30 m above the Kootenay River (Figure 5-33). An unnamed creek that flows eastward (roughly parallel to exposure 47B) has deeply incised and bisected the bench near site 47 (Figure 5-33a).

At site 47, 25 m (vertical, dGPS) of sediment are exposed along a single, winding bulldozer road that reveals five lithostratigraphic units, which are described from three exposures (Exposures 47A, 47B and 47C; Figure 5-34). Some lithostratigraphic units are designated by letter rather than by number, because these units are interpreted to be emplaced out of sequence with the rest of the deposit (i.e. they record an inset stratigraphy). Sequential letters and numbers are used for simplicity, though it is acknowledged that the record is incomplete (i.e. the full sequence is not exposed) (Figure 5-34).

Exposure 47A

Exposure 47A is the lowest exposure at site 47 (maximum elevation of 509 m asl, dGPS) (538 m asl, DEM) and is >7 m long and up to 3 m high (Figure 5-34). It contains two subunits (1a, and 1b) of lithostratigraphic unit 1 and lithostratigraphic unit W (Figure 5-34, Figure 5-35a). Subunit 1a (~1 m thick, lower contact not visible) contains deformed (faulted and sheared) and cross-laminated sand lithofacies (Sd and Sr, Table 4-1) described as parcels 1a-i, 1a-ii and 1a-iii, differentiated on the basis of sediment texture and structure, and arranged laterally across the exposure (Figure 5-35b). Parcels are sheared to the north and southeast (Figure 5-35b).

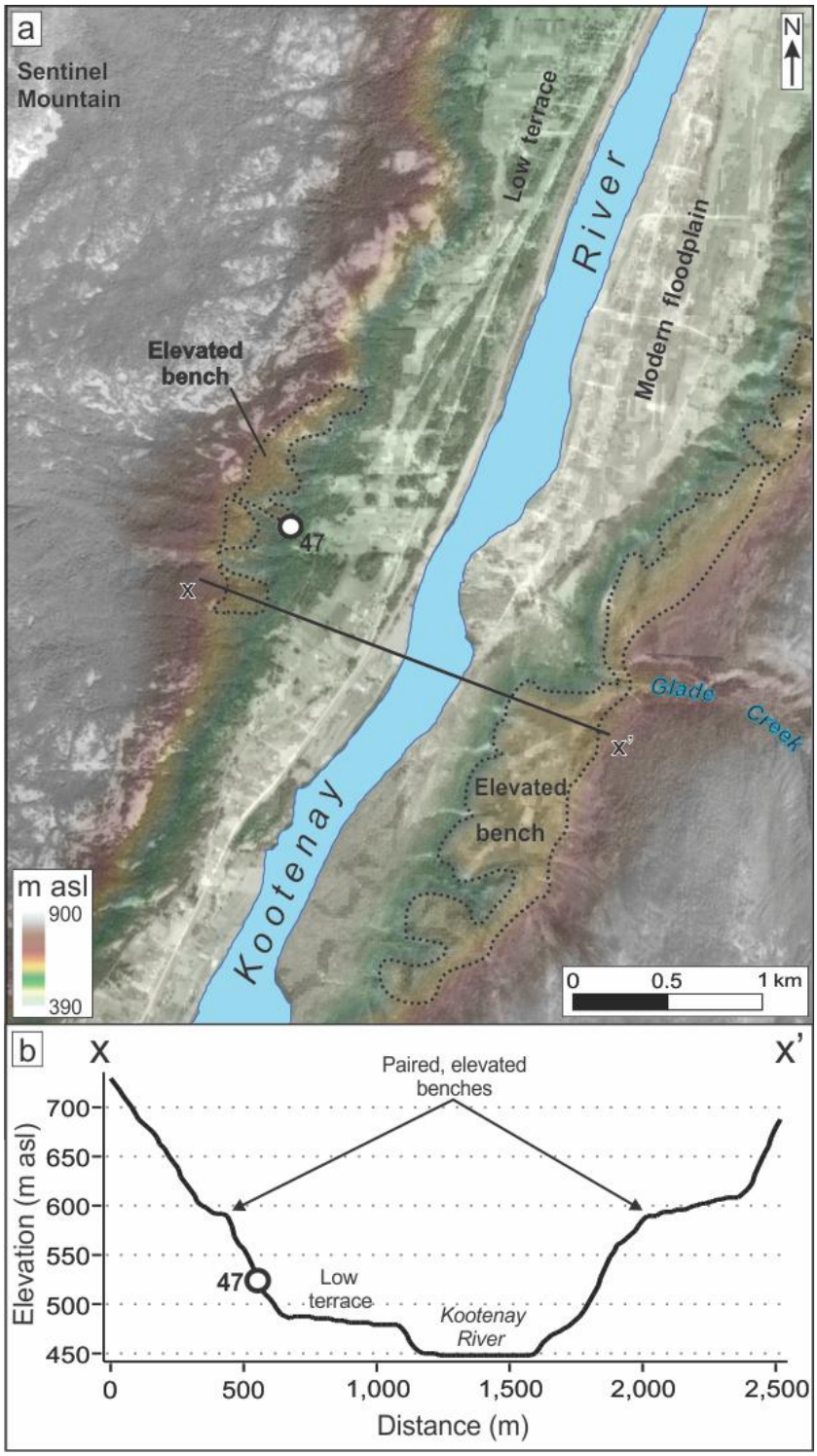

Figure 5-33: a) Hillshaded DEM (Geobase®) overlain by an aerial photograph (A22007-20; © Department of Natural Resources Canada. All rights reserved.) showing site 47 (white dot) located in an elevated bench above the floodplain of Kootenay River. The remnant, elevated (~590 m asl) bench surfaces are outlined with dotted lines. Line X-X' denotes location of the topographic profile in "b". Refer to Figure 3-4 for location of site in KRv. b) The topographic profile (X-X') shows the paired elevations of the elevated benches and location of site 47 (labeled white dot). Vertical exaggeration ~3.75x.

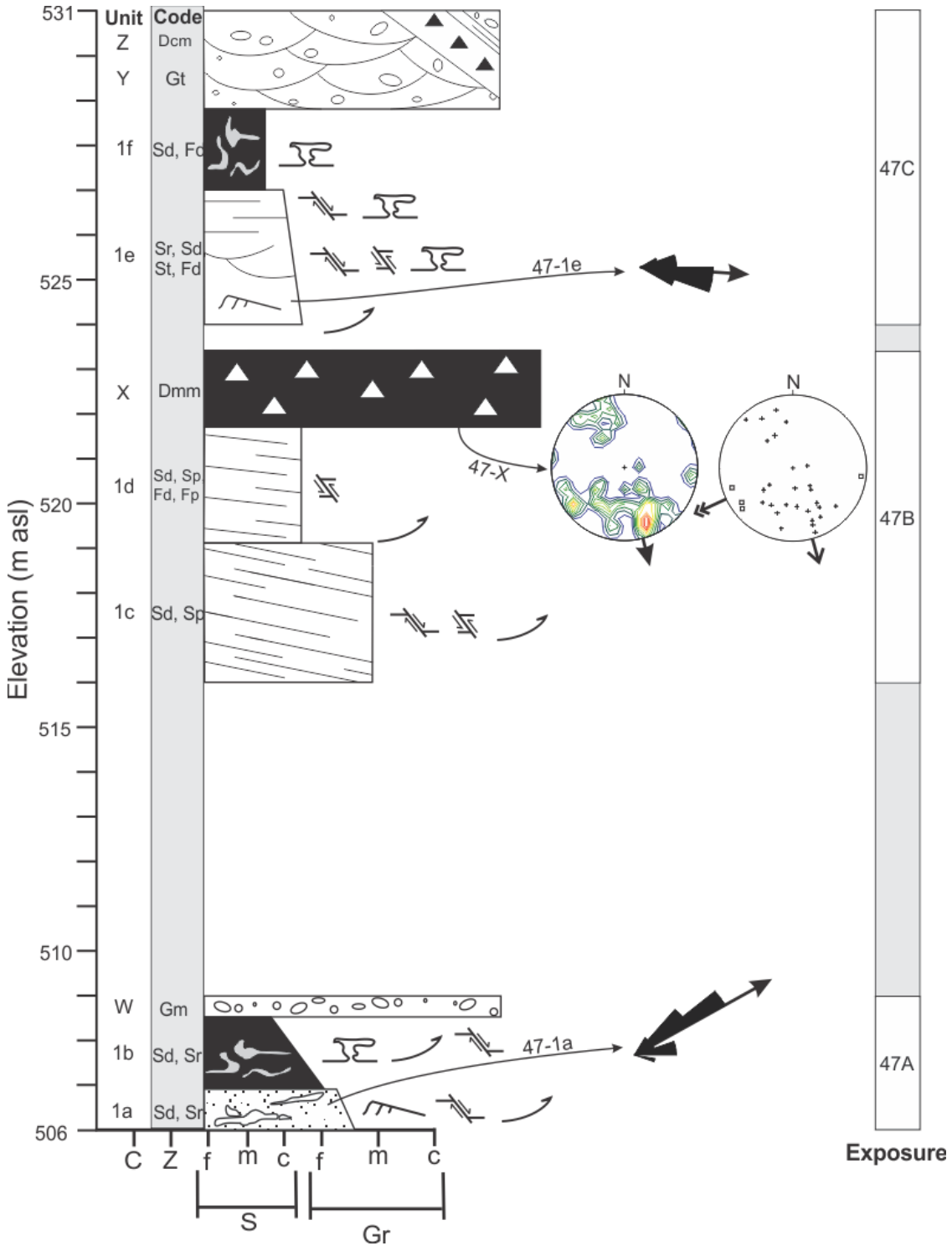

Figure 5-34: Composite sedimentary log of site 47 exposures 47A, 47B and 47C (labeled on right; grey bars denote unexposed areas between exposures). Units and subunits denoted with numbers record sequential stratigraphy, units denoted with letters record inset stratigraphy. The thickness of some units differs from that reported in the text because laterally varying unit thicknesses have been collapsed into a single log (refer to text for maximum thicknesses). Refer to Figure 4-2 for sedimentary log legend, Table 4-1 for lithofacies symbols and codes, Figure 4-1 for stereogram legend, and Table 5-2, and Table 5-3 for fabric and paleoflow data, respectively.

Parcel 1a-i is 0.8 m thick and is composed of cross-laminated (type-B ripples), normally-graded medium and fine sand that has undergone varying amounts of deformation from shearing (Figure 5-35b). Paleoflow is towards the northeast (47-1a, Figure 5-34, Figure 5-35b; Table 5-3), and the angle of climb of the type B ripples decreases towards the top of the subunit and ranges from 15°-46°.

Parcel 1a-ii is ~0.7 m thick (Figure 5-35b) and is comprised of deformed (microfaulted and sheared) alternating fine and medium sand beds (Sd, Table 4-1). This parcel has been faulted and sheared out of its original stratigraphic position, which is presumed to have been directly above parcel 1a-i. The extensive remobilization and shearing of this subunit has left no evidence of primary sedimentary structures. The lower contact of parcel 1a-ii (dotted line between parcels 1a-i and 1a-ii, Figure 5-35b) is sharp, microfaulted, truncates the sand beds of parcel 1a-i, and dips 16° towards 286° (Figure 5-35b).

Parcel 1a-iii is ~0.7 m thick and composed of deformed (sheared and microfaulted) and planar-bedded (Sd and Sp, Table 4-1), normally-graded coarse and medium sand. The Sp beds are tilted with apparent dips that range from 35°-45° towards ~170°. The lower contact of parcel 1a-iii (dotted line between parcels 1a-ii and 1a-iii, Figure 5-35b) is sharp, microfaulted, truncates the Sd beds of parcel 1a-ii, and dips 24° towards 186° (Figure 5-35b).

Subunit 1b is 1.3-2.5 m thick (Figure 5-34, Figure 5-35a) and composed of deformed medium and fine sand and silt and clay (Sd and Fd, Table 4-1). Deformation in the subunit is recorded by faults, shear planes, boudinage

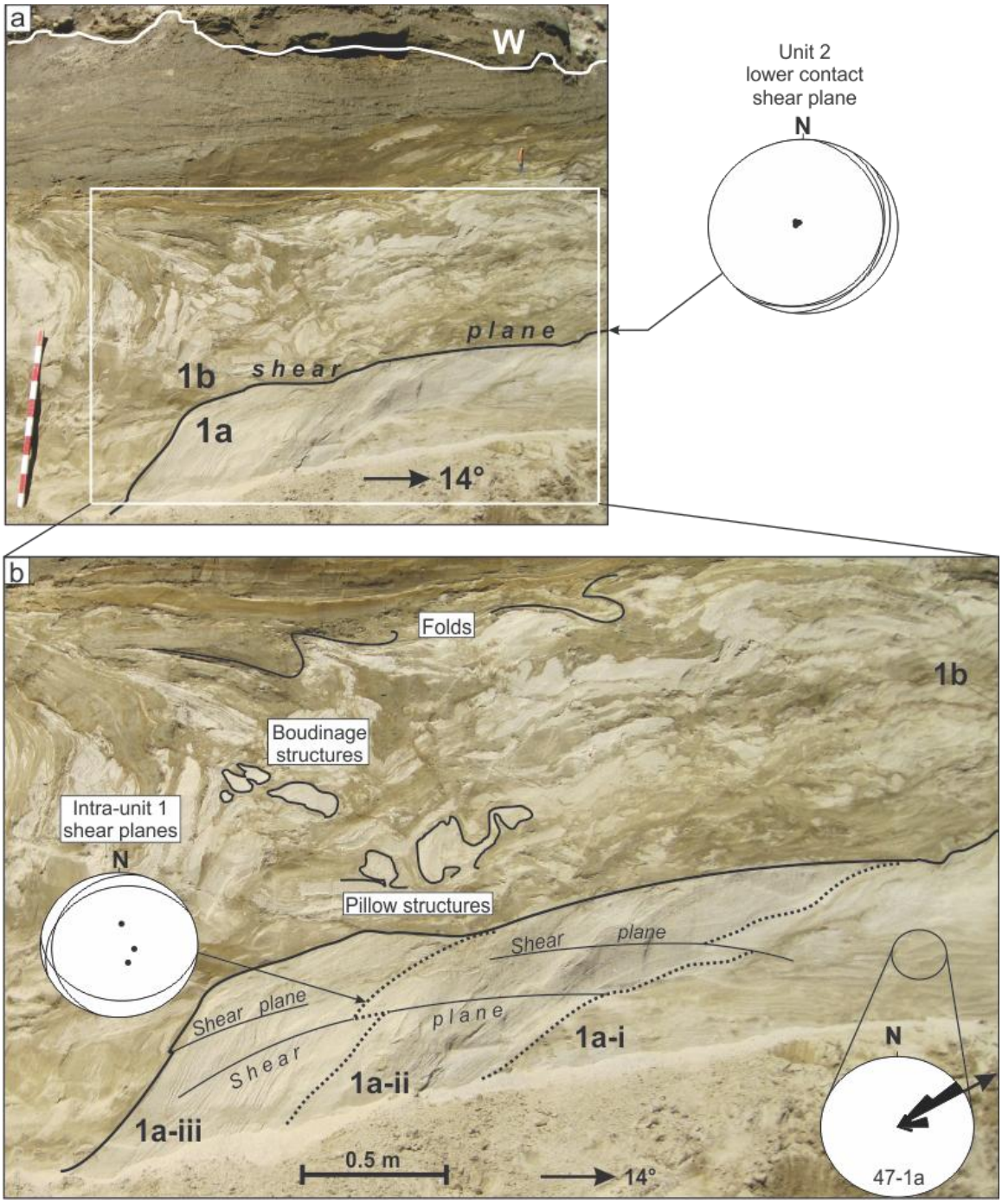

Figure 5-35: a) Exposure 47A reveals subunits 1a and 1b separated by a shear plane (black line) and unit W with an irregular lower contact (white line). Shear plane orientations and dips are plotted as arcs and poles-to-planes on a stereogram. Metre stick has decimetre markings. b) Close-up of subunit 1a and 1b sedimentology. Subunit 1a contains three parcels (i-iii, delimited by large shear planes (dotted lines)) that are transected by smaller shear planes (thin black lines). The orientations and dips of the parcel-delineating shear planes (dotted lines) are shown on the stereogram as arcs and poles-to-planes. Paleoflow directions for some relatively undisturbed ripples (47-1a) are shown in the rose diagram. Some folds, pillow structures, and boudinage structures are highlighted (black lines) and labeled.

structures, pillow structures, and folds (Figure 5-35b). The unit displays an overall upward fining from medium sand at its lower contact to sandy silt and clay near the lower contact of unit W (Figure 5-35a). The lower contact of subunit 1b is sharp and delineated by a shear plane that truncates the Sd beds of subunit 1a (Figure 5-35a). The attitude of this shear plane is shown in Figure 5-35a as arcs and corresponding poles to planes on a stereogram, which reveals a down-dip direction of shear towards the southeast.

Unit W at the top of exposure 47A, consists of massive gravel (Gm, Table 4-1) with rounded to angular clasts (pebble to cobble sized) supported by a poorly-sorted sand matrix. Unit W has a sharp lower contact that truncates the deformed laminae of subunit 1b (Figure 5-35a).

Exposure 47B

Exposure 47B is >15 m long and ~8 m high, reaching a maximum elevation of 523.5 m asl (dGPS) (538 m asl, DEM) (Figure 5-34, Figure 5-36). It is oriented roughly parallel to a nearby unnamed creek that has deeply incised the bench (Figure 5-33a) and exposes two lithostratigraphic subunits (1c and 1d) and one lithostratigraphic unit (unit X) (Figure 5-36).

Subunit 1c is at least 3 m thick (lower contact not exposed) (Figure 5-36) and is composed of deformed (faulted and tilted) planar-stratified sand lithofacies (Sd and Sp, Table 4-1) that consist of unconsolidated, normally-graded coarse to medium sand. The beds have an apparent tilt of 34° towards 80° and shear planes show apparent eastward displacements. Fine sand and clay intrusions,

apparently originally deposited as part of subunit 1d, have been sheared into subunit 1c.

Subunit 1d is ~3 m thick (Figure 5-36) and composed of deformed (tilted and faulted) planar-bedded fine sand and sandy clay lithofacies (Sd, Sp, Fd and Fp, Table 4-1). The beds average ~10 cm thick, are normally-graded, and consist of unconsolidated fine sand and clay. Sand from subunit 1c has been sheared into the base of subunit 1d (Figure 5-36).

Unit X overlies subunit 1d and is at least 1.5 m (Figure 5-36) thick and composed of a massive, clast-poor (~20% clasts) diamicton (Dmm, Table 4-1). Clasts range in size from pebbles to small boulders (b-axes up to 0.5 m), are supported by a poorly-sorted silty sand matrix and are dominantly subrounded to angular (47-X, Table 5-2). Unit X has a sharp lower contact that truncates the sand beds of unit 1d. A diamicton fabric (47-X, Table 5-2) reveals a bimodal distribution with many clasts exhibiting high plunge angles, and a principal eigenvector towards the south-southeast (Figure 5-36) and the unnamed creek.

Exposure 47C

Exposure 47C is >60 m long and up to ~5 m high (Figure 5-37), reaching a maximum elevation of 531 m asl (dGPS) (535 m asl, DEM) (Figure 5-34). The top of the 47C exposure is ~25 m higher (dGPS) than, and located almost directly above the base of exposure 47A (a result of the steep and winding bulldozer road).

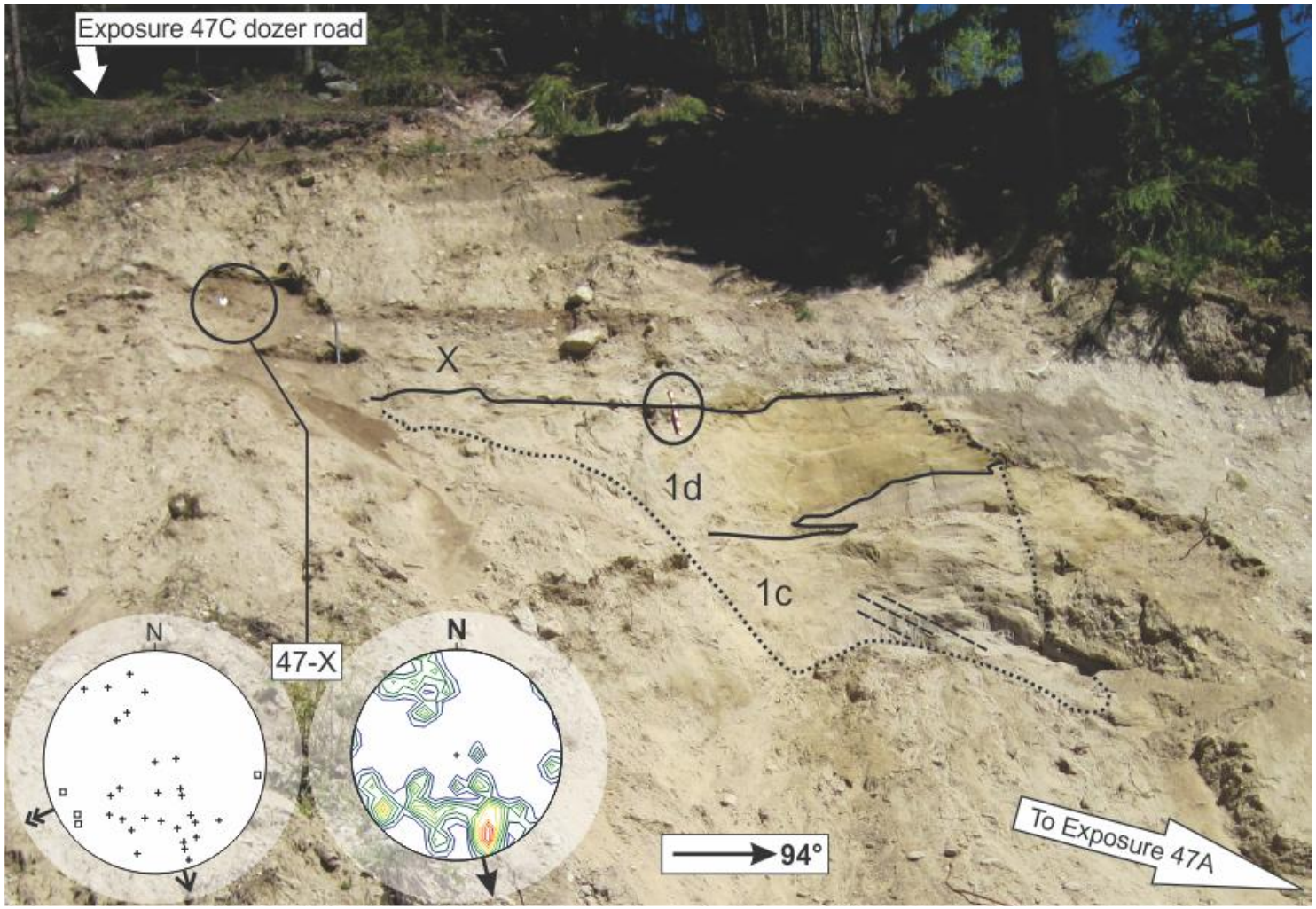

Figure 5-36: Exposure 47B reveals subunits 1c and 1d, and unit X. Bold lines delineate unit contacts. Tilted beds in Unit 3a are highlighted (dashed black lines). The top of the talus is indicated with a dotted line. The location and stereograms of diamicton fabric 47-X (Table 5-2) are provided. Refer to Figure 4-1 for stereogram legend. The relative positions of exposures 47A and 47C are shown. Metre stick is circled.

Two lithostratigraphic subunits (subunits 1e and 1f) and two lithostratigraphic units (units Y and Z) are revealed in exposure 47C (Figure 5-37). Subunit 1e is ~4 m thick and composed of upward fining, deformed (sheared) cross-laminated fine sand beds (Sr, Table 4-1) (Figure 5-37b) that are truncated and overlain by faulted, sheared and dewatered trough cross-stratified fine sand and clay lithofacies (Sd, St and Fd; Table 4-1) (Figure 5-37b). The trough cross-stratified sand is truncated and overlain by deformed (faulted, Figure 5-37b), dewatered and tilted (apparently 6° towards 70°), planar-bedded and laminated coarse to fine sand, silt and clay (Sp, Sd, Fl and Fd; Table 4-1). Trough width decreases upwards through the subunit from ~1 m near the bottom of the exposure to <0.25 m near the top. Three prominent arcuate shear planes with dips ranging from 58°-85° down towards ~300°cut through the Sr and St of subunit 1e, the largest of which is >1 m long. Type-A climbing ripples low in subunit 1e record a paleoflow direction towards the east (47-1e, Figure 5-37c).

Subunit 1f is 1.5-5 m thick and consists of tilted (apparent tilt 6° towards 70°) and dewatered fine sand with some medium sand and large amounts of silt and clay (Sd, Fd, Table 4-1). This subunit displays many large dewatering structures (sand and clay dikes, convolute bedding, flame structures, and ball-and-pillow structures) that increase in size and frequency with proximity to the overlying gravel of unit Y (Figure 5-37).

Unit Y is 2-7 m thick and composed of trough cross-bedded gravel (Gt, Table 4-1) in a well-sorted coarse sand matrix (Figure 5-37d). The clasts range in size from pebbles to cobbles (up to 0.09 m b-axes), are well-rounded, and

highly spherical (Figure D-3). Clasts are matrix supported in small (less than ~4 m wide) fine-textured troughs and clast supported in the large (> 5 m wide) coarse-grained troughs. The lower contact of unit Y is sharp, irregular and truncates the Sd and Fd beds and laminae of subunit 1f.

The highest stratigraphic unit at site 47 is unit Z (Figure 5-34, Figure 5-37), which is comprised of interbedded planar-stratified coarse sand, planar-stratified pebbles, massive pebble beds, massive clast-supported diamicton, and laminated silt and clay (Sp, Gp, Gm, Dcm, Fl, Table 4-1). The sand beds are ~0.10 m thick, possess frequent granules and have sharp lower contacts. The pebble gravel beds average ~0.20 m thick, rarely contain outsized cobbles (b-axes up to 0.25 m), and have sharp lower contacts. The diamicton beds consist of subrounded pebbles in a silty fine sand matrix, average ~0.10 m thick, and have sharp lower contacts. The granule beds average ~0.05 m thick and have sharp lower contacts. The unit is saturated and weeps groundwater and a slurry of fine-grained sediment.

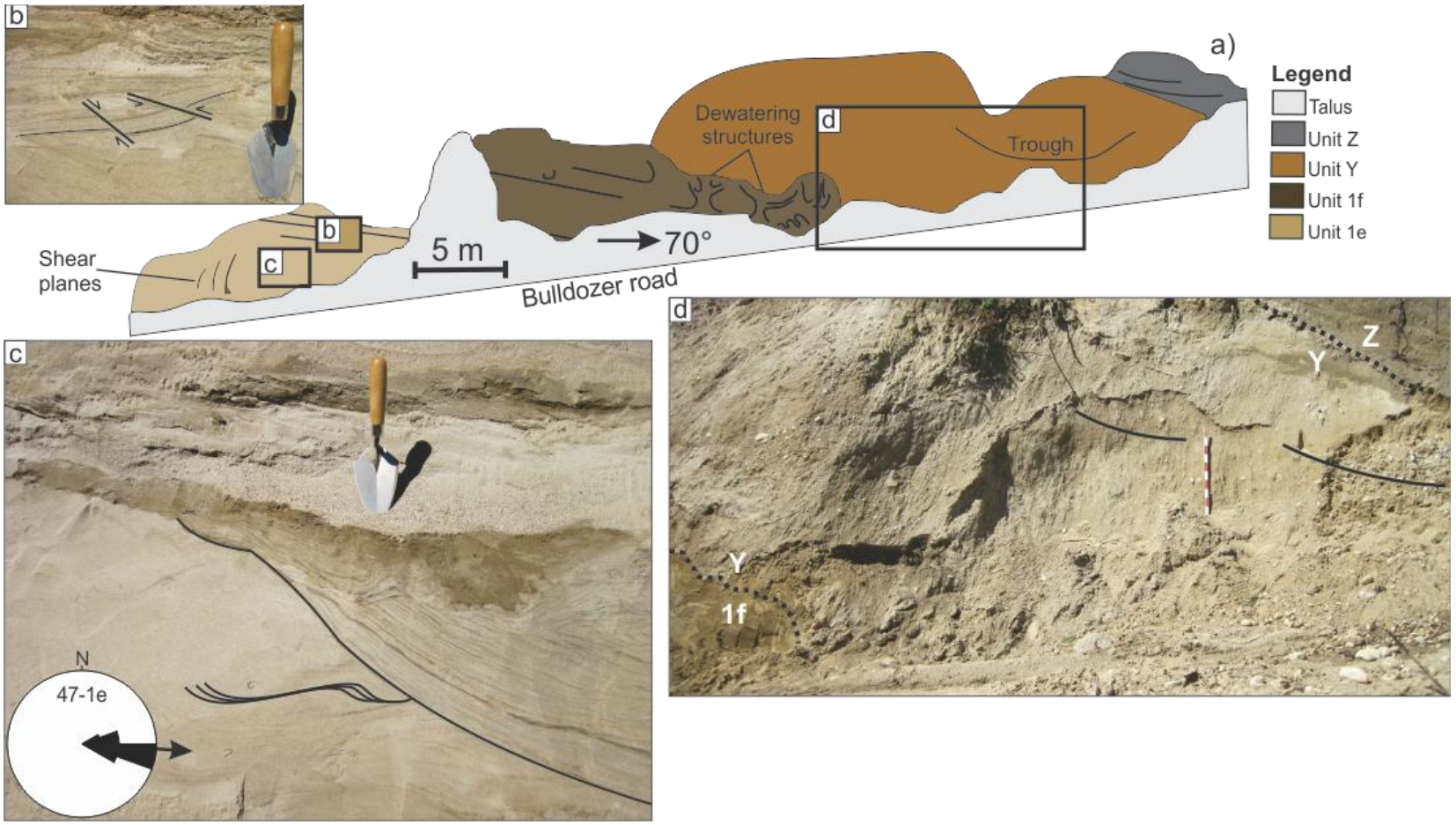

Figure 5-37: a) Sketch of exposure 47C illustrating stratigraphy and some sediment structures (labeled black lines). Boxes locate photographs in b-d. b) Faults within subunit 1e. c) Deformed (sheared and dewatered) trough cross-stratified sand (bottom of trough highlighted with a black line), silt and clay truncates cross-laminated sand (type-A ripples highlighted by black lines; occasionally sheared), and is overlain by deformed (dewatered, faulted and sheared) planar-bedded sand silt and clay in subunit 1e. Rose diagram displays the paleoflow of the type-A ripples (47-1e, Table 5-3). d) Trough cross-stratified gravel in unit Y (some troughs highlighted by black lines) and contacts with unit Z and subunit 1f (black dotted lines). Trowel is 0.27 m long. Metre stick has decimetre subdivisions.

5.4.6.2 Interpretation

The paired elevations of the terrace at site 47 and the terrace on the east side of the Kootenay River (Figure 5-33), and their similar gullied morphology suggest that the terraces record an elevated valley fill (to ~600 m asl). Below I argue that the fine-grained sediments in subunits 1a-1f record a lake bottom depositional environment in the valley-fill, and the coarse-grained, poorly-sorted sediments of units W-Z record deposition by debris flows and streams during valley-fill incision. Accordingly, the pre-gLP drainage valley-fill (subunits 1a-1f) is first interpreted, and then the inset stratigraphy (units W-Z) is interpreted.

Unit 1 (valley fill sediment)

Subunits 1b and 1f are interpreted as recording deposition from suspension settling on a lake bed because they are composed of sorted fine sand, silt and clay laminae (Smith & Ashley 1985). Shearing at the lower contact of subunit 1b records mobilization over subunit 1a during deposition on a gently sloping (valley-wall proximal) lake bed. Soft sediment deformation structures indicate strain from extension (boudinage structures) and compression (folds) (McCarroll & Rijsdijk 2003) as sediments were remobilized.

Subunits 1a, 1c and 1e are interpreted as recording relatively higher-energy deposition on the lake bed because they are composed of well sorted, normally-graded, planar-stratified and cross-laminated sand (Smith & Ashley 1985). Type-B climbing ripples may indicate the inflow of turbidity currents into the lake (e.g., Smith & Ashley 1985; Johnsen & Brennand 2006). Trough cross-stratified fine sand in unit 1e records scour and fill during high-density turbidity

flows (Lowe 1982). Intra-unit shear planes in subunits 1a and 1e are interpreted as syn-depositional because they do not extend into overlying subunits; they provide a record of saturated sand remobilization on a gently-sloped lake bed.

Units W-Z (inset stratigraphy)

Unit W is interpreted as fluvial sediment that was remobilized into a non-cohesive debris flow deposit because it contains rounded clasts suggesting fluvial wear (Mills 1979; Lindsey et al. 2007), and a massive matrix-supported structure consistent with non-cohesive debris flows (Eyles et al. 1987; Blair & McPherson 1994). Its lower contact is interpreted as erosional.

Unit X is interpreted as a cohesive debris flow deposit because it is composed of massive matrix–supported diamicton that contains clasts without glacigenic wear features (Lowe 1982). The bimodal diamicton fabric including clasts with high plunge angles may record compressive and extensional stresses in a cohesive debris flow (Lowe 1982; Eyles et al. 1987). Its lower contact is interpreted as erosional.

Unit Y is interpreted as recording fluvial sedimentation because of its texture and structure. It is well sorted and contains well-rounded, highly spherical clasts indicative of wear and sorting during fluvial transport (Mills 1979; Lindsey et al. 2007). The large lenses of Gt (Table 4-1) likely record channel fills in a braided stream environment (Miall 1977; Allen 1984; Salamon 2008). Consequently, unit Y may have been deposited in a local stream responding to the evolving gullied geometry of the elevated sediment bench. Its lower contact is interpreted as erosional.

The steeply dipping, crudely stratified and massive sand, gravel and diamicton lithofacies of unit Z record small, periodic colluvial events (Hein 1982; Lowe 1982; Eyles et al. 1987) within the over-steepened gully of the unnamed creek. The inverse grading in some Gp granule beds may record grain flows (Sallenger 1979). The sharp lower contact of unit Z, which truncates the gravel of unit Y, is interpreted as erosional.

In summary, unit 1 records sedimentation in a lake within the pre-gLP drainage valley fill, and units X-Z record alluvial and colluvial sedimentation during or following valley fill incision. Unit 1 may have been deposited into the same lake that occupied the Slocan River valley ("glacial Lake Slocan", site 54, Appendix B).

5.4.7 Sites 48A and 48B

5.4.7.1 Observations

Sites 48A and 48B occupy the northern half of a large, terraced fan-shaped deposit at the confluence of the Kootenay and Columbia Rivers (Figure 5-38a). The landform extends radially from a bedrock constriction (near Brilliant Dam) in the Kootenay River valley (Figure 3-4) and has been bisected by the Kootenay River, leaving a series of terraces within the fan (mapped from aerial photographs and numbered according to elevation, Figure 5-38, Figure 5-39) that were first mapped by Fulton (1970). The nearby Columbia River valley is terraced to the north and south of sites 48A and 48B (Figure 5-38a).

Geologic cross sectional diagrams (Figure 5-38b, c) constructed (using field observations and well logs, Appendix E) along lines X-X' and Y-Y' reveal valley fill stratigraphy near the confluence of the KRv and the Columbia River valley. Cross section X-X' reveals the inset and shallow (~10-30 m below the surface) nature of the terraced, fan-shaped deposit at sites 48A and 48B (Figure 5-38b). Terrace 8, at the foot of the fan, is shown to be capped by compact silty clay with pebbles and boulders (unit 2, Figure 5-38b). Cross section Y-Y' illustrates the paired elevations of terraces 1 and 7 (Figure 5-38c).

Site 48A is a small road-cut exposure within the riser of terrace 6 (maximum elevation ~492 m asl) that reveals a single lithostratigraphic unit (unit 1) composed of crudely-bedded massive gravel (Gm, Table 4-1). The gravel is comprised of mainly clast-supported, rounded to well-rounded and highly spherical pebbles to boulders (up to 0.5 m b-axis) in a poorly-sorted sand matrix with a small percentage of silt; some gravel beds (~10%) are openwork (Figure 5-40).

Figure 5-38: (Next page) a) Hillshaded DEM (Geobase®) overlain by an aerial photograph (A22007-8, NAPL; © Department of Natural Resources Canada. All rights reserved.) showing locations of sections at sites 48A and 48B (white dots labeled A and B, respectively). Terraces are outlined (solid black lines) and numbered according to elevation with 1 and 11 being the highest and lowest, respectively. Terraces that share a label are within 5 m in elevation of one another. Bedrock contact (from field and aerial photograph observations) is outlined by dotted black lines and rock slides (from aerial photograph observations) are labeled "rs". Boxed area is shown in Figure 5-39a. Lines X-X' and Y-Y' mark the location of geologic cross-sections in b and c. X-X' (b) and Y-Y' (c) cross-sections showing simplified valley fill stratigraphy consisting of five lithostratigraphic units. Known bedrock (BR) locations are shown as dotted lines, and inferred bedrock contacts are shown as dashed lines; areas of uncertainty are marked with question marks. Well log data is shown in Appendix E. Note that the fan-shaped deposit emerging from the Kootenay River valley is a thin, terraced carapace on the valley-wall bedrock. Vertical exaggeration = ~2x (b) and ~3x (c).

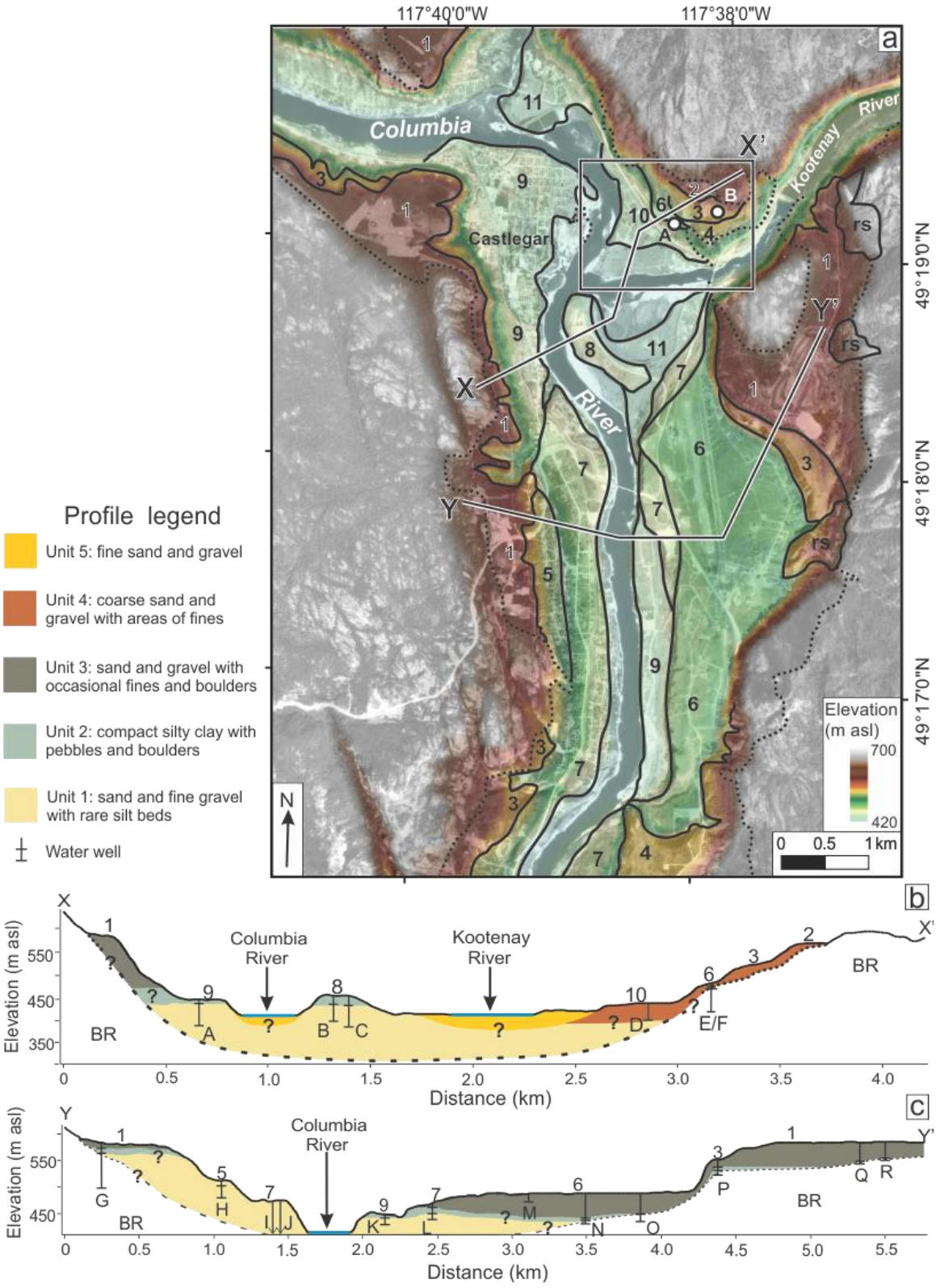
117°40'0"W
117°38'0"W
49°19'0"N
49°18'0"N
49°17'0"N
a
Columbia
River
Kootenay
River
Castlegar
X
X'
Y
Y'
Profile legend
Unit 5: fine sand and gravel
Unit 4: coarse sand and gravel with areas of fines
Unit 3: sand and gravel with occasional fines and boulders
Unit 2: compact silty clay with pebbles and boulders
Unit 1: sand and fine gravel with rare silt beds
Water well
Elevation (m asl)
700
420
0 0.5 1 km
N
b
Columbia River
Kootenay River
BR
Elevation (m asl)
Distance (km)
c
Columbia River
BR
Elevation (m asl)
Distance (km)

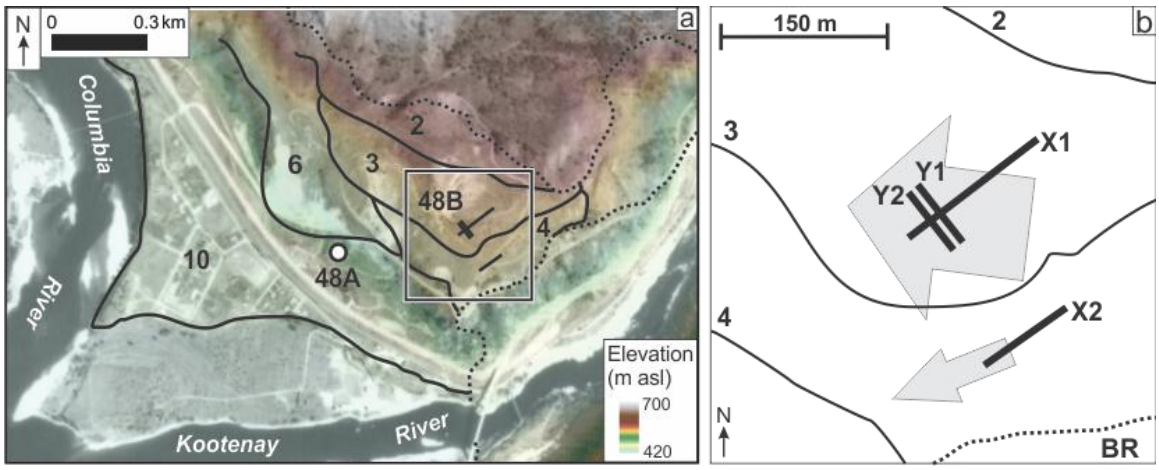

Figure 5-39: a) Hillshaded DEM (Geobase®) overlain by an aerial photograph (A22007-8, NAPL; © Department of Natural Resources Canada. All rights reserved.) showing boxed area from Figure 5-38a and locations of sites 48A (labeled white dot) and 48B (labeled black lines). Terraces are numbered by elevation and correspond to those numbered in Figure 5-38a. Black dotted lines delineate bedrock contacts. b) GPR grid at site 48B (line labels are placed at 0 m along the line). Grey arrows denote ~paleoflow direction inferred from radar reflections. Dotted line delineates bedrock (BR) location.

Figure 5-40: Crudely-bedded, clast-supported, massive gravel in a poorly-sorted silty sand matrix with areas of openwork structure exposed at site 48A. Ruler is 0.36 m long.

Site 48B is an inactive, privately-owned gravel pit that occupies two terraces (terrace 3 at 550 m asl, and terrace 4 at 532 m asl; dGPS) (~539 m asl, DEM) above the north shore of the Kootenay River, near its confluence with the Columbia River (Figure 5-39a). Although there are no vertical sediment exposures in the pit, the surface material exposed on the pit floor consists of coarse sand and rounded to well-rounded pebbles and cobbles; well-rounded boulder (up to ~1 m along b-axes) piles are also present.

Because there were no exposures at site 48B, sedimentary architecture was documented using ground-penetrating radar (GPR) (Figure 5-39a, b). Two KRv-parallel (X-lines) and two KRv-perpendicular (Y-lines) lines were collected on terraces 3 and 4 (Figure 5-39b). Lines X1 and X2 are 145 and 90 m long, respectively; lines Y1 and Y2 are both 65 m long (Figure 5-39b, Figure 5-41).

Radar bounding surfaces define 31 radar elements on terrace 3, labelled a to ee, and 16 radar elements on terrace 4, labelled a to p (Figure 5-41). Radar elements (RE) are ~1-4 m thick and most have a concave-up lenticular geometry and lower bounding surfaces that truncate deeper reflections (Figure 5-41). Radar elements in line X1 have KRv-parallel lengths ranging from ~12 m to >130 m (RE c and h, respectively, Figure 5-41b) with a mode of ~25 m; radar elements in line X2 have KRv-parallel lengths ranging from ~10 to >45 m (RE b and a, respectively, Figure 5-41e) with a mode of ~30 m (Figure 5-41b, e). Internally these radar elements have varied reflection geometries, including subhorizontal (e.g., RE a, b, c, h, n, o, Figure 5-41e), shallowly-dipping towards the northeast or southwest (upstream and downstream along the KRv) with dip angles up to

~15° (e.g., RE d, g, j, k, l, Figure 5-41e), or concave-up, particularly in Y-lines (e.g., RE g, i, j, m, n, bb, Figure 5-41c). Reflections are typically moderately continuous, subparallel to one another, and on-lap radar element lower boundaries (e.g., RE f, h, k, q, s, Figure 5-41b,). Rarely, reflections dip northeast (i.e., in a direction that is upstream relative to the Kootenay River) (e.g., radar elements s, u, p; ~10-45 m, Figure 5-41b). Some out-of-line reflectors (boulders) have resulted in hyperbolic diffractions in the GPR lines; the diffractions have been removed through the migration function (§ 4.2.2; Figure 5-41a). There is no evidence of distortion (faulting) of primary reflection geometry.

5.4.7.2 Interpretation

The well-rounded clast-supported and openwork gravel lithofacies at site 48A were deposited by river flows. A paucity of matrix and areas of openwork gravel indicate deposition in a fluvial environment with high-energy flows (Smith 1974; Lunt & Bridge 2007), rapidly waning flows (Steel & Thompson 1983), or sorting due to flow separation in the lee of bedforms (Rust 1984; Carling & Glaister 1987; Carling 1996). Thus, terrace 6 contains alluvium deposited by relatively high-energy flows.

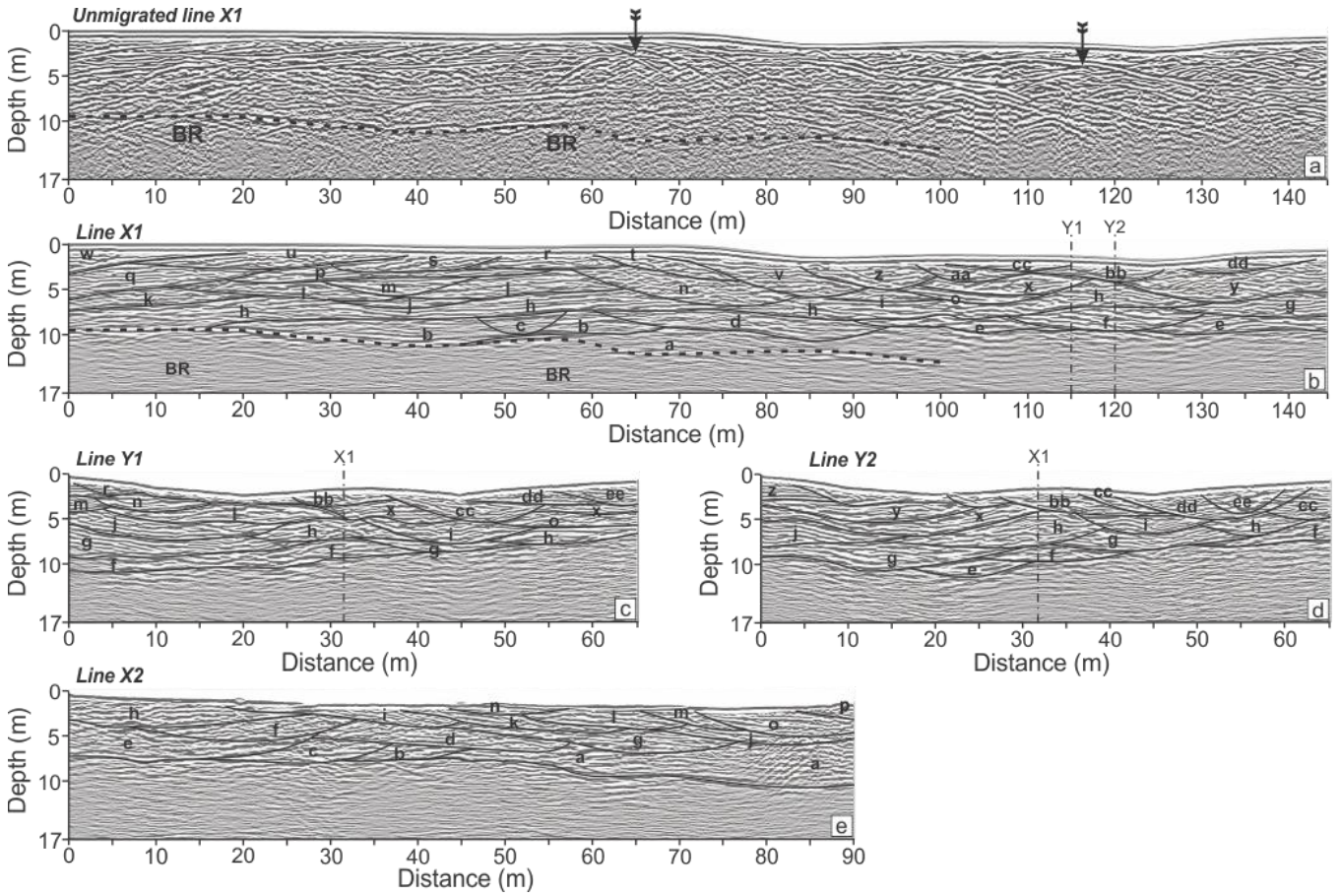

Figure 5-41: GPR data from site 48B. a) Unmigrated line X1 showing hyperbolic diffractions (select examples highlighted by arrows) caused by out-of-line reflectors (boulders) (Neal 2004; § 4.2.2). b), c) and d) Lines X1, Y1 and Y2, respectively, taken from surveys on terrace 3 (Figure 5-39) showing lenticular radar elements a-ee delineated by black lines that mark the radar bounding surfaces. Dashed line near bottom of X1 marks the inferred bedrock (BR) contact. The vertical dashed-dotted lines mark ~90° intersections with other lines (label at top identifies intersecting line). e) Line X2, surveyed on terrace 4 (Figure 5-39) showing lenticular radar elements a-p delineated by black lines marking radar bounding surfaces (radar element labels letters do not correlate to those used in lines X1, Y1, or Y2). X-lines run from northeast (0 m) to southwest, and Y-lines run from northwest (0 m) to southeast (Figure 5-42b).

The GPR data from terraces 3 and 4 is interpreted to record deposition in a braided river environment (Miall & Jones 2003; Skelly et al. 2003; Woodward et al. 2003). The lenticular radar elements with concave-up, KRv-perpendicular internal reflection geometries are consistent with deposition during scour-and-fill (Miall & Jones 2003; Skelly et al. 2003; Sambrook Smith et al. 2006; Kostic & Aigner 2007). Subhorizontal reflections record deposition from gravel sheets (Skelly et al. 2003; Sambrook Smith et al. 2006). Inclined reflections may record bar slip-face progradation (Skelly et al. 2003; Sambrook Smith et al. 2006). The pseudo-three-dimensional reflection geometries derived from lines X1, Y1 and Y2, suggest a paleoflow to the west-northwest on terrace 3, and, by extension, reflections geometries from line X2 suggest a paleoflow direction to the west-southwest on terrace 4 (Figure 5-42b).

Paired terraces in the Columbia (both north and south of the Kootenay River) and Kootenay River valleys near sites 48A and 48B suggest the existence of an elevated (~590 m asl on terrace 1, Figure 5-38) original valley fill that has undergone incision by the Columbia and Kootenay Rivers (cf. Figure 5-26). Paired terraces suggest an interpretation of thick postglacial valley fill over the previous interpretation of ice-marginally deposited kame terraces (Fulton 1970). Thus, the geomorphology at sites 48A and 48B is interpreted as a thick (~175 m) and fluvially-incised valley fill.

The valley fill sediment (Figure 5-38b, c) at the confluence of the Kootenay and Columbia Rivers is interpreted as a record of advance-phase (unit 1) and retreat-phase (unit 3) outwash deposition, separated by a till (unit 2). The river

terraces exposed at sites 48A and 48B are inset into this valley fill and drape bedrock (Figure 5-38b). Terraces 2-6 lie within the elevational zone of putative jökulhlaup incision (Figure 5-26, Figure 5-38b). Terrace preservation in this elevational zone at Castlegar may support the notion that KRv valley fill incision was gradual, and accomplished by the Holocene Kootenay River, rather than a gLP jökulhlaup. However, expansion bar deposition and terracing during the waning stages of jökulhlaups has been reported elsewhere (e.g., Baker 1984; Russell et al. 2001; Carrivick et al. 2004), and preservation of such terraces is favoured in the valley widening at Castlegar.

5.4.8 GLP drainage summary and discussion

The sites in this § reveal sedimentary deposits that have been interpreted to record a glacial lake, river terraces, and alluvial and colluvial fans in the >100 m thick KRv valley fill (Figure 5-27). Smoothed and potholed bedrock near the top of the valley fill (624 m asl, site 44, §5.4.5) confirm energetic water flows at that elevation. In the absence of independent dating, these sites are assumed to record late MIS 2 (during and/or following late stages of ice decay) events in KRv.

The geomorphic evidence for a jökulhlaup from gLP along the KRv is equivocal. Topographic profiles across KRv reveal zones of steep, non-terraced incision through the upper ~100 m (thickness) of the valley fill, and terraced incision through the lower 20-30 m of the valley fill (Figure 5-28). It is plausible that incision through the upper 100 m (possibly more if waning jökulhlaup flows and Holocene alluvial and colluvial action resulted in significant post-gLP

drainage aggradation) of the valley fill may have been accomplished by a jökulhlaup from gLP. Previous reports on jökulhlaup incision confirm that even much smaller volumes of water (by an order of magnitude) than gLP are capable of eroding large amounts (~25 x 10^6 m^3, Skeiðarársandur, Smith et al. 2000) of sediment (e.g., Smith et al. 2000; Magilligan et al. 2002; Carrivick et al. 2004; Russell 2009). However, it is equally plausible that a powerful, early-Holocene Kootenay River incised into the elevated valley-fill sediment in the KRv. The preservation of terraces in the upper 100 m of the valley fill at Castlegar may favour the latter interpretation, though such terraces could have formed in the waning stages of a jökulhlaup (Carrivick et al. 2004).

The sedimentary record for a jökulhlaup from gLP along the KRv is equivocal because none of the lithofacies observed are diagnostic of jökulhlaups. If the rising stage of a jökulhlaup is mainly erosive, then deposition may be more likely on the waning stage (Maizels 1993; Russell 2009). If the putative gLP jökulhlaup incised through the top ~100 m of the valley fill, jökulhlaup deposits may be preferentially located near the floor of this incision in KRv. It is possible that the sand and gravel sediment bench (bench tread ~590 m asl) at the junction between the Purcell Trench and the West Arm (sites 21 and 24, §5.4.2) may record the waning stage of a gLP jökulhlaup. In this scenario, the changes in texture and structure of the deposits at sites 21 and 24 record fluctuations in flow energy during the waning stage. Similar lithofacies have been reported in waning-stage jökulhlaup deposits elsewhere (Maizels 1993; Carling 1996; Carrivick et al. 2004; Russell 2009), though they are also reported from non-

jökulhlaup river deposits (Hein & Walker 1976; Miall 1977; Allen 1983). The fan-shaped deposit at the confluence of the Kootenay and Columbia River valleys (sites 48A and 48B) is similar in morphology and sedimentology to expansion bars deposited by large flood events (Baker 1978a, 1984), though it also resembles an alluvial fan that could have been deposited by the Kootenay River.

5.5 Sites recording post-gLP drainage processes

This § describes sites that are interpreted as a record of post-gLP drainage (very late MIS 2 and Holocene) processes. The sites exist in the northern Purcell Trench and the West Arm and are representative (not exhaustive) of post-gLP drainage processes.

5.5.1 Site 34

5.5.1.1 Observations

Site 34 is located on the eastern valley wall of the Purcell Trench near the shore of Duncan Lake on the tread of an elevated (maximum elevation of ~635 m asl, DEM (Geobase ®)), sloping (~5° towards 265°) sediment bench that radiates from the mouth of Glacier Creek (Figure 3-3; Figure 5-42a). The elevated deposit is positioned ~25 m above the modern Glacier Creek delta (Figure 5-42a), which formed after the completion of Duncan Dam in 1967 (Kyle 1938). At site 34 >5 m of sediment are exposed to the top of the bench due to incision by Glacier Creek (Figure 5-42b).

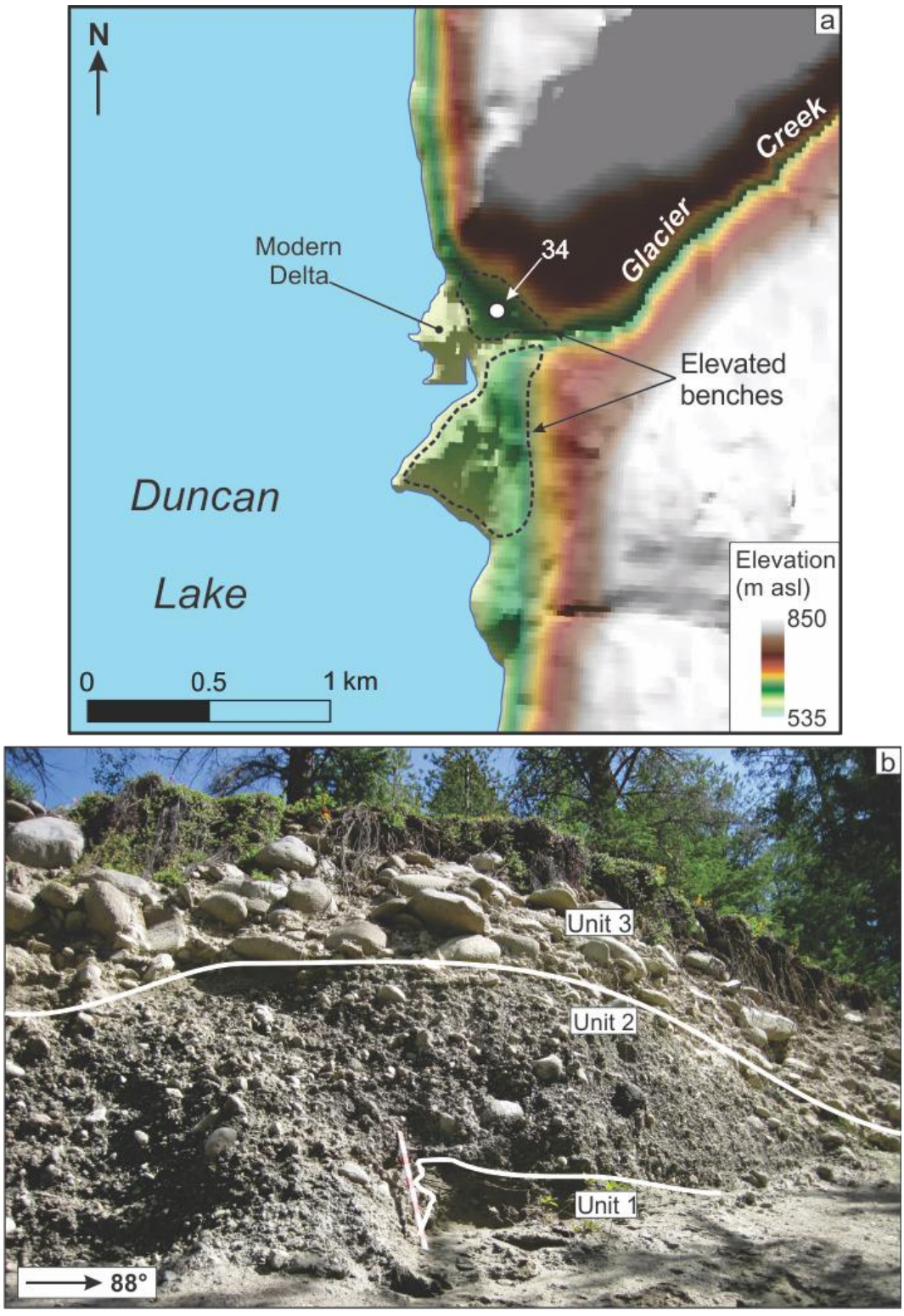

Figure 5-42: a) Hillshaded DEM (Geobase®) showing the location of site 34 (white dot) on the tread of the northern elevated gravel bench. The elevated gravel benches are outlined with dashed lines. The smaller, and lower modern (post-Duncan Dam) Glacier Creek delta is labeled. Refer to Figure 3-3 for location of site 34 in the Purcell Trench. B) Three units are exposed at site 34. Metre stick with decimetre markings for scale.

Three lithostratigraphic units are identified at site 34 (Figure 5-42b). Unit 1 is at least 0.5 m thick (its lower contact is not exposed) (Figure 5-42b). It is composed of consolidated and deformed (tilted and faulted) planar cross-stratified coarse, medium and fine sand (Sd and Sc, Table 4-1) with occasional pebbles. The sand beds are ~0.01 m thick and display both normal and reverse grading. Some of the sand beds within unit 1 have been tilted at angles up to 45° down towards an apparent azimuth of 90°. There are also thrust faults present in the tilted sand beds that extend through the entire unit and are oriented nearly horizontally with displacements of 0.01 – 0.02 m. The westernmost edge of the exposed unit ends abruptly at a sharp and irregular contact with the overlying gravel of unit 2 (Figure 5-42b).

Unit 2 is 2.3 m thick and has a sharp lower contact that truncates the sand beds of unit 1. It is composed of dipping (8° towards 265°, apparent), tabular, crudely cross-stratified gravel beds (Gc, Table 4-1) that are ~1 m thick (Figure 5-42b). The gravel is composed of rounded, clast-supported pebbles to small boulders in a matrix of granules and coarse sand; some areas consist of openwork pebbles and cobbles. The entire unit fines upwards and is capped in places by pebble gravel.

Unit 3 is up to 3 m thick and has a sharp lower contact that truncates the gravel beds of unit 2 (Figure 5-42b). It is composed of tabular cross-stratified, upward fining gravel beds (Gc, Table 4-1) that exhibit apparent dips of 9° towards ~268° (Figure 5-42b). The gravel clasts range in size from pebbles to boulders

with b-axis measurements of up to ~0.8 m (Figure 5-42b). The boulders are imbricated with dips of 35° - 50° towards (down dip) ~92°.

5.5.1.2 Interpretation

The elevated, sloping (~5° towards the Purcell Trench) and dissected sediment bench at site 34 (Figure 5-42a) is suggestive of an alluvial or colluvial fan (Church and Ryder 1972; Blair & McPherson 1994; Ballantyne 2002) that was built by flows along an elevated Glacier Creek, and later incised by Glacier Creek following a decrease in sediment supply and/or a lowering of the Glacier Creek base level (the floor of the Purcell Trench, which was likely incised by the south-flowing pre-Duncan-Dam Duncan River). The composition of the fan is consistent with this interpretation. The well-sorted, normally-graded planar cross-stratified, and reverse-graded sand lithofacies in unit 1 record deposition from stream flows (Smith 1974; Lowe 1982; Allen 1984; Kjaer et al. 2004) and grain flows (Lowe 1982). The planar cross-stratified rounded gravel beds of unit 2, and the cross-stratified and imbricated, well rounded boulder beds of unit 3 likely record deposition on the slipface of gravel bars (Nemec 1990; Postma 1990). The dip of the gravel beds and clast imbrication direction (towards the Purcell Trench) confirms that the fan prograded west away from Glacier Creek valley. The shearing and faulting in unit 1 indicates a post-depositional, compressional stress associated with erosion by the flows responsible for deposition of unit 2.

In summary, the units exposed at site 34 record a period of alluvial fan progradation onto an elevated, postglacial Purcell Trench floor. Postglacial

timing is inferred because the bench projects out into the Purcell Trench (there is no signature of truncation by glacial erosion or due to removal of ice support), the sediments display no evidence of glacial overriding, and the bench elevation is ~25 m higher than the elevation of the Purcell Trench valley fill prior to ice occupation. The fan was bisected by Glacier Creek when the Duncan River incised into the Purcell Trench valley fill prior to the completion of the Duncan Dam (Hooke 1967; Ryder 1971).

5.5.2 Site 35

5.5.2.1 Observations

Site 35 is located on the floor of the Purcell Trench next to the eastern valley wall ~2.4 km north of Kootenay Lake on an elevated (~615 m asl maximum, DEM (Geobase®)) ~55 m thick sediment bench (Figure 5-43a). The bench is fan-shaped, radiates from the Hamill Creek valley, and its tread slopes ~6° towards 285° (Figure 5-43b). The riser and tread of the bench are exposed by a combination of gravel pits, access roads and incision by Hamill Creek.

A single upward-finning lithostratigraphic unit (unit 1) is exposed at site 35. Near the base of the riser (560 m asl, DEM (Geobase®)), the bench is composed of steeply dipping (26° towards 320°) normally-graded, planar-stratified and massive beds (Gp and Gm, Table 4-1) of large, rounded to well-rounded, cobble and boulder-sized gravel in a matrix of poorly sorted sand (Figure 5-44b). On the bench tread (at 615 m asl, DEM (Geobase®); Figure 5-44a, c), the unit exhibits similar structures, but its composition has fined to poorly-sorted, very angular to well-rounded (35-1, Table 5-1) pebble and cobble gravel (average ~3 cm along

their b-axes) with some large, well-rounded boulders (b-axes > 0.6 m; Figure 5-44a). These gravel beds are also steeply dipping (apparently ~20° down towards 300°) and tabular with sharp lower contacts. They are interbedded with poorly-sorted lenses (lateral extents of 3 m to >12 m and thicknesses ranging from 0.1 m to 0.35 m) of massive sand with sharp lower contacts (Sm, Table 4-1) that dip 37° towards 293° (measured from an exposed fine sand bed at the northernmost exposure, northeast of the exposure in Figure 5-44a). A gravel fabric from the inclined, planar-stratified gravel beds near the top of the bench tread is unimodal with a principal eigenvector towards the northeast and a dominance of a(p) clasts (35-1, Figure 5-44c; Table 5-1).

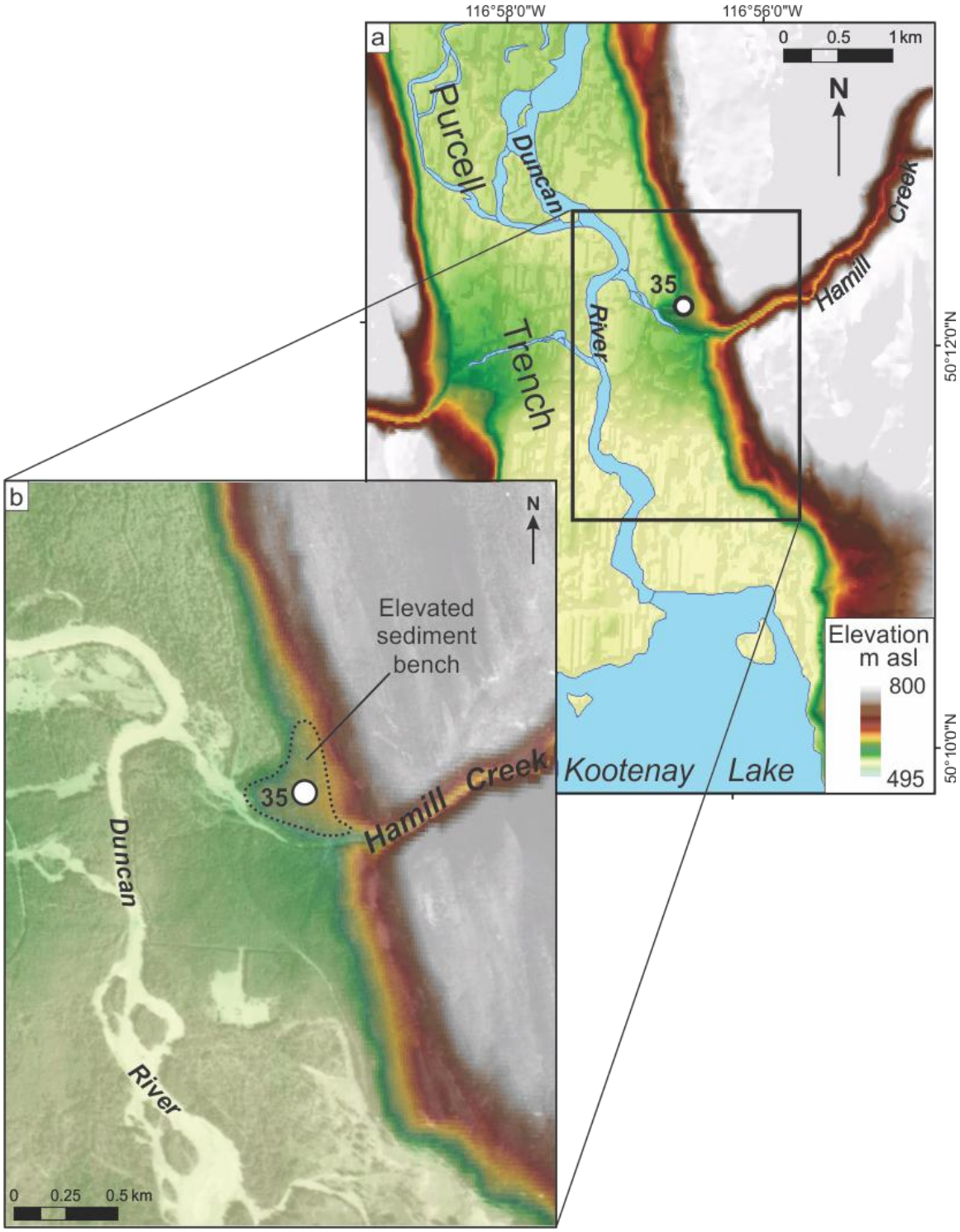

Figure 5-43: a) Hillshaded DEM (Geobase®) showing location of site 35 (white dot) at the mouth of the Hamill Creek valley. Black box shows location of b. Refer to Figure 3-3 for site location in the Purcell Trench). b) Hillshaded DEM (Geobase®) overlain by an aerial photograph (A13796_18, © Department of Natural Resources Canada. All rights reserved.) that shows the location of site 35 (white dot) on an elevated sediment fan (outlined by black dotted line).

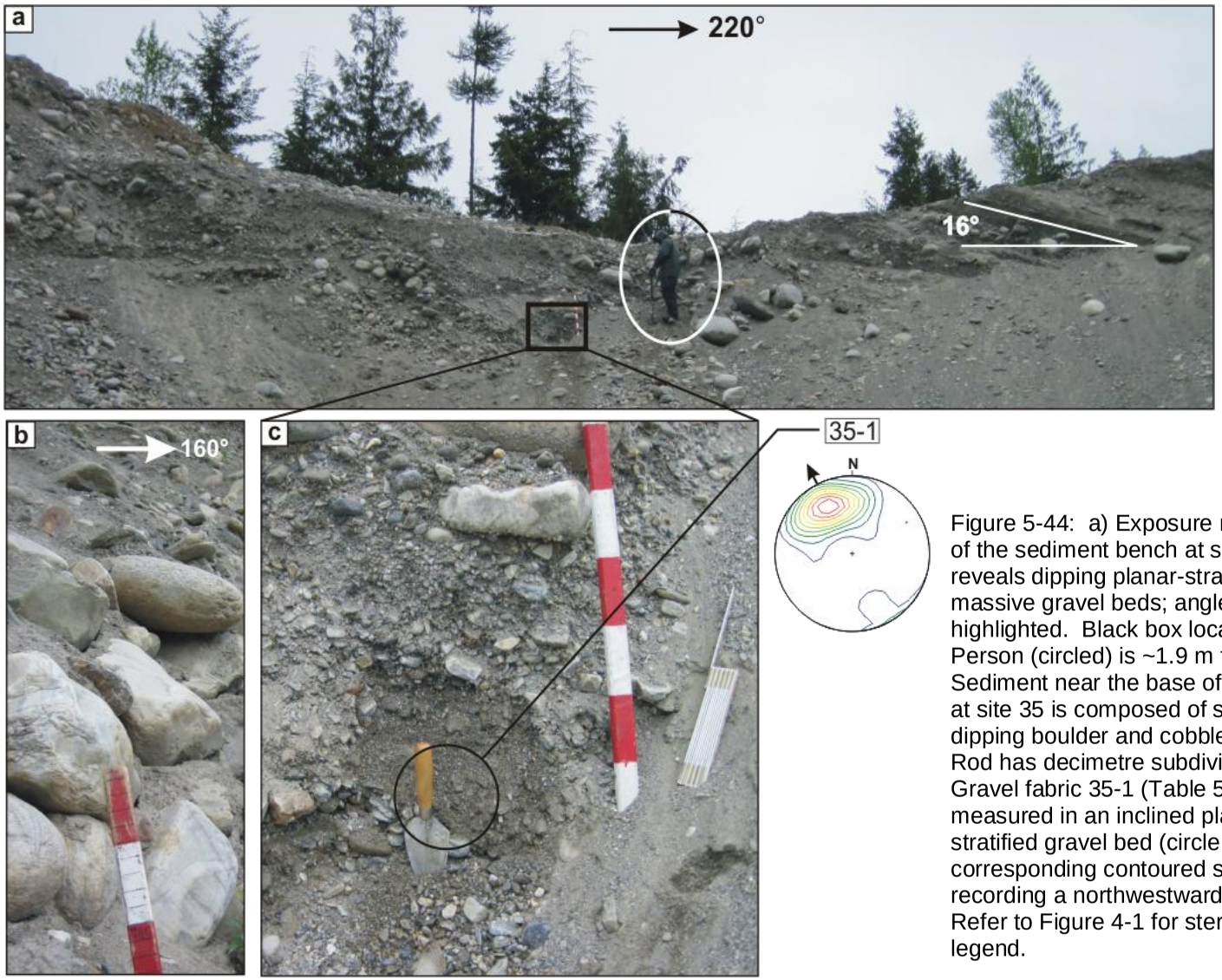

Figure 5-44: a) Exposure near the top of the sediment bench at site 35 reveals dipping planar-stratified and massive gravel beds; angle of dip is highlighted. Black box locates c. Person (circled) is ~1.9 m tall. b) Sediment near the base of the deposit at site 35 is composed of steeply-dipping boulder and cobble beds. Rod has decimetre subdivisions. c) Gravel fabric 35-1 (Table 5-1) was measured in an inclined planar-stratified gravel bed (circle with corresponding contoured stereogram, recording a northwestward paleoflow). Refer to Figure 4-1 for stereogram legend.

5.5.2.2 Interpretation

The elevated, sloping (~6° towards the Purcell Trench) and fan-shaped sediment bench at the mouth of Hamill Creek investigated at site 35 is suggestive of an alluvial or colluvial fan (Church and Ryder 1972; Blair & McPherson 1994; Ballantyne 2002) that was built by flows along an elevated Hamill Creek, and later incised by Hamill Creek following a decrease in sediment supply and/or a lowering of the Hamill Creek base level (the floor of the Purcell Trench, which was likely incised by the south-flowing pre-Duncan-Dam Duncan River). The composition of the fan is consistent with this interpretation. Steeply dipping, normally-graded, massive and planar-stratified gravel and sand beds are commonly found in alluvial fans (e.g., Ryder 1971; Blair 1987; Blair & McPherson 1994), and record fluvial transport and deposition. The presence of angular clasts suggests short transport distances for some beds (Ryder 1971). The gravel fabric is dominated by sliding clasts (clast a-axis parallel to the maximum dip of the a-b plane) and so records a northwestward paleoflow, consistent with the westward dip of the gravel beds.

In summary, the sediment exposed at site 35 records a period of alluvial fan progradation onto an elevated, postglacial Purcell Trench floor. Postglacial timing is inferred because the bench projects out into the Purcell Trench (there is no signature of truncation by glacial erosion or due to removal of ice support) and the sediments display no evidence of glacial overriding. Much of the fan was likely removed by Hamill Creek flows when the Duncan River incised into the

Purcell Trench valley fill prior to the completion of the Duncan Dam (Hooke 1967; Ryder 1971).

5.5.3 Site 46

5.5.3.1 Observations

Site 46 is located in the KRv ~1 km northwest of the confluence of the Slocan and Kootenay Rivers on an elevated (~486 m asl, DEM (Geobase®)) sediment bench (Figure 3-4, Figure 5-45a), which is ~35 m above the Kootenay River. The site is located east of the bedrock ridge of Sentinel Mountain, which is situated west of the Kootenay River valley (Figure 5-45a). Two exposures (46A and 46B) reveal the composition of the bench (Figure 5-45a). Exposure 46A is located in a roadcut along highway 3A, in the bench riser (~470 m asl, DEM (Geobase®)) and exposure 46B is located in a small, privately-owned gravel pit (restricted access) on the bench tread (~485 m asl, DEM (Geobase®). Each site exposes a single lithostratigraphic unit. Sequential unit numbers are used for simplicity though it is acknowledged that the sedimentary record of the bench is incomplete (i.e. the full sedimentary sequence is not exposed).

Exposure 46A is ~5 m wide and 2 m tall and reveals one lithostratigraphic unit (unit 1) consisting of cross-laminated fine sand (Sr, Table 4-1, Figure 5-45b). The sand beds display type-A ripples with shallow angles of climb (46-1, Table 5-3) and type-S ripples (Figure 5-45b). The type-A ripples record a paleoflow direction towards the south east (46-1, Figure 5-45b, Table 5-3).

Exposure 46B is ~5 m tall and 15 m wide and reveals lithostratigraphic unit 2, which consists of trough cross-stratified gravel (Gt, Table 4-1) (Figure 5-45c). Cross-sets average ~7 m in length and ~1.5 m high, and have sharp lower contacts that truncate underlying cross-strata (Figure 5-45c). The gravel consists of clast-supported rounded to well-rounded pebbles and cobbles in a small amount of coarse sand matrix; rarely, the gravel is openwork. A paleoflow estimate from trough geometries is southward.

5.5.3.2 Interpretation

The normally-graded rippled sand of unit 1 records deposition from traction and suspension in relatively low magnitude uni-directional flows (Ashley et al. 1982), perhaps an underflow in a lake or pond. The alternation between type A and type S ripples suggests that flow power varied during deposition of unit 1. Southeastward paleoflows are consistent with flow out of the Slocan River valley towards KRv.

The trough cross-bedded, well-rounded gravel of unit 1 records channel scour and fill, dune or barform migration (Miall 1977; Postma 1990) in a river. The presence of some openwork gravel may suggest relatively high-energy flows (Smith 1974; Lunt & Bridge 2007), rapidly waning flows (Steel & Thompson 1983), or sorting due to flow separation in the lee of bedforms (Rust 1984; Carling & Glaister 1987; Carling 1996).

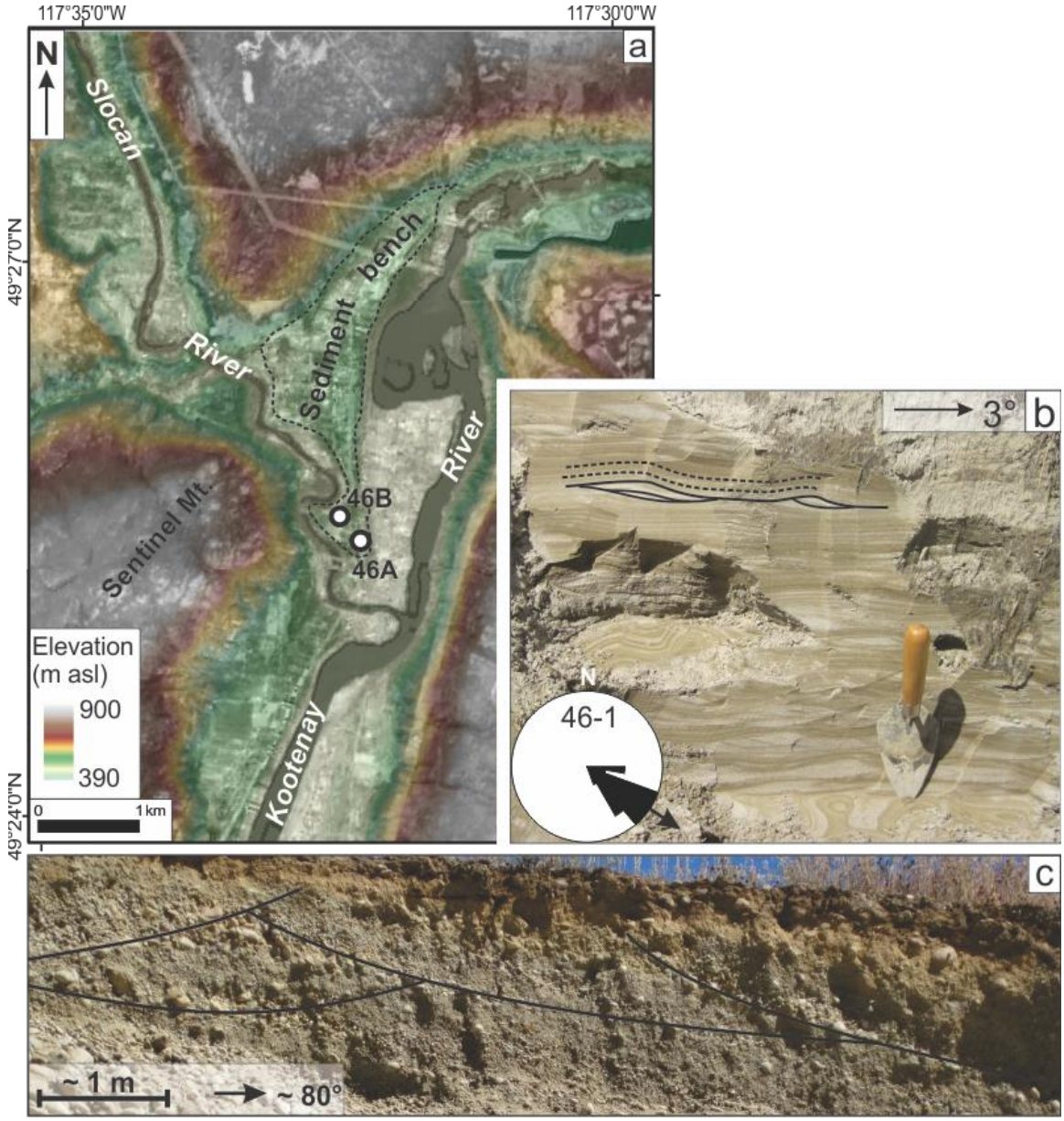

Figure 5-45: a) Hillshaded DEM (Geobase®) overlain by an aerial photograph (A22007-21; © Department of Natural Resources Canada. All rights reserved.) showing locations of site 46 exposures 46A and 46B (labeled white dots) on a sediment bench (delineated by a black dashed line) at the junction between the KRv and the Slocan River valley. Refer to Figure 3-4 for site location within the KRv. b) Unit 1 in exposure 46A contains some type-A ripples (one set indicated by solid black lines) and type-S ripples (several sets indicated by dashed black lines). Trowel is ~27 cm long. Ripples record southeastward paleoflows (rose diagram) (46-1, Table 5-3). c) Unit 2 in exposure 46B contains trough cross-stratified gravel (Gt, Table 4-1); some trough lower contacts are highlighted (solid black lines).

In summary, the sediment bench at site 46 is interpreted as a river terrace because it is capped by alluvial gravels (unit 2). These gravels were likely

deposited by an elevated (485 m asl) Kootenay River during the Holocene because they record southward paleoflows, are not capped by till, contain no evidence of glacier over-riding (e.g., glacitectonic structures), and they occur in a sediment bench that is ~100 m below the inferred elevation of the pre-gLP drainage valley fill in KRv (Figure 5-25). Unit 1 is more enigmatic. It may record sedimentation in a small pond on a river floodplain, or it may record earlier (i.e. be part of the pre-gLP drainage KRv valley fill) deposition in the same glacial lake(s) recorded at sites 47 (§ 5.4.6) and 54 (Appendix B).

5.5.4 Post-gLP drainage processes summary

The numerous, elevated alluvial fans in the Kootenay River valley and the Purcell Trench possess similar sedimentology (fluvial and mudflow gravel) and morphology (toe truncation, incision) to the fans described by Ryder (1971a, 1971b) in the Fraser, Thompson and Similkameen valleys. Sites 34 and 35 record the formation and subsequent incision of postglacial alluvial fans on the floor of the Purcell Trench. Site 46 records sedimentation on a Holocene Kootenay River floodplain, and floodplain abandonment (river terrace formation) due to Kootenay River incision. Sites 34 and 35 record 35 m and 55 m, respectively, of incision through alluvial fan deposits in the Purcell Trench. The Kootenay River has incised 35 m since it deposited the terrace gravel at site 46. Aggradation, incision and abandonment of alluvial fans and river floodplains are typical postglacial adjustments to changes in sediment supply and base level (Hooke 1967; Ryder 1971; Eyles & Clague 1991).

6: DISCUSION

"We are like a judge confronted by a defendant who declines to answer, and we must determine the truth from the circumstantial evidence."

Alfred Wegener (1966, page viii)

6.1 Ice dam evidence

The presence of the Purcell Lobe of the CIS in the Purcell Trench during MIS 2 is inferred from the presence of advance outwash (valley fill at least 610 m asl at site 19) and subglacial till at/near the top of the valley fill at sites 19, 41 and 53 (§ 5.1; Figure 6-1). In the absence of dating, MIS 2 age is inferred from the presence of a geoclimatic marker (till) at/near the top of the valley-fill sequence.

The continued occupation of the Purcell Trench by the Purcell Lobe during associated CIS decay (downwasting and backwasting) is evidenced by the presence of kame terraces at sites 27, 30, and 38-40 (§ 5.2, Figure 6-1). These kame terraces were deposited marginal to the Purcell Lobe and are differentiated from the elevated advance-phase outwash gravel mapped elsewhere in the study area by their elevation, geomorphology, stratigraphy and sedimentology. In places (site 27, bench tread at sites 38-40), the kame terraces are ~100 m higher than the till/advance-phase outwash contact. Geomorphically, most of the kame

terraces (except site 27) are located in areas devoid of any shelter (e.g., upflow bedrock knobs, etc) from glacial erosion by the advancing Purcell Lobe, a condition that appears necessary for the preservation of advance outwash in the Purcell Trench (§ 5.1). The Purcell Lobe is responsible for at least 167-202 m of incision in places where its flow was unobstructed (§ 5.1, sites 19 and 41). Stratigraphically, none of the sites are capped by subglacial till. Sedimentologically, many of the sites yield paleoflow directions against regional hydraulic grade (i.e., into the valley wall at site 30 and towards the north at sites 38 and 39), a condition most simply explained in an ice-marginal depositional environment. Furthermore, ice-marginal paleoflows to the north may suggest a degraded ice mass without a regional slope towards its southern terminus during kame terrace formation. A scenario in which the Purcell Lobe recloses after failure through ice creep (§ 2.1.2) and allows multiple drainings of gLP may be negated if this degraded ice is assumed to record ice stagnation.

Kame terrace formation north of the KRv indicates that the Purcell Lobe was likely grounded and supported ice-marginal meltwater streams and lakes. Although the synchronicity of the kame terraces and gLP cannot be confirmed without dating their respective deposits, given the relatively low elevation (~600-700 m asl, § 5.2) of some of the kame terraces, the kame terraces likely record post-gLP ice-marginal processes (because they are ~56 m below the likely water surface of gLP, § 6.2). However, their presence suggests that the Purcell Lobe could have functioned as an ice dam for gLP in the Purcell Trench preventing drainage west into the KRv.

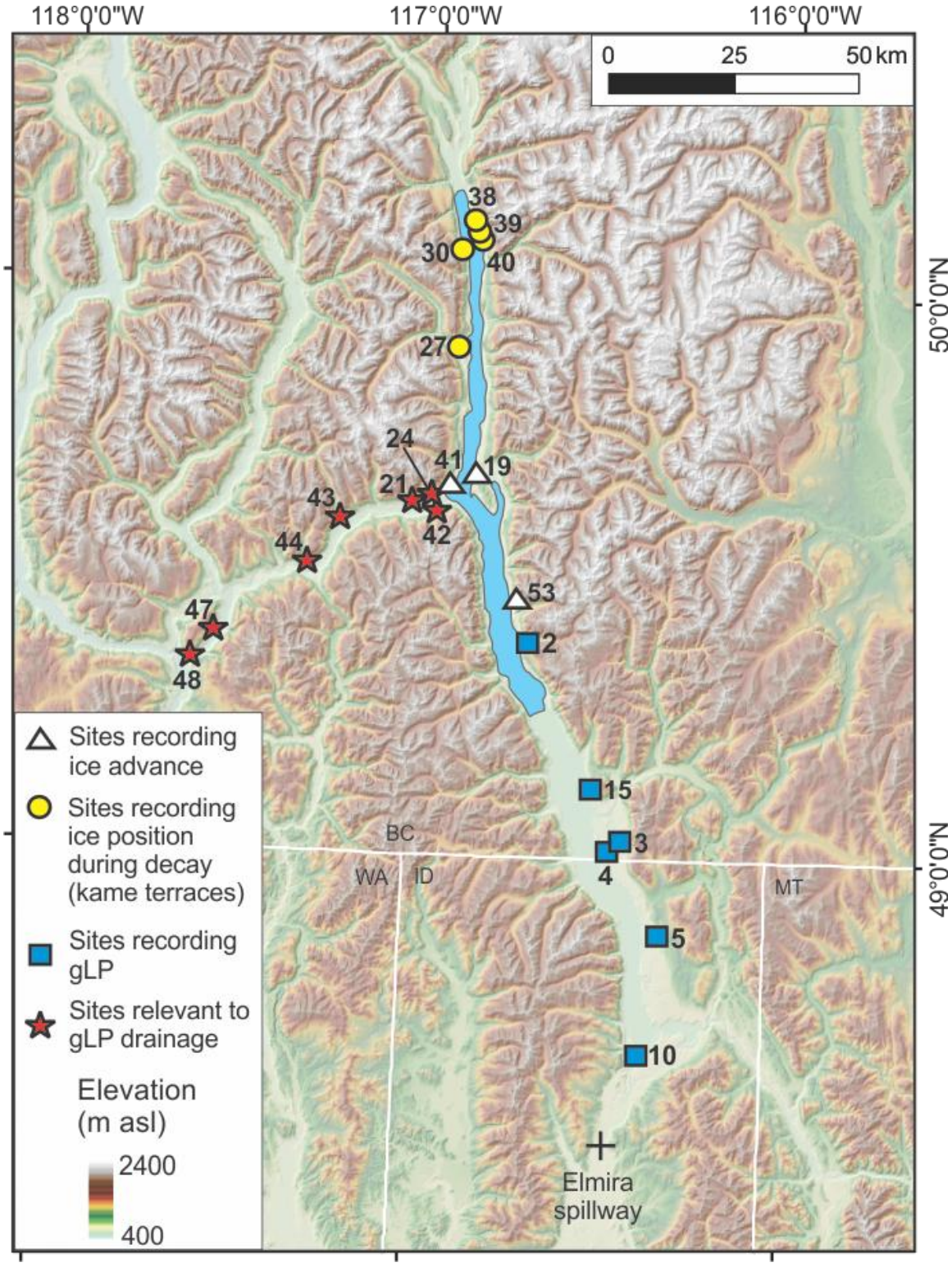

Figure 6-1: Hillshaded DEM mosaic (Geobase® in CA, NED in USA; data available from U.S. Geological Survey) showing the study area with field sites referenced in the discussion chapter demarcated by symbols according to their interpretations. Kootenay Lake, in the Purcell Trench, is shown as blue.

6.2 GLP paleogeography and evolution

Given the topography of the Purcell Trench basin, and the presence of the Purcell Lobe in the Purcell Trench preventing drainage west down KRv, meltwater would have ponded in front of the decaying Purcell Lobe to the level of the Elmira spillway (655 m asl). This would have occurred even without any glacioisostatic depression, because the Elmira Spillway is currently a drainage divide. Thus gLP would have extended north into BC as far as allowed by the downwasting and backwasting Purcell Lobe. Eventually its northern margin (the Purcell Lobe snout) would have been near the KRv (74 km north of the 49th parallel).

A minimum (although, possibly non-synchronous) areal extent of gLP is recorded by the extant gLP lake bed bench (~444 km^2) that stretches from Elmira, ID to Creston, BC (Figure 5-21); sites 3, 4, 5, 10 and 15 are located in this bench (§ 5.3; Figure 6-1). However, given that the northern lake boundary was the backwasting Purcell Lobe, gLP was likely much more extensive. The dearth of discovered gLP deposits on the eastern valley wall north of Creston (site 2 was the only other site containing lake sediments between Creston and KRv) is mainly attributed to Holocene fluvial and colluvial action, and/or poor preservation on the steep valley walls of the Purcell Trench. The presence of gLP sediments on the floor of Kootenay Lake or on the inaccessible valley wall west of Kootenay Lake is unknown. Consequently, a more accurate estimate of gLP extent is derived through GIS modeling: using the DEM (cf. Leverington et al. 2002; DeVogel et al. 2004), assuming a glacioisostatic tilt direction parallel to

the PT axis, and applying water-plane tilts appropriate for gLP (refer to § 4.2.3 for methodology).

The range of plausible glacioisostatic water-plane tilts for gLP was determined through consideration of previously reported water-plane tilts from MIS 2 CIS glacial lakes (Table 6-1). The geographic centre of gLP was ~40 km from the late glacial maximum (LGM) limit and it may have drained ~11.6 ^{14}C ka BP (13.5 cal. ka BP) (Waitt et al. 2009). The tested range of gLP water-plane tilts (0-1.25 m/km) encompasses the reported water-plane tilts of MIS 2 CIS glacial lakes within geographic proximity to gLP ("glacial Lake Arrow", glacial Lake Invermere, Table 6-1) and those that were similar distances from the LGM ice limit (glacial Lake Russell-Hood, glacial Lake Bretz, Table 6-1). The average water-plane tilt of these four lakes is 0.73 m/km. The Puget Lowland lakes existed earlier than gLP and thus may record higher water-plane tilts than those experienced by gLP (some glacioisostatic rebound having already occurred prior to gLP having formed). "Glacial Lake Arrow" is perhaps the most similar in age to gLP (Table 6-1) but its water-plane tilt is poorly constrained (Fulton et al. 1989). A glacioisostatic water-plane tilt of 0.75 m/km is deemed the most likely at the time of gLP drainage.

Table 6-1: Previously reported glacioisostatic tilts associated with the CIS during MIS 2.

Tilt[1] (m/km)	**Location (glacial lake name)**	**Distance from CIS LGM limit**[2] (km)	**Upslope direction**	**Age** (^{14}C ka BP)	**Reference**
0	Rocky Mountain Trench (Invermere)	120	NA	10 ± 140	Sawicki & Smith (1992)
0.2	SW Yukon Territory (Champagne)	<100	South	Unknown	Gilbert and Desloges (2006)
~0.4	Peace Basin (Peace, Clayhurst stage)	100	West	~11	Mathews (1978)
0.6	Shuswap Basin (Shuswap, Rocky Point stage)	200	East	Unknown	Fulton (1969)
0.7	Okanogan Valley (Penticton, B.X. stage)	140	North	8.41 ± 100	Nasmith (1962)
0.85	Puget Lowland (Russell-Hood)	20	North	13.7-13.8	Thorson (1989)
0.9	Columbia River valley ("glacial Lake Arrow")	100	North	10.1 ± 150	Fulton et al. (1989)
1.15	Puget Lowland (Bretz, western)	10	North	13.5	Thorson (1989)
1.6 ± 0.7	Nicola Basin (Hamilton, lower stage)	200	North (347° ± 7°)	Unknown	Fulton & Walcott (1975)
1.7 ± 0.4	Thompson Basin (Deadman, lowest stage)	200	Northwest (321° ± 6.1°)	9.32 ±160 (likely)	Johnsen & Brennand (2004)
1.8 ± 0.6	Nicola Basin (Merritt)	200	Northwest (341° ± 18°)	Unknown	Fulton & Walcott (1975)
1.8 ± 0.6	Nicola Basin (Hamilton, upper stage)	200	North (354° ± 11°)	Unknown	Fulton & Walcott (1975)
1.8 ± 0.7	Thompson Basin (Thompson, high stage)	200	Northwest (332° ± 9.9°)	9.32 ±160 (likely)	Johnsen & Brennand (2004)
3.8 ± 10	Nicola Basin (Quilchena)	200	Northwest	9.32 ±160	Fulton & Walcott (1975)

[1] Rate of land surface tilt caused by glacioisostatic depression, as recorded by paleo-lake-level indicators.

[2] Approximate distances between the glacial lake and the nearest margin of the CIS during the late-glacial maximum extent (LGM) from Ehlers & Gibbard (2004). GLP was ~40 km from the LGM limit, perhaps 11.6 ^{14}C ka BP (13.5 cal. ka BP) (Waitt et al. 2009).

While gLP was dammed in the north by the Purcell Lobe, its lake level was controlled by the Elmira Spillway in the south. The spillway is composed of drift (Alden 1953) that has been incised leaving a terrace at 710 m asl, which is ~55 m above the bottom of the spillway (~655 m asl). Most or all of this incision is interpreted to be the result of gLP drainage through the spillway because there is no evidence of significant post-gLP drainage in the area. Indeed the spillway is now the drainage divide between the Kootenai and Pend Oreille River systems. Thus, the tilted planes representing the glacioisostatically-tilted water surface of gLP are projected from 655 m asl at the Elmira spillway.

The estimated areal extents and volumes for gLP for the tested range of glacioisostatic tilts are presented in Table 6-2. Lake area estimates are derived from the intersection of the selected water planes with the reconstructed gLP lake bed and the surrounding terrain (refer to § 4.2.3 for methodological details). Lake volume and drainable volume are estimated from lake area, topographic and bathymetric data, and assume that there was sufficient meltwater supplied to the Purcell Trench to fill the lake to the projected water plane (refer to § 4.2.3 for methodologic details). The 0.75 m/km water-plane tilt is inferred to produce the most likely estimate of the actual extent and volume of gLP just before drainage (Table 6-2).

Lake extent and volume vary with the amount of tilt applied to the water plane (Table 6-2, Figure 6-2). For glacioisostatic tilts of ≤ 1.00 m/km, differences in lake area are relatively small (Table 6-2, Figure 6-2). Increasing the water-plane tilt from 1.00 m/km to 1.25 m/km results in a large areal increase (increase

of 481 km^2, Table 6-2) because, at this water plane tilt, the lake partially covers and extends beyond the Kootenai River alluvial fan (Figure 6-2, Figure 6-3). A similar trend is seen in lake volume (and drainable volume), though the volume increase between the 1.00 and 1.25 m/km water-plane tilt reconstructions is minimized by the presence of the Kootenai River alluvial fan (Table 6-2, Figure 6-3). When the water plane is tilted ≤ 1.00 m/km, the lake is impounded behind the Kootenai River alluvial fan and drains towards the Elmira spillway along the western wall of the Purcell Trench (Figure 6-2, Figure 6-3, Figure 6-4). Just prior to drainage gLP is estimated to have had an area of ~670 km^2, a volume of ~70 km^3, a maximum drainable volume of ~50 km^3 and a depth of >350 m against its dam (Table 6-2; Figure 6-4). The Purcell Lobe would have had to be at least 400 m thick (assuming structurally-sound clean ice) in order to dam gLP at this water depth (Table 6-2).

Table 6-2: Dimensions of gLP and its ice dam for the tested range of glacioisostatic tilts.

Water-plane tilt (m/km)	**Lake area**[1] (km^2)	**Lake volume**[1] (km^3)	**Maximum drainable volume**[2] (km^3)	**Water surface elevation**[3] (m asl)	**Water depth**[4] (m)	**Minimum ice dam thickness**[5] (m)	**Height of water surface above KRv valley fill**[6] (m)
0	600	40	14	655	257	286	10
0.50	663	69	43	723	325	361	78
0.75[7]	**667**	**73**	**47**	**756**	**358**	**398**	**111**
1.00	671	93	67	788	390	433	143
1.25	1152	142	116	817	419	466	172

[1] Location of ice dam placed at 49°36'55.7"N, 116°52'21.9"W (~132 km north of the Elmira spillway).

[2] Lake volume minus the volume of Kootenay Lake within the paleolake extent.

[3] Measured against the ice.

[4] Maximum depths, measured against the ice.

[5] Clean ice thickness required to resist flotation at the dam (following the $9/10^{ths}$ ratio of ice to water densities (~900 kg m^{-3} : ~1000 kg m^{-3}; Thorarinsson 1939; Fowler 1999)).

[6] Height of water surface above the elevated, pre-drainage KRv valley fill (~645 m asl at site 42).

[7] 0.75 m/km water-plane tilt is inferred to produce the most likely estimate of the actual extent and volume of gLP just before drainage (refer to text in § 6.2 for explanation).

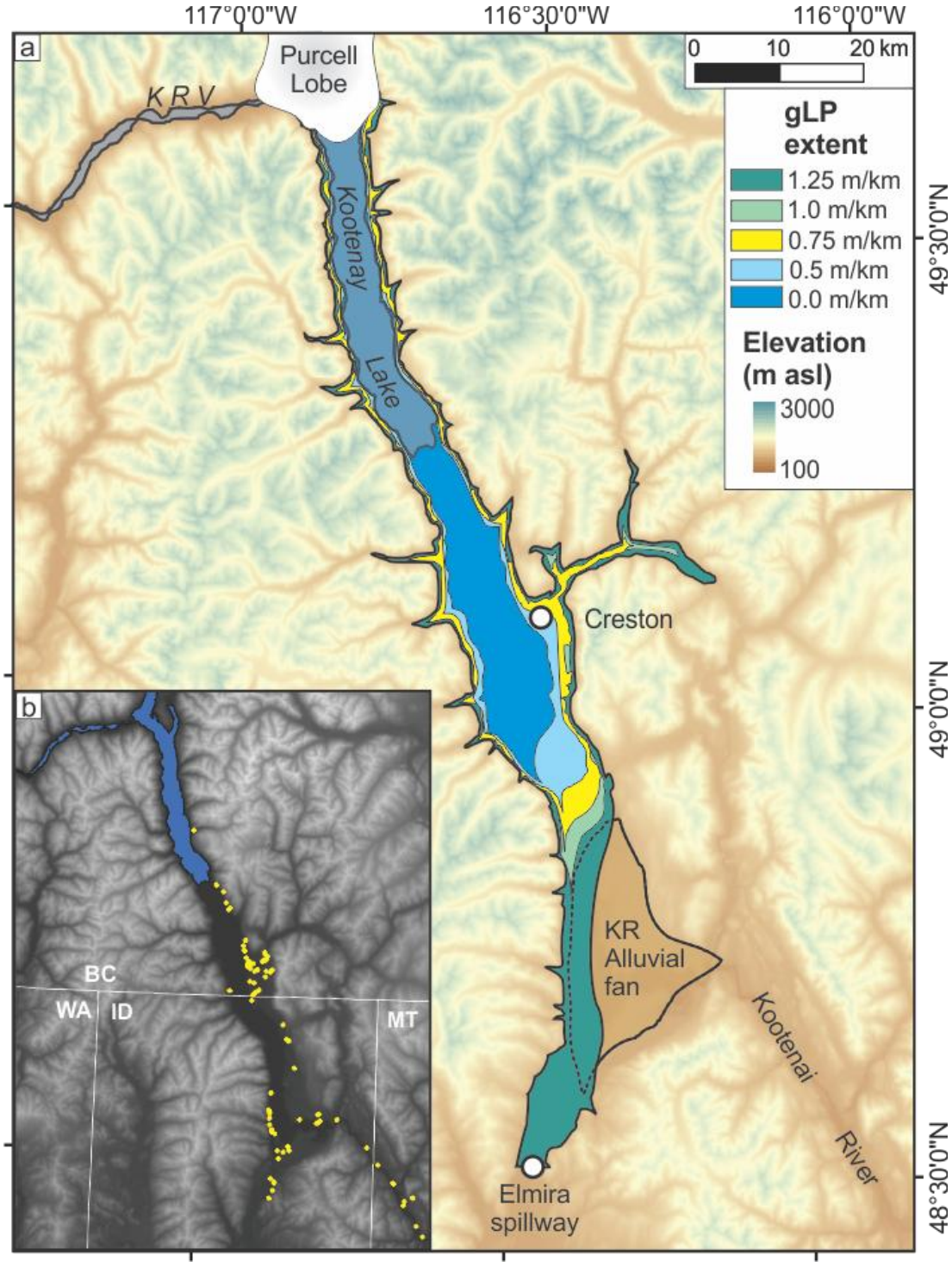

Figure 6-2: a) DEM mosaic (Geobase® in CA, NED in USA; data available from U.S. Geological Survey) showing the Purcell Trench in BC and ID and the extent of gLP for a range of glacioisostatic tilts. Also shown is the pre-incision Kootenai River (KR) alluvial fan, which forced the southern shore of gLP to migrate northward, away from the Elmira spillway. North of Creston, BC, the shorelines of gLP for tilts of 1.0-0.5 m/km are nearly indistinguishable at this scale. This diagram assumes that the Purcell Lobe terminates at an ice cliff. b) DEM mosaic (lower elevations are darker shades, Kootenay Lake is outlined with a black line) showing locations of 83 field sites where lacustrine or silty alluvial fan sediments (yellow dots) were observed.

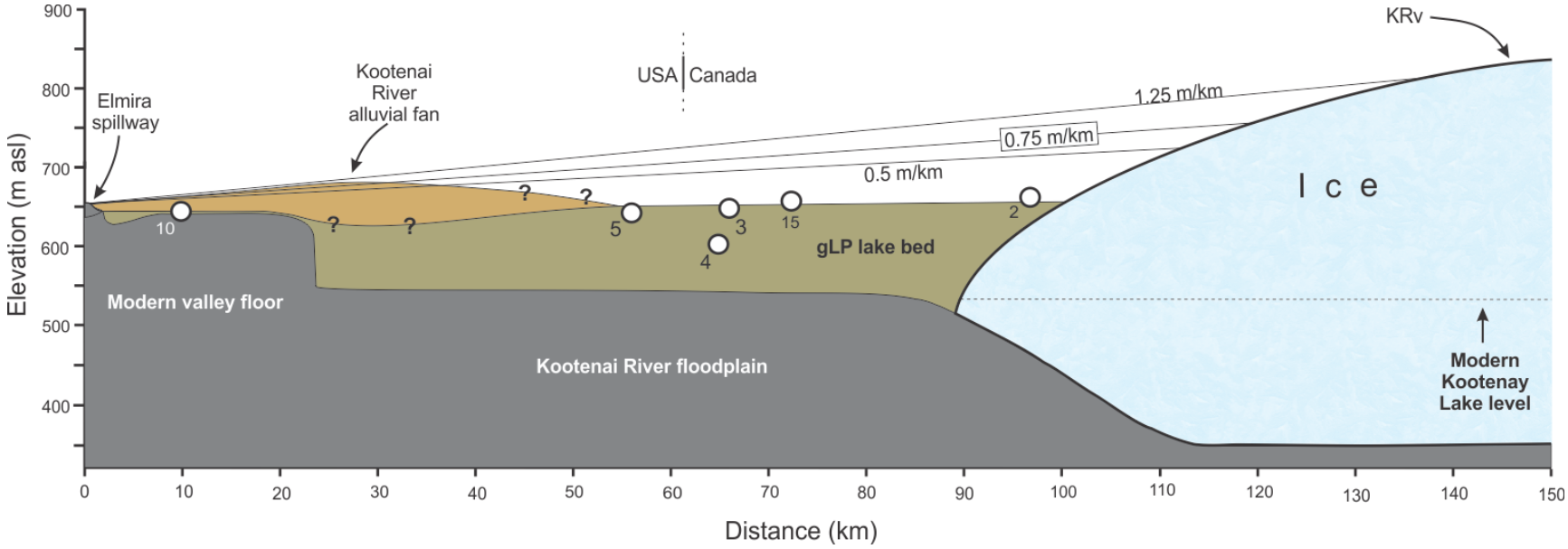

Figure 6-3: Schematic long-valley profile of gLP just prior to its drainage. Field sites (chapter 5) are indicated by white dots. The range of possible glacioisostatic tilts are represented by the 0.5, 0.75 and 1.25 m/km tilt planes. Note that at 1.25 m/km of tilt the Kootenai River alluvial fan is overtopped by gLP. Vertical exaggeration = 87x.

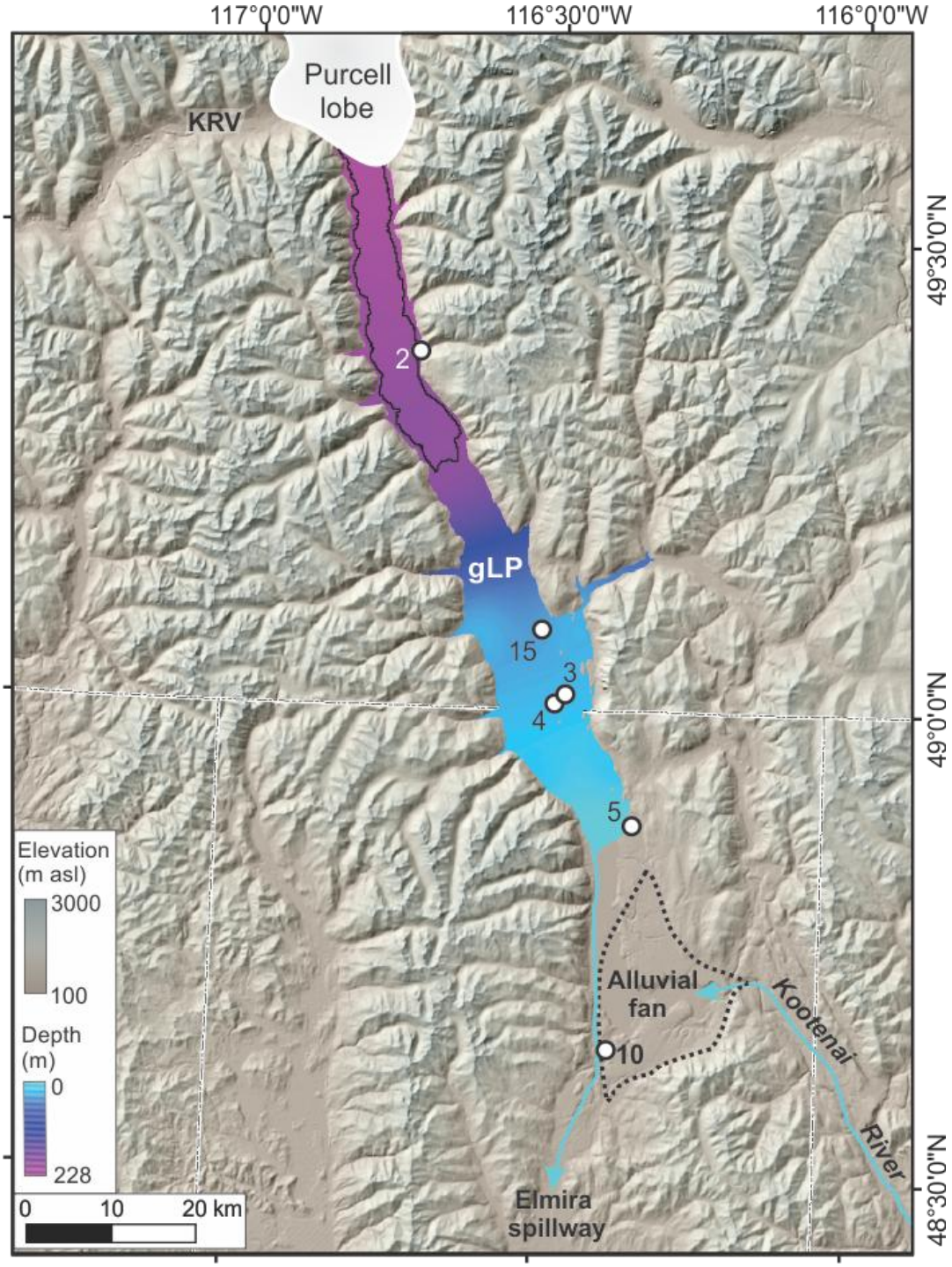

Figure 6-4: Hillshaded DEM mosaic (Geobase® in CA; NED in USA, data available from U.S. Geological Survey) showing approximate extent and simplified maximum depth (for valley center line only, assuming a 0.75 m/km glacioisostatic tilt, and minus the depth of Kootenay Lake (outlined in black; refer to Figure 4-5 for derivation) of gLP just prior to its drainage. Locations of field sites recording lake-bottom sediments (§ 5.3) are also shown (labeled white dots). The southern shore of gLP, which was initially controlled by the Elmira spillway, was forced to migrate northwards as the Kootenai River alluvial fan (outlined by black dotted line) grew. The depth of water below the modern surface of Kootenay Lake (outlined by a thin black line) would not have drained, but would have added ~180 m of depth to gLP at the ice dam.

In summary, glacial Lake Purcell was a proglacial, ice-contact lake that was constrained laterally by the steep valley walls of the Purcell Trench in ID and BC (Figure 4-5). It was dammed to the north by the Purcell Lobe to an elevation of ~750 m asl and was probably >350 m deep against its ice dam (Table 6-2; Figure 6-3). It drained south into the Pend Oreille River system over the Elmira spillway (Alden 1953; Table 3-1, Figure 3-5) until the Purcell Lobe decayed sufficiently to allow drainage into the KRv. Following the decanting of gLK into gLP (Figure 3-5), gLP lake level and southern extent were governed by a large fan (Figure 6-3, Figure 6-4) that evolved from a fan delta (during gLK decanting and while gLP occupied the southern part of the Purcell Trench, Figure 3-5) to an alluvial fan (with the reestablishment of Kootenai River in the Purcell Trench).

6.3 Evidence for catastrophic drainage of gLP through the KRv

GLP is a proglacial, ice-dammed lake. Such lakes tend to drain catastrophically when their ice dam is breached by overtopping, hydrofracture or flotation (Thorarinsson 1939; Glen 1954; Nye 1976; Clarke 1982, Waitt 1985; Walder & Fowler 1994; Anderson et al. 2003; Roberts 2005). Consequently, it seems reasonable to expect that gLP likely drained catastrophically. In the pre-drainage lake basin itself (Figure 6-4) there are no shoreline sets or deltas to provide clues as to the nature of lake drainage (gradual or catastrophic). Evidence for catastrophic drainage down KRv is also somewhat equivocal.

Some of the lithofacies revealed by sites in the KRv valley fill (§ 5.4; Figure 6-1) are consistent with previously reported jökulhlaup deposits (Sp, St, Sr, Gp, Gt, Gc and Gm lithofacies, Table 4-1; e.g. Maizels 1989, 1993; Carrivick et al. 2004; Marren et al. 2009); however, none of these lithofacies are unique to jökulhlaup deposits (i.e., many are also consistent with braided river deposits; Smith 1974; Hein & Walker 1976; Miall 1977) and thus cannot be considered confirmation of the catastrophic drainage of gLP. Furthermore, diffusely-graded sand and soft-sediment rip-up clasts that would suggest rapid deposition during hyperconcentrated flows (Russell & Arnott 2003) were not seen in the KRv.

The top of the KRv valley fill forms a sloping surface from ~650 m asl at the junction of the West Arm and the Purcell Trench to ~600 m asl at Castlegar (~0.0007 m/m slope) (Figure 5-26). This valley fill is mainly interpreted to have formed following MIS 2 ice decay in the KRv because it contains no till, (except at dept around Castlegar, site 48) but rather evidence of glacial lakes, river and slope processes attributed to a time following MIS 2 ice decay in the KRv (§ 5.4). Today this fill is deeply incised, and exhibits a paired terrace marking the top of the pre-gLP drainage valley fill (~150 m above the West Arm; ~200 m above the Kootenay River at Castlgar), and multiple unpaired terraces and truncated alluvial fans below ~50 m above current grade (the top of the inferred Holocene fill) (Figure 5-26). The lack of additional terraces between the top of the valley fill and ~50 m above modern grade (Figure 5-26) suggests that the steep slope in-between may be attributed to incision by a single event (a jökulhlaup), though the possibility for sediment removal by Holocene fluvial and colluvial processes must

be acknowledged. Potholes at ~624 m asl (site 44, Figure 6-1, § 5.4) are further evidence of elevated and energetic water flows above the level of inferred pre-gLP drainage valley fill in the KRv. Such energetic flow may have occurred within a gLP jökulhlaup or an elevated Kootenay River.

Making the simplifying assumptions that the volume of incision through the KRv fill approximates a half cylinder, that the average incision depth is 150 m and valley length is 68 km, yields ~2.4 km^3 of postglacial sediment removal. Smith et al. (2000) have previously reported on sand and gravel incision by jökulhlaups that drained much smaller volumes of water (3.6 km^3; Grimsvötn Lake, Iceland) and have removed ~0.3 km^3 of sediment in unconfined (sandur) ice-proximal locations. This suggests that if gLP drained catastrophically through the KRv the flood flow may have removed enough sediment to reach bedrock.

The possibility of jökulhlaup erosion to bedrock in KRv raises the question of whether the deep bedrock canyon reaches (at the Corra Linn and Brilliant dams, Figure 3-4) in the KRv may record jökulhlaup incision. Rapid bedrock incision from high-energy (flow powers up to 5-15 kW/m^2, Denlinger & O'Connell 2010) fluvial processes has been reported over stratified sedimentary and basaltic rocks (e.g., Baker & Bunker 1985; Reusser et al. 2006; Lamb & Fonstad 2010). Rates of fluvial incision into bedrock are a function of the tensile strength of the bedrock being eroded: intrusive igneous rocks, such as those in the KRv, tend to have the lowest erosion rates (cf. Sklar & Dietrich 2001, 2006). Furthermore, massive, relatively unjointed rock (such as that in the KRv) typically undergoes erosion from incremental wear processes—usually abrasion (Whipple

et al. 2000). Plucking-dominated erosion is only enabled when fractures are pervasive at a submetre scale (Whipple et al. 2000). The most rapid fluvial incision into bedrock typically occurs when powerful flows flow over stratified (easily plucked) sedimentary (easily abraded) bedrock. Thus, the massive, intrusive igneous and metamorphic bedrock (granite and granitic gneiss) of the Kootenay River valley is likely to be more resistant to both abrasion and plucking than sedimentary or stratified extrusive igneous rocks (e.g., basalt). A full assessment of the likely geomorphic impact of gLP drainage in KRv requires a paleohydraulic reconstruction of the event and is beyond the scope of this thesis.

7: CONCLUSIONS AND SUGGESTIONS FOR FUTURE WORK

"The gradual recession of the ice northward, and, therefore, the first uncovering of the southern half of the drift region must have taken place... That during these long ages, the rivers must have been deepening their channels and emptying the lake basins, is a fact which needs only to be stated; and hence we have all the facts the hypothesis requires."

Isaac Kinley on glacial lake evolution—while not sweating the little things.

(Kinley 1886, p.40)

7.1 Conclusions

This thesis explores whether the Purcell Trench could have held a large amount of water and delivered it suddenly to the Columbia River system. The study addresses three detailed research questions and a primary research question. Research findings are summarized below.

7.1.1 Detailed research questions

7.1.1.1 Is there evidence of an ice dam in the Purcell Trench?

Kame terrace formation in the Purcell Trench indicates that the Purcell Lobe was grounded in the Purcell Trench and could have impounded gLP until downwasting and backwasting allowed drainage into the KRv. Although these

kame terraces likely formed after the drainage of gLP (as evidenced by their relatively low elevations), the evidence they provide for grounded ice most likely also pertains to the Purcell Lobe during the existence of gLP.

7.1.1.2 What is the paleogeography of gLP and how did it evolve?

GLP began as a small lake confined by the Purcell Lobe to the southern part of the Purcell Trench, and expanded northward as the Purcell Lobe downwasted and backwasted to the north. Northward retreat of the Purcell Lobe caused gLK to decant into gLP, and resulted in deposition of a fan-delta at the confluence of the Kootenai River and the Purcell Trench. The fan-delta evolved into an alluvial fan as Kootenai River re-established its course in the Purcell Trench. The alluvial fan caused the southern shore of gLP to migrate northwards. Just prior to drainage, gLP is estimated to have had an area of ~670 km^2, a volume of ~70 km^3, a drainable volume of ~50 km^3 and a depth of >350 m against its dam.

7.1.1.3 Is there evidence of catastrophic drainage from gLP through the Kootenay River Valley?

Although somewhat equivocal, the distribution of valley-fill terraces in the KRv may record a rapid erosional event through thick valley fill, consistent with jökulhlaup incision. Elevated potholes are further evidence of vigorous flows atop the valley fill. Whether the bedrock canyon reaches of KRv were eroded by a gLP jökulhlaup remains uncertain.

7.1.2 Primary research question

Could the Purcell Trench have held a large amount of water and delivered it suddenly to the Columbia River system?

Late in MIS 2, from ~12.5 ^{14}C ka BP (14.8 cal. ka BP) to ~11.5 ^{14}C ka BP (13.1 cal. ka BP) the Purcell Lobe was grounded and decayed northward across the section of Purcell Trench that contained gLP (Easterbrook 1992; Carrara et al. 1996; Clague & James 2002; Dyke et al. 2003; Waitt et al. 2009). During this ice retreat, gLP was impounded in the Purcell Trench. The lake elongated over this ~1,700 year period, eventually covering ~670 km^2 and containing ~70km^3 of water. Lake drainage occurred, likely catastrophically, into the KRv following a failure of the Purcell Lobe ice dam. Drainage may have occurred suddenly and would have delivered ~50 km^3 of water into the Columbia River valley via the KRv.

7.2 Suggestions for future work

7.2.1 Paleohydraulic model of gLP drainage

Paleohydraulic modelling could best address the potential geomorphic impact of gLP drainage through the Kootenay River and Columbia River valleys. An example of such2-D modelling is presented by Denlinger and O'Connell (2010).

7.2.2 Quaternary history of the Slocan River valley

The Slocan River valley (SRv) is a potential area of interest to the history of the KRv. The SRv is devoid of previous study and seems to have contained a glacial lake ("glacial Lake Slocan", site 54, Appendix B) that may have extended

into the KRv (cf. site 46, § 5.5.3 and site 47, § 5.4.6). Near its confluence with the Kootenay River valley, the SRv is choked with thick deposits of fine-grained lacustrine sediment. If the sediment is indeed the signature of a large lake, its drainage may have contributed to erosion of the KRv fill.

7.2.3 Dating glacial lakes in the Kootenays and their drainage into the Columbia River valley

Constraints on the timing of events discussed in this thesis rely on previous reports of CIS chronology (e.g., Easterbrook 1992; Clague & James 2002; Dyke et al 2003; Waitt et al. 2009), lithostratigraphy and geoclimatic markers (till). In order to constrain the age of gLP and its drainage, associated sediments must be dated. Although no datable organics or tephra were found in the strata below the modern topsoil in the study area, optical or cosmogenic dating techniques could be employed. Absolute dating of gLP lacustrine sediments may be possible from optical dating (Lian & Hicock 2001; Lian & Roberts 2006); and cosmogenic dating of potholed bedrock using isotopes ^{10}Be and ^{26}Al could provide direct dates of incision in the KRv (Hein et al. 2011). The timing of the KRv valley fill incision could be used to confirm or reject a temporal correlation between gLP drainage and post-Missoula Channeled Scablands flood deposits (Waitt et al. 2009).

The ages of gLP, “glacial Lake Slocan” (site 54, Appendix B), and “glacial Lake Arrow” (Fulton et al. 1989) and the dates they drained into the Columbia River valley remain unknown (although Fulton et al. (1989) speculate from radiocarbon dates of detrital plant debris that “glacial Lake Arrow” drained ~8.3

^{14}C ka BP (9.3 cal. ka BP), yet age is vital to assessing the potential geomorphic work accomplished by their drainage to the Columbia Valley. ”Glacial Lake Arrow” appears to have been impounded behind the thick sediment deposit at the confluence of the KRv and the Columbia River near Castelgar, BC (Fulton et al. 1989; site 48, §5.4.7). Also, “glacial Lake Slocan” appears to have been controlled by the elevated KRv sediment fill (to which it may have contributed). Because these sediment dams lie within the path of the putative gLP jökulhlaup, it is possible that a gLP jökulhlaup could have triggered the release of these two sediment-dammed lakes. Consequently, a gLP jökullhlaup could have caused a cascading series of drainage events that resulted in a much larger flow of water into the Columbia River system than possible from gLP alone.

APPENDICES

Appendix A: Site coordinates

Site #	Latitude	Longitude
1	49° 00’ 40.29”	116° 34’ 17.61”
2	49° 22’ 42.85”	116° 43’ 06.57”
3	49° 00’ 53.20”	116° 28’ 08.72”
4	49° 00’ 18.08”	116° 29’ 08.06”
5	48° 50’ 11.78”	116° 20’ 09.66”
10	48° 38’ 35.59”	116° 23’ 22.89”
15	49° 07’ 05.56”	116° 31’ 46.87”
19	49° 42’ 08.78”	116° 52’ 00.64”
21	49° 37’ 22.87”	116° 58’ 35.56”
24	49° 37’ 47.68”	116° 57’ 59.30”
27	49° 54’ 10.42”	116° 55’ 37.32”
30	50° 04’ 38.31”	116° 55’ 32.47”
34	50° 17’ 11.00”	116° 55’ 11.34”
35	50° 12’ 08.72”	116° 56’ 30.87”
38	50° 06’ 41.51”	116° 54’ 13.62”
39	50° 05’ 38.00”	116° 53’ 22.31”
40	50° 05’ 21.00”	116° 53’ 02.00”
41	49° 39’ 03.40”	116° 56’ 42.23”
42	49° 36’ 44.00”	116° 58’ 02.37”
43	49° 35’ 08.59”	117° 13’ 51.93”
44	49° 29’ 51.94”	117° 18’ 27.55”
46	49° 25’ 26.57”	117° 31’ 49.22”
47	49° 23’ 02.54”	117° 33’ 47.52”
48A	49° 19’ 28.49”	117° 37’ 50.11”
48B	49° 19’ 18.37”	117° 38’ 14.10”
49	49° 19’ 33.40”	117° 41’ 22.80”
51	49° 20’ 04.81”	117° 45’ 30.49”
53	49° 26’ 00.88”	116° 45’ 17.20”
54	49° 27’ 40.24”	117° 33’ 49.62”

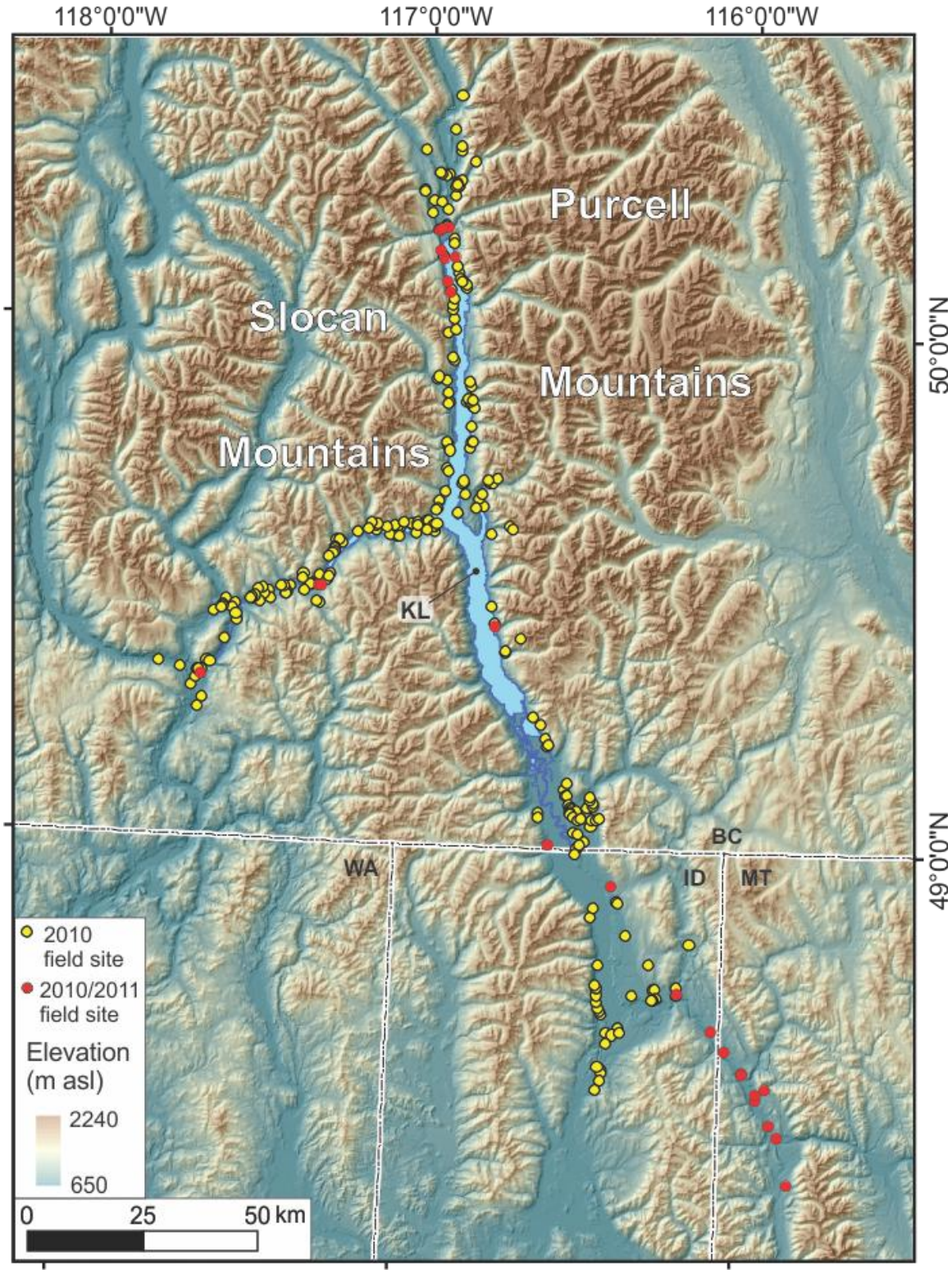

Figure A-1: Hillshaded DEM mosaic (Geobase® in CA, NED in USA; data available from U.S. Geological Survey) showing the locations of >250 field sites explored in 2010 and 2011.

Appendix B: Additional site descriptions

B.1 Site 1

B.1.1 Observations

Site 1 is located on the floor of the Purcell Trench (~610 m asl) near the western valley wall just north of the 49th parallel (Figure 3-2, Figure B-1). It is one of the few sediment deposits associated with glacial Lake Kootenai that has been preserved on the western side of the Purcell Trench in BC because the Kootenai River (flowing north from Idaho State) has removed most of the lake sediments from the western side of the valley (Figure B-1).

This site consists of four lithostratigraphic units (Figure B-2). Unit 1 is at least 0.75 m thick (lower contact not visible) and consists of indurated, planar-stratified, slightly convolute, normally-graded coarse sand beds (~1 cm average bed thickness) (Sp, Table 4-1). Occasional intra-unit pebble lenses are present (at a small exposure not shown in Figure B-2), becoming more abundant towards the top of unit 1. The largest pebble lenses extend laterally in excess of 7 m; the average lateral extent is 4 m. Lens thickness varies from 0.10 m to 0.30 m. In the lenses, well-rounded massive gravel is supported by a matrix of indurated coarse sand with ~10% granules.

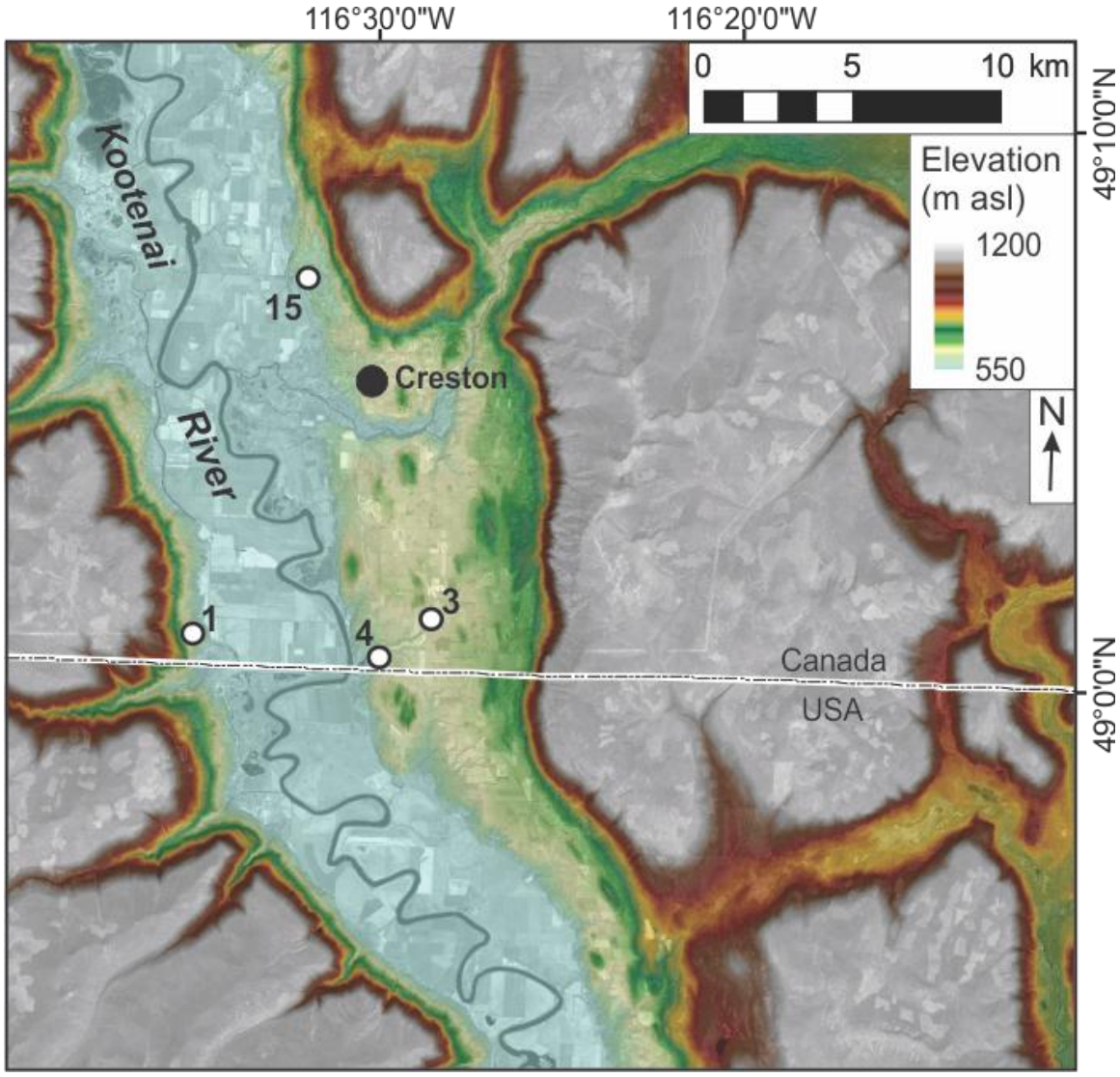

Figure B-1: DEM mosaic (Geobase® in CA, NED in USA; data available from U.S. Geological Survey) overlain with an orthophotograph (clip from 1:250 000 orthophotograph mosaic, 82F, Province of British Columbia) of the floor of the Purcell Trench near Creston, BC. Sites (white dots) that expose gLP lake-bottom sediment are shown.

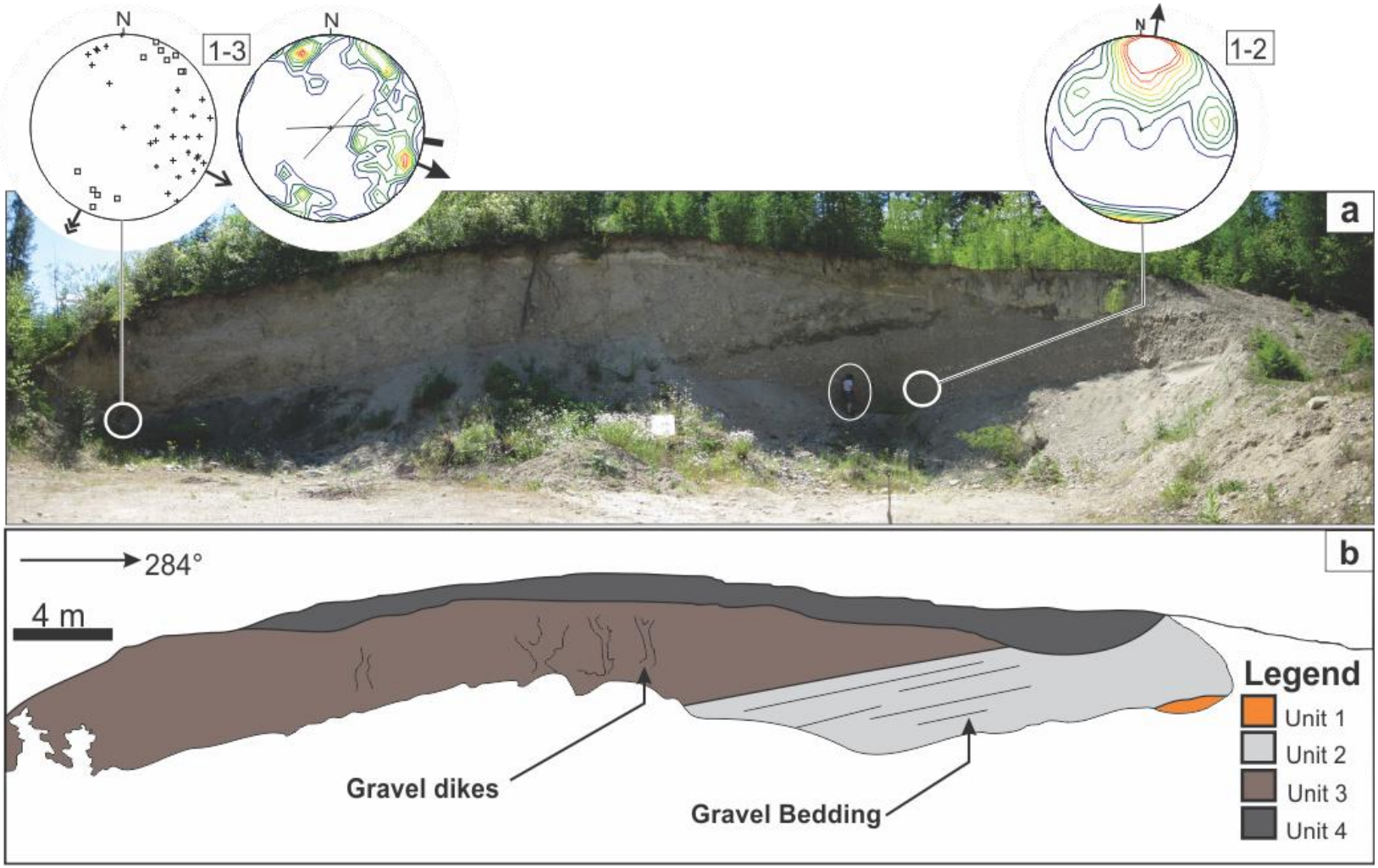

Figure B-2: a) Exposure at site 1 showing locations and stereograms for diamicton fabric 1-3 (Table 5-2) and gravel fabric 1-2 (Table 5-1). Person (circled) is 1.7 m tall. b) Sketch of lithostratigraphic units and major sedimentary structures in the exposure at site 1. Only part of unit 1 is exposed here. Refer to Figure 4-1 for stereogram legend.

Unit 2 is ~4 m thick (Figure B-2), has a sharp lower contact and consists of dipping, planar cross-stratified, imbricated gravel beds (Gc, Table 4-1). The apparent trend and plunge of the bedding are 124° and 18°, respectively. Beds exhibit upward fining from small cobbles (average b-axis length ~10 cm) to medium pebbles, and have sharp lower contacts. Most beds are matrix-supported (matrix composed of coarse sand and granules); some cobble beds are clast-supported. A gravel fabric on rounded, imbricated, dominantly a(t) pebbles records a southward paleoflow dominated by rolling clasts (i.e., clast are aligned perpendicular to flow) (1-2, Figure B-2, Table 5-1).

Unit 3 is ~4.5 m thick (Figure B-2) and composed of massive, clast-supported diamicton (Dcm, Table 4-1). It consists of large cobbles (up to 20 cm along their b-axes) to small pebbles supported by a sandy silt matrix. Clast roundness ranges from well-rounded to angular with most clasts being well-rounded (1-3, Table 5-2). Rarely, large cobbles are draped by silt laminae. A diamicton fabric in unit 3 is bimodal with a principal eigenvector toward 116° (1-3, Figure B-2, Table 5-2). Several massive, vertically-oriented gravel dikes occur within unit 4. These dikes consist of clast-supported, rounded and well-rounded cobbles and pebbles with very little sandy matrix.

Unit 4 is ~0.6 m thick that widens into a distinct trough-shaped depression near the west side of the exposure, where it is up to 2 m thick (Figure B-2). It consists of massive silt with few areas of discernible convolute or planar laminae and very few small pebbles.

B.1.2 Interpretation

Unit 1 is interpreted as a fluvial deposit based on the well-sorted, stratified sand with lenses of gravel indicating a scour-and-fill fluvial depositional environment (Miall 1977, Ashley 1990). Gravel lenses are more abundant towards the top of the unit 1 sands indicating an upwards increase in energy through unit 1.

Unit 2 is interpreted as a fluvial deposit, deposited by southeastward flows based on its texture, clast roundness, the planar cross-stratified, normally-graded character of its beds, its fabric and the apparent dip of its beds (Miall 1977; Allen 1982).

Unit 3 is interpreted as a debris flow that originated on the western wall of the Purcell Trench because of its texture, structure, lack of glacigenic surface wear features on clasts, and fabric (Lowe 1982; Eyles et al. 1987). The bimodal fabric suggests both extensional and compressional stresses during deposition (a dominance of compressional stress recorded in fabric 1-3, B-2). The abundance of rounded clasts suggests a possible remobilization of upslope fluvial sediments. The texture of the gravel dikes intruded into unit 3 is similar to that of the underlying gravel of unit 2; this indicates unit 2 dewatered following deposition of unit 3 (cf. Rijsdijk et al. 1999). The gravel dikes are interpreted as burst-out structures from hydrofracturing caused by excessive water pressure within the underlying unit 2 gravel beds (Rijsdijk et al. 1999; Jolly & Lonergan 2002).

The massive silt in unit 4 could record lake bed or eolian deposition. The areas of bedded silts in unit 4 are typically well sorted, suggesting deposition via suspension settling (Smith & Ashley 1985) and the presence of rare pebbles in the unit also suggest lacustrine, rather than eolian, sedimentation. In this light, and given its proximity to the land surface, unit 4 is interpreted as bioturbated (or cryoturbated) lake bed sediment. Given the elevation of site 1 and its proximity to other gLP lake bed sediment exposures (Figure 3-2, Figure B-1), unit 4 was most likely deposited within gLP. The lenticular trough at the contact between units 2/3 and 4 is interpreted as an erosional unconformity that was later filled with gLP lacustrine sediment.

B.2 Site 54

B.2.1 Observations

Site 54 is located in the Slocan River valley (SRv) ~7 km upstream of the Slocan/Kootenay River confluence at an elevation of ~513 m asl (~50 m above the Slocan River and ~60 m above the Slocan/Kootenay confluence) (Figure 3-4, Figure B-3a). The site exposes >5 m of fine-grained sediment, which is characteristic of the sediment exposed in bluffs along the southern SRv (the northern SRv was not explored during this study) (Figure B-3). The site was investigated from a distance using binoculars because it is on private land and the owners could not be contacted.

Exposed at site 54 are massive silt and cross-laminated fine sand lithofacies (Fm and Sr, Table 4-1, Figure B-3b). The lithofacies are planar-stratified and have sharp lower contacts. Type-A climbing ripples are present.

B.2.2 Interpretation

The silt beds at site 54 indicate deposition from suspension settling in a lake bed environment (Smith & Ashley 1985). The cross-laminated sands record higher-energy turbidity flows onto the lake bed (Johnsen & Brennand 2006).

The location of the deposit (in the riser of an extensive silt bluff) suggests that it is part of a lake bed bench that was deposited in a large SRv-occupying lake. This was likely a glacial lake because its geomorphic and geographic similarities to deposits in the Arrow Lakes basin (Fulton et al. 1989) suggest a similar paleoenvironment. The name “glacial Lake Slocan” (gLS) is hereby proposed to describe the putative water body once located in the SRv (and potentially in part of the KRv). Whether or not the lake bed sediments recorded at sites 46 and 47 were part of the same lake remains to be determined.

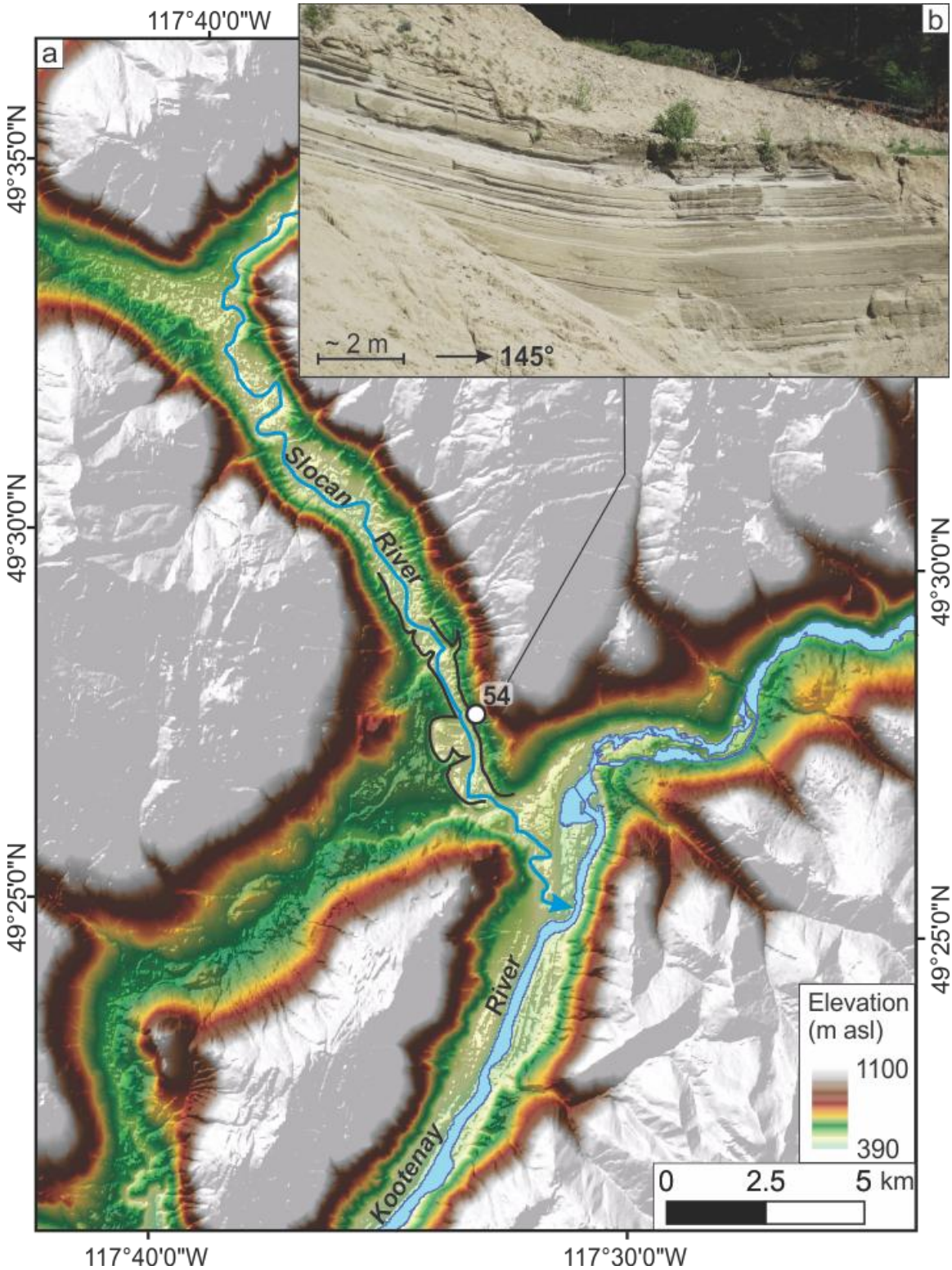

Figure B-3: a) Hillshaded DEM (GeoBase®) showing the location of site 54 (white dot) and the surrounding fine sediment bluffs (outlined with black lines). Refer to Figure 3-4 for location along the KRv. b) 5 m thick exposure of fine sand and silt at site 54.

B.3 History of the Columbia River valley

B.3.1 Site 49

B.3.1.1 Observations

Site 49 is located along the southern bank of the Columbia River ~4.4 km upstream from its confluence with Kootenay River (Figure 3-4, Figure B-4a). The site exposes ~33 m of sediment (~11 m of colluvium separates the unit 1 exposure from the unit 2 exposure) and reaches a maximum elevation of ~540 m asl. The exposure forms a steep (near vertical) cliff near the top of a dry (not stream-cut), arcuate scarp in the riser of a sloping (towards the Columbia River) valley-wall bench (Figure B-4a; cf. Figure 5-38a). Below the exposure a long (~0.3 km), steep (~20° - 30°) ramp of colluvium stretches to the Columbia River. Access to the exposure was very limited and most of the observations were gathered using binoculars.

Four lithostratigraphic units are exposed at site 49 (Figure B-4b). Unit 1 is revealed only by small isolated exposures through the silty colluvium but appears to be at least 3-6 m thick. It is composed of planar-laminated, rhythmically-bedded silt and clay (Fl, Table 4-1). Unit 2 is at least 10 m thick (its lower contact is covered by colluvium) (Figure B-4b), and is composed of massive diamicton with dominantly subrounded to subangular clasts (49-2, Table 5-2) (small pebbles to boulders) supported by a silty matrix (Dmm, Table 4-1) and including small (~0.1–0.25 m wide, ~0.02 m thick) lenses of planar-laminated clay and silt (Fl, Table 4-1). A diamicton fabric from unit 2 reveals a bimodal distribution with a principal eigenvector towards 219° and steep clast a-axis plunge angles (49-2, Figure B-4c, Table 5-2). Unit 3 is ~10 m thick and has a sharp lower contact

(Figure B-4b). It is composed of planar-stratified sand (Sp, Table 4-1). The sand appears well sorted and the beds appear tabular. Unit 4 is ~9 m thick and has a sharp lower contact (Figure B-4b). It is composed of planar-stratified, rounded large-pebble to cobble-sized gravel (Gp, Table 4-1) in a sandy matrix. Bed geometry is tabular and lenticular.

B.3.1.2 Interpretation

Unit 1 is interpreted as a lake deposit because it contains well-sorted, laminated silt and clay rhythmites (Smith & Ashley 1985). The textural variations within it suggest diurnal or seasonal variations in the lake influx (Shaw et al. 1978; Smith & Ashley 1985; Johnsen & Brennand 2006). Unit 2 is interpreted as a debris flow deposited into a lake because of its massive, matrix-supported character, intra-unit silt and clay lenses and lack of glacigenic wear features on pebbles (Eyles et al. 1987). The bimodal diamicton fabric with high plunge angles records extensional stress (flow) to the northeast, into the Columbia River basin, and more minor compressional stress.

The planar-stratified sand of unit 3 may record deposition from traction transport in a river, on an alluvial fan, or from underflows on the lake bottom. The well-rounded, tabular and lenticular gravel beds of unit 4 are consistent with deposition in a braided river (Miall 1977; Miall & Jones 2003).

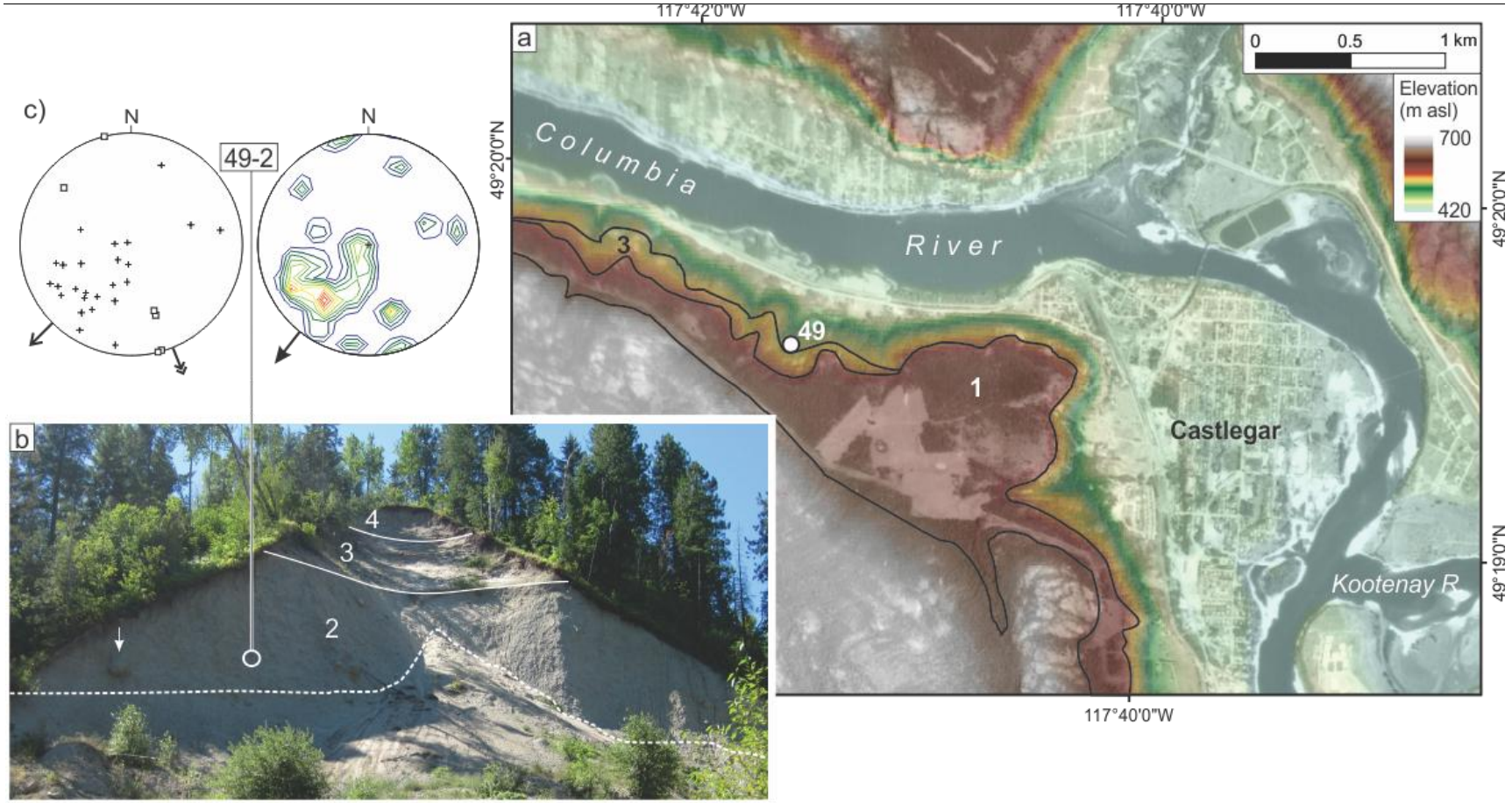

Figure B-4: a) Hillshaded DEM (Geobase®) overlain by an aerial photograph (A22007-7; © Department of Natural Resources Canada. All rights reserved.) showing the location of site 49 (white dot) along the steep-walled Columbia River and the surrounding terraced geomorphology (terrace numbers are consistent with Figure 5-38). b) Site 49 stratigraphy showing unit contacts (solid white lines) and the exposure-colluvium contact (dashed white line). Location of diamicton fabric 49-2 (Table 5-2) measurements is marked (white circle). For scale, the white arrow points to a ~1 m wide boulder. c) Equal area scatter plot and corresponding contoured stereogram of fabric 49-2 in unit 2. Refer to Figure 4-1 for stereogram legend.

The stratigraphic sequence of lacustrine sediments (unit 1) overlain by debris flow deposits (unit 2) may be explained by a deglacial depositional environment in which a glacial lake (previously identified by Fulton et al. (1989)) received debris flows off of steep glacially-conditioned valley walls. This lake (called “glacial Lake Arrow” in this thesis) formed in the glacioisostatically-depressed Columbia River valley north of Castlegar, BC and lake level was controlled by the thick valley fill delivered at the convergence of the Columbia, Kootenay, Slocan and Norns valleys (Fulton et al. 1989; § 5.4.6). Lake level was lowered through incision of the valley fill (Fulton et al. 1989) and likely from decanting during glacioisostatic rebound (cf. Teller 2004). Progressive lake level lowering resulted in the subaerial exposure of the valley floor and the reestablishment of river flow (units 3 and 4). The Columbia River has now incised through its floodplain, leaving a river terrace at site 49.

B.3.2 Site 51

B.3.2.1 Observations

Site 51 is located on the southern wall of the Columbia River valley ~1 km east of the Hugh Keenleyside Dam at an elevation of ~507 m asl (Figure 3-4; Figure B-5a). Two lithostratigraphic units are exposed by a small (~3 m high and <15 m wide) roadcut at this site. Unit 1 is at least 3 m thick (lower contact not exposed) and composed of planar-stratified and deformed silty sand beds (Sp, Sd; Table 4-1) that range in thickness from <0.01 - ~0.05 m (Figure B-5c). The unit fines upwards from coarse and medium sand with a few laminae of very fine silty sand to laminated very fine silty sand (Figure B-5b). Deformation decreases

upwards through the unit, low in the exposure the coarse sand is highly convoluted with some dewatering structures and pillows of fine sand, whereas higher in the unit the fine sand laminae are tilted but still planar. Some small (<0.06 m long) coarse sand rip-up clasts are present within the fine sand laminae (Figure B-5b).

Unit 2 is ~4 m thick and composed of massive, well-rounded, poorly-sorted imbricated gravel (Gm, Table 4-1) (Figure B-5c). The gravel clasts range in size from pebbles to cobbles and are clast supported in a coarse sand matrix (Figure B-5c). A-b plane measurements of ten imbricated clasts reveal an eastward paleoflow (Figure B-5a).

B.3.2.2 Interpretation

The planar-stratified, laminated and deformed silty sand of unit 1 likely records sedimentation in a lake (Smith & Ashley 1985). The presence of a sand rip-up clast suggests rapid transport and deposition of frozen sediment (Knight 2009). Convolute beds and ball-and-pillow structures indicate a loading-induced dewatering associated with rapid sedimentation. The well rounded, imbricated gravel of unit 2 records sedimentation on a river terrace by an east-flowing river.

The lithostratigraphy at site 51 is interpreted as lacustrine valley fill capped by fluvial gravels. This lithostratigraphy is interpreted to record deposition in a glacial lake (“glacial Lake Arrow”, Fulton et al. 1989) and deposition by the Columbia River following lake drainage. The Columbia River has now incised through its floodplain, leaving a river terrace at site 51.

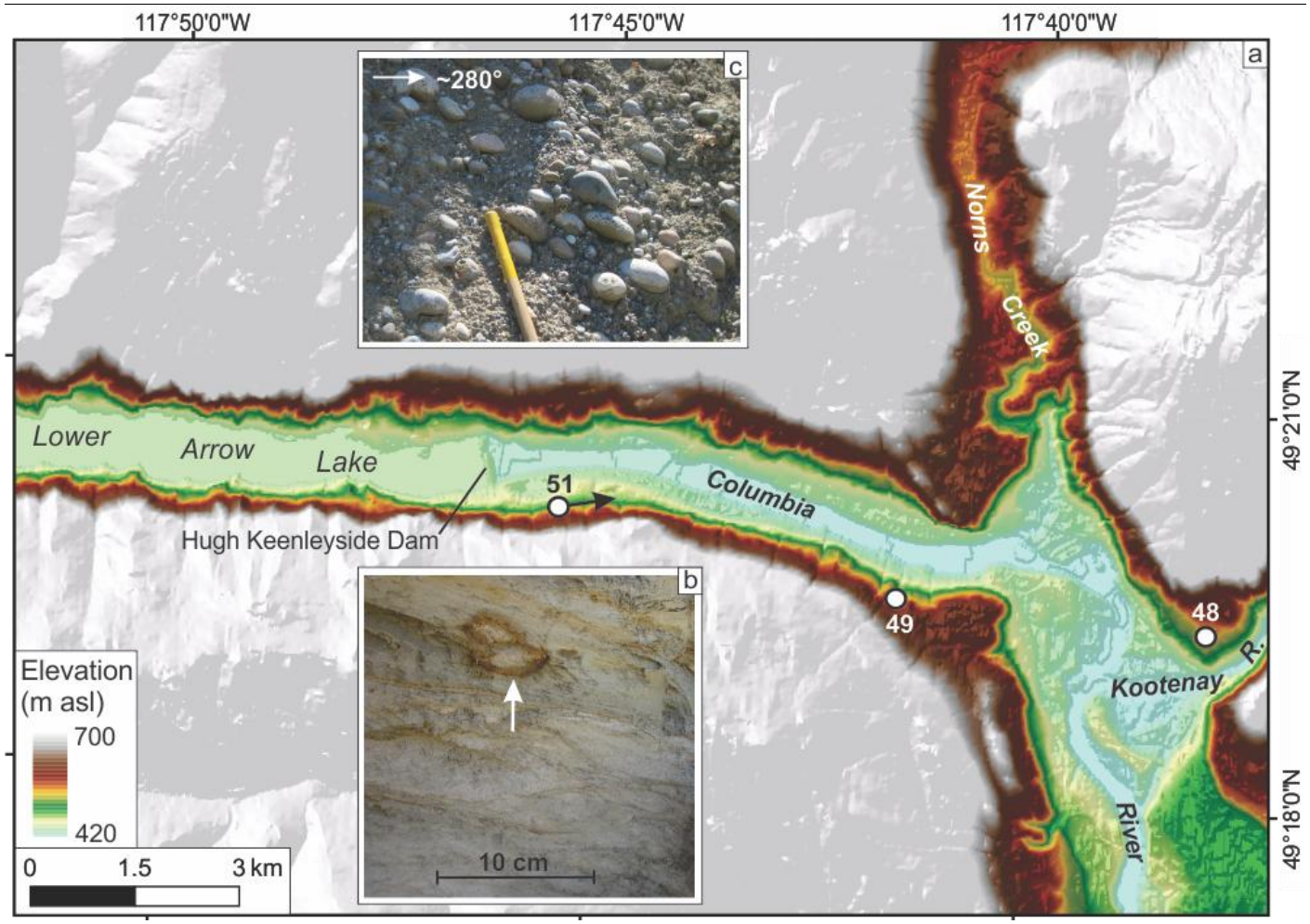

Figure B-5: a) Hillshaded DEM (Geobase®) showing locations of sites 51, 49 and 48 (white dots) in the steep-walled Columbia River valley geomorphology. Eastward paleoflow direction (78°) from imbricated gravel in unit 2 at site 51 is shown as a black arrow. b) Deformed sand of unit 1 containing a coarse sand rip-up clast (white arrow). c) Imbricated, well-rounded gravel of unit 2. The yellow section of the mattock handle is 0.23 m long.

B.3.3 Columbia River valley summary

Sediment exposed at sites 49 and 51 records the postglacial history of the Columbia River valley north of Castlegar, BC. The ponded water deposits lowest in the stratigraphic record may record the southernmost extent of “glacial Lake Arrow” (Fulton et al. 1989) and the imbricated gravel overlying the lacustrine deposits likely records the flow of the Columbia River following “glacial Lake Arrow” drainage past its sediment dam at the Kootenay-Columbia River confluence (Fulton 1970; Fulton et al. 1989).

Appendix C: Raw paleoflow data

C.1 Gravel fabric data

In the data tables below: 1) “a-b trend” is the down-dip direction of the maximum dip of the a-b plane corrected for declination; 2) “a-b dip” is the maximum dip of the a-b plane; 3) “a orient” is the orientation of the a-axis of the clast with respect to the maximum dip of the a-b plane. Where p = parallel, t = transverse and o = oblique; 4) clast axial dimensions (a, b, c) are in cm; and 5) roundness is after Wentworth (1922), Wadell (1933) and Olsen (1983), where WR = well rounded, R = rounded, SR = subrounded, SA = subangular, A = angular, VA = very angular and (fr) indicates that the clast is fractured.

24-1a

Clast #	a-b trend	a-b plunge	A orient (P, T, O)	A	B	C	roundness
1	82	20	O	4.8	4.7	2.2	SA
2	77	34	T	4	3.3	2	R
3	311	27	T	2.9	2.3	1.9	A
4	66	24	O	3	2.2	1.4	SA
5	21	23	O	7	5.3	3.4	SR
6	96	31	T	3	2.2	1.5	SA
7	70	32	O	2.5	1.8	0.8	WR
8	64	32	P	3.1	2.5	1	WR
9	186	30	T	3.9	2.8	2.2	SR
10	71	33	O	3.7	2.1	1.6	SA
11	25	43	P	3	2.1	1.2	SR
12	60	10	T	3.8	3.4	1.8	SR
13	1	22	O	3.5	2.5	1.7	SR
14	342	35	T	4	2.6	2.3	WR
15	74	41	T	4.9	4	1.6	R
16	78	50	O	4.9	3.6	2.7	WR
17	66	39	O	3	2.5	2	R
18	70	40	O	3.6	1.7	1.1	R
19	34	46	T	4.5	3.8	2.7	R
20	70	41	T	5.9	4	2.3	SR
21	25	50	O	4.3	3.7	2.2	SR
22	65	28	T	3.4	2.9	1.8	SR
23	23	24	T	7.8	4.6	3.2	R
24	71	44	T	10	6.4	4.6	SR
25	355	27	T	8.7	5.2	5	R
26	62	15	T	4.4	3.7	2.7	WR
27	152	28	O	6.7	3.8	1.7	SR
28	41	49	T	5.5	4.2	2.9	R
29	341	31	O	5	3.6	3	SR
30	349	17	O	5.6	3.6	2.7	R

24-1b

Clast #	a-b trend	a-b plunge	A orient (P, T, O)	A	B	C	roundness
1	106	25	P	14	10.5	8	WR
2	356	16	O	4.6	4.6	2.2	R
3	301	46	O	6	3.5	2	SR
4	160	32	O	7	4.1	2.5	SR
5	278	18	T	6.2	4.9	3.5	R
6	86	24	T	10.5	8	4	R
7	63	29	O	4.2	3.2	2	R
8	106	20	T	6.5	4	3	WR
9	146	25	O	4	2.2	1	SR
10	82	30	T	3.5	3	1.7	SR
11	111	19	O	5	3.8	2.6	R
12	30	59	O	3.4	2.5	2.1	SR
13	11	16	T	5.5	3.4	2.5	SR
14	97	18	T	5.4	2.6	1.6	R
15	52	52	O	5.5	3	2	R
16	61	26	P	5.5	3.9	1.3	SR
17	38	30	O	3.6	2.4	1	R
18	71	44	O	6.6	5	3.4	SR
19	41	38	O	3.5	3.4	1.6	WR
20	16	72	T	4.2	2.7	1.2	R
21	28	31	O	4.5	2.7	1.2	SR
22	92	38	T	5.5	4.5	2.5	WR
23	33	54	P	5	4	3.2	SR
24	75	29	O	11	5	3.7	R
25	11	44	T	7.5	4	3.2	WR
26	93	36	T	7.5	5	4	WR
27	76	37	T	5.5	3.5	3.3	WR
28	23	14	T	4.5	4	2	WR
29	8	22	O	9.8	6.5	3.8	R
30	72	27	T	12	7.8	7	R

24-1c

Clast #	a-b trend	a-b plunge	A orient (P, T, O)	A	B	C	roundness
1	93	40		14	13.4	8.5	WR
2	89	31	P	6.6	5.7	4.4	R
3	373	56	O	6.7	6.3	4.6	R
4	372	20	O	10	5.5	2.3	SR
5	51	20	O	5.4	3	1.6	R
6	62	36	O	10.5	5.5	2.5	SA
7	45	28	P	8.4	5.7	3.5	R
8	96	60	T	4.1	2.9	2.6	WR
9	83	13	O	10.5	8.2	6	WR
10	76	20	P	7	5.1	4.9	WR
11	89	18	O	5.2	5.2	2.7	R
12	77	21	O	4.5	2.7	1.3	SR
13	74	14	P				WR
14	106	35	T	9	7	4.7	WR
15	22	16	O	7.5	5.2	2.9	SR
16	52	21	P	5.4	3.9	2.8	R
17	31	45	O	6.8	5	4	WR
18	72	56	O	14.2	6.7	6	SR
19	86	45	T	6	4.8	3.8	SR
20	75	33	O	10.5	8.2	5	R
21	81	9	P	7	4.5	1.5	SR
22	126	22	P	7	4	3.2	SR
23	110	30	O	5.4	4	2.9	WR
24	84	40	T	9.3	5.3	4.3	WR
25	115	45	O	6.9	4.7	3.8	SR
26	370	21	T	5.5	4.6	2.7	R
27	62	20	O	9.5	7.5	5.8	WR
28	71	26	T	9	6.5	4	R
29	18	39	T	9.5	8.5	5.5	WR
30	34	29	O	9.5	8.5	5.7	R

24-1d

Clast #	a-b trend	a-b plunge	A orient (P, T, O)	A	B	C	roundness
1	51	18					
2	102	27					
3	116	12					
4	78	28					
5	31	82					
6	26	39					
7	60	44					
8	53	14					
9	28	44					
10	15	20					
11	50	46					
12	77	42					
13	21	39					
14	8	45					
15	51	53					
16	68	22					
17	38	38					
18	40	36					
19	27	45					
20	101	46					
21	66	43					
22	56	40					
23	31	46					
24	56	32					
25	104	38					
26	340	23					
27	18	51					
28	24	60					
29	11	19					
30	60	45					

41-4

Clast #	a-b trend	a-b plunge	A orient (P, T, O)	A	B	C	roundness
1	44	19	T	5	2.7	0.9	SR
2	177	18	T	2.9	2.4	1	SR
3	48	21	T	3	2.5	0.7	SA
4	188	5	T	2.4	1.8	1	SA
5	7	33	T	4.1	2	1.7	SA
6	60	10	T	4.2	3.5	2.5	SA
7	172	32	T	5.5	3.5	2.3	SR
8	116	20	T	3.6	2.8	1.7	SR
9	96	21	T	3.7	2.3	1	SR
10	204	39	P	4	2.3	1.6	A
11	149	15	T	4.2	2.1	1	SA
12	196	25	T	7.5	4.5	2.5	SR
13	346	27	O	4	2.7	1.4	WR
14	191	51	O	7.5	6.5	2.7	R
15	30	27	T	6.2	4.4	3.7	SR
16	166	25	O	7.2	4.8	3.2	SR
17	96	12	T	2.7	1.5	0.5	A
18	298	25	O	3.2	2.2	0.9	R
19	115	23	O	6	3.8	2.3	SR
20	171	30	T	3.3	2	1.5	SA
21	167	16	T	3.3	3	1	VA
22	151	12	O	7	5.6	2.7	A
23	341	55	T	4.4	2.5	1.8	SR
24	271	34	T	8.5	6	3.1	SA
25	162	28	O	6.3	5	2.2	SR
26	301	35	T	4	3.2	2.4	SA
27	191	40	O	5.5	3.3	1.6	R
28	241	18	T	2.6	2	0.6	SR
29	165	10	O	5	4	2.5	WR
30	316	25	T	6	4	1.1	SR

35-1

Clast #	a-b trend	a-b plunge	A orient (P, T, O)	A	B	C	roundness
1	296	26	O	9.2	5.5	4.2	SR
2	329	39	T	8.5	5	3.5	R
3	326	50	P	5.4	3.7	2.9	SR
4	338	35	O	10.8	6.7	4.7	SR
5	311	32	P	5.7	2.9	2.5	R
6	266	51	O	5.6	3.8	2	SR
7	337	18	P	5.5	3.6	1.2	SA
8	350	33	P	4.6	3.2	2.5	SA
9	13	37	O	8.6	5.2	2.2	SA
10	305	46	P	6.5	2.7	1.6	WR
11	333	15	P	5	4	1.1	WR
12	328	36	P	9	2.9	2	A
13	341	24	P	5.1	4.4	2.5	WR
14	303	27	O	4.4	3.2	1.5	SA
15	327	12	O	4.8	3.3	1.8	SR
16	62	18	O	4.1	2.2	1.5	R
17	297	10	P	7	5	1.5	R
18	357	54	P	3.7	3	1.5	WR
19	319	12	P	5.9	2.8	1.4	VA
20	9	27	T	3.8	3.1	1.5	WR
21	338	36	P	4.9	3.4	2	SA
22	157	34	O	4.5	2.5	1	R
23	42	62	T	5.2	3.3	1.3	R
24	324	23	P	9.5	5.9	4.5	SA
25	355	41	O	6.8	4.9	3	SR
26	358	33	P	5.2	3.9	1.5	
27	155	25	P	2.5	2	1.1	WR (fr)
28	313	23	O	4.4	1.9	1.5	A
29	10	13	O	4.3	2.3	0.5	SA
30	332	40	P	6.3	3.7	1.8	SA

38-1a

Clast #	a-b trend	a-b plunge	A orient (P, T, O)	A	B	C	roundness
1	174	40	P	9	6.8	4.5	SR
2	171	62	T	6.6	5.6	2	R
3	230	47	O	4.9	3	2.5	A
4	192	25	T	3.8	2	1.4	R
5	173	32	O	8.3	3.4	2.3	SA
6	197	79	T	3.7	3	1.1	SR
7	186	61	T	4	3	1.8	A
8	193	45	O	4.5	2.7	1.8	SR
9	149	56	O	4.6	3.1	1.4	R
10	132	36	T	8.4	7	2	R
11	141	16	P	4.4	3.4	1.7	SA
12	142	35	T	3.5	2.7	0.9	R
13	164	26	O	10.3	6.3	3.5	A
14	147	51	O	10.2	5.5	4	SA
15	157	46	P	7.4	5.7	1.9	SA
16	128	41	T	4	2.5	0.8	WR
17	161	46	T	11.5	8	2.9	A
18	191	63	T	3.7	3.2	1	SR
19	140	63	T	6.6	3.8	2	SR
20	156	59	T	5.5	3.5	1.5	R
21	176	42	O	9	6.5	2.5	WR
22	163	58	P	5.7	4.9	2	SR
23	170	38	T	5.5	5	1.8	WR
24	175	55	O	3.6	2.3	1.2	R
25	165	35	O	3	2.4	1.5	WR
26	171	40	T	4.5	3.8	1.7	SR
27	221	46	O	4.4	3.4	1.7	SA
28	230	38	P	3	2	1.4	WR
29	151	53	P	3.6	2.5	1.2	SR
30	177	51	T	5.7	2.9	1.1	VA

38-1b

Clast #	a-b trend	a-b plunge	A orient (P, T, O)	A	B	C	roundness
1	212	27	O	5.8	3.5	2	SA
2	191	45	O	6.3	6	1.9	R
3	161	16	T	7.7	6.6	1	SR
4	204	26	P	7.3	4.7	1.5	SA
5	206	15	T	6.5	4	1.7	R
6	210	32	O	4.7	3.3	1.4	SR
7	236	57	T	6	3.5	1.5	SA
8	190	21	P	7.8	5.4	1.8	R
9	171	10	T	4.3	2.7	1.5	R
10	234	52	O	4.7	3.4	0.9	WR
11	176	10	P	5.9	4	2.1	SA
12	131	45	O	4.6	3	1.5	SA
13	145	19	T	3	2.2	1	SR
14	216	28	O	4.5	4	2	SA
15	106	49	O	11	6	5	R
16	171	33	P	3.4	3	1.2	R
17	241	35	O	6.3	3.7	2	WR
18	316	17	O	5	3	1.5	SA
19	145	37					
20	229	2	T	6	4.7	1.8	SA
21	174	44	O	3.5	2.7	0.8	WR
22	173	46	O	6.7	3.7	1.5	R
23	219	12	O	7	5	2.6	SA
24	220	19	P	6.5	4.2	1.7	VA
25	181	20	T	5.5	3.5	0.8	R
26	206	6	T	6	3.7	1.8	SR
27	221	28	O	6	4.8	2.5	SA
28	192	35	O	4.6	3.3	1.5	SA
29	241	18					
30	176	30	O	4.8	2.8	1.6	SA

31	185	66	T	7	4	2	A
32	207	57	P	3.3	2.5	1	SR
38-1c							
Clast #	**a-b trend**	**a-b plunge**	**A orient (P, T, O)**	**A**	**B**	**C**	**roundness**
1	186	44	T	5.6	3.7	2.2	SA
2	194	26	O	8	3.6	3	SR
3	140	19	T	4.1	2.5	1.6	SA
4	176	34	T	7.2	5.3	2.5	R
5	198	36	O	6.2	4.2	2.8	SA
6	202	19	O	5.5	3.8	2	R
7	221	31	O	3.5	3.3	1.4	A
8	314	38	O	5	3	2	A
9	334	31	O	4.6	3.3	1.4	VA
10	236	3	T	3.5	2	1	R
11	242	30	O	7	4.6	2.2	SR
12	236	35	P	6.7	5.6	2	SA
13	168	25	P	4.8	4	0.8	R
14	187	20	T	12	7.7	2	R
15	241	35	O	5.7	3.1	1.4	SR
16	166	51	T	4.8	4	1.8	R
17	201	14	P	4.2	2.5	0.6	SA
18	271	28	T	5.5	3.6	2.9	R
19	101	57	T	5.2	4.7	0.7	R (fr)
20	111	20	P	6.5	4	2.5	SA
21	203	25	P	3.9	2.1	1.1	SA
22	322	21	T	3.8	2.5	1.5	WR
23	214	16	O	5.7	3	2.1	SA
24	239	34	T	4.5	2.8	1.6	R
25	236	51	T	6.4	5.1	1.4	SA
26	108	27	T	8	4.4	1.9	WR
27	231	10					
28	223	27	O	6.5	4.6	2	R

29	211	41	T	7.9	6.9	4.2	SR
30	186	40	P	4.5	2.4	1.2	SA
31	176	24	T	3.9	3.4	1.3	R

39-6

Clast #	**a-b trend**	**a-b plunge**	**A orient (P, T, O)**	**A**	**B**	**C**	**roundness**
1	204	24	P	6.2	4.8	1.9	SR
2	65	36	P	9	8	5	A
3	264	38	P	9.5	8.4	4	SR
4	240	27	P	7	4.9	1.7	VA
5	366	44	O	6.6	5	2.5	SR
6	216	31	T	4.4	3.1	1.4	A
7	262	39	P	9.5	5.8	3.4	A
8	280	35	P	4.8	2.6	1.7	SA
9	216	58	P	5.9	5.5	3.7	A
10	316	37	O	6	3.5	2.8	R
11	241	35	T	5.9	3	2.5	A
12	260	20	T	5.6	4.1	2.4	A
13	205	18	T	7.6	6	2.8	SA
14	246	21	P	5	3.5	1.7	SA
15	220	32	P	4.7	2.5	2	SA
16	166	17	O	6.5	4.8	2	SA
17	201	35	P	5.6	5	3.4	SA
18	311	37	T	4.8	3.8	1.6	SA
19	176	32	O	7.5	3.4	2.3	A
20	271	10	P	6	3.8	2.4	SR
21	261	16	O	4	3.3	1.6	WR
22	178	17	P	5.5	4.5	3.5	R
23	293	45	O	4	2.8	1.4	A
24	220	36	O	7.2	4	2.2	A
25	183	43	T	5.4	2.1	1.5	A
26	272	46	P	5.8	4.3	2.1	SA
27	240	37	O	4.2	2.7	1.7	SR

28	248	29	O	5.9	3	2	R
29	279	26	P	6.4	4.8	3.7	SA
30	301	30	T	4	3.5	1.9	R

39-7

Clast #	**a-b trend**	**a-b plunge**	**A orient (P, T, O)**	**A**	**B**	**C**	**roundness**
1	172	15	O	4.5	4	2.3	SR
2	244	56	T	5.1	4.4	2	SR
3	223	61	T	7.8	5	4	R
4	336	56	O	4.7	3.2	1.9	SR (fr)
5	301	19	P	8.4	6.1	3	SR
6	260	55	T	4.7	3.6	2.5	WR
7	249	20	P	9.6	6.8	4	VA
8	263	49	O	7.1	4.4	2	A (fr)
9	165	35	T	5	3.5	2.1	A
10	78	40	T	7	4	2.5	A
11	254	45	P	7	4.5	2.7	SA
12	319	35	O	5	2.9	2	WR
13	276	30	T	6.5	5.5	3.3	SR
14	210	59	T	4.5	3.5	2.6	SA
15	209	56	O	5.7	4	2.2	A
16	319	61	T	5	4	2.4	A
17	244	42	O	6.5	5.4	2	SA
18	245	44	P	7.6	5	2.5	A
19	228	45	T	6	4	3.2	R
20	66	47	T	8	5.5	3.4	SR
21	277	28	P	4.3	2.3	1.3	WR
22	204	60	P	5	2.8	2.5	SA
23	299	12	T	4.4	3.6	3	A
24	159	40	O	6.9	3	2	SA
25	276	47	T	3.4	2.7	1	SR
26	273	48	T	5.5	2.8	1	VA
27	236	37	O	5.5	4	2.5	SA

28	338	48	P	7.5	4	2	WR (fr)
29	191	20	O	4.5	2.8	2	SR
30	16						
31	227	30	O	5	4	2	R

40-1

Clast #	a-b trend	a-b plunge	A orient (P, T, O)	A	B	C	roundness
1	360	38	T	8	5	3.5	SA
2	261	22	O	6.7	5.8	1	R
3	265	26	P	4.8	3	1	R
4	236	25	P	3.5	2.5	1	R
5	306	54	O	4.4	2.8	1.8	A
6	234	14	P	6.4	4	1.5	A
7	243	11	P	4.5	3	1.4	SA
8	176	20	P	4.4	3.6	1.3	SR
9	216	26	O	4	2	1	A
10	188	55	O	2.9	2.5	1.3	SR
11	246	14	P	5	3.8	1.7	R
12	234	45	O	2.5	1.6	1.3	WR
13	262	21	O	3	2.6	0.6	R
14	131	26	O	3.3	2	0.7	SR
15	280	20	P	5	2.7	1.1	WR
16	109	15	T	4	2.7	1.7	SA
17	134	29	P	6	4.8	1	SA
18	202	27	O	3.7	2.2	0.8	SA
19	178	15	O	3.4	1.6	0.9	R
20	225	17	O	4.8	2.6	1.9	A
21	333	39	T	3.5	2.3	1.5	WR
22	248	18	P	3.7	2.9	1.9	WR
23	76	15	P	3.2	1.7	1	SR
24	326	38	P	4.7	3.5	2.8	SA
25	325	15	P	5.5	3.3	2.2	WR
26	240	29	O	4	3.2	2	SR

27	251	28	T	3.5	2	1	SA
28	157	26	O	4.1	1.8	0.7	SA
29	196	18	P	6.7	5	1.3	SA
30	328	52	O	4.5	2.8	1.3	SA
31	200	9	P	4.3	3.8	1	SR
32	253	23	P	4	2.4	0.9	SR
33	276	32	P	2.5	1.4	0.6	SA
34	230	22	O	3.9	2.8	1	SA
35	231	23	O	6	3.5	2	WR
36	235	36	P	2.8	1.8	1.1	SR
37	121	58	O	5.5	4.2	2.2	SA
38	149	42	O	6.5	4.2	3	SR
39	218	48	P	3.4	2	1.8	SA
40	296	53	T	4.6	3.3	1.2	R
41	291	27	P	4.2	3.5	1.7	R
42	298	32	O	4.5	2.4	1.5	WR
43	268	33	O	3.2	1.5	0.8	WR
44	219	17	O	3.5	2.5	1.3	R
45	273	43	O	3	2.2	1.8	A
46	184	56	T	3.1	2.2	0.7	R
47	305	67	T	3	2	1.6	SR
48	246	13	P	4.3	2.8	0.9	SR
49	301	14	T	3.3	2.9	1.4	R
50	246	64	O	5.5	3.2	1.8	R

19-1c

Clast #	**a-b trend**	**a-b plunge**	**A orient (P, T, O)**	**A**	**B**	**C**	**roundness**
1	358	50	T	8	6	3.4	WR
2	343	41	T	7.1	3.7	1.3	R
3	332	17	T	8.9	5.6	3.2	R
4	331	11	P	6.2	5	2.8	SR
5	319	21	P	7.1	5	4	WR
6	348	39	T	9.6	7.4	6	R

7	4	15	T	5	4.3	3	R
8	346	17	O	6.7	5.6	2.6	WR
9	338	16	P	4.5	3.7	2	R
10	315	25	T	5.5	3.4	1.5	SR
11	346	37	O	6.6	4.9	3.6	SR
12	311	27	P	4.9	2.5	1.8	SA
13	331	24	P	4.6	3.7	1.9	SR
14	322	27	O	4.6	3.5	1.5	R
15	339	72	T	5.5	4.4	2.5	WR
16	316	21	P	16	12	7.5	R
17	341	35	O	6.4	3.7	2	SR
18	290	71	P	4.1	2.7	1.1	SR
19	321	67	T	6.4	4.2	2.5	WR
20	347	20	T	8.2	5	2	A
21	353	17	O	6.8	5.8	2.5	SA
22	340	20	O	5.8	3.5	1.6	R
23	7	27	T	9	5.8	3	SR
24	331	45	T	6.2	4	2.5	SR
25	356	46	P	5.5	5.2	3	A
26	341	23	P	8.4	6.8	2.3	SR
27	121	27	O	11.4	8	5	R
28	334	11	O	10.5	8.5	3.7	SR
29	320	35	T	4.8	3.8	2.7	WR
30	342	30	T	12	9.5	3.5	SA

19-1b

Clast #	a-b trend	a-b plunge	A orient (P, T, O)	A	B	C	roundness
1	316	24	T	10.4	6.4	3.7	SR
2	6	15	P	5.5	4	1.4	SR
3	221	29	O	8	7	2	SA
4	313	19	P	5	4	2.5	R
5	233	28	T	4.4	2.3	1	WR
6	314	22	T	7.3	5.3	3.5	WR

7	305	34	P	5.5	3.8	2	WR
8	321	18	O	8	5.5	2.5	R
9	312	35	O	6	5	3.2	WR
10	326	24	T	8	5.2	3.7	WR
11	346	29	O	7.2	5.2	1.2	R
12	313	13	P	8.5	3.5	2.2	SA
13	286	31	T	9.5	7.8	4.2	SR
14	314	37	O	5.4	4	3	SA
15	325	34	T	3.8	3.5	2.6	WR
16	265	12	P	5.1	3.7	3	R
17	316	37	T	5.4	3.5	2.6	SR
18	56	27	T	6	4.7	2.4	R
19	229	23	O	4.8	3	1.2	WR
20	277	12	P	6	4.8	2.2	SA
21	1	12	P	4.8	2.2	1.9	R
22	254	28	T	6	3.9	2.5	SR
23	329	52	T	7.4	5	3.4	SA
24	319	10	O	7.5	6.5	2	SR
25	311	7	T	8	4.7	2.2	WR
26	317	38	T	5.7	4.2	2.5	SA
27	328	12	T	5.8	4.1	2	SA
28	285	10	T	6.3	4.6	4.1	SR
29	258	8	P	10.5	4.3	2.5	SR
30	315	55	O	5.6	5.2	2.6	SA

19-1d

Clast #	**a-b trend**	**a-b plunge**	**A orient (P, T, O)**	**A**	**B**	**C**	**roundness**
1	26	21	P	2.6	1.2	0.5	R
2	346	70	T	1.6	0.8	0.2	R
3	21	19	P	2.4	2	1	SA
4	342	35	O	1.5	1	0.6	SR
5	346	22	O	3.7	2.4	0.6	R
6	346	29	O	1.5	1.1	0.7	WR

7	321	23	O	1.5	0.9	0.5	WR
8	354	42	P	1.2	0.5	0.4	SA
9	41	12	P	3.6	2.5	1.1	SA
10	291	6	P	1.8	1.1	0.7	WR
11	358	25	T	2.3	1.8	0.4	SA
12	346	30	T	3	1.6	0.8	A
13	334	28	P	3.2	2	1.5	SA
14	5	16	P	2.5	2.1	0.7	WR
15	343	20	P	2.2	1.9	1.2	SA
16	11	29	O	2	1.3	1	SR
17	41	30	P	2.5	1.6	1	SR
18	46	8	O	1.9	1	0.4	WR
19	360	20	P	3.3	1.3	1	SR
20	341	29	P	2.2	1.2	0.7	SR
21	20	25	P	2.2	1.7	0.6	A
22	342	20	P	2.4	2	1.4	WR
23	350	10	P	1.6	1.1	0.6	SA
24	6	12	P	4.5	1.1	0.9	WR
25	26	26	P	3	2.5	1.4	SR
26	336	18	O	1.7	1	0.8	WR
27	326	51	P	1.2	0.7	0.6	SA
28	358	21	P	1.3	0.7	0.5	SR
29	76	47	P	3.1	2.1	1.5	WR
30	348	23	T	1.9	1.5	0.9	WR

19-1a

Clast #	**a-b trend**	**a-b plunge**	**A orient (P, T, O)**	**A**	**B**	**C**	**roundness**
1	314	28	O	8.3	6	3.1	WR
2	304	50	O	5.7	5	2.8	WR (fr)
3	331	21	P	10	4.7	3.5	R
4	313	44	P	13	11.5	3.5	R
5	340	40	P	13.7	7.2	3	SA
6	293	21	O	8.5	7.5	3.9	SR

7	320	76	P	4.6	3.3	1.3	SR
8	260	29	P	5.8	4.7	4	WR
9	291	55	O	12	5.5	3	WR
10	307	40	P	6.5	4.7	3	WR
11	305	40	T	7	4.5	1.7	SR
12	186	23	T	4.5	3.2	1.1	WR
13	324	62	O	7.5	4.7	2	SR
14	236	45	T	5	3.7	3	SR
15	245	24	P	11.3	9	5.2	R
16	268	35	T	6.5	5	2.1	WR
17	289	21	O	4.6	4	3.1	WR
18	287	24	O	13	11	5	R
19	255	42	O	6	4	3.8	SA
20	316	59	T	11.5	5.8	2.8	WR
21	296	24	P	7	4.8	3.5	SR
22	309	40	P	4.1	3.1	2.3	WR
23	296	39	P	6.3	3.5	2.3	SA
24	301	49	T	4.3	3.1	2.2	R
25	301	20	P	6	5.5	3.9	WR
26	303	37	O	7	4.8	4	SR
27	319	43	P	4.5	4	2	R (fr)
28	316	69	T	3.8	3.2	1.4	R
29	311	70	O	3.5	2.7	0.7	SR
30	316	25	T	5.5	5.1	2.5	SA

1-2

Clast #	**a-b trend**	**a-b plunge**	**A orient (P, T, O)**	**A**	**B**	**C**	**roundness**
1	352	5	T	4.4	3.4	1.6	R
2	346	37	T	4.7	3.6	2.5	WR
3	34	47	O	3	2.5	1.5	WR
4	39	28	T	4	3	2.3	WR
5	355	45	O	3.6	2.7	1.5	SR
6	38	14	T	4	3.3	2.5	R

7	17	66	T	3.2	2.1	2	WR
8	84	30	P	2.8	2	1.4	A
9	12	45	T	3.8	2.4	1.5	SA
10	11	9	T	4.6	2.8	2.2	WR
11	13	10	T	2.9	2.5	1.5	R
12	19	16	O	3.3	2.4	1.1	R
13	171	86	T	6	4.5	3	WR
14	10	11	O	3.5	2.5	1.4	WR
15	353	34	O	4	3.1	1.6	A
16	2	15	T	3.3	2.2	1.6	WR
17	22	55	T	2.7	1.5	1	SA
18	307	33	P	2.5	2.1	1	SR
19	290	23	T	2.3	2.1	1.5	R
20	4	25	T	3.2	2.5	1.2	WR (fr)
21	306	19	O	2.7	2.2	1.2	R
22	3	24	O	2.5	2.1	1.1	A
23	318	51	T	4.3	1.8	1.6	WR
24	89	73	O	4	3.2	2.4	R
25	21	5	T	3.2	1.8	1	A
26	267	251	T	3.5	2.5	1.5	SR
27	90	74	P	3.6	2.8	1.3	SA
28	352	336	P	2.5	2.3	1	WR
29	360	344	T	4.3	2.6	1.7	WR
30	72	56	P	3.5	2.1	1.6	WR

27-1

Clast #	a-b trend	a-b plunge	a orient (P, T, O)	A	B	C	roundness
1	342	38	T	10.5	5.9	2.6	WR
2	347	17	T	4.5	3.2	1.6	WR
3	20	22	P	6.4	3.5	2.3	WR
4	303	30	O	5.9	4	1.5	WR
5	37	23	P	3.5	1.6	0.7	R
6	342	23	T	10.8	7	3.1	WR

7	332	20	T	11.7	7.8	4	WR(FR)
8	360	69	T	8.7	5.5	4.4	R
9	338	45	T	3.9	1.8	0.9	R
10	354	24	T	4.3	2.3	1.6	R
11	288	19	O	4.2	2.6	1	WR
12	356	18	T	4.4	3	1.5	R
13	266	2	T	3.5	1.7	1	WR
14	312	41	T	5.4	3.3	2.6	RF
15	90	4	O	4.7	2.1	1	SA
16	22	31	T	8.7	5.9	4.9	WR
17	353	52	T	5.8	4	3	SR
18	330	30	T	13	10	3.2	WR
19	22	21	T	2.9	2.5	1	SA
20	356	22	T	5	2.3	1.1	SR
21	358	39	T	5.6	3.5	2	R
22	117	36	T	3.7	2.5	1.1	SA
23	338	29	T	3.6	1.3	1.2	R
24	92	36	O	3.5	2.1	0.8	A
25	368	39	T	5.4	3	2.4	R
26	368	8	T	6.9	4.5	1.2	R
27	337	28	T	5	3.3	1.6	R
28	321	20	T	4.9	3.5	2	R
29	168	39	T	5.4	2.5	1.5	SA
30	306	30	T	3.7	2.3	1.3	R
31	257	30	T	3.1	1.9	1.1	SA

30-1

Clast #	a-b trend	a-b plunge	a orient (P, T, O)	A	B	C	roundness
1	30	31	P	7.5	4.6	3.7	SR
2	65	17	P	9	5	3.5	SR
3	371	25	O	4.2	2.4	1.5	SA
4	60	15	O	5.8	3.3	1.3	WR(FR)

5	193	29	T	6.1	3.2	2.5	R
6	72	5	P	3.7	2.6	0.8	WR
7	24	6	P	3	2.5	1	SR
8	212	45	O	3.6	3.2	1.5	R
9	41	19	O	6.5	4	3.6	SR
10	338	52	T	5.5	4.8	1.8	SA
11	66	45	T	3.7	3	1.9	A
12	361	25	T	5	4.5	2.8	SA
13	359	10	P	4	3.9	2.4	SR
14	347	18	O	3.4	2.1	0.9	SA
15	31	37	T	4.9	3.7	2.3	SA
16	120	15	P	3.2	2.5	1.8	SA
17	114	54	T	5.9	4.7	2.6	SR
18	226	58	O	3.4	1.8	1.5	WR
19	292	23	O	4.7	3.5	2	SR
20	224	37	P	6.5	5.6	2.5	R
21	289	15	P	3.8	3.5	2	R
22	123	46	T	4.5	3.4	1.1	SR
23	25	5	P	3.2	2.6	1.5	R
24	271	28	O	3.5	2.6	1.7	R
25	39	21	O	3.1	2.2	1.7	A
26	225	30	P	4.8	3.3	2.5	SA
27	42	24	O	5.5	3	2.3	R
28	143	42	T	5.2	2.9	2.7	WR
29	26	37	T	7.5	5	4.8	SR
30	185	45	T	6.9	4	1.8	SR

C.2 Diamicton fabric data

In the data tables below: 1) “a trend” is the down-plunge direction of the a-axis corrected for declination; 2) “a plunge” is the plunge of the a-axis; 3) clast axial dimensions (a, b, c) are in cm.; 4) roundness is after Wentworth (1922), Wadell (1933) and Olsen (1983), where WR = well rounded, R = rounded, SR = subrounded, SA = subangular, A = angular, and VA = very angular; 5) “plucked lee” records the direction in which the plucked lee was pointing (corrected for declination); 6) “bullet nose” records the direction in which the bullet nose was pointing (corrected for declination); 7) “keel” records the orientation of keels on clast bottoms; and 8) “striae” records the orientation of the most recent striae on the clast and whether they are present on the clast top (T), bottom (B) or side (S).

47-X

Clast #	a trend	a plunge	A	B	C	roundness	plucked lee	bullet nose	Keel	striae
1	233	37	5.4	4	2.5	SA				
2	132	14	5.2	3	2.8	SA				
3	141	48	5	3	2.7	SA				
4	174	59	4	2.4	1.3	A				
5	161	26	6.8	3.8	3.3	SA				
6	199	24	8.5	6.3	4.7	A				
7	231	7	3.8	3	2	SA				
8	210	29	2.8	2	1.4	A				
9	161	4	2.2	1.5	1	A				
10	199	25	3.6	2.1	1.1	A				
11	231	11	3.3	1.7	1.2	SA				
12	210	10	8.9	7.5	3	A				
13	161	34	6.9	5.5	3	SR				
14	352	53	4.5	3.5	3.1	SA				
15	344	5	4.8	2.8	1.7	A				
16	81	68	3.2	4.5	1.3	SA				
17	234	47	3	1.8	1.5	R				
18	97	4	12.6	7.4	4	SA				
19	191	10	3.8	3.3	2.2	SA				
20	252	8	2.3	1.4	1.2	A				
21	160	15	2.2	1.6	1	SA				
22	161	11	4	2.2	2.2	A				
23	328	13	5	2.6	1.6	A				
24	190	36	2.5	2	1.4	A				
25	151	15	4	2.8	1.9	A				
26	146	30	5.5	3	2.3	SA				
27	317	36	7.4	5.6	3	SA				
28	221	26	3.5	2.4	1.2	SR				
29	146	24	2.4	1.2	0.8	SA				
30	331	36	5	3.5	2	A				

41-6a

Clast #	a trend	a plunge	A	B	C	roundness	plucked lee	bullet nose	Keel	striae
1	44	12								

2	148	16								
3	336	16								
4	194	4								
5	157	61								
6	212	2								T
7	271	3								B
8	182	8								
9	189	25								
10	206	6								T
11	326	16								B
12	3	13								
13	322	5								
14	352	19								TB
15	151	13						S128		S135
16	254	6								
17	154	3								
18	19	0								B
19	167	1					151			TB
20	220	8								
21	256	21								T
22	173	25								
23	186	8					347			B
24	196	13								
25	46	13								
26	68	1								
27	316	39								T
28	230	32								
29	111	19								
30	352	36								

41-6b

Clast #	**a trend**	**a plunge**	**A**	**B**	**C**	**roundness**	**plucked lee**	**bullet nose**	**Keel**	**striae**
1	129	12								B105
2	104	21								
3	136	22								
4	216	3								
5	149	35								

6	88	40								TB252
7	170	30								
8	166	27								T114
9	194	15								
10	131	7								
11	351	4								
12	149	7								
13	74	30								
14	188	1								
15	263	17								
16	41	19								T25
17	138	5								
18	7	7								T35B340
19	196	15								
20	186	18								
21	141	29								
22	19	5								
23	6	1					176			T140
24	157	22								
25	288	20								
26	20	8								
27	47	10								
28	160	9								
29	157	23								
30	144	14								S128

19-2

Clast #	a trend	a plunge	A	B	C	roundness	plucked lee	bullet nose	Keel	striae
1	257	70	3.5	2	1.8	SR				T241
2	146	5	7	5	2.9	SR	130			
3	171	24	4	2.4	1.2	SR				
4	31	85	4.1	3.6	1	SR	15			
5	21	3	3	2.1	0.8	SA				
6	316	35	3.5	1.8	1	SA				
7	181	34	2.2	1.8	1.5	SA				T110S137
8	171	38	5.1	3.1	0.9	SA				S160
9	45	45	4.2	2.6	2.5	SR				
10	79	15	4.5	3.5	2.5	SA				

11	344	9	1.9	1.5	0.7	SA				B69
12	124	7	3.7	2.1	1.3	SR				S116
13	338	15	12.5	11.3	5.5	SA				T149S159B162
14	332	17	6.8	4.2	2	SR				T146
15	164	13	3.6	2.9	1.5	A				
16	54	4	3.2	1.7	1	A				
17	371	1	2.9	1.7	0.7	R				B108T74
18	176	3	6.8	3.4	2.7	SA				B199
19	46	13	2.8	2	1.6	SA				B30
20	340	17	3.4	2.4	2.4	SR				
21	266	24	5	4	2.1	A	59			T125
22	185	4	13	9.2	5	SA				
23	354	12	2.4	1.3	0.8	R	161			T340
24	31	20	5	2.5	1.6	A	195			T30
25	222	13	3.7	3	1.6	WR				
26	47	30	3.3	1.5	1	SA				
27	153	11	3	2.1	0.8	R				
28	349	2	3	2.5	1.1	R				
29	326	8	3	2.6	1.1	SR				T132
30	245	18	3	1.8	0.8	SA				T46

53-1

Clast #	**a trend**	**a plunge**	**A**	**B**	**C**	**roundness**	**plucked lee**	**bullet nose**	**Keel**	**striae**
1	7	6	2.6	2.2	1.2	A				
2	341	24	6	4.2	2.9	R				
3	54	9	3.2	2	1.5	SA				
4	340	27	3.4	2.4	1	SA				
5	246	33	5.4	3.5	1.8	SA				T226
6	16	20	10.1	5	3.3	A				
7	31	6	4	2.9	1.4	SR				T333B15
8	10	18	4.3	2.7	0.9	SA				T350
9	50	14	4	2.9	1.1	SR				T346B346
10	23	4	2	1.5	0.7	SR				
11	261	2	2.5	2	1	A				
12	235	7	5.2	3	2.5	A				T6
13	196	3	2.9	2	0.7	R				T346
14	15	16	3.4	2	1.3	SA				

15	57	29	3.1	2.4	1.3	SA				
16	344	34	2.7	1.9	1.2	A				
17	85	59	2.6	2	1.4	SR				
18	44	4	3	1.5	1.3	SA				
19	18	23	2.7	1.7	1.1	A				
20	371	14	6	3.4	2	SA	172			
21	271	14	3.5	2.5	1.6	A				
22	8	11	3.2	2.4	1.2	SR	352	154		
23	215	27	2.4	1.7	0.9	SA				
24	11	18	2.5	1	0.8	SR	175	355		T7
25	36	30	3.8	2	0.8	A				
26	351	31	2.6	2	0.9	SR	170			
27	257	21	2.2	1.8	0.3	SA				
28	44	44	4.8	2.1	2	SA				
29	20	9	5.6	2.3	1.7	A				
30	29	21	3.2	1.3	0.5	SA	192			T30

1-3

Clast #	**a trend**	**a plunge**	**A**	**B**	**C**	**roundness**	**plucked lee**	**bullet nose**	**Keel**	**striae**
1	84	7	4.9	3.9	1.7	R				
2	71	42	3.6	2.5	2	WR				
3	124	36	3.7	2.9	2.6	WR				
4	33	15	4	2	1.8	WR				
5	348	12	7	5.7	2.7	WR				
6	71	11	3.6	1.9	1.8	R				
7	121	62	2.7	1.9	1.2	SR				
8	81	25	4	2.8	2	WR				
9	146	15	3.2	2	1.9	R				
10	56	30	2.8	1.8	0.8	SA				
11	334	14	3.9	1.5	1	WR				
12	113	59	3.5	3	2.5	R				
13	132	21	6.7	5.8	3.6	WR				
14	111	26	8.8	8.1	4.6	R				
15	16	23	3.9	2.5	1.5	A				
16	140	44	3	2.5	2	WR				
17	114	6	3.7	2.4	1.6	SR				
18	47	13	4.3	2.4	1.5	SR				
19	226	32	2.5	1.3	1.1	SR				

20	97	19	5.2	4.5	2.8	R				
21	99	32	4.5	3.1	2.2	SA				
22	101	45	6.7	3.8	3	SA	85			T88
23	201	23	3.5	2.7	1.2	A				T41
24	46	15	5.2	3.9	2.8	SR				
25	359	1	3.8	2.4	1.2	SA				
26	89	60	6.3	5.8	4.5	VWR				
27	21	2	4.1	3	1.9	WR				
28	333	26	2.7	1.8	1.3	SA				
29	342	49	3.8	3.1	2.8	WR				
30	341	14	2.6	1.5	1.3	SA				
31	111	15	2.5	1.9	1.2	R				
32	206	26	2.7	1.9	1.2	SA				
33	185	24	6.2	4.5	2.6	SA				
34	113	15	4.5	3	3	WR				
35	36	5	3	2.2	1.9	WR				
36	122	12	3	1	0.8	SA				
37	201	9	2.5	1.7	1.1	R				
38	341	12	2.1	1.5	1	SR				
39	144	2	3.7	2.5	1.8	WR				
40	26	9	3.2	1.6	1.5	SA				

39-2

Clast #	a trend	a plunge	A	B	C	roundness	plucked lee	bullet nose	Keel	striae
1	312	50	10.5	5.4	4	A				
2	336	29	5.6	3.7	3	A				
3	278	16	6	5.2	2.9	SA				
4	76	33	4.6	2.5	2.4	A				
5	342	9	3.3	2.5	1.8	SA				
6	162	23	3.5	2.6	1.3	A				
7	337	55	3	2.2	1.5	A				
8	338	20	4	2	1.6	A				
9	288	26	4	2.7	1.2	SR				
10	206	38	3.3	2.5	2	SA				
11	343	20	2.5	2.2	1.7	SR				
12	176	14	3.5	2.2	1.6	A				
13	321	19	3.5	2.6	1.7	A				
14	121	14	6.4	4.4	2.5	A				

15	306	7	3.1	2.3	1.5	A				
16	144	20	7.5	5.5	3.2	SR				T128
17	126	1	7	5.2	4.3	A				
18	314	24	10	8.8	4.5	A				
19	270	20	3.4	2.1	1.1	A				
20	351	10	9.5	5.3	3	A				
21	122	19	4	3	2.2	A				
22	221	4	4.1	3	2.5	A				
23	331	10	3.3	3.1	1.6	VA				
24	177	6	3.3	2	1.7	A				
25	318	11	6.3	3.5	3.4	A				
26	254	15	4	2.8	1.4	SR				T66 B64
27	331	0	3	2	0.9	A				
28	116	29	4.5	3.5	2.3	VA				
29	137	5	2.6	1.5	0.8	SA				
30	82	46	5.5	5	3.2	SA				

40-2

Clast #	a trend	a plunge	A	B	C	roundness	plucked lee	bullet nose	Keel	striae
1	351	15	7.7	5	2.7	5.9	A			
2	314	0	4.6	3.1	1.8	4.2	SA			
3	366	24	4.7	2.2	2.2	4.4	SA			
4	204	10	5.5	3.1	2.9	5.4	SA			
5	195	5	6.8	5.1	3.4	6.2	SR			
6	256	13	5.1	3.2	1.8	4.9	SR			
7	276	49	6.7	5.2	2.5	5.5	SR			
8	196	89	6.2	3.6	3.1	5.2	SR			
9	304	19	3.6	1.7	1.2	2.5	SR			
10	276	38	4.4	2.6	2.6	4.1	A			
11	18	9	6	3.9	2	5.9	SR			
12	332	28	4.5	2.9	1.5	4.4	SR			
13	366	15	3.8	2.5	1.6	35	SA			
14	191	9	7.5	5.5	3.7	7	RF			
15	359	14	4	2.9	2	3.4	SR			
1	208	10	8.7	6.3	4	8.4	R			
17	300	3	6.1	3	2.6	6.1	R			
18	316	14	5.4	3	2.6	4.6	SA			
19	333	10	6.6	3.3	2.1	6.6	R			

20	231	7	5.5	3.9	2.4	4.5	SR	
21	66	23	4.4	3	1.8	4.1	SR	
22	149	22	4.9	4	1.6	4.9	R	
23	346	25	9.4	6	4	7.3	SA	
24	152	4	5.1	2.7	2.2	4.5	R	
25	321	5	5	3.5	1.7	4.5	SR	
26	81	3	6.3	3.6	1.8	5.5	SA	
27	274	43	5	2	1.4	4.4	A	
28	111	19	4	1.9	0.9	3	A	
29	329	27	7.4	4.5	3.6	7	SR	
30	188	2	6.2	5	2.5	5.3	SR	

49-2

Clast #	a trend	a plunge	A	B	C	roundness	plucked lee	bullet nose	Keel	striae
1	316	20	6	3.8	3.8	R				
2	321	43	3.5	2.3	2	WR				
3	322	2	8.5	3.9	2.6	R				
4	36	8	5	3.9	2.9	SR				
5	225	19	4	3	1.7	SA				
6	51	15	7.5	5.3	5	SR				
7	191	28	6.5	3.6	3	R				
8	186	10	5.5	3.7	1.7	SA				
9	354	35	8	5.5	5	SR				
10	302	15	7.7	5	3.6	SA				
11	313	15	6.6	5	3.5	SR				
12	346	37	5.7	4.8	3.4	R				
13	340	0	8.6	4.7	3	A				
14	316	6	4.6	2.7	2.7	SR				
15	46	16	4.6	3.8	2.7	SA				
16	328	32	2.9	2	1.7	SR(fr)				
17	276	15	8.6	6	4.3	SA				
18	310	38	4.6	3.3	2.6	WR				
19	190	10	14	10	6.5	SR				
20	161	5	5.5	4.4	3	SR				
21	188	28	3.5	2.5	2	SA				
22	350	50	4.6	3	1.9	SA				
23	121	13	5.6	2.9	2.4	SA				
24	269	13	5	4.1	3.4	SR				

25	20	40	4.6	3.2	2.3	WR
26	128	20	5.2	4	3	WR
27	164	29	5.6	4.5	2.8	WR
28	210	37	4	3.3	2.3	SA
29	336	44	3.6	2.4	2.2	WR
30	365	31	4.7	3.6	3	SA

C.3 Ripple drift data

In the data tables below: 1) “azimuth” is paleoflow direction inferred from ripple cross-laminae; and 2) “angle of climb” is the angle of climb of the ripple set in which the azimuth was measured.

47-1a
TYPE B

Azimuth	Angle of climb
34	36
35	37
30	15
28	25
35	31
41	46
59	38
71	33
31	
46	
68	
85	
59	
40	
35	

47-1e
TYPE A

Azimuth	Angle of climb
65	32
80	54
94	25
53	15
70	
86	
79	
89	
78	
88	
55	
100	

92

85

60

46-1
TYPE A

Azimuth	Angle of climb
90	15
98	17
105	21
114	19
101	
115	
110	
108	
94	
121	
126	
125	
115	
97	
80	

21-1b
TYPE A

Azimuth	Angle of climb
288	28
289	30
290	27
314	
294	
288	
224	
214	
208	

213

210

202

230

221

207

208

220

238

222

218

205

200

41-1
TYPE A

Azimuth	Angle of climb
160	7
246	15
224	8
205	11

204

225

150

186

181

164

160

140

169

172

221

41-6i

TYPE A

Azimuth	Angle of climb
162	2
192	15
170	6
210	6
162	7
189	8
178	
178	
185	
182	
184	
178	
190	
180	
182	

Appendix D: Clast sphericity

Clast sphericity charts were constructed for one sample used for gravel fabric measurements and one sample used for diamicton fabric measurements. These samples were taken from deposits with anomalously high numbers of spherical clasts. The charts in this appendix display the sphericity of the sampled clasts, which typically represent the least equant clasts in the deposit (because spherical clasts cannot be used for gravel or diamicton fabric analysis).

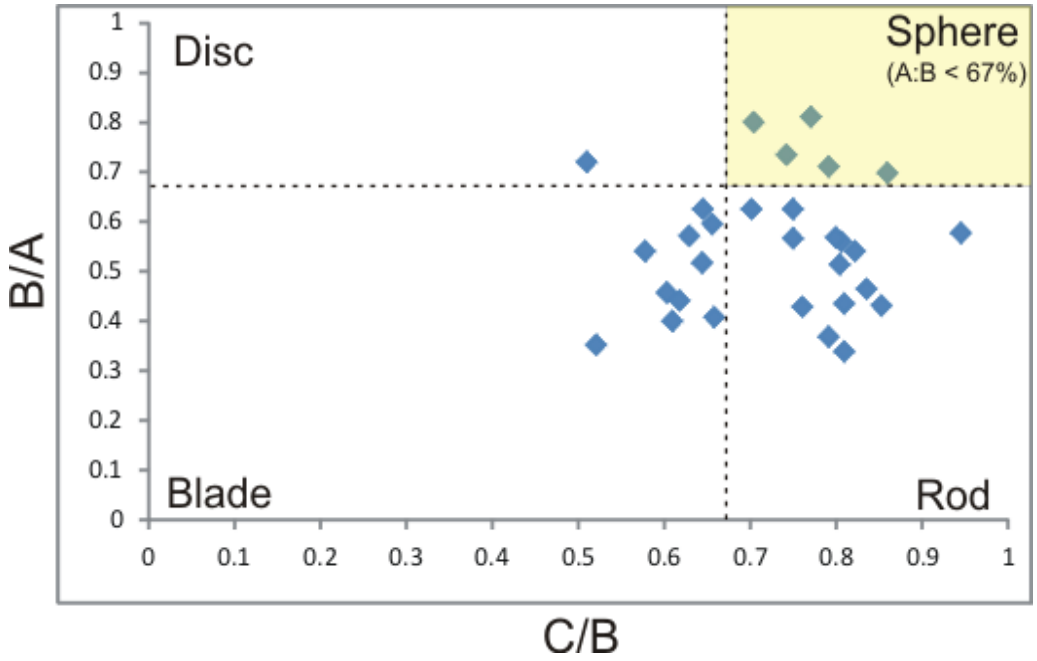

Figure D-1: Sphericity of clasts measured for the 19-1c (Table 5-1) gravel fabric.

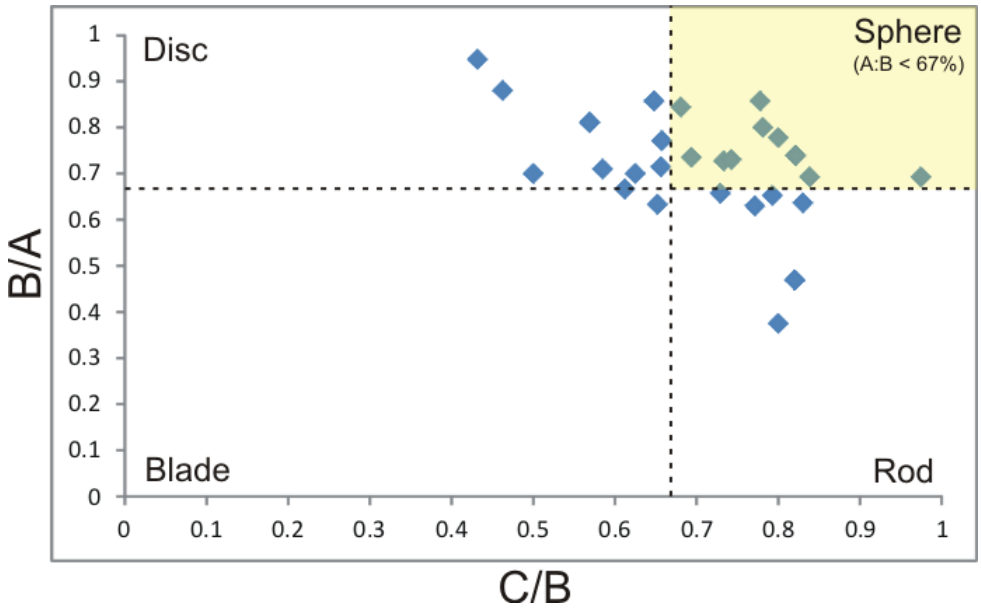

Figure D-2: Sphericity of clasts measured for the 40-2 (Table 5-2) diamicton fabric.

Appendix E: Uninterpreted GPR lines

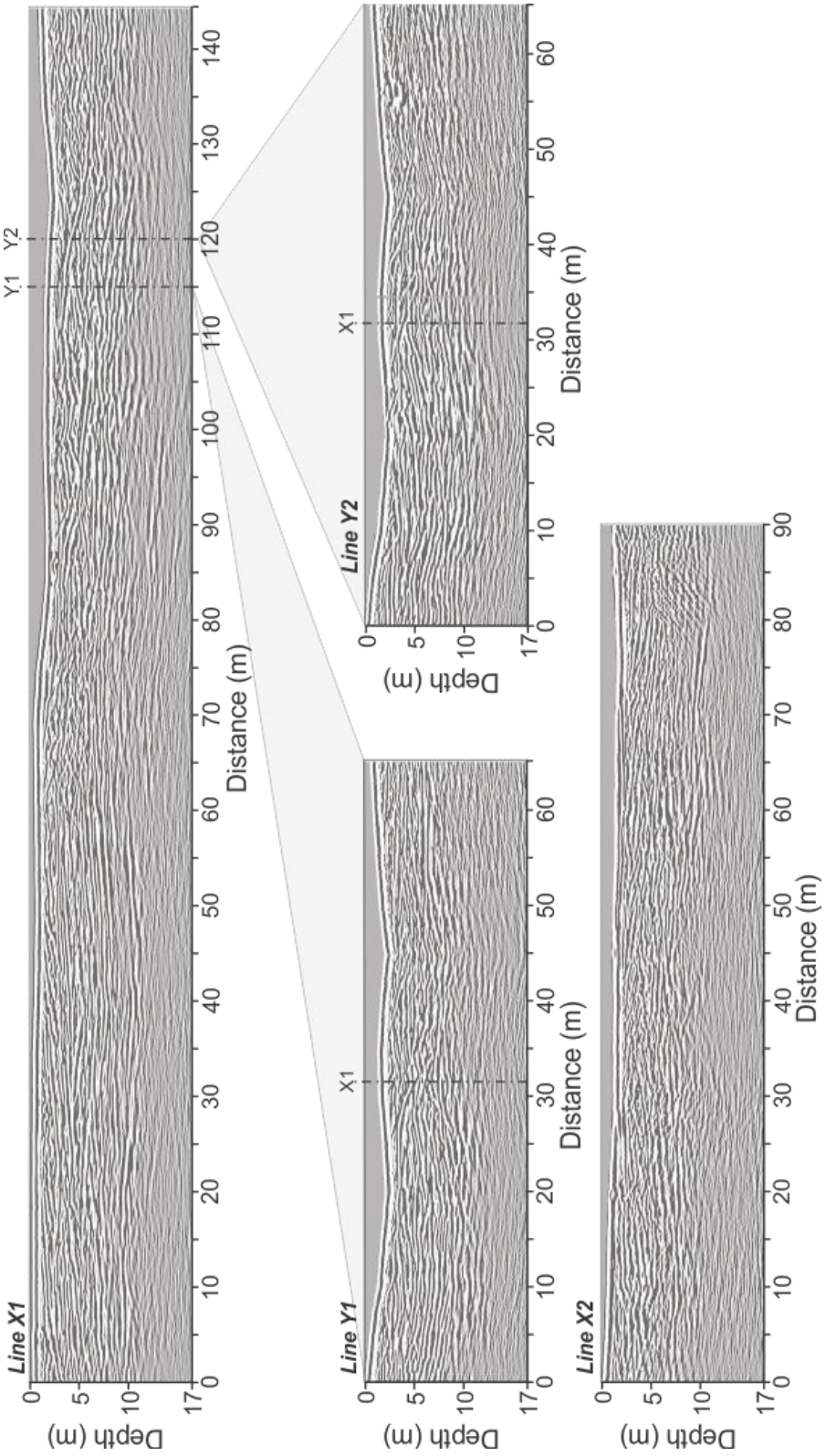

Figure E-1: Uninterpreted GPR lines from site 48B (Figure 5-39).

Appendix F: Well log data

Table F-1: Well log data used in the construction of the Columbia River-Kootenay River cross-sectional profiles (lines X-X' and Y-Y', Figure 5-38, Figure 5-39c, d). Tag numbers are from the British Columbia Groundwater Association (Ministry of Environment).

Well	Tag number	Depth (m)	Geographic coordinates
A	16556	35	49°18'58"N 117°39'49"W
B	31358	52	49°18'40"N 117°38'59"W
C	36328	49	49°18'39"N 117°38'57"W
D	19471	43	49°19'15"N 117°38'31"W
E	99659	68	49°19'15"N 117°38'15"W
F	89102	21	49°19'03"W 117°38'07"W
G	88525	146	49°17'34"W 117°39'58"W
H	74637	59	49°17'35"W 117°39'14"W
I	18377	119	49°17'24"W 117°38'57"W
J	18372	106	49°17'16"W 117°38'56"W
K	57096	43	49°17'22"W 117°38'23"W
L	40991	73	49°17'18"W 117°38'07"W
M	42102	18	49°17'20"W 117°37'37"W
N	5074	95	49°17'29"W 117°37'21"W
O	98788	134	49°17'42"W 117°37'32"W
P	81562	50	49°17'57"W 117°36'55"W
Q	20571	52	49°18'30"W 117°36'54"W
R	21002	50	49°18'40"W 117°36'49"W

Appendix G: CD-ROM Data

The CD-ROM, attached, forms a part of this work.

The GIS data file can be opened with ESRI ArcGIS® 10.3 or later.

The stereogram data can be viewed as text in Microsoft Notepad®, or opened with Stereo32 software (Roeller 2008).

Fabric and paleoflow spreadsheets can be opened with Microsoft Excel® 2010 or later.

Data Files:

- GIS data
- Stereogram data
- Fabric and paleoflow spreadsheets

REFERENCE LIST

Aitken, J. F. (1995). Lithofacies and depositional history of a late Devensian ice-contact deltaic complex, northeast Scotland. *Sedimentary Geology, 99*(2), 111-129.

Alden, W. C. (1953). Physiography and glacial geology of western Montana and adjacent areas: U.S. Geological Survey Professional Paper 231.

Alexander, H. S. (1932). Pothole erosion. *The Journal of Geology, 40*(4), 305-337.

Alho, P., Roberts, M. J., & Käyhkö, J. (2007). Estimating the inundation area of a massive, hypothetical jökulhlaup from northwest Vatnajökull, Iceland. *Natural Hazards, 41*(1), 21-42.

Alho, P., Russell, A. J., Carrivick, J. L., & Käyhkö, J. (2005). Reconstruction of the largest Holocene jökulhlaup within Jökulsá á Fjöllum, NE Iceland. *Quaternary Science Reviews, 24*(22), 2319-2334.

Alho, P., Baker, V. R., & Smith, L. N. (2010). Paleohydraulic reconstruction of the largest glacial Lake Missoula draining(s). Quaternary Science Reviews, 29(23–24), 3067-3078.

Allen, J. R. L. (1983). Studies in fluviatile sedimentation; bars, bar-complexes and sandstone sheets (low-sinuosity braided streams) in the brownstones (L. Devonian), welsh borders. *Sedimentary Geology, 33*(4), 237-293.

Allen, J. R. L. (1982). *Sedimentary Structures, their Character and Physical Basis; Volume II,* Elsevier Science Publishers, the Netherlands, 679.

Anderson, S. P., Walder, J. S., Anderson, R. S., Kraal, E. R., Cunico, M., Fountain, A. G., & Trabant, D. (2003). Integrated hydrologic and hydrochemical observations of hidden creek lake jökulhlaups, Kennicott Glacier, Alaska. *Journal of Geophysical Research, 108*(F1), 6003-6022.

Ashley, G. M. (1990). Classification of large-scale subaqueous bedforms; a new look at an old problem. *Journal of Sedimentary Research, 60*(1), 160-172.

Ashley, G. M., Southard, J. B., & Boothroyd, J. C. (1982). Deposition of climbing-ripple beds: A flume simulation. *Sedimentology, 29*(1), 67-79.

Atkins, C. B. (2003). *Characteristics of striae and clasts in glacial and non-glacial environments.* Unpublished PhD thesis. Victoria University of Wellington, Wellington, New Zealand.

Atwater, B. F. (1987). Status of glacial Lake Columbia during the last floods from glacial Lake Missoula. *Quaternary Research, 27*(2), 182-201

Baker, V. R., & Bunker, R. C. (1985). Cataclysmic late Pleistocene flooding from glacial Lake Missoula: A review. *Quaternary Science Reviews, 4*(1), 1-41.

Baker, V. R., Pickup, G., & Polach, H. A. (1985). Radiocarbon dating of flood events, Katherine gorge, northern territory, Australia. *Geology, 13*(5), 344-347.

Baker, V. R. (1978a). Large-scale erosional and depositional features of the Channeled Scabland. In V. R. Baker, & D. Nummedal (Eds), *The Channeled Scabland*. Washington D.C.: The National Aeronautics and Space Administration, pp. 81-116.

Baker, V. R. (1978b). Paleohydraulics and hydrodynamics of Scabland floods. In V. R. Baker, & D. Nummedal (Eds), *The Channeled Scabland*. Washington D.C.: The National Aeronautics and Space Administration, pp. 59-80.

Baker, V. R. (1978c). Quaternary geology of the Channeled Scablands and adjacent areas. In V. R. Baker, & D. Nummedal (Eds), *The Channeled Scabland*. Washington D.C.: The National Aeronautics and Space Administration, pp. 17-36.

Baker, V. R. (1978d). The Spokane flood controversy. In V. R. Baker, & D. Nummedal (Eds), *The Channeled Scabland*. Washington D.C.: The National Aeronautics and Space Administration, pp. 3-16.

Baker, V. R. (1984). Flood sedimentation in bedrock fluvial systems. *Memoir, Canadian Society of Petroleum Geologists, 10*, 87-97.

Baker, V. R. (2002). High-energy megafloods; planetary settings and sedimentary dynamics. *International Association of Sedimentologists, Special Publication, 32*, 3-15.

Baker, V. R. (2008a). Paleoflood hydrology: Origin, progress, prospects. *Geomorphology, 101*(1-2), 1-13.

Baker, V. R. (2008b). The Channeled Scabland: A retrospective. *The Annual Review of Earth and Planetary Sciences, 37*, 393-411.

Baker, V. R. (2009a). Overview of megaflooding: Earth and mars. In D. M. Burr, P. A. Carling & V. R. Baker (Eds.), *Megaflooding on Earth and Mars*. New York: Cambridge University Press, pp. 1-12.

Baker, V. R. (2009b). Channeled Scabland morphology. In D. M. Burr, P. A. Carling & V. R. Baker (Eds.), *Megaflooding on Earth and Mars*. New York: Cambridge University Press, pp. 65-77.

Baker, V. R., Benito, G., & Rudoy, A. N. (1993). Paleohydrology of late Pleistocene superflooding, Altai Mountains, Siberia. *Science, 259*(5093), 348-350.

Baker, V. R., & Pickup, G. (June, 1987). Flood geomorphology of the Katherine Gorge, Northern Territory, Australia. *Geological Society of America Bulletin, 98*(6), 635-646.

Ballantyne, C. K. (2002). Paraglacial geomorphology. *Quaternary Science Reviews, 21*(18-19), 1935-2008.

Barrett, P. J. (1980). The shape of rock particles, a critical review. *Sedimentology, 27*(3), 291-303.

Baylor, J. W. (1935). Geography of the glaciated north Idaho panhandle. *Economic Geography, 11*(2), 191-205.

Beaulieu, A., Clavet, D. (2007) Accuracy assessment of Canadian Digital Elevation Data using ICESAT. Centre d'Information Topographique de Sherbrooke, Quebec, Canada.

Benito, G., & Thorndycraft, V. R. (2005). Palaeoflood hydrology and its role in applied hydrological sciences. *Journal of Hydrology, 313*(1-2), 3-15.

Benito, G., & O'Connor, J. E. (2003). Number and size of last-glacial Missoula floods in the Columbia River valley between the Pasco basin, Washington, and Portland, Oregon. *Bulletin of the Geological Society of America, 115*(5), 624-638.

Benn, D. I., & Evans, D. J. A. (1996). The interpretation and classification of subglacially-deformed materials. *Quaternary Science Reviews, 15*(1), 23-52.

Benn, D. I., & Evans, D. J. A. (2010). *Glaciers and glaciation* (Second Edition). London: Hodder.

Berthelsen, A. (1979). Recumbent folds and boudinage structures formed by subglacial shear: An example of gravity tectonics. *Geologie En Mijnbouw, 58*(2), 253-260.

Bjornsson, H. (1976). Marginal and supraglacial lakes in Iceland. *Jökull, 26*, 40-50.

Björnsson, H. (2009). Jökulhlaups in Iceland: Sources, release and drainage. In D. M. Burr, P. A. Carling & V. R. Baker (Eds.), *Megaflooding on Earth and Mars*. New York: Cambridge University Press, pp. 50-64.

Blachut, S. P., & Ballantyne, C. K. (1976). *Ice dammed lakes: A critical review of their nature and behaviour. Discussion Paper 6*. Hamilton, Ontario: Department of Geography, McMaster University, pp. 78-90.

Blair, T. C. (1987). Sedimentary processes, vertical stratification sequences, and geomorphology of the Roaring River alluvial fan, Rocky Mountain National Park, Colorado. *Journal of Sedimentary Research, 57*(1), 1-18.

Blair, T. C., & McPherson, J. G. (1994). Alluvial fans and their natural distinction from rivers based on morphology, hydraulic processes, sedimentary processes, and facies assemblages. *Journal of Sedimentary Research, 64*(3a), 450-489.

Boothroyd, J. C., & Ashley, G. M. (1975). Processes, bar morphology, and sedimentary structures on braided outwash fans, northeastern Gulf of Alaska. *Society of Economic Paleontologists and Mineralogists, Special Publication, 1*(23), 193-222.

Boulton, G. S. (1975). Till genesis and fabric in Svalbard, Spitsbergen. In Goldthwait, R. P. (Ed.) *Till, a symposium*. Pp. 41-72.

Breckenridge, R. M., Burmester, R. F., McFaddan, M. D., Lewis, R. S. (2009), Geologic map of the Bonners Ferry Quadrangle, Boundary County, Idaho. Idaho Geologic Survey. Moscow, Idaho.

Breckenridge, R. M., & Garwood, D. L. (2009). Ice age floods research and mapping in Idaho; results from STATEMAP. *Geological Society of America, Abstracts with Programs, 41*(7), 283.

Brennand, T. A., Shaw, J., & Sharpe, D. R. (1996). Regional-scale meltwater erosion and deposition patterns, northern Quebec, Canada. *Annals of Glaciology, 22*, 85-92.

Brennand, T. A., & Shaw, J. (1994). Tunnel channels and associated landforms, south-central Ontario; their implications for ice-sheet hydrology. *Canadian Journal of Earth Sciences, 31*(3), 505-520.

Bretz, J. H. (1923). The Channeled Scablands of the Columbia Plateau. *Journal of Geology, 31*(8), 617-649.

Bretz, J. H. (1925). The Spokane flood beyond the Channeled Scablands. *Journal of Geology, 33*(2), 97-115.

Bretz, J. H. (1928). The Channeled Scabland of eastern Washington. *Geographical Review, 18*(3), 446-477.

Bretz, J. H., Smith, H. T. U., & Neff, G. E. (1956). Channeled Scabland of Washington; new data and interpretations. *Geological Society of America Bulletin, 67*(8), 957-1049.

Bretz, J. H. (1969). The lake Missoula floods and the Channeled Scabland. *The Journal of Geology*, 77(5), pp. 505-543.

Bristow, C. S., & Jol, H. M. (2003). An introduction to ground penetrating radar (GPR) in sediments. *Geological Society, London, Special Publications, 211*(1), 1-7.

Burbidge, G. H., & Rust, B. R. (1988). A Champlain sea subwash fan at St. Lazare, Quebec. *Special Paper - Geological Association of Canada, 35*, 47-61.

Burke, M. J. (2008). *GPR investigations of the sedimentary architecture of jökulhlaup eskers; Skeidararjökull, Iceland and Bering glacier, Alaska.* Unpublished PhD thesis, University of Northumbria.

Burmester, R. F., Breckenridge, R. M., McFaddan, M. D., & Lewis, R. S. (2010). *Geologic map of the Meadow Creek quadrangle, boundary County, Idaho*. Moscow, Idaho: Idaho Geological Survey.

Carling, P. A., Burr, D. M., Johnsen, T. F., & Brennand, T. A. (2009a). A review of open-channel megaflood depositional landforms on earth and mars. In D. M. Burr, P. A. Carling & V. R. Baker (Eds.), *Megaflooding on Earth and Mars*. New York: Cambridge University Press, pp. 33-49.

Carling, P. A., Martini, I. P., Herget, J., Borodavko, P., & Parnachov, S. (2009b). Megaflood sedimentary valley fill: Altai Mountains, Siberia. In D. M. Burr, P. A. Carling & V. R. Baker (Eds.), *Megaflooding on Earth and Mars*. New York: Cambridge University Press, pp. 243-262.

Carling, P. A., Herget, J., Lanz, J. K., Richardson, K., & Pacifici, A. (2009c). Channel-scale erosional bedforms in bedrock and loose granular material: Character, processes and implications. In D. M. Burr, P. A. Carling & V. R. Baker (Eds.), *Megaflooding on Earth and Mars*. New York: Cambridge University Press, pp. 13-32.

Carling, P. A. (1996). Morphology, sedimentology and palaeohydraulic significance of large gravel dunes, Altai Mountains, Siberia. *Sedimentology, 43*(4), 647-664.

Carling, P. A., Goelz, E., Orr, H. G., & Radecki-Pawlik, A. (2000). The morphodynamics of fluvial sand dunes in the River Rhine near Mainz, Germany; I, sedimentology and morphology. *Sedimentology, 47*(1), 227-252.

Carling, P. A., Williams, J. J., Goelz, E., & Kelsey, A. D. (2000). The morphodynamics of fluvial sand dunes in the River Rhine, near Mainz, Germany; II, hydrodynamics and sediment transport. *Sedimentology, 47*(1), 253-278.

Carling, P. A., & Glaister, M. S. (1987). Rapid deposition of sand and gravel mixtures downstream of a negative step: The role of matrix-infilling and particle-overpassing in the process of bar-front accretion. *Journal of the Geological Society, 144*(4), 543-551.

Carling, P., Villanueva, I., Herget, J., Wright, N., Borodavko, P., & Morvan, H. (2010). Unsteady 1D and 2D hydraulic models with ice dam break for Quaternary megaflood, Altai Mountains, southern Siberia. *Global and Planetary Change, 70*(1-4), 24-34.

Carrara, P. E., Kiver, P. E., & Stradling, D. F. (1996). The southern limit of cordilleran ice in the Colville and Pend Oreille valleys of northeastern Washington during the late Wisconsin glaciation. *Canadian Journal of Earth Sciences*, 33(5), 769-777.

Carrivick, J. L. (2006). Application of 2D hydrodynamic modelling to high-magnitude outburst floods: An example from Kverkfjöll, Iceland. *Journal of Hydrology, 321*(1-4), 187-199.

Carrivick, J. L. (2007). Hydrodynamics and geomorphic work of jökulhlaups (glacial outburst floods) from Kverkfjöll Volcano, Iceland. *Hydrological Processes, 21*(6), 725-740.

Carrivick, J. L. (2009). Jökulhlaups from Kverkfjöll Volcano, Iceland: Modeling transient hydraulic phenomina. In D. M. Burr, P. A. Carling & V. R. Baker (Eds.), *Megaflooding on Earth and Mars*. New York: Cambridge University Press, pp. 273-289.

Carrivick, J. L., Russell, A. J., & Tweed, F. S. (2004). Geomorphological evidence for jökulhlaups from Kverkfjöll Volcano, Iceland. *Geomorphology, 63*(1), 81-102.

Carrivick, J. L., Russell, A. J., Tweed, F. S., & Twigg, D. (2004). Palaeohydrology and sedimentary impacts of jökulhlaups from Kverkfjöll, Iceland. *Sedimentary Geology, 172*(1), 19-40.

Cary, A. S. (1950). Origin and significance of openwork gravel. *Proceedings of the American Society of Civil Engineers, 76*(17), 1-13.

Cassidy, N. J., Russell, A. J., Marren, P. M., Fay, H., Knudsen, Ó., Rushmer, E. L., & Van Dijk, T. A. G. P. (2003). GPR derived architecture of November 1996 jökulhlaup deposits, Skeiðarársandur, Iceland. *Geological Society, London, Special Publication, 211*(1), 153-166.

Cheel, R. J. (1990). Horizontal lamination and the sequence of bed phases and stratification under upper-flow-regime conditions. *Sedimentology, 37*(3), 517-529.

Church, M., & Gilbert, R. (1975). Proglacial fluvial and lacustrine environments. In A. V. Jopling, & B. C. McDonald (Eds.), *Glaciofluvial and glaciolacustrine sedimentation*. Tulsa, Oklahoma: Society of Economic Paleontologists and Mineralogists, pp. 22-100.

Church, M., & Ryder, J. M. (1972). Paraglacial sedimentation. *Geological Society of America Bulletin, 83*(10), 3059-3072.

Church, M. (2006). Bed material transport and the morphology of alluvial river channels. *Annual Review of Earth and Planetary Sciences, 34*, 325-349.

Church, M., & Ryder, J. M. (1989). Sedimentology and clast fabric of subaerial debris flow facies in a glacially-influenced alluvial fan; a discussion. *Sedimentary Geology, 65*(1-2), 195-196.

Clague, J. J., Barendregt, R., Enkin, R. J., & Foit, F. F. (2003). Paleomagnetic and tephra evidence for tens of Missoula floods in southern Washington. *Geology, 31*(3), 247-250.

Clague, J. J., & James, T. S. (2002). History and isostatic effects of the last ice sheet in southern British Columbia. *Quaternary Science Reviews, 21*(1), 71-87.

Clarke, G. K. C., Mathews, W. H., & Pack, R. T. (1984). Outburst floods from glacial Lake Missoula. *Quaternary Research, 22*(3), 289-299.

Clarke, G. K. C. (1982). Glacier outburst flood from 'Hazard Lake', Yukon Territory, and the problem of flood magnitude precision. *Journal of Glaciology, 28*, 3-21.

Clarke, G. K. C., & Waldron, D. A. (1984). Simulation of the August 1979 sudden discharge of glacier-dammed Flood Lake, British Columbia. *Canadian Journal of Earth Sciences, 21*, 502-504.

Colpron, M., & Price, R. A. (1995). Tectonic significance of the Kootenay terrane, southeastern Canadian Cordillera: An alternative model. *Geology, 23*(1), 25-28.

Costa, J. E. (1983). Paleohydraulic reconstruction of flash-flood peaks from boulder deposits in the Colorado Front Range. *Geological Society of America Bulletin, 94*(8), 986-1004.

Costa, J. E., & Schuster, R. L. (1988). The formation and failure of natural dams. *Geological Society of America Bulletin, 100*(7), 1054-1068.

Crosby, P. (1968). Tectonic, plutonic, and metamorphic history of the central Kootenay Arc, British Columbia, Canada. *Geological Society of America, Special Paper, 1*, 81-86.

Davies, T. R. H., Smart, C. C., & Turnbull, J. M. (2003). Water and sediment outbursts from advanced Franz Josef Glacier, New Zealand. *Earth Surface Processes and Landforms, 28*(10), 1081-1096.

Davis, W. M. (1920). Features of glacial origin in Montana and Idaho: A Shaler memorial study. *Annals of the Association of American Geographers, 10*(1), 75-147.

Delaney, P. T., Pollard, D. D., Ziony, J. I., & McKee, E. H. (1986). Field relations between dikes and joints; emplacement processes and paleostress analysis. *Journal of Geophysical Research, 91*(B5), 4920-4920-4938.

Doughty, P. T., & Price, R. A. (2000). Geology of the Purcell Trench rift valley and Sandpoint conglomerate; Eocene en echelon normal faulting and synrift sedimentation along the eastern flank of the Priest River metamorphic complex, northern Idaho. *Geological Society of America Bulletin, 112*(9), 1356-1374.

Dyke, A. S., Moore, A., & Robertson, L. (2003). Deglaciation of North America. *Geological Survey of Canada. Open File 1574.*

Easterbrook, D. J. (1992). Advance and retreat of Cordilleran Ice Sheets in Washington, U.S.A. *Geographie Physique et Quaternaire, 46*(1), 51-68.

Ehlers, J., & Gibbard, P. L. (Eds.). (2004). *Quaternary glaciations - extent and chronology. part II: North America* (First ed.). Netherlands: Elsevier.

Embleton, C., & King, C. A. M. (1975). *Glacial geomorphology* (Second ed.). London: Edward Arnold Ltd, pp. 489-491.

Evans, D. J. A. (2000). A gravel outwash/deformation till continuum, Skalafellsjokull, Iceland. *Geografiska Annaler.Series A: Physical Geography, 82*(4), 499-512.

Evans, D. J. A., Owen, L. A., & Roberts, D. (1995). Stratigraphy and sedimentology of Devensian (Dimlington Stadial) glacial deposits, east Yorkshire, England. *Journal of Quaternary Science, 10*(3), 241-265.

Eyles, C. H., & Eyles, N. (1984). Glaciomarine sediments of the Isle of Man as a key to late Pleistocene stratigraphic investigations in the Irish Sea basin. *Geology, 12*(6), 359-364.

Eyles, N., & Clague, J. J. (1987). Landsliding caused by Pleistocene glacial lake ponding; an example from central British Columbia. *Canadian Geotechnical Journal, 24*(4), 656-663.

Eyles, N., & Miall, A. D. (1984). Glacial facies. In R. G. Walker (Ed.), *Facies models*. Geoscience Canada Reprint Series, pp. 15-38.

Eyles, N., Clark, B. M., & Clague, J. J. (1987). Coarse-grained sediment gravity flow facies in a large supraglacial lake. *Sedimentology, 34*(2), 193-216.

Eynon, G., & Walker, R. G. (1974). Facies relationships in Pleistocene outwash gravels, southern Ontario; a model for bar growth in braided rivers. *Sedimentology, 21*(1), 43-70.

Finnegan, N. J., Roe, G., Montgomery, D. R., & Hallet, B. (2005). Controls on the channel width of rivers; implications for modeling fluvial incision of bedrock. *Geology, 33*(3), 229-232.

Fisheries and Oceans Canada. (2011). *Lakes and rivers of British Columbia* (Canadian Hydrographic Service Digital Charts ed.) Fisheries and Oceans Canada.

Foit, Franklin F.,Jr, Mehringer, Peter J.,Jr, & Sheppard, J. C. (1993). Age, distribution, and stratigraphy of Glacier Peak tephra in eastern Washington and western Montana, United States. *Canadian Journal of Earth Sciences, 30*(3), 535-552.

Fowler, A. C. (1999). Breaking the seal at Grimsvötn, Iceland. *Journal of Glaciology, 45*(151), 506-515.

Fulton, R. J. (1965). Silt deposition in late-glacial lakes of southern British Columbia. *American Journal of Science, 263*(7), 553-570.

Fulton, R. J. (1967). Deglaciation studies in Kamloops region, an area of moderate relief, British Columbia. *Geological Survey of Canada Bulletin, 154*, 1-36.

Fulton, R. J. (1968). Olympia interglaciation, Purcell Trench, British Columbia. *Geological Society of America Bulletin, 79*(8), 1075-1080.

Fulton, R. J., Achard, R. A., & Smith, G. W. (1970). Two surficial geology maps of southern British Columbia; twenty-four less detailed surficial geology maps of the valley bottom parts of Arrow and Duncan Lake reservoir areas, British Columbia. *Geological Survey of Canada, Open-File* 25*.*

Fulton, R. J., & Pullen, M. J. L. T. (1969). Sedimentation in Upper Arrow Lake, British Columbia. *Canadian Journal of Earth Sciences, 6*(4), 785-791.

Fulton, R. J., Shetsen, I., & Rutter, N. W. (1984). Surficial geology, Kootenay Lake, British Columbia, Alberta. *Geological Survey of Canada. Open-File Report 1084.*

Fulton, R. J., & Walcott R. I. (1975). Lithospheric flexure as shown by deformation of glacial lake shorelines in southern British Columbia. In E. H. T. Whitten (Ed.), *Quantitative studies in the geological sciences*. Boulder, CO: Geological Society of America, pp. 163-173.

Fulton, R. J. (1969). Glacial lake history, southern Interior Plateau, British Columbia. *Geological Survey of Canada. Paper 69-37, 1-14.*

Fulton, R. J. (1991). A conceptual model for growth and decay of the Cordilleran Ice Sheet. *Géographie physique et Quaternaire, 45*(3), 281-286.

Fulton, R. J., & Smith, G. W. (1978). Late Pleistocene stratigraphy of south-central British Columbia. *Canadian Journal of Earth Sciences, 15*, 971-980.

Fyles, J. T. (1964). Geology of the Duncan Lake area, British Columbia; *British Columbia Department of Mines and Petroleum Resources, 49*, 1-87.

Gasparini, N. M., & Brandon, M. T. (2011). A generalized power law approximation for fluvial incision of bedrock channels. *Journal of Geophysical Research. 116*, 1-16.

Geertsema, M., & Clague, J. J. (2005). Jökulhlaups at Tulsequah Glacier, northwestern British Columbia, Canada. *The Holocene, 15*(2), 310-316.

Ghienne, J., Girard, F., Moreau, J., & Rubino, J. (2010). Late Ordovician climbing-dune cross-stratification; a signature of outburst floods in proglacial outwash environments? *Sedimentology, 57*(5), 1175-1198.

Gilbert, R., & Desloges, J. R. (2005). The record of glacial Lake Champagne in Kusawa Lake, southwestern Yukon Territory. *Canadian Journal of Earth Sciences, 42*(12), 2127-2140.

Gilbert, R., & Shaw, J. (1981). Sedimentation in proglacial Sunwapta Lake, Alberta. *Canadian Journal of Earth Sciences, 18*(1), 81-93.

Glen, J. W. (1954). The stability of ice-dammed lakes and other water-filled holes in glaciers. *Journal of Glaciology, 2*, 316-318.

Glen, J. W. (1955). The creep of polycrystalline ice. *Proceedings of the Royal Society of London Series A Mathematical and Physical Sciences, 228*(1175), 519-538.

Goedhart, M. L., & Smith, N. D. (1998). Braided stream aggradation on an alluvial fan margin; Emerald Lake fan, British Columbia. *Canadian Journal of Earth Sciences, 35*(5), 534-545.

Gregory, J. W. (1912). The relations of kames and eskers. *The Geographical Journal, 40*(2), 169-175.

Gunn, J. P. (1930). The Shyok flood, 1929. *The Himalayan Journal, 2*, 35-47.

Gustavson, T. C., Ashley, G. M., & Boothroyd, J. C. (1975). Depositional sequences in glaciolacustrine deltas. *Society of Economic Paleontologists and Mineralogists, Special Publication* 23, 264-280.

Hakon Wadell. (1933). Sphericity and roundness of rock particles. *The Journal of Geology, 41*(3), 310-331.

Hanson, M. A., Lian, O. B., & Clague, J. J. (2012). The sequence and timing of large late Pleistocene floods from glacial Lake Missoula. *Quaternary Science Reviews, 31*, 67-81.

Harms, J. C., & Fahnestock, R. K. (1965). Stratification, bed forms, and flow phenomena (with an example from the Rio Grande) *Society of Economic Paleontologists and Minerologists, 12*(84), 84-115.

Hart, J. K., Hindmarsh, R. C. A., & Boulton, G. S. (1990). Styles of subglacial glaciotectonic deformation within the context of the Anglian Ice-Sheet. *Earth Surface Processes and Landforms, 15*(3), 227-241.

Hart, J. K., & Roberts, D. H. (1994). Criteria to distinguish between subglacial glaciotectonic and glaciomarine sedimentation, I. deformation styles and sedimentology. *Sedimentary Geology, 91*(1-4), 191-213.

Havholm, K. G., Bergstrom, N. D., Jol, H. M., & Running, G. L. (2003). GPR survey of a Holocene aeolian/fluvial/lacustrine succession, Lauder Sandhills, Manitoba, Canada. *Geological Society, London, Special Publication, 211*(1), 47-54.

Hein, A. S., Dunai, T. J., Hulton, N. R. J., & Xu, S. (2011). Exposure dating outwash gravels to determine the age of the greatest Patagonian glaciations. *Geology, 39*(2), 103-106.

Hein, F., & Walker, R. (1977). Bar evolution and development of stratification in the gravelly, braided, Kicking Horse River, British Columbia. *Canadian Journal of Earth Sciences, 14*(4), 562-570.

Hein, F. J. (1982). Depositional mechanisms of deep-sea coarse clastic sediments, Cap Enrage formation, Quebec. *Canadian Journal of Earth, 19*(2), 267-287.

Heinz, J., & Aigner, T. (2003). Three-dimensional GPR analysis of various Quaternary gravel-bed braided river deposits (southwestern Germany). *Geological Society, London, Special Publication, 211*(1), 99-110.

Helgi, B. (2003). Subglacial lakes and jökulhlaups in Iceland. *Global and Planetary Change, 35*(3–4), 255-271.

Hesse, R., Rashid, H., & Khodabakhsh, S. (2004). Fine-grained sediment lofting from meltwater-generated turbidity currents during Heinrich events. *Geology, 32*(5), 449-452.

Hicock, S. R. (1996). On the interpretation of subglacial till fabric. *Journal of Sedimentary Research A: Sedimentary Petrology and Processes, 66*(5), 928-934.

Holmes, C. D. (1947). Kames. American Journal of Science, 245(4), 240-249.

Hooke, R. L. (1967). Processes on arid-region alluvial fans. *The Journal of Geology, 75*(4), 438-460.

Huang, L., & Chiang, Y. (2001). The formation of dunes, antidunes, and rapidly damping waves in alluvial channels. *International Journal for Numerical and Analytical Methods in Geomechanics, 25*(7), 675-690.

Hutchinson, G. E. (1957). *A Treatise on Limnology. Volume 1*. New York: Wiley & Sons, 660 pp.

International Kootenay Lake Board of Control. (2003). *2003 Annual Report to the International Joint Commission*. Vancouver, BC: International Kootenay Lake Board of Control.

James, T. S., Clague, J. J., Wang, K., & Hutchinson, I. (2000). Postglacial rebound at the northern Cascadia subduction zone. *Quaternary Science Reviews, 19*(14–15), 1527-1541.

Jansen, J. D. (2006). Flood magnitude-frequency and lithologic control on bedrock river incision in post-orogenic terrain. *Geomorphology, 82*(1-2), 39-57.

Jasper, K. (2009). Significance of soft-sediment clasts in glacial outwash, Puget Sound, USA. *Sedimentary Geology, 220*(1-2), 126-133.

Johns, W. M. (1970). Geology and mineral deposits of Lincoln and Flathead counties, Montana. *Montana Bureau of Mines and Geology, Bulletin 79*, 10-13.

Johnsen, T. F., & Brennand, T. A. (2004). Late-glacial lakes in the Thompson basin, British Columbia: Paleogeography and evolution. *Canadian Journal of Earth Sciences, 41*(11), 1367-1383.

Johnsen, T. F., & Brennand, T. A. (2006). The environment in and around ice-dammed lakes in the moderately high relief setting of the southern Canadian Cordillera. *Boreas, 35*(1), 106-125.

Johnson, J. P. L., Whipple, K. X., & Sklar, L. S. (2010). Contrasting bedrock incision rates from snowmelt and flash floods in the Henry Mountains, Utah. *Geological Society of America Bulletin, 122*(9-10), 1600-1615.

Jol, H. M., & Bristow, C. S. (2003). GPR in sediments: Advice on data collection, basic processing and interpretation, a good practice guide. *Geological Society, London, Special Publication, 211*(1), 9-27.

Jolly, R. J. H., & Lonergan, L. (2002). Mechanisms and controls on the formation of sand intrusions. *Journal of the Geological Society of London, 159*, 605-617.

Kinley, I. (1886). North American Lakes. Historical Society of Southern California, Los Angeles, 1(2), pp. 37-43.

Kjaer, K. H., Sultan, L., Kruger, J., & Schomacker, A. (2004). Architecture and sedimentation of outwash fans in front of the Myrdalsjökull ice cap, Iceland. *Sedimentary Geology, 172*(1-2), 139-163.

Knight, P. G., Waller, R. I., Patterson, C. J., Jones, A. P., & Robinson, Z. P. (2000). Glacier advance, ice-marginal lakes and routing of meltwater and sediment; Russell Glacier, Greenland. *Journal of Glaciology, 46*(154), 423-425.

Kovanen, D. J., & Slaymaker, O. (2004). Glacial imprints of the Okanogan lobe, southern margin of the Cordilleran Ice Sheet*. Journal of Quaternary Science, 19*(6), 547.

Krüger, J. (1979). Structures and textures in till indicating subglacial deposition. *Boreas, 8*(3), 323-340.

Krüger, J. (1984). Clasts with stoss-lee form in lodgement tills: A discussion. *Journal of Glaciology,* (30), 241-243.

Krumbein, W. C. (1941). Measurement and geological significance of shape and roundness of sedimentary particles. *Journal of Sedimentary Research, 11*(2), 64-72.

Kuehn, S. C., Froese, D. G., Carrara, P. E., Foit Jr., F. F., Pearce, N. J. G., & Rotheisler, P. (2009). Major- and trace-element characterization, expanded distribution, and a new chronology for the latest Pleistocene Glacier Peak tephras in western North America. *Quaternary Research*, 71(2), 201-216.

Kyle, G. W. (1938). *1938 Kootenay Lake order*. New York: International Joint Commission.

Lecce, S. A. (1990). The alluvial fan problem. In A. H. Rachocki, & M. Church (Eds.), *Alluvial fans: A Field Approach*. West Sussex: John Wiley and Sons Ltd, pp. 3-24.

Lesemann, J., & Brennand, T. A. (2009). Regional reconstruction of subglacial hydrology and glaciodynamic behaviour along the southern margin of the Cordilleran Ice Sheet in British Columbia, Canada and northern Washington State, USA. *Quaternary Science Reviews, 28*(23), 2420-2444.

Lesemann, J., & Shaw, J. (2000). An additional water source for the formation of the Channeled Scablands in south-central British Columbia, Canada. *Geological Society of America, Abstracts with Programs, 32*(7), 116.

Levson, V. M., & Rutter, N. W. (1989). Late Quaternary stratigraphy, sedimentology, and history of the Jasper townsite area, Alberta, Canada. *Canadian Journal of Earth Sciences, 26*(7), 1325-1342.

Lewis, D. (1984). *Practical Sedimentology*. United States (USA): Hutchinson Ross Publishing Co., Stroudsburg, PA, United States (USA).

Lian, O. B., & Hickin, E. J. (1996). Early postglacial sedimentation of lower Seymour valley, southwestern British Columbia. *Géographie physique et Quaternaire, 50*(1), 95.

Lian, O. B., & Hicock, S. R. (2000). Thermal conditions beneath parts of the last Cordilleran Ice Sheet near its centre as inferred from subglacial till, associated sediments, and bedrock. *Quaternary International, 68-71*(0), 147-162.

Lian, O.B, Hicock S.R. (2001). Lithostratigraphy and limiting optical ages of the Pleistocene fill in Fraser River valley near Clinton, south-central British Columbia. *Canadian Journal of Earth Sciences, 38*(5), 839-850.

Lian, O. B., & Huntley, D. J. (1999). Optical dating studies of postglacial aeolian deposits from the south-central interior of British Columbia, Canada. *Quaternary Science Reviews, 18*(13), 1453-1466.

Lian, O. B., & Roberts, R. G. (2006). Dating the Quaternary: Progress in luminescence dating of sediments. *Quaternary Science Reviews, 25*(19), 2449-2468.

Liboriussen, J. (1975). A study of gravel fabric. *Sedimentary Geology, 14*(3), 235-251.

Lindsey, D. A., Langer, W. H., & Van Gosen, B. S. (2007). Using pebble lithology and roundness to interpret gravel provenance in piedmont fluvial systems of the Rocky Mountains, USA. *Sedimentary Geology, 199*(3–4), 223-232.

Lowe, D. R. (1982). Sediment gravity flows. *Journal of Sedimentary Petrology, 52*(1), 279-297.

Lunt, I., & Bridge, J. S. (2007). Formation and preservation of open-framework gravel strata in unidirectional flows. *Sedimentology, 54*(1), 71-87.

Lutz, P., Garambois, S., & Perroud, H. (2003). Influence of antenna configurations for GPR survey: Information from polarization and amplitude versus offset measurements. *Geological Society, London, Special Publications, 211*(1), 299-313.

Maag, H. (1969). *Ice dammed lakes and marginal glacial drainage on Axel Heiberg Island. Axel Heiberg Island research report*. Montreal: McGill University.

Mackin, J. H. (1961). A stratigraphic section in the Yakima basalt and the Ellensburg formation in south-central Washington. *Washington Department of Conservation, 19*, 1-45.

Magilligan, F. J., Gomez, B., Mertes, L. A. K., Smith, L. C., Smith, N. D., Finnegan, D., & Garvin, J. B. (2002). Geomorphic effectiveness, sandur development, and the pattern of landscape response during jökulhlaups; Skeiðhararsandur, southeastern Iceland. *Geomorphology, 44*(1-2), 95-113.

Maizels, J. (1989). Sedimentology, paleoflow dynamics and flood history of jökulhlaup deposits; paleohydrology of Holocene sediment sequences in southern Iceland sandur deposits. *Journal of Sedimentary Research, 59*(2), 204-223.

Maizels, J. (1993). Lithofacies variations within sandur deposits. *Sedimentary Geology, 85*(1-4), 299-325.

Maizels, J. K. (1990). Paleoflow dynamics of bedforms and sediment sequences produced during catastrophic floods on Icelandic sandurs. *Geological Society of America, Abstracts with Programs, 22*(2), 53.

Maizels, J. K. (1997). Jökulhlaup deposits in proglacial areas. *Quaternary Science Reviews, 16*, 793-819.

Major, J. J. (1998). Pebble orientation on large, experimental debris-flow deposits. *Sedimentary Geology, 117*(3-4), 151-164.

Marcus, M. G. (1960). Periodic drainage of glacier-dammed Tulsequah Lake, British Columbia. *Geographical Review, 50*(1), pp. 89-106.

Marren, P. M., Russell, A. J., & Rushmer, E. L. (2009). Sedimentology of a sandur formed by multiple jökulhlaups, Kverkfjöll, Iceland. *Sedimentary Geology, 213*(3-4), 77-88.

Marren, P. M., & Schuh, M. (2009). Criteria for identifying jökulhlup deposits in the sedimentary record. In D. M. Burr, P. A. Carling & V. R. Baker (Eds.), *Megaflooding on Earth and Mars*. New York: Cambridge University Press, pp. 225-242.

Marston, R. A. (1983). Supraglacial stream dynamics on the Juneau Icefield. *Annals of the Association of American Geographers, 73*(4), pp. 597-608.

Mathews, W. H. (1978). Quaternary stratigraphy and geomorphology of Charlie Lake (94a) map-area, British Columbia. *Geological Survey of Canada Paper,* 76-20.

Mathews, W. H. (1980). Retreat of the last ice sheets in northeastern British Columbia and adjacent Alberta. *Geological Survey of Canada Bulletin,* 331, 1-22.

Matthes, G. H. (1947). Macroturbulence in natural stream flow. *American Geophysical Union, 28*, 255-262.

McCarroll, D., & Rijsdijk, K. F. (2003). Deformation styles as a key for interpreting glacial depositional environments. *Journal of Quaternary Science, 18*(6), 473-489.

McDonald, E. V., & Busacca, A. J. (August, 1988). Record of pre-late Wisconsin giant floods in the Channeled Scabland interpreted from loess deposits. *Geology, 16*(8), 728-731.

Menzies, J. (Ed.). (1996). *Past Glacial Environments: Sediments Forms and Techniques* (2nd ed.). Oxford: Butterworth and Heinemann.

Miall, A. D. (1976). Palaeocurrent and palaeohydrologic analysis of some vertical profiles through a Cretaceous braided stream deposit, Banks Island, arctic Canada. *Sedimentology, 23*(4), 459-483.

Miall A. D. (1977). A review of the braided-river depositional environment. *Earth Science Reviews*. 13, 1-62.

Miall, A. D. (1978). Lithofacies types and vertical profile models in braided river deposits; a summary. *Canadian Society of Petroleum Geologists Memoir, 1*(5), 597-604.

Miall, A. D., & Jones, B. G. (2003). Fluvial architecture of the Hawkesbury sandstone (Triassic), near Sydney, Australia. *Journal of Sedimentary Research, 73*(4), 531-545.

Mills, H. H. (1979). Downstream rounding of pebbles; a quantitative review. *Journal of Sedimentary Petrology, 49*(1), 295-302.

Mitchum, R. M., Vail, P. R., & Sangree, J. B. (1977). Stratigraphic interpretation of seismic reflection patterns in depositional sequences. In C. E. Payton (Ed.), *Seismic stratigraphy - applications to hydrocarbon exploration* American Association of Petroleum Geologists, pp. 117-123.

Miyamoto, H., Komatsu, G., Baker, V. R., Dohm, J. M., Ito, K., & Tosaka, H. (2007). Cataclysmic scabland flooding: Insights from a simple depth-averaged numerical model. *Environmental Modelling & Software, 22*(10), 1400-1408.

Munro-Stasiuk, M., Shaw, J., Sjogren, D. B., Brennand, T. A., Fisher, T. G., Sharpe, D. R., Rains, B. B. (2009). The morphology and sedimentology of landforms created by subglacial megafloods. In D. M. Burr, P. A. Carling & V. R. Baker (Eds.), *Megaflooding on Earth and Mars*. New York: Cambridge University Press, pp. 78-103.

Nasmith, H. (1962). Late glacial history and surficial deposits of the Okanagan Valley, British Columbia. *British Columbia Department of Mines and Petroleum Resources, Bulletin 46*.

Neal, A. (2004). Ground-penetrating radar and its use in sedimentology; principles, problems and progress. *Earth-Science Reviews, 66*(3-4), 261-330.

Neal, A., Richards, J., & Pye, K. (2002). Structure and development of shell cheniers in Essex, southeast England, investigated using high-frequency ground-penetrating radar. *Marine Geology, 185*(3-4), 435-469.

Nemec, W., Lønne, I., & Blikra, L. H. (1999). The Kregnes moraine in Gauldalen, west-central Norway: Anatomy of a Younger Dryas proglacial delta in a palaeofjord basin. *Boreas, 28*(4), 454-476.

Nemec, W., & Steel, R. J. (Eds.). (1988). *Fan deltas: Sedimentology and tectonic settings*. London: Blackie and Son Ltd.

Newberry, J. S. (1871). The ancient lakes of western America: Their deposits and drainage. *The American Naturalist, 4*(11), pp. 641-660.

Nichols, R. L., & Miller, M. M. (1952). The Moreno Glacier, Lago Argentino, Patagonia, advancing glaciers and nearby simultaneously retreating glaciers. *Journal of Glaciology, 2*, 41-50.

Nichols, R., Sparks, R., & Wilson, C. (1994). Experimental studies of the fluidization of layered sediments and the formation of fluid escape structures. *Sedimentology, 41*(2), 233-253.

Normark, W., & Reid, J. (2003). Extensive deposits on the Pacific Plate from late Pleistocene North American glacial lake outbursts. *The Journal of Geology, 111*(6), 617-637.

Nye, J. F. (1976). Water flow in glaciers: Jökulhlaups, tunnels and veins. *Journal of Glaciology, 17*, 181-207.

O'Connor, J. E., & Baker, V. R. (1992). Magnitudes and implications of peak discharges from glacial Lake Missoula. *Geological Society of America Bulletin, 104*(3), 267-279.

O'Connor, J. E., & Webb, R. H. (1988). Hydraulic modeling for paleoflood analysis. *Flood Geomorphology,* 393-402.

O'Connor, J.,E., & Beebee, R. A. (2009). Floods from natural rock-material dams. In D. M. Burr, P. A. Carling & V. R. Baker (Eds.), *Megaflooding on Earth and Mars*. New York: Cambridge University Press, pp. 128-171.

O'Connor, J.,E., Waitt, R. B., Johnston, D. A., Benito, G., Cordero, D., & Burns, S. (1995). Beyond the Channeled Scabland; a field trip to Missoula flood features in the Columbia, Yakima, and Walla Walla valleys of Washington and Oregon, part 2; field trip, day one. *Oregon Geology, 57*(4), 1-75.

Oviatt, C. G., Currey, D. R., & Sack, D. (1992). Radiocarbon chronology of Lake Bonneville, eastern Great Basin, USA. *Palaeogeography, Palaeoclimatology, Palaeoecology, 99*(3–4), 225-241.

Paradis, S. (2007). Carbonate-hosted zn-pb deposits in southern British Columbia - potential for Irish-type deposits. *Geological Survey of Canada, Current Research, 2007-A10*, 1-7.

Pardee, J. T. (1910). The glacial Lake Missoula. *The Journal of Geology, 18*(4), 376-386.

Pardee, J. T. (1942). Unusual currents in glacial Lake Missoula, Montana. *Geological Society of America Bulletin, 53*(11), 1569-1599.

Patton, P. C., & Baker, V. R. (1978). Origin of the Cheney-Palouse Scabland tract. In V. R. Baker, & D. Nummedal (Eds.), *The Channeled Scabland*. Washington D.C.: The National Aeronautics and Space Administration, pp. 117-130.

Pattyn, F., De Smedt, B., & Souchez, R. (2004). Influince of subglacial Vostok on the regional ice dynamics of the Antarctic ice sheet: A model study. *Journal of Glaciology, 50*(171), 583-589.

Philip M., M. (2005). Magnitude and frequency in proglacial rivers: A geomorphological and sedimentological perspective. *Earth-Science Reviews, 70*(3–4), 203-251.

Postma, G. (1990). Depositional architecture and facies of river and fan deltas: A synthesis. In Colella, A., Prior, D. B (Eds.), *Coarse-Grained Deltas*. Blackwell Publishing Ltd., Oxford, UK.

Price, R. J. (1973). Glacial and fluvioglacial landforms. Oliver and Boyd, Edinburgh; *Geomorphology Texts, 5*.

Pugin, A. (1989). Facies model for deglaciation in an overdeepened alpine valley (Bulle area, western Switzerland). *Palaeogeography, Palaeoclimatology, Palaeoecology, 70*(1-3), 235-248.

Rappol, M. (1985). Clast-fabric strength in tills and debris flows compared for different environments. *Geologie En Mijnbouw, Netherlands. Journal of Geosciences, 64*(3), 327-332.

Raymond, C. F., & Nolan, M. (2000). Drainage of a glacial lake through an ice spillway. International Union of Geodesy and Geophysics. *Debris-Covered Glaciers, In Nakawo, M., Raymond, C.F. and Fountain, A. (Eds), Debris-Covered Glaciers, International Association of Hydrological Sciences Publication.* 264, 199-207.

Reading, H. G. (Ed.). (1986). *Sedimentary Environments and Facies* (Second ed.). Oxford: Blackwell.

Reusser, L., Bierman, P., Pavich, M., Larsen, J., & Finkel, R. (2006). An episode of rapid bedrock channel incision during the last glacial cycle, measured with ^{10}Be. *American Journal of Science, 306*(2), 69-102.

Rijsdijk, K. F., Owen, G., Warren, W. P., McCarroll, D., & van der Meer, J. J. M. (1999). Clastic dykes in over-consolidated tills: Evidence for subglacial hydrofracturing at Killiney Bay, eastern Ireland. *Sedimentary Geology, 129*(1-2), 111-126.

Roberts, M. J. (2005). Jökulhlaups: A reassessment of floodwater flow through glaciers. *Reviews of Geophysics, 43*, 1-21.

Roberts, M. J., Palsson, F., Gudmundsson, M. T., Bjornsson, H., Tweed, F. S., Hulbe, C. (2005). Ice-water interactions during floods from Gaenalon glacier-dammed lake, Iceland. *Annals of Glaciology, 40*, 133-138.

Roeller, K. (2008). *Software for Geoscientists: Stereo32 and StereoNett,* Bochum, DE: Ruhr University Bochum.

Rovey, C. W.,II, & Borucki, M. K. (1995; 1995). Subglacial to proglacial sediment transition in a shallow ice-contact lake. *Boreas, 24*(2), 117-127.

Rudoy, A. N. (2002). Glacier-dammed lakes and geological work of glacial superfloods in the late Pleistocene, southern Siberia, Altai Mountains. *Quaternary International, 87*, 119-140.

Ruffner, R. A., Kleinspehn, K. L., Paola, C., & Vondra, C. F. (1996). Gravel fabric; implications for paleocurrent analyses. *Geological Society of America, Abstracts with Programs, 28*(6), 63.

Russell, A. J. (2009). Jökulhlaup (ice-dammed lake outburst flood) impact within a valley-confined sandur subject to backwater conditions, Kangerlussuaq, west Greenland. *Sedimentary Geology, 215*(1-4), 33-49.

Russell, H. A. J., & Arnott, R. W. C. (2003). Hydraulic-jump and hyperconcentrated-flow deposits of a glacigenic subaqueous fan; oak ridges moraine, southern Ontario, Canada. *Journal of Sedimentary Research, 73*(6), 887-905.

Russell, H. A. J., Arnott, R. W. C., & Sharpe, D. R. (2003). Evidence of rapid sedimentation from high-energy flows and hyperconcentrated flows in glacifluvial deposits; subaqueous fan examples. *Journal of Sedimentary Research, 35*(6), 387-387.

Russell, H. A. J., Sharpe, D. R., & Bajc, A. F. (2007). Sedimentary signatures of the Waterloo moraine, Ontario, Canada. *International Association of Sedimentologists, Special Publication, 39*, 85-108.

Rust, B. R. (1988). Ice-proximal deposits of the Champlain Sea at south Gloucester, near Ottawa, Canada. *Geological Association of Canada, Special Paper, 35*, 1-37.

Ryder, J. M. (1971). The stratigraphy and morphology of para-glacial alluvial fans in south-central British Columbia. *Canadian Journal of Earth Sciences, 8*(2), 279-298.

Ryder, J. M., Fulton, R. J., & Clague, J. J. (1991). The Cordilleran Ice Sheet and the glacial geomorphology of southern and central British Columbia. *Géographie physique et Quaternaire, 45*(3), 365-377.

Sagan, C. (1995). *Demon-haunted world* (Kindle ed.) Random House Inc.

Salamon, T. (2009). Origin of Pleistocene outwash plains in various topographic settings, southern Poland. *Boreas, 38*(2), 362-378.

Sallenger, A. H., J. (1979). Inverse grading and hydraulic equivalence in grain-flow deposits. *Journal of Sedimentary Petrology, 49*(2), 553-562.

Sambrook Smith, G., Ashworth, P. J., Best, J. L., Woodward, J., & Simpson, C. J. (2006). The sedimentology and alluvial architecture of the sandy braided South Saskatchewan River, Canada. *Sedimentology, 53*(2), 413-434.

Sandmeier, S. K. (2011). *REFLEXW (version 6.0) processing program for seismic, acoustic and electromagnetic reflection, refraction and transmission data* (v 6.0). Germany: Karlsruhe.

Schiefer, E., & Gilbert, R. (2008). Proglacial sediment trapping in recently formed Silt Lake, upper Lillooet valley, Coast Mountains, British Columbia. *Earth Surface Processes and Landforms, 33*(10), 1542-1556.

Schlee, J. S. (1957). Fluvial gravel fabric. *Journal of Sedimentary Petrology, 27*(2), 162-176.

Sharp, M. (1982). Modification of clasts in logement tills by glacial erosion. *Journal of Glaciology, 28*(100), 475-480.

Shaw, J., & Archer, J. (1979). *Deglaciation and glaciolacustrine sedimentation conditions, Okanagan Valley, British Columbia, Canada,* In C. Schluchter, ed.,Moraines and Varves, Origin/genesis/classification. A. A. Balkema, Rotterdam, 347-355.

Shaw, J., Gilbert, R., & Archer, J. J. J. (1978). Proglacial lacustrine sedimentation during winter. *Arctic and Alpine Research, 10*(4), 689-699.

Shaw, J., Munro-Stasiuk, M., Sawyer, B., Beaney, C., Lesemann, J., Musacchio, A., Young, R. R. (1999). The Channeled Scabland: Back to Bretz? *Geology, 27*(7), 605-608.

Siegert, M. J., Carter, S., Tabacco, I., Popov, S., & Blankenship, D. D. (2005). A revised inventory of antarctic subglacial lakes. *Antarctic Science, 17*(3), 453-460.

Skelly, R. L., Bristow, C. S., & Ethridge, F. G. (2003). Architecture of channel-belt deposits in an aggrading shallow sandbed braided river; the Lower Niobrara River, northeast Nebraska. *Sedimentary Geology, 158*(3-4), 249-270.

Sklar, L. S., & Dietrich, W. E. (2001). Sediment and rock strength controls on river incision into bedrock. *Geology, 29*(12), 1087-1090.

Sklar, L. S., & Dietrich, W. E. (2006). The role of sediment in controlling steady-state bedrock channel slope: Implications of the saltation–abrasion incision model. *Geomorphology, 82*(1–2), 58-83.

Smith, D. R., & Leeman, W. P. (1982). Mineralogy and phase chemistry of Mount St. Helens tephra sets W and Y as keys to their identification. *Quaternary Research, 17*(2), 211-227.

Smith, L. N. (2006a). Pleistocene glacial deposits in the Libby and Lake River valley areas, Lincoln County, Montana. *Northwest Geology, 35*, 87-90.

Smith, L. N. (2006b). Stratigraphic evidence for multiple drainings of glacial Lake Missoula along the Clark Fork River, Montana, USA. *Quaternary Research, 66*(2), 311-322.

Smith, L. C., Alsdorf, D. E., Magilligan, F. J., Gomez, B., Mertes, L. A. K., Smith, N. D., & Garvin, J. B. (2000). Estimation of erosion, deposition, and net volumetric change caused by the 1996 Skeiđararsandur jökulhlaup, Iceland, from synthetic aperture radar interferometry. *Water Resources Research, 36*(6), 1583-1594.

Smith, N. D. (1974). Sedimentology and bar formation in the upper Kicking Horse River, a braided outwash stream. *The Journal of Geology, 82*(2), 205-223.

Smith, N. D., & Ashley, G. M. (1985). Proglacial lacustrine environment. *Society of Economic Petrologists and Mineralogists, Short Course 16*, 135-215.

Smith, N. D., Vendl, M. A., & Kennedy, S. K. (1982). Comparison of sedimentation regimes in four glacier-fed lakes of western Alberta. In R. Davidson-Arnott, W. Nickling & B. D. Fahey (Eds.), *Research in Glacial, Glaciofluvial, and Glaciolacustrine Systems*. Norwich: Geo Books, pp. 203-238.

Sneed, E. D., & Folk, R. L. (1958). Pebbles in the lower Colorado River, Texas a study in particle morphogenesis. *The Journal of Geology, 66*(2), pp. 114-150.

Southard, J. B., & Boguchwal, L. A. (1990). Bed configuration in steady unidirectional water flows; part 2, synthesis of flume data. *Journal of Sedimentary Petrology, 60*(5), 658-679.

Sparks, R. S. J., Bonnecaze, R. T., Huppert, H. E., Lister, J. R., Hallworth, M. A., Mader, H., & Phillips, J. (1993). Sediment-laden gravity currents with reversing buoyancy. *Earth and Planetary Science Letters, 114*(2–3), 243-257.

Steel, R. J., & Thompson, D. B. (1983). Structures and textures in Triassic braided stream conglomerates ("bunter" pebble beds) in the Sherwood sandstone group, north Staffordshire, England. *Sedimentology, 30*(3), 341-376.

Stokes, C. R., & Clark, C. D. (2004). Evolution of late glacial ice-marginal lakes on the northwestern Canadian Shield and their influence on the location of the Dubawnt Lake palaeo-ice stream. *Palaeogeography, Palaeoclimatology, Palaeoecology, 215*(1-2), 155-171.

Stumpf, A. J., Broster, B. E., & Levson, V. M. (2000). Multiphase flow of the late Wisconsinan Cordilleran Ice Sheet in western Canada. *Geological Society of America, Bulletin, 112*(12), 1850-1863.

Sugden, D. E., Clapperton, C. M., & Knight, P. G. (1985). A jökulhlaup near Sondre Stromfjord, west Greenland, and some effects on the ice-sheet margin. *Journal of Glaciology, 31*(109), 366-368.

Swanson, D. A., & Wright, T. L. (1978). Bedrock geology of the northern Columbia Plateau and adjacent areas. In V. R. Baker, & D. Nummedal (Eds.), *The Channeled Scabland*. Washington D.C.: The National Aeronautics and Space Administration, pp. 37-58.

SWANSON, D. A. (1967). Yakima basalt of the Tieton River area, south-central Washington. *Geological Society of America Bulletin, 78*(9), 1077-1110.

Teller, J. T., Leverington, D. W., & Mann, J. D. (2002). Freshwater outbursts to the oceans from glacial Lake Agassiz and their role in climate change during the last deglaciation. *Quaternary Science Reviews, 21*(8–9), 879-887.

Thorarinsson, S. (1939). The ice-dammed lakes of Iceland with particular references to their value as indicators of glacier oscillations. *Geografiska. Annaler, 21*(3-4), 216-242.

Thorson, R. M. (1989). Glacio-isostatic response of the Puget Sound area, Washington. *Geological Society of America Bulletin, 101*(9), 1163-1174.

Tweed, F. S., & Russel, A. J. (1999). Controls on the formation and sudden drainage of glacier-impounded lakes: Implications for jökulhlaup characteristics. *Progress in Physical Geography, 23*(1), 79-110.

Valla, P. G., van der Beek, P.,A., & Lague, D. (2010). Fluvial incision into bedrock; insights from morphometric analysis and numerical modeling of gorges incising glacial hanging valleys (western Alps, France). *Journal of Geophysical Research, 115*.

Waitt Jr, R. B. (1984). Periodic jökulhlaups from Pleistocene glacial Lake Missoula - new evidence from varved sediment in northern Idaho and Washington. *Quaternary Research, 22*(1), 46-58.

Waitt Jr, R. B. (1985). Case for periodic, colossal jökulhlaups from Pleistocene glacial Lake Missoula. *Geological Society of America Bulletin, 96*(10), 1271-1286.

Waitt, R. B. (1980). About forty last-glacial Lake Missoula jökulhlaups through southern Washington. *The Journal of Geology, 88*(6), 653-679.

Waitt, R.B. (1994). Scores of gigantic, successively smaller Lake Missoula floods through Channeled Scabland and Columbia valley. In: Swanson, D.A. & Haugerud, R.A. (Eds.), Geologic field trips in the Pacific Northwest. Seattle, Department of Geological Sciences, University of Washington, 1 (Chapter 1K), pp. 88.

Waitt, R. B., Denlinger, R. P., & O'Connor, J. E. (2009). Many monstrous Missoula floods down Channeled Scabland and Columbia valley. *Geological Society of America Field Guide* 15, pp. 775-844.

Waitt, R. B. (2009). Routes to Wenatchee of Columbia valley megafloods from glacial Lake Missoula and other sources. *Geological Society of America, Abstracts with Programs, 41*(5), 33.

Walder, J. S., & Fowler, A. C. (1994). Channelized subglacial drainage over a deformable bed. *Journal of Glaciology, 40*(134), 3-14.

Walder, J. S., & O'Connor, J.,E. (1997). Methods for predicting peak discharge of floods caused by failure of natural and constructed earthen dams. *Water Resources Research, 33*, 2337-2348.

Walker, R. G. (1992). *Facies, facies models and modern stratigraphic concepts*. In Walker, R. G. & James, N. P. (Eds.) *Facies models – response to sea level change. Geological Association of Canada, St. John's Newfoundland*, pp. 1-14.

Ward, B., & Rutter, N. W. (2000). Deglacial valley fill sedimentation, Pelly River, Yukon Territory, Canada. *Quaternary International, 68(71)*, 309-328.

Wentworth, C. K. (1919). A laboratory and field study of cobble abrasion. *The Journal of Geology, 27*(7), 507-521.

Whipple, K. X., Hancock, G. S., & Anderson, R. S. (2000). River incision into bedrock: Mechanics and relative efficacy of plucking, abrasion, and cavitation. *Geological Society of America, Bulletin, 112*(3), 490-503.

Woodward, J., Ashworth, P. J., Best, J. L., Sambrook Smith, G. H., & Simpson, C. J. (2003). The use and application of GPR in sandy fluvial environments: Methodological considerations. *Geological Society, London, Special Publication, 211*(1), 127-142.

Zen, E., & Prestegaard, K. L. (1994). Possible hydraulic significance of two kinds of potholes: Examples from the paleo-potomac river. *Geology, 22*(1), 47-50.

Zuffa, G. G., Normark, W. R., Serra, F., & Brunner, C. A. (2000). Turbidite megabeds in an oceanic rift valley recording jökulhlaups of late Pleistocene glacial lakes of the western United States. *The Journal of Geology, 108*(3), 253-274.